The role of intraflagellar transport during the disassembly of the *Leishmania mexicana* flagellum

Lauren Wilburn

THIS THESIS IS SUBMITTED IN PARTIAL FULFILMENT OF THE REQUIREMENTS OF THE AWARD FOR THE DEGREE OF DOCTOR OF PHILOSOPHY

AWARDED BY OXFORD BROOKES UNIVERSITY

SUBMISSION DATE: NOVEMBER 2022

Declaration

I declare that the material contained in this thesis has not been used in any other submission for an academic award. I confirm that all the research and findings presented in this thesis are my own work unless otherwise indicated through the use of a clear referencing system.

Abstract

The ability of the *Leishmania* parasites to remodel its flagellum is important for its survival as it navigates through multiple host environments during its lifecycle. The most striking remodelling step is during the differentiation from the long, motile flagellum of promastigotes to the short, sensory flagellum of amastigotes. Previous work has suggested a large reduction in the intraflagellar transport (IFT) system can lead to flagellum disassembly in *Leishmania*. However, it is not clear how or when the IFT system changes during this disassembly process.

Here, we show that the flagellum disassembly is associated with a large drop in IFT numbers and a slight decrease in IFT velocity. This drop occurs within 30 minutes of differentiation suggesting the 'shock' of the change in environmental conditions is the likely trigger of the IFT reduction. The potential role of post-translational modifications in regulating IFT was investigated but no major changes in modification patterns were observed.

We also looked at a previously documented naturally occurring *Leishmania* mutant, known as the dysflagellar mutant. It had a very short but otherwise normal axoneme but a large mass of unorganised material at the exit of the flagellar pocket, which created a bulge. The underlying cause of this mutant was hypothesised to be a defect in IFT. However, analyses showed that a large 27 kb deletion, containing four genes, on chromosome 35 was present. We found when the deletion of a serine kinase was replicated it led to a similar phenotype as the dysflagellar mutant. This could be rescued when the serine kinase was reintroduced.

Overall, we have provided initial observations regarding flagellum remodelling of *Leishmania* that can be used to address unanswered questions such as what is controlling flagellum (dis)assembly.

Acknowledgments

I would firstly like to thank my supervisor Dr Jack Sunter for his ongoing support, guidance, and patience during this PhD as without him this thesis would not have been possible. The genuine passion he has for parasitology is evident. I have thoroughly appreciated his willingness is letting me follow ideas (even if they mostly didn't work!), make mistakes and learn from them and provide invaluable insights in every topic.

I would also like to thank past and present members of the Sunter and Vaughan labs and members of the bioimaging team for discussions, advice and showing me the ropes. Special thanks to Clare Halliday, Laura Smithson, Shahaan Shafiq, Manu Ahmed and Heloisa Berti Gabriel for your training, patience and genuinely making the PhD more enjoyable both in and out of the lab!

I'd like to mention the wonderful humans at Linacre boat club who have kept me exercised, entertained and sane throughout this PhD. With thanks to my family, friends and Humps who have supported me throughout this experience. In particular, Abbey who has always been at the other end of the phone and my grandma who kindly sacrificed her dining room to allow me to write.

And a very special thanks to my partner Phil who has proofread work, listened endlessly to my practice presentations, and provided a huge deal of support (and many snacks) throughout.

Lastly, I recognize the BBSRC for funding this project.

Contents

List of Figures and Tables

1. Introduction

1.1 Flagella are highly conserved across eukaryotes.

Flagella and cilia (terms used interchangeably) are microtubule-based organelles found throughout eukaryotes. The flagella ultrastructure is highly conserved, but flagella have evolved to perform a range of biological functions, including sensing, motility, and signalling (Moran et al., 2014).

The typical structure of the flagellum consists of a microtubule axoneme, which is nucleated from a specialised microtubule organising centre known as the basal body (Vaughan & Gull, 2016). Usually, the microtubules are ordered in either a 9+2 arrangement in motile flagella or a 9+0 arrangement in non-motile flagella (Scholey, 2008). The 9+2 structure has nine sets of microtubule doublets and a central pair of microtubule singlets whereas the 9+0 structure lacks the central pair (Figure 1.1a). Notable examples of deviation from this classical structure include insect sperm. For example, the sperm of *Platycotis,* a species of small insect, have motile sperm with a modified 9+9+2 axoneme structure, with an additional set of nine singlet microtubules outside the 9+2 structure (Phillips, 1969).

As flagella are present in most eukaryotic lineages, the evolutionary origins of these organelles have garnered a lot of interest. Previously it was though that eukaryotic flagella had originated from prokaryotic flagella, however they are fundamentally different in their ultrastructure and function (Silverman & Simon, 1974; Smith, 2013). There are three common theories of how the eukaryotic flagellum evolved: i) from an endosymbiotic relationship with a spirochete, ii) a viral infection with a virus with a nine-fold symmetry or iii) evolved independently with the eukaryotic cell (Carvalho-Santos et al., 2011). Comparative genomics are starting to suggest that most of the axoneme and associated proteins are duplicates of cytoplasmic proteins (Jékely & Arendt, 2006), therefore lending the most support to autogenous evolution of the eukaryotic flagellum.
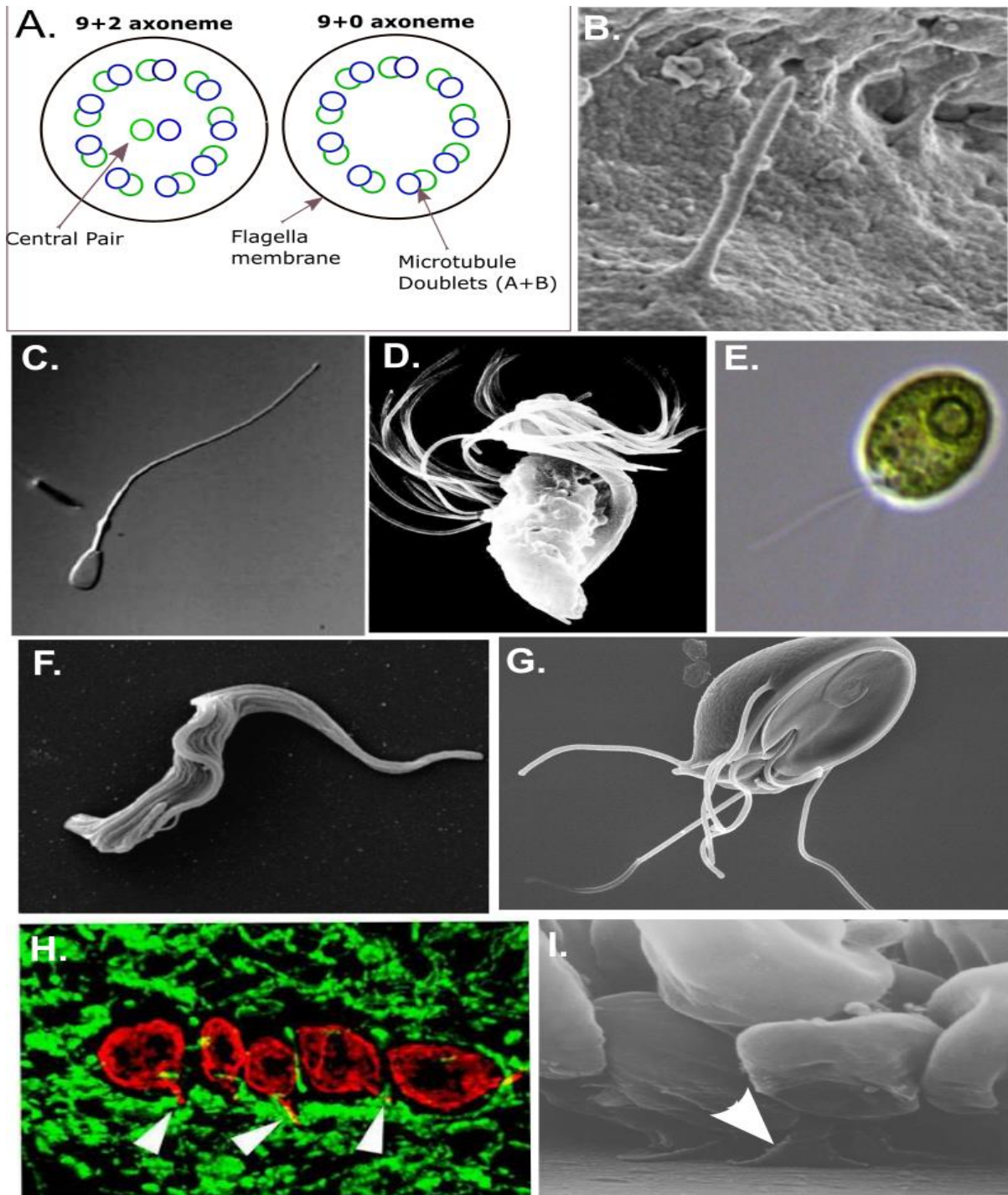
Figure 1.1. The diversity of flagella and cilia across the eukaryotic kingdom. A. Cross sections of flagella axonemes show 9 pairs of A/B microtubule doublets with a defined, which form a ring. There may be the presence of a central pair (9+2) found in motile flagellum or may lack the central pair (9+0) as found in non-motile flagellum. **B.** SEM of non-motile primary cilium (9+0 axoneme) found on the mammalian epidermis (Van Der Heiden et al., 2006). **C**. Highly mobile (9+2 axoneme) mammalian sperm (Ounjai et al., 2012) **D**. Multi-flagellated, motile, spermazatoid of *Equisetum* (Horsetail fern) (Renzaglia & Garbary, 2001). **E.** Bi-flagellated algae, *Chlamydomonas*, an important model for understanding flagellum biology (Neofotis et al., 2021) **F.** A *Trypanosoma brucei* parasite undergoing early division with two flagella (Price et al., 2010)**. G.** The parasite, *Giardia*, has eight flagella that can independently assemble and disassemble from one another (CDC, 2020). **H.** *Trypanosoma cruzi* intracellular amastigote flagellum overlapping and possibly interacting with host mitochondria. White arrows indicate the flagella (Lentini et al., 2018)**. I.** *Leishmania* haptomonads (attached forms of the parasite) have an extended flagellar base that adheres to the sandfly stomedal valve, glass slides *in vitro*. White arrow indicates the flagellum (Wakid & Bates, 2004).

1.2 Diverse flagella can fulfil a wide range of biological functions.

Flagella display huge diversity in form and function and can adapt to serve specific functions across different organisms and even within a single cell. Yet, the ultrastructure is remarkably conserved and so these adaptations are thought to arise from flagellum accessory structures, changes in the flagella number or differences in flagellum regulation (Moran et al., 2014). Examples of the broad range of functions of flagella are discussed below.

1.2.1 The cells' 'antenna'

For many years, primary, non-motile cilia (Figure 1.1b) were thought to be non-functional remnants of their motile predecessors. In fact, it is now known that primary cilia are involved in key signal transduction in pathways such as Hedgehog (Huangfu et al., 2003), Notch (Ezratty et al., 2011) and mTOR (Shillingford et al., 2006). The important role of cilia in signalling means that defects in the organelle can lead to a broad range of serious human diseases, known as ciliopathies. Well documented examples include Bardet-Biedl and Joubert syndrome (Reiter & Leroux, 2017).

1.2.2 Sexual reproduction

Flagella mediated motility is common in metazoan to facilitate sexual reproduction. This can be seen in mammalian sperm with its long, single whip-like flagellum (Figure 1.1c) or the spermatozoids of the lower plants that display a range of unusual morphologies including the example from the horsetail sperm with its numerous, staggered flagellum that are organised in a helical pattern (Figure 1.1d) (Renzaglia & Garbary, 2001).

Protozoa also utilise flagella in sexual reproduction by differentiating into specialised flagellated gametes. *Chlamydomonas* is a biflagellated algae that is common model of flagella biology (Figure 1.1e). The algae undergo division and emerge as biflagellated zoospores, a stage capable of sexual reproduction. They first use their flagella for motility to find a partner cell then they fuse together, first with their flagellum, which triggers intracellular signalling to begin complete fusion and germination (Dentler & Rosenbaum., 1977). These examples highlight the importance of motility in reproduction and the role that flagella may have played from the switch from asexual to sexual reproduction.

1.2.3 An integral factor in pathogenesis.

Motility is also an important part of pathogenicity. A pathogen needs to be able to reach its host, invade, and colonise single or multiple hosts, and the flagellum is often a key part of this.

Protozoan pathogens such as *Trypanosoma brucei* maintain their flagellum and remain motile throughout the different stages of their life cycle, both in the tsetse fly and in the bloodstream of their mammalian hosts (Figure 1.1f). Other parasites such as *Giardia* (Figure 1.1g) have up to eight flagella that are used for motility in the host intestine. *Giardia* then loses flagella by internalising all eight,

then disassemble them whilst differentiating to dormant cysts in order to infect their next host (Einarsson & Svärd, 2015).

Parasites such as *Trypanosoma cruzi* and *Leishmania spp* will differentiate into amastigote forms whilst inside their mammalian host cells, in order to help evade the host's immune system. Amastigotes have a very short flagellum that barely extends out of the flagellar pocket (Gluenz et al., 2010). The amastigote flagellum was originally thought to be rudimentary, however, the short flagellum likely has a specialised role and may be involved in recruitment of organelles to the parasite (Reignault et al., 2019). For example, the amastigote flagellum of *T. cruzi* (Figure 1.1h) shows a close interaction with the host mitochondria and may be involved in recruitment of organelles to the parasite. In *Leishmania spp* the amastigote flagellum has been associated with signalling between the host cell and parasite in addition to sensing of glucose in the external environment (Gluenz et al., 2010).

Leishmania and *T. brucei* also utilise their flagellum to mediate attachment in the insect hosts (Figure 1.I). *T. brucei* epimastigotes will squeeze their flagellum between the epithelial cells of the Tsetse fly's salivary glands and form membranous outgrowths of the flagellum, which develop a hemidesmosome-like structure and facilitate attachment (Tetley & Vickerman, 1985). *Leishmania* have two attached stages, first with the flagellum-mediated attachment of nectomonads and leptomonads to the midgut microvilli (Tetley & Vickerman, 1985). Secondly, at the cuticle surface of the stomodeal valve where haptomonads are attached via the expansion of the flagellum tip and a hemidesmosome-like plaque (Gossage et al., 2003; Pimenta et al., 1992). This attachment allows parasites to persist inside the insects therefore continuing the infection cycle.

1.3 The flagellar proteome; the building blocks of the flagellum.

Flagella are complex organelles capable of performing a variety of biological functions. They have a distinct protein composition that is physically separated from the cell body by a barrier known as the ciliary gate (Breslow et al., 2013; Kee et al., 2012). The collection of proteins required for flagellar assembly and function is known as the flagellar proteome.

The flagellar proteome is composed of roughly 400-900 proteins, depending on species (Beneke et al., 2019; Ostrowski et al., 2002; Pazour et al., 2005). The proteome is made up of a wide variety of proteins including structural proteins (e.g., tubulins, radial-spoke proteins), motor proteins (kinesins and dynein's), enzymes, flagella associated proteins, membrane proteins, intraflagellar transport proteins (IFT) etc. (Diniz et al., 2012). Although the size of the flagella proteome varies between species (potentially due to differences in identification and validation methods of the studies documenting them) many of these genes are conserved across species.

Flagella assemble from the basal body and the axoneme is built by incorporating proteins at the flagellum tip (Deane et al., 2001). However, flagella do not contain protein synthesis machinery,

therefore all proteins are synthesised in the cell body. This creates a problem; how does a cell transit the whole proteome out of the cell body into the flagellum and then to the flagellum tip? Ciliates have evolved a system to orchestrate protein trafficking in the flagellum. This is known as the intraflagellar transport system (IFT). The IFT system, actively transports proteins between the base of the flagellum, known as the IFT pool, and the flagellum tip. IFT machinery is highly conserved and present in almost all ciliates, with the exception of *Plasmodium spp* that lack IFT genes and assemble their flagellated gametes via an alternative pathway (Briggs et al., 2004).

1.4 The Intraflagellar Transport System; a builder, maintainer, and disassembler(?) of flagella

In the early 1990s whilst examining *Chlamydomonas,* Kozminski observed rapidly moving 'lumps' moving along the flagellum from the cell body to the distal tip (Kozminski et al., 1993). These would later be identified as IFT trains.

The majority of IFT research has remained focused upon *Chlamydomonas,* which has provided a wealth of information regarding trafficking. However, recent data is starting to suggest there are large differences in how IFT operates across species.

As the main body of this thesis focuses on, *Leishmania mexicana,* the following section will also present IFT data in the closely related parasite, *T. brucei. T. brucei* is a useful system to analyse IFT in due to its genetic tractability and ease of culture. Schematics with the overviews of IFT in *Chlamydomonas* and *T. brucei* are shown in Figure 1.2 and 1.3 to highlight key differences between the two models.
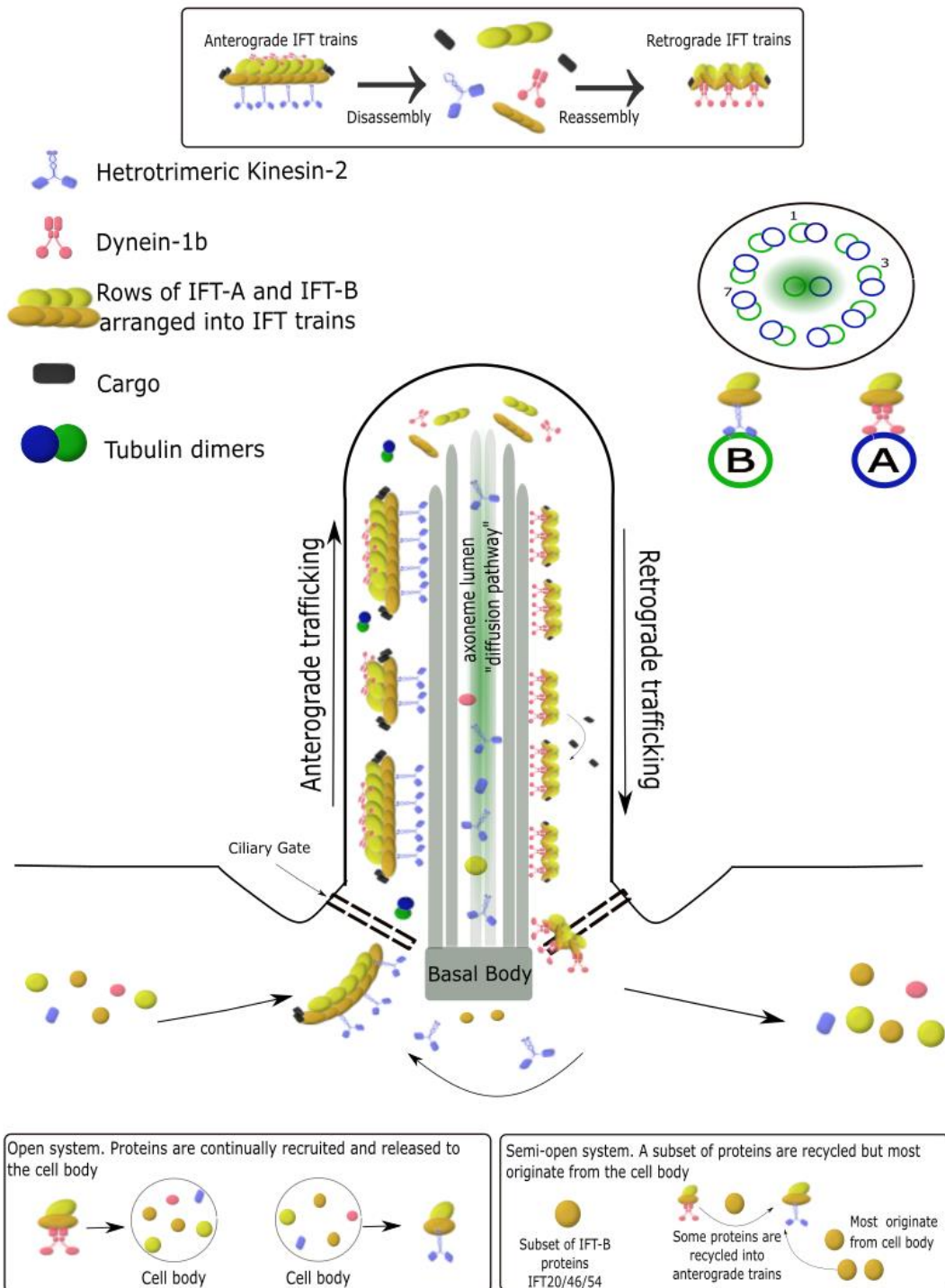
Figure 1.2. The Intraflagellar transport system in *Chlamydomonas* flagella. The IFT pool of *Chlamydomonas* has an open system for the majority of its proteins. Meaning that IFT proteins and cargoes are continually recruited and discarded, and very little recycling of proteins occurs. A few IFT-B proteins are recycled but most are newly recruited from the cell body. Only the anterograde motor, kinesin-2, is recycled. Proteins dock to nine docking sites around the ciliary gate, associate with kinesin-2 and form into IFT trains, which queue to enter the flagellum. Trains are organised in rows with IFT-B rows closer to the motor and IFT-A rows situated between IFT-B and the flagellar membrane. Dynein is loaded onto trains in an inhibited state so that is does not impede trafficking. Trains travel along axoneme on the B tubule of tubulin in an anterograde direction powered by heterotrimeric kinesin-2. Some tubulin dimers can diffuse to the flagellum tip, independently of IFT. At the tip IFT trains remodel into retrograde trains, powered by dynein motors. These trains then return to the IFT pool along the A tubule of tubulin.

17

Intraflagellar transport in *T. brucei*
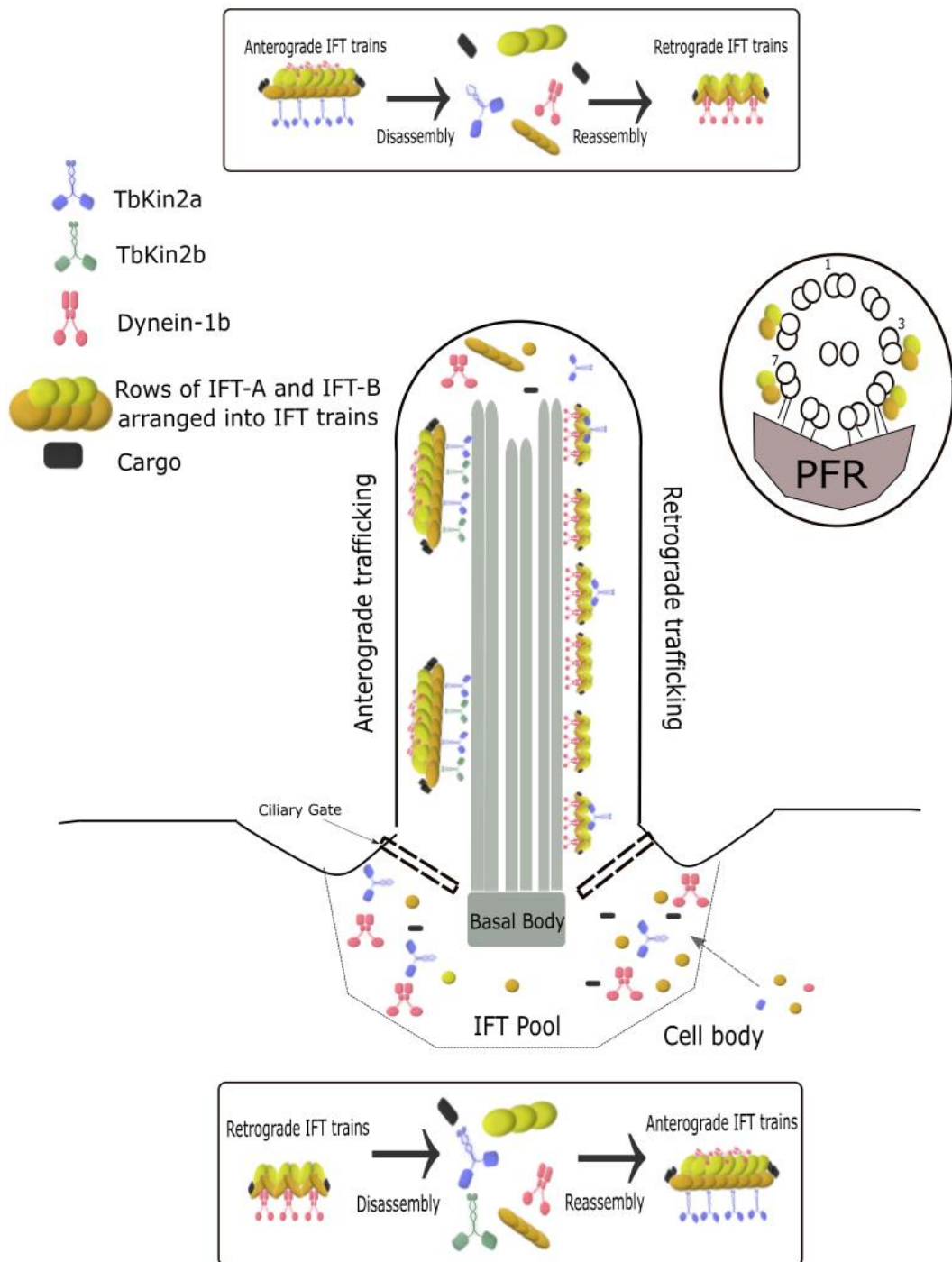
Figure 1.3. The Intraflagellar transport system in *T. brucei* flagella. The IFT pool of *T. brucei* has a closed system for the majority of its proteins, meaning that, IFT proteins and cargoes are continually recycled between retrograde and anterograde trains. Proteins dock around the ciliary gate, associate with kinesin-2 and form into IFT trains where they queue to enter the flagellum. Trains are organised in rows with IFT-B rows closer to the motor and IFT-A rows situated between the IFT-B and the flagellar membrane. Dynein is loaded in an inhibited state. There is evidence that anterograde trains may be powered by two motors, TbKin2a and TbKin2b. The action of both these kinesins have yet to be shown in vivo. If the two motors are functional it is not clear whether they share the motor role or have a spatially divided role. Both motors travel on both the A and B tubules of tubulin but all IFT trains are restricted to doublets 3-4 and 7-8. Dynein motors power the retrograde trains back to the cell body.

1.4.1 Trains travel as multi-protein complexes.

There are at least 24 proteins (this number may vary with species) in the IFT system, which organise into multi-protein complexes; IFT-A and IFT-B (Lacey et al., 2022). Rows of IFT-A/B arrange themselves into larger polymers known as IFT trains (Figure 1.4a-b). These trains are powered by the motor proteins, kinesin-2 and dynein-1b (Scholey, 2008). The IFT-A and IFT-B complexes are biochemically different and are associated with distinct roles within the IFT system.

There are at least six IFT-A proteins, species dependent, (Table 3.1) that form the structural core of the IFT-A complex (IFT140/144/122) and three that form the peripheral section, namely IFT43/121/139 where IFT139 is the most distal (Hirano et al., 2017; Piperno et al., 1998). The IFT-A proteins, apart from IFT43, are all large proteins (> 1000 amino acids) (Taschner et al., 2012). They contain many tetratricopeptide repeats (TPR) and WD-repeat domains, which are both domains associated with protein-protein interactions. In general, IFT-A mutations cause less severe defects in flagella assembly and disease. The typical IFT-A mutant can generate a short flagellum with an accumulation of IFT-B proteins at the flagellum tip, or in some cases can lead to complete flagellum loss (Fowlkes-Comninellis & Beverley, 2015; Hirano et al., 2017; Kobayashi et al., 2021). In these mutants, IFT-A recruitment and protein expression is decreased but the IFT-B expression levels remain unaffected. As IFT-A mutants can assemble a flagellum and successfully traffic IFT-B proteins to the flagellum tip, IFT-A proteins are associated with roles in retrograde transport.

There are at least 15 IFT-B proteins (species dependent) that form the core and the peripheral domains of the subcomplex. IFT-B proteins are typically smaller than IFT-A proteins (~ 800 aa), except for IFT172, which is the largest of all the IFT proteins (>1700 aa). Similar to IFT-A, IFT-B proteins are enriched with protein-protein interaction domains such as WD-repeats, TPR and coiled-coils. IFT-B proteins are associated with IFT docking, regulation and IFT-cargo interactions (Deane et al., 2001; Hazime et al., 2021; Lechtreck, 2015a). Loss of IFT-B proteins often leads to failure to assemble a flagellum however, this may be species dependent. For example, in *Chlamydomonas* IFT22 is not needed within the flagellum but is required at the basal body, but in *T. brucei* IFT22 is essential for flagellum assembly (Nakayama & Katoh, 2020; Xue et al., 2020). As IFT-B knockouts generally fail to build a flagellum, IFT-B proteins are linked to the anterograde transport.

In *Chlamydomonas,* cryo-electron microscopy has generated a detailed structure of IFT trains (Jordan et al., 2018a; Lacey et al., 2022; Van Den Hoek et al., 2021). Trains are assembled as distinct rows of IFT-A and IFT-B complexes (Figure 1.4a, b, d). The IFT-A row lies directly under the flagellum membrane and the IFT-B row is situated between the IFT-A and microtubule tracks, the cargo binding regions are located on the periphery of the IFT-B rows (Lacey et al., 2022). These repeating subunits of IFT-A and IFT-B do not perfectly overlap so there are bridging structures between the two to hold the trains together.

Anterograde and retrograde trains are distinct in structure. Anterograde trains vary in length from ~250 nm to ~700 nm (Vannuccini et al., 2016). In *Chlamydomonas* regenerating flagellum, short, rapidly growing flagellum had an equal number of short and long anterograde IFT trains but as the flagellum reached its full length the number of short trains were seven-fold higher than the number of longer trains, suggesting that larger trains can carry more material when flagella are undergoing rapid growth. In contrast, retrograde trains were always detected as shorter ~250 nm (Pigino et al., 2009). Although retrograde trains are a similar length to short anterograde trains they are typically wider and have lateral extensions, which extend around the microtubule doublet (Vannuccini et al., 2016).

Prior to entering the beginning the IFT cycle, the components of both anterograde and retrograde trains must first gather at the base of the flagellum to undergo docking and cargo loading.

1.4.2 The IFT pool is the site of IFT recruitment, docking and loading.

The cycle of IFT proteins begins at the base of the flagellum, an area known as the IFT or basal body pool. Here over 90% of IFT proteins are located and start to form complexes, commonly referred to as trains, comprised of a mix of IFT-A, IFT-B, BBSome (a complex implicated in the transport of membrane proteins), cargo and motor proteins (Lechtreck et al., 2009a; Wingfield et al., 2017).

In *Chlamydomonas* the IFT pool, is thought to be an open system whereby most of the IFT proteins are recruited from the cell body into the pool (Wingfield et al., 2017). When IFT proteins have completed the cycle, they are released back into the cell body and are not immediately recycled into new trains. Instead, the authors propose that proteins are released into a large, soluble cell body pool and are randomly recruited back into IFT trains. A small proportion of IFT-B proteins, including IFT20/46/54, have a semi-open system meaning that small amounts of these proteins are recycled between retrograde and anterograde trains, but most are newly recruited from the cell body (Wingfield et al., 2017). The exception is the anterograde motor, kinesin 2, as it is synthesised at such low levels in the cell body that it must be recycled between trains (Wingfield et al., 2017). *T. brucei* on the other hand has a closed IFT pool, meaning that there is minimal recruitment from the cell body and proteins are continually recycled between trains. Bleaching of IFT52 in the pool shows that most of the IFT material is recycled and over 80% of the fluorescent signal in anterograde trains is retained in retrograde trains (Buisson et al., 2013). Continued synthesis of IFT proteins could be energy intensive for the cell and it would therefore be interesting to see if the balance between open and closed systems remains during periods of rapid growth and disassembly.

At the junction between the basal body and flagellum lies the ciliary gate, which is composed of two sub-domains: the transition fibres and the transition zone. These work in unison to act as a barrier into the flagellum (Takao & Verhey, 2016). The transition fibres dock the mature basal body to the cell membrane and provides a physical barrier to the entrance of the flagellum. The transition zone is located distal to the fibres and is made up of Y-links, which attach the outer microtubule doublets of

the axoneme to the ciliary membrane. The gate has important roles in recruitment and docking of IFT proteins including: IFT27, 46, 52, 54, 57, 81, 122, 140 and 144 (Deane et al., 2001; Hazime et al., 2021; Sedmak & Wolfrum, 2010; Wei et al., 2013a). It is likely that other IFT proteins also dock with the ciliary gate, but their interaction has yet to be investigated.

In species such as *Chlamydomonas* and *Tetrahymena*, IFT proteins are recruited to nine distinct docking sites at the base of the flagellum (Figure 1.4c) (Hazime et al., 2021; Van Den Hoek et al., 2021). These docking sites are arranged in a ring with IFT-B proteins in the centre and IFT-A proteins localising on the outside. In *Chlamydomonas* trains form by a 'front-to-back' assembly, first with the IFT-B row forming the backbone, then IFT-A attaches, followed by the loading of inactive dynein-1b, and the trains associate with kinesin-2 at the transition fibres (Figure 1.4a) (Van Den Hoek et al., 2021). The trains then enter the flagellum at a rate of 1 per second, with the next in the queue occupying the place and new trains joining the back of the queue (Wingfield et al., 2017).

For many species, defects in the transition zone can lead to impaired cilia assembly. In vertebrates, defects in transition zone genes can lead to severe ciliopathies such as Joubert syndrome and Bardet-Biedl syndrome (Szymanska & Johnson, 2012a; Vieillard et al., 2016a). However, it has been shown that other species can facilitate IFT entry with either non-functioning or no transition zone at all. For example, in wild-type *C. elegans*, IFT entry into the sensory cilia is mediated by the transition zone. If multiple mutations are introduced in this region, the axoneme is unaffected and IFT continues; independent of a functional transition zone, suggesting possible compensatory mechanisms (Schouteden et al., 2015). Alternatively, *Giardia* completely lacks transition zone protein homologues and instead the IFT proteins gather at regions, known as flagellar pores (McInally et al., 2019). These are situated around the base of the eight flagella and can control the injection of proteins into flagella. Flagellar pores are thought to be analogous to the transition zone and, to date, have not been detected in other species. Why *Giardia* have developed this unique strategy is unclear, perhaps this may be related to *Giardia's* ability to independently control the length of its four sets of flagella.
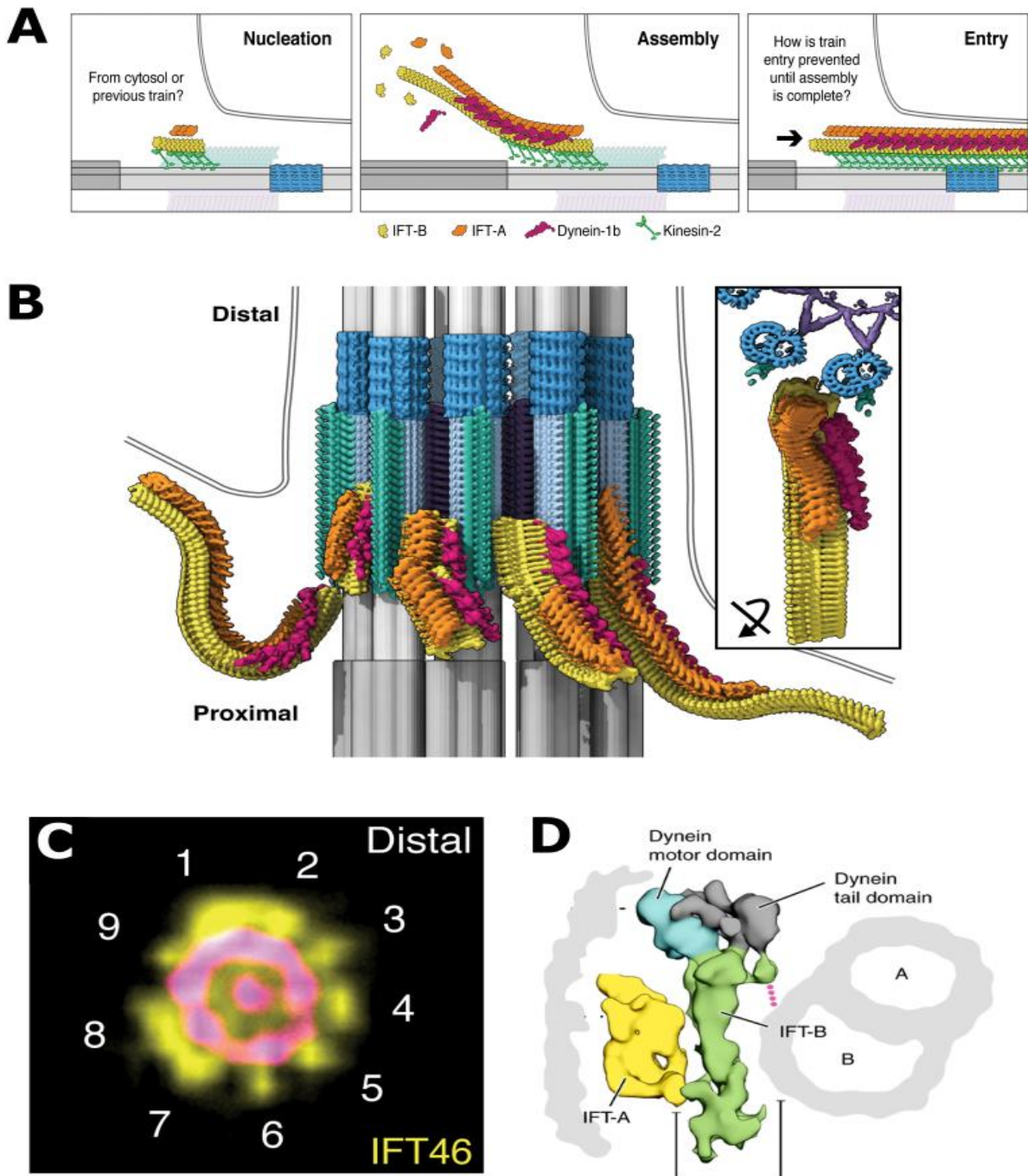
Figure 1.4 IFT train structure and assembly at the flagellum base. A. Schematic showing that IFT proteins gather at the ciliary gate. Here, IFT proteins assemble into rows of IFT-A and IFT-B, which form IFT trains. Trains elongate by the recruitment of proteins, motors, and cargoes. When fully formed, trains enter the flagellum to begin the IFT cycle. The mechanism that restricts IFT entry until the train is assembled is unknown (Van den Hoek et al., 2021). **B.** Tomograms show that *Chlamydomonas* train assembly occurs around the nine doublets of the axoneme (Van den Hoek et al., 2021).. **C.** Cross section of the ciliary base shows that IFT proteins gather at nine distinct locations around the axoneme. Tubulin shown in magenta, imaging method ultrastructure expansion microscopy (Van den Hoek et al., 2021). **D.** In anterograde trains in *Chlamydomonas* the kinesin motor (shown by the pink dotted line in the image) interacts with the B tubule of the microtubule doublets with the dynein motor is transported as cargo in an inactive position so it cannot interact with the microtubules (Imaging method cryo-electron tomography) (Jordan et al., 2018).

1.4.3 Anterograde trains travel from the IFT pool to the flagellum tip

After proteins enter the flagellum, they travel to the flagellum tip. Anterograde trains travel along the microtubule axoneme from the base to the tip, powered by kinesin motors. In *Chlamydomonas* this can occur on all nine sets of microtubule doublets, with anterograde trains traveling on the B tubule, and retrograde trains traveling along the A tubule (Stepanek & Pigino, 2016). Whereas in *T. brucei,* IFT trains are restricted to doublets 3-4 and 4-7 but transport can happen bi-directionally and on either the A or B tubule (Bertiaux et al., 2018). It is unclear why this restriction of doublets happens in *T. brucei* and how the retrograde and anterograde trains do not collide. Kinetoplast parasites have a large dense structure known as the paraflagellar rod that runs partway along the 9+2 axoneme (Deflorin et al., 1994). This may block IFT access to certain doublets and therefore restrict the potential IFT pathways however, how these trains do not collide is unclear.

Anterograde trains are powered by flagella-specific members of the kinesin-2 family. In most organisms, such as *Chlamydomonas,* kinesin-2 acts as the sole anterograde motor and carries trains along the length of the flagellum (Cole, 2003; Li et al., 2020). Some taxa have multiple kinesins thought to be involved in anterograde transport. For example, in vertebrates both the primary kinesin-2, KIF3, and an additional kinesin-2, KIF17, localise to the flagellum. However, it is unclear what role the KIF17 plays in IFT. *In vitro* purified, recombinant mouse and human KIF17 and KIF3 can co-operate to transport IFT trains along microtubules (Milic et al., 2017). The train velocity was determined by whether the significantly slower KIF3 was bound to the microtubule. In cases where KIF3 was bound, the train speed decreased because KIF3 created drag on the train and slowed it down. When KIF3 remained attached to the train but not bound to the microtubule, KIF17 was the sole motor which resulted in quicker moving IFT trains. Although these results provide valuable mechanistic insight into how these proteins could co-operate, it has been shown that KIF17 is not required for mammalian ciliogenesis and there is no evidence for co-operation *in vivo* (Engelke et al., 2019; Funabashi et al., 2017; Ishida et al., 2022). In fact, in order to enter the flagellum, KIF17 had to interact with IFT-B proteins and also possess an intact nuclear localisation signal (Funabashi et al., 2017). Inside the flagellum KIF17's motor region is not active and instead the kinesin acts only as a passenger. KIF17 has many varied roles including transport of vesicles and neurotransmitters along neuronal microtubules and potential roles in developing the outer segment of the primary cilium of photoreceptors (Wong-Riley & Besharse, 2012). However, as of yet, the evidence suggests that KIF17 does not play a significant role in powering mammalian ciliogenesis.

However, this motor co-operation is present in the sensory flagellum of *C. elegans.* There is substantial evidence that the homologues of KIF3 and KIF17 (kinesin-2 and OSM-3, respectively) have a division on labour in anterograde transport (X. Pan et al., 2006). The axoneme of the specialised sensory cilium in *C. elegans* is split into a middle segment of microtubule doublets (~ 4 μm) and a thinner distal segment with microtubule singlets (~2.5 μm) (Ward et al., 1975). After IFT

trains enter the flagellum they travel along the middle segment, powered by both the heterotrimeric kinesin, kinesin-2, and the homodimeric kinesin, OSM-3. When trains reach the thinner segment, trains release the kinesin-2 and are only powered by the OSM-3 (Snow et al., 2004). Interestingly, the trains in the distal segment, powered only by OSM-3, have a higher velocity than those powered by both kinesins in the middle segment. Motors were purified and found that the uninhibited velocity was 0.5 μm/s and 1.3 μm/s for kinesin-2 and OSM-3, respectively, yet the average velocity of IFT movement in the middle segment is roughly 0.7 μm/s (Snow et al., 2004). The mechanical competition model proposes that the two motors work together to move along the microtubules, but the slower kinesin-2 creates drag and slows trains down (X. Pan et al., 2006). When the train reaches the distal section of the axoneme, kinesin-2 dissociates from the train, where it is thought to diffuse back to the IFT pool, and the train, solely powered by OSM-3, increases in velocity.

T. brucei have two divergent kinesins, TbKin2a and TbKin2b (Douglas et al., 2020). In bloodstream forms, TbKin2a localises along the length of the flagellum with a stronger signal at the IFT pool, a typical distribution for IFT proteins. TbKin2a only colocalised with IFT144 and IFT172 when close to the IFT pool but once inside the flagellum TbKin2a and the IFT proteins no longer showed colocalisation. The study did not determine the localisation of TbKin2b nor its colocalisation with other IFT proteins. Knockdown of these kinesins resulted in a flagellum length decrease of 16% and 21% for TbKin2a and TbKin2b, respectively and double knockdown showed a 42% decrease in length. Single knockdown of either kinesin also resulted a reduction of total IFT144 in the flagellum and reduced localisation to the basal body, yet IFT172 remained unaffected. The authors propose that the divergent kinesin-2s co-operate in a similar manner to *C. elegans* kinesins. Data from TrypTag shows that TbKin2b does have a typical IFT localisation, so it would be beneficial to determine whether these kinesins colocalise inside the flagellum (Dean et al., 2017). Further work to show how these motors are interacting with IFT trains would be useful, similar to the dissection of the role of KIF17 that was carried out in mammals. It should also be noted that there is emerging evidence of members of kinesin-2 families having alternative functions outside the flagellum such as in mitosis and roles in Golgi and endoplasmic reticulum transport (Marszalek & Goldstein, 2000; Vashishtha et al., 1996).

The velocities of different kinesin motors are highly variable depending on the species and cell type, examples of the different IFT velocities are shown in Table 1.1. These differences are likely due to differences in the structure and function of the flagellum and adaptations to their environment. It is important to take these differences into consideration when trying to apply IFT findings across species.

Table 1.1 IFT Velocity across species

Organism	Anterograde (Reported as average or range)	Retrograde (Reported as average or range)
C. reinhardtii (Kozminski et al., 1993)	1.9-2.1 μm/s	2.7-3.1 μm/s
C. elegans (Snow et al., 2004) (Yi et al., 2017)	0.7 μm/s (middle segment of sensory cilium) 1.3 μm/s (distal segment of sensory cilium)	1.2 μm/s (distal segment) 1.5 μm/s (middle segment) 1 μm/s (proximal segment)
Mouse OSN (Williams et al., 2014)	0.22-0.24 μm/s	0.14 μm/s
Tetrahymena (Jiang et al., 2015)	0.98 μm/s	1.43 μm/s
Trypanosoma brucei, Procyclics (27°C) (Buisson et al., 2013)	2.4 μm/s Slow particles 1.5 μm/s	5.6 μm/s
Trypanosoma brucei, Procyclics (37°C) (Buisson et al., 2013)	3.2 μm/s Slow particles 2.2 μm/s	7.4 μm/s
Leishmania mexicana (Wheeler et al., 2015)	1.6 μm/s	1.5 μm/s
Leishmania mexicana, Promastigotes Present study	2.8 μm/s	3.3 μm/s
Leishmania mexicana, Early amastigotes (8 hours post differentiation) Present study	2.2 μm/s	2.5 μm/s

1.4.4 Proteins are transported as cargo by the IFT trains.

For IFT-mediated transport, roughly 24 proteins (including motors) must co-ordinate the movement of the flagellar proteome into the flagellum. Both IFT-A and B proteins are involved with import in and out of the flagellum, but IFT-B proteins are mainly responsible for cargo entry and key cargo carrying sites have been identified along the IFT-B rows of the trains (Lechtreck, 2015a). The binding properties between IFT trains and their cargoes are thought to be weak and transient to allow easy dissociation of proteins and imaging has showed that random dissociation of cargo from IFT trains can occur along the flagellum (Wren et al., 2013).

Tubulin as a cargo, has been well studied. It is a highly abundant flagella protein, which forms the structural backbone of the axoneme. Tubulin forms dimers of α and β subunits of roughly ~110 kDa and can be transported via IFT or diffusion (Van De Weghe et al., 2021). In *Chlamydomonas* when tubulin is transported by IFT, it has a dedicated binding site on the IFT-B sub complex of IFT74/81 (Bhogaraju et al., 2013). The IFT74 binds to the tubulin globular region to provide binding specificity and IFT81 binds the tubulin tail to increase binding affinity. When double mutants of IFT74 and 81 were generated, the algae had very short flagella (<1 μm) that retained a normal axoneme ultrastructure (Kubo et al., 2016). The flagellum was too short to track IFT, so it was unclear if the flagellum defect was due to inhibition of tubulin transport or a non-functional IFT system.

IFT cargo needs to be loaded onto trains, but does this happen haphazardly or is there another layer of organisation here? Dynein, the retrograde motor, is transported to the flagellum tip by anterograde trains. In *C. elegans* mechanical competition occurs between two kinesin motors that travel in the same direction, resulting in variable motor velocities (X. Pan et al., 2006). In order for dynein to be transported to the flagellar tip dynein would need to be inactivated to avoid a 'tug-of-war' between the dynein and the kinesin. In *Chlamydomonas,* this tug-of-war is mitigated as dynein-1b molecules are loaded onto anterograde trains in an auto-inhibited form and orientated so that the motor domain is situated away from the microtubules (Jordan et al., 2018a). Dynein molecules are tessellated so that the tail region of one dynein interacts with the motor domain of another and will block the motor domain. This suggests some level of loading organisation for at least some cargoes.

Additional organisation for loading is provided via cargo adaptor proteins. These are not essential for IFT function but can assist in the loading and transport of certain cargo proteins. Adaptor proteins such as ODA16, TULP3, MRJ, Cluap1, TTC26, ARMC2 may have various roles in trafficking, localisation, increasing IFT efficiency and regulating cargo transport (Ahmed et al., 2008; Bhowmick et al., 2009; Katoh et al., 2016; Lechtreck et al., 2022; Mukhopadhyay et al., 2010). For example, ODA16 is a specific adaptor for the transport of the outer dynein arm complex. Outer dynein arms (ODA) enter the flagellum as complexes that are bound by an IFT46/ODA16 module (Ahmed et al., 2008; Taschner et al., 2017). Knockdown analyses have shown that ODA16 is not essential for ODA transport, but instead it is thought to enhance the ability of IFT46 to transport ODA (Ahmed et al.,

2008). ODA16 is found at significantly lower levels in the flagellum than in the cell body that may suggest ODA16 needed for the initial entry of ODA into the flagellum but is then immediately released.

Co-migration of cargo and IFT protein in transit provides strong evidence of true IFT cargo. Studies have successfully imaged the trafficking of proteins including members of the nexin-dynein regulatory complex DRC4 and DRC2, the central pair protein, PF16, outer dynein arms (ODA), tubulin, members of the BBSome BBS4 and radial spoke proteins such as RSP3/4 (Craft et al., 2015; Dai et al., 2018; Hao et al., 2011; Lechtreck, 2013; Lechtreck et al., 2009b; Wren et al., 2013). It was previously thought that cargo had to travel to the flagellum tip for release. However, this idea appears too rigid and in organisms, a combination of IFT and diffusion facilitates cargo transport. DRC4 is an axonemal protein that co-localises with IFT20 during transport. In *Chlamydomonas*, IFT is required for cargo entry into the flagellum but is not needed for transport to the tip (Wren et al., 2013). In fact, only 53% of trains successfully transported DRC4 to the flagellum tip, many of the cargoes dissociated at various points along the flagellum and diffused along to the tip. In the case of retrograde transport, the majority of DRC4 left the tip via diffusion and rarely left transported by trains. In the IFT mediated exports, the cargo randomly dissociated at various points along the flagellum.

The traditional model of IFT trains carrying cargo to the flagellum tip for release may be over simplistic. In this section and section 1.4.5 it is clear that both IFT and diffusion play key roles in transport.

1.4.5 Diffusion may be important in the transport of some proteins.

IFT is the primary mechanism for the transport of particles along the flagellum. However, emerging research is showing that a combination of both IFT and diffusion is important for flagellum assembly and maintenance.

The ciliary gate is a physical barrier at the base of the flagellum, which can exclude proteins by size or permeability (Garcia-Gonzalo & Reiter, 2017). The gate usually restricts proteins larger than 40-70 kDa from diffusing into the flagellum (Breslow et al., 2013; Kee et al., 2012). For example, in human primary cilia, dextrans smaller than 10 kDa could diffuse into the cilia but dextrans larger than 40 kDa were restricted from entering (Kee et al., 2012). However, this size restriction may vary between proteins and species. In *Chlamydomonas* both tubulin and the microtubule tracking protein EB1 (both predicated to traffic as dimers) can diffuse into the flagellum and they are ~110 kDa and ~120 kDa, respectively (Harris et al., 2016; Van De Weghe et al., 2021). This may suggest additional factors such as protein shape and surface charge distribution also may influence diffusional entry (Takao & Verhey, 2016).

Tubulin is a highly abundant flagellum protein and appears to be transported by both IFT and diffusion. In *Chlamydomonas,* tubulin is a dedicated cargo of an IFT-B sub-complex of IFT74/81 (Bhogaraju et al., 2013). However, calculations predict that IFT can only provide roughly 60% of the tubulin that a rapidly assembling flagellum needs, suggesting the other 40% is transported via diffusion (Van De Weghe et al., 2021). When the IFT74/81 binding module was mutated it could no longer bind to tubulin, however overall IFT functionality remained. When tubulin transport via IFT was blocked this successfully induced a 90% reduction of IFT of tubulin. However, the amount of tubulin incorporated into the axoneme was only moderately reduced and imaging showed tubulin still entering the flagellum. This suggests that diffusion plays a key role in tubulin transport.

In the primary cilium of mammals, diffusion of some proteins may be important. The axonemal lumen is located inside the axoneme. It was first detected as a site for diffusion in primary cilium of mice, which lack a central pair (Luo et al., 2017). Unbound GFP, a protein with no role in the flagellum, was transported exclusively by diffusion inside the axoneme lumen. In contrast, IFT20 was only detected co-migrating with IFT trains, and not via diffusion. Moreover, the motor KIF17 was transported both by IFT and diffusion. IFT was found to carry KIF17 to the tip 93% of the time, but to return the flagellum base it travelled predominately (55%) via diffusion within the axonemal lumen (Luo et al., 2017). Suggesting that anterograde and retrograde transport may also show differences in how they transport the cargo i.e., either IFT or diffusion mediated.

This division between anterograde and retrograde transport can be seen in *Chlamydomonas.* The kinesin-2 is transported in the anterograde direction but once it reaches the flagellum tip and IFT trains disassemble the kinesin-2 returns to the IFT pool via diffusion (Engel et al., 2009). The retrograde direction seems to utilise diffusion more commonly. In *Chlamydomonas,* other cargoes have also been shown to dissociate from retrograde IFT at random locations along the flagellum and then return to the IFT pool via diffusion (Wren et al., 2013).

IFT and diffusion seem to play a role in both anterograde and retrograde transport of some proteins. Diffusion seems to be more common in retrograde transport than in anterograde, but most findings show that IFT is the primary mechanism of flagellum assembly.

1.4.6 The flagellum tip is a site of protein turnover.

At the end of the microtubule tracks lies the flagellum tip. This is the site of flagellum turnover, maintenance and plays a key role is signalling (Croft et al., 2018). Although the tip is important across organisms as the site of elongation the underlying structure of this tip varies between organisms. For example, *Chlamydomonas* have a tapered flagellum tip with a large microtubule cap structure present in some cells and not others (Dentler & Rosenbaum, 1977; Ringo, 1967). Whilst in *T. brucei* there are no microtubule singlets, which gives the flagellum a blunt tip with the addition of an electron-dense cap (Croft et al., 2018; Woolley et al., 2006). There are few studies that focus on the regulation and

dynamics of the flagellum tip, but these structural differences should be taken into consideration when trying to compare findings across species.

Once the trains have travelled to the flagellum tip, here they must unload their cargo and undergo remodelling to become structurally distinct retrograde trains (Chien et al., 2017; Jordan et al., 2018a; Porter et al., 1999). The remodelling itself, can trigger cargo unloading and in some cargo, such members of the dynein regulatory complex, the cargo is unloaded towards the end of the IFT remodelling (Wren et al., 2013). The turnaround from anterograde to retrograde trains happens remarkably quickly; less than four seconds in *T. brucei* (Buisson et al., 2013) and in under one second in *Chlamydomonas* (Nievergelt et al., 2022). The current model suggests that the kinesin motors of anterograde trains either stops or 'walk off' the microtubule tracks. Once unattached from the microtubules the trains are more flexible, and the previously structurally confined dynein can be freed and activated. Anterograde trains are broken down into large sub-complexes and then these larger sections are restructured into retrograde trains (Wingfield et al., 2021).

Older electron microscopy data suggested that anterograde trains were three times as long as their retrograde counterparts, which disputed the idea that anterograde trains could simply convert to retrograde (Cole et al., 1993). However, new data suggests that, in *Chlamydomonas* at least, the retrograde and anterograde trains are a similar size ~200-250 nm, so a straight conversion could be plausible (Stepanek & Pigino, 2016). In *T. brucei* there is a 3:1 ratio of anterograde to retrograde trains suggesting that they break up into three smaller trains to traffic back (Buisson et al., 2013). So simple conversion of anterograde to retrograde train may not be possible here and different species may have different train sizes and methods of converting anterograde to retrograde trains.

Although the final destination for anterograde trains is the flagellum tip, the ability to remodel anterograde trains into retrograde trains is an intrinsic property of the trains (Nievergelt et al., 2022). In *Chlamydomonas,* anterograde IFT trains can be 'forced off' the microtubules by applying mechanical pressure to the flagellum. Anterograde trains then convert to retrograde ones and traffic back to the flagellum base. This surprising finding shows that despite the presence of various kinases and flagellum tip complexes trains do not need to reach the tip to be remodelled. However, the conversion time at the flagellum tip (~0.74 seconds) compared to an artificial block of IFT movement (~2.6 seconds) was over three times quicker, suggesting the extra tip structures make the process more efficient. There is also no evidence that these newly formed retrograde trains are effectively transporting cargo.

1.4.7 Retrograde transport travels from the flagellum tip to the base

Once trains have entered the flagellum, travel along the axoneme and deliver their cargo they finally convert to retrograde trains. Retrograde transport is responsible for trafficking material the flagellum tip to the cell body. There are two main functions of retrograde transport, the first being its

responsibility for returning IFT machinery back to the cell body. In *Chlamydomonas* mutants that lack retrograde transport ability, anterograde IFT components accumulate at the flagellum tip and do not complete the IFT cycle (Pazour et al., 1998). However, as discussed components such as kinesin motors may return to the cell body via diffusion (Engelke et al., 2019).

The second role of retrograde transport is to return proteins from the flagellum tip back to the base of the flagellum. Experiments in different *Chlamydomonas* mutants lacking various IFT components demonstrate this (Qin et al., 2004). When flagellum resorption was induced in mutants that did not have a functional IFT system, they found an accumulation of flagellar structural proteins such as radial spoke proteins and tubulin at the flagellum tip; caused by the lack of retrograde IFT to remove them. Retrograde transport was also shown to be important for the physical transport of the components back to the cell body. Algae with normal anterograde transport but lacking retrograde IFT failed to transport these components back to the cell body. Although retrograde IFT clearly has important roles in the transport of flagellum components, other factors such as diffusion are also involved with retrograde transport (Van De Weghe et al., 2021).

Cytoplasmic dynein-1b in non-vertebrates and dynein-2 in vertebrates, powers retrograde transport (Pazour et al., 1998). The dynein motor is made up of several components including a core homodimer plus the intermediate, light intermediate and light chain subunits (Toropova et al., 2019). *T. brucei* and *Leishmania* are slightly unusual as they have two additional heavy chain isoforms where one is required for flagellum assembly and has roles in maintaining the cell body shape and the other copy may be essential as knockout parasites are not viable (Adhiambo et al., 2005).

Once the retrograde trains have returned to the IFT pool and released their cargo and/or IFT material the IFT cycle continues as anterograde trains enter the flagellum. The IFT cycle is continually delivering and removing material in order to assemble, maintain or disassemble a flagellum.

1.5 Is the balance point model a universal explanation of flagellum length control?

Detailed research regarding the structures and functions of IFT and its components have been generated. However, there are still key questions to be resolved about how flagella grow, are maintained, and disassemble. Trying to apply a one-fits-all model of flagellum length control, is challenging both due to the variety of flagellum morphologies (section 1.1) and differences in how IFT functions across different species. However, there are several proposed models to explain flagellum assembly including: diffusion, grow and lock, time-of-flight and limiting pool (Bertiaux et al., 2018; Bertiaux & Bastin, 2020; Moran et al., 2014; Patra et al., 2020). One of the most accepted models, the balance point model, suggests that flagellum length is maintained via the balance between flagellum assembly and disassembly (Marshall & Rosenbaum, 2001). If there is a higher rate of assembly then the flagellum will grow, a higher rate of disassembly the flagellum shrinks and a balance between the two results in the length being maintained. One of the models' key predictions is

that all flagella contain the same amount of IFT material. The revised version of the model states that there is the same amount of IFT material in all flagella, but shorter flagella have longer IFT trains and longer flagella have shorter IFT trains (Engel et al., 2009). This may be applicable in *Chlamydomonas* as different lengths of IFT trains have been observed and vastly more shorter trains are seen in long flagella than short ones (Vannuccini et al., 2016).

However, in species such as *Leishmania* the amount of IFT material in the flagellum drastically decreases in smaller flagella compared to longer ones (Wheeler et al., 2015). The revised balance point model also ignores the role of diffusion in flagellum assembly and disassembly. As previously discussed, diffusion plays a key role in the transport of major flagellum components, such as tubulin (Van De Weghe et al., 2021). The balance-point-model uses IFT retrograde transport as the sole proxy for disassembly and ignoring the role of diffusion. Thereby incorrectly predicting the balance between anterograde and retrograde transport.

At the core of this model is the idea that more material entering the flagellum than leaving results in elongation and less material means disassembly. This principle may be relevant for many species but currently the details of the balance point model cannot explain flagellum length control in species outside of *Chlamydomonas* and in fact a mixture of the models, along with tailoring to individual species, may provide a better explanation.

1.6 Factors driving flagellum disassembly.

The flagellum tip is a site of continued flagellum assembly and disassembly if the rate of one is faster than the other, then the flagellum will either elongate or shorten. Flagella disassembly is a key step to many life and cell cycle stages. For example, in primary cilia prior to mitosis the cilia must disassemble and in parasites such as *Leishmania* disassembling of the flagellum is a mechanism to evade host immunity (Liang et al., 2016; Wheeler et al., 2011). Although not well understood, triggers such as post-translational modifications, modulation of protein kinases, changes in IFT trafficking, and cargo loading have all been linked to driving disassembly (Chien et al., 2017; Sloboda, 2009).

Flagella can be lost in two ways deflagellation (also known as autonomy) or resorption. Deflagellation is the complete severing of the axoneme and loss of the flagellum. This occurs in response to external stressors such as pH, heat, and some drugs. In *Chlamydomonas,* complete deflagellation is mediated by calcium influx and occurs in the presence of certain drugs (W. Dentler, 2005). There is also evidence to suggest *T. cruzi* completely severe the flagellum before differentiation to amastigotes (Kurup & Tarleton, 2014). Resorption is the controlled disassembly of the flagellum. This occurs in well-regulated steps in the cell cycle or in cell differentiation. Examples of this are seen in mammals as primary cilia are resorbed before early mitosis and in *Chlamydomonas* cell resorption occurs prior to mating (W. Dentler, 2005; Plotnikova et al., 2009).

During the life cycle of *Leishmania*, the parasite disassembles its long promastigote flagellum into the short one found in the amastigote form (discussed in section 1.8.1). In comparison to the well-studied flagellum model *Chlamydomonas*, this flagellum disassembly occurs much more slowly. It takes roughly 8-10 hours for *Leishmania* to disassemble the flagellum (up to 72 hours to fully remodel to amastigotes) whilst *Chlamydomonas* flagella are rapidly shortened before mating within 2 hours (Fiebig et al., 2015; Morga & Cilia, 2013; Wheeler et al., 2015).

The role of IFT in the disassembling flagellum of the two species may also vary. In *Chlamydomonas* the amount of IFT in disassembling flagella remains the same regardless of the flagella length (Engel et al., 2009). The flagella of *Chlamydomonas* can disassemble without IFT but shortening occurs significantly quicker when IFT is present (Marshall et al., 2019; Marshall & Rosenbaum, 2001; Qin et al., 2004). However, in *Leishmania* during flagellum shortening the amount of IFT in the flagellum is drastically reduced in comparison to the full-length flagellum (Wheeler et al., 2015).

Both species have different environmental pressures driving flagellum disassembly. *Chlamydomonas* must rapidly loose its flagellum in order to mate whilst *Leishmania spp* slowly disassemble their flagellum whilst encased inside the parasitophorous vacuole of macrophages (Gluenz et al., 2010). These key differences in biology could contribute to the different roles of IFT in disassembly. The stark difference of the potential roles between the two makes *Leishmania* an interesting system to study IFT during this slower, controlled disassembly step.

1.7 Do post-translational modifications play a role in regulating flagellum length?

Flagellar axonemes have a 9+2 microtubule structure with nine sets of outer microtubules comprised of an A and B tubule and a central pair with the C1 and C2 tubule (Figure 1.1) (Ma et al., 2019). The microtubules themselves are comprised of repeating subunits of tubulin heterodimers, which are formed of α and β tubulins. Despite high structural conservation of the axoneme structure, motile flagella can perform a wide variety of biological functions, suggesting there could be additional levels of specialisation. One way to generate this diversity is by the 'tubulin code' which is encoded by both 1) different αβ tubulin isotypes and 2) the decoration of tubulin subunits with various post-translational modifications (PTMs) (Gadadhar *et al.*, 2017). This code is interpreted by various microtubule associated proteins and is thought to have functions in microtubule organisation, regulation, and dynamics.

Homologues of enzymes involved in glutamylation and glycylation (common flagellar PTMs) are not present in non-ciliated yeasts and plants yet are always present in flagellated organisms (Janke & Magiera, 2020). Recent evidence is beginning to show that the dysregulation of tubulin PTMs in flagella may be linked to severe human disease including Joubert disease, infertility, and potential roles in the development of some cancers (He et al., 2020; Kato et al., 2004; Latour et al., 2020). These factors demonstrate the importance of PTMs in the flagellum.
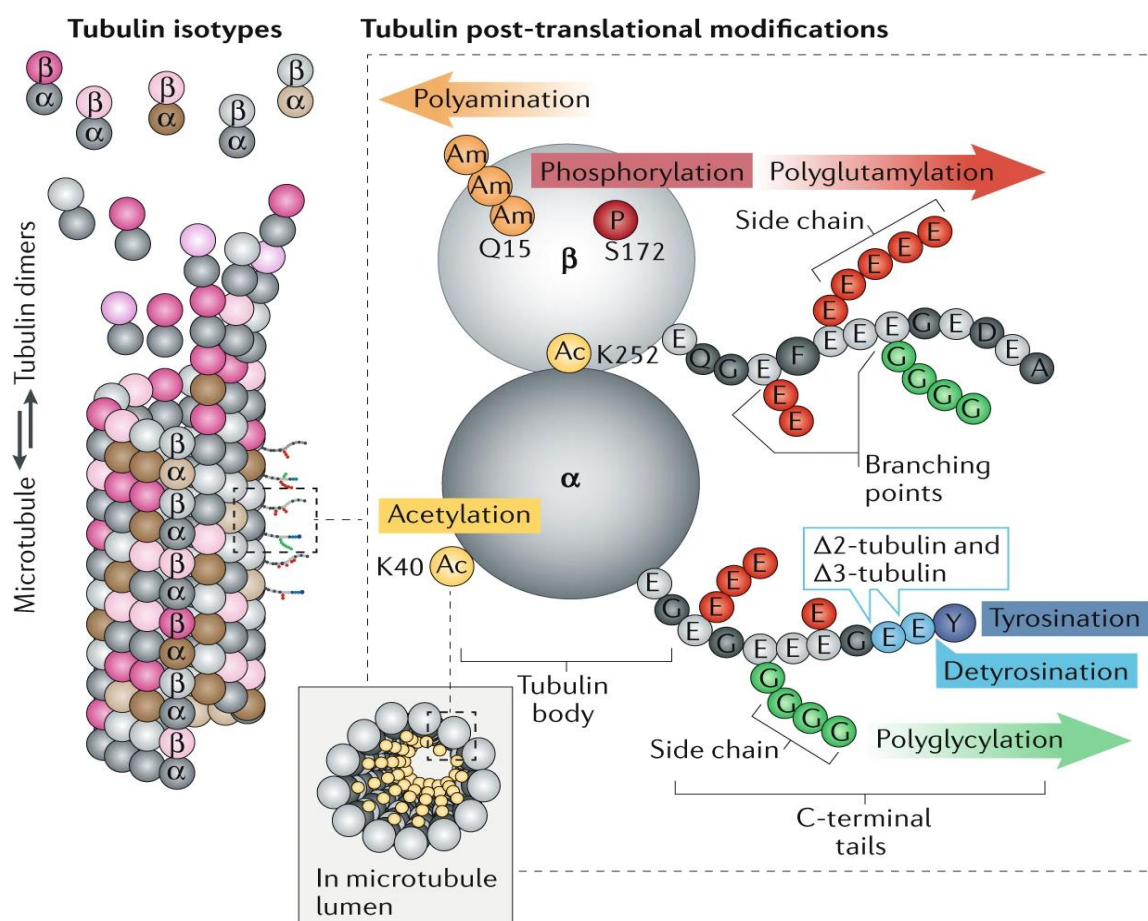
Figure 1.5. A variety of post-translational modifications decorate the tubulin lattice. Most PTMs occur on the outside of microtubules with the notable exception of acetylation that occurs in the microtubule lumen. Schematic highlights the position of various PTMs of tubulin (Janke & Magiera, 2020)

The first element of the tubulin code are tubulin isotypes, these are important drivers of diversity, particularly in higher eukaryotes. On average, higher eukaryotes encode many more tubulin isotypes genes. For example, humans encode over nine α and ten β tubulin isotypes, whilst unicellular *Chlamydomonas* only has two α tubulin and two β tubulin isotypes, with the two α genes encoding identical proteins that have the same expression levels (Brunke et al., 1982; McKeithan et al., 1983; Silflow & Rosenbaum, 1981; Ti, 2022). Although the exact mechanism of how isotypes create diversity is unclear, loss of individual isotypes can lead to defects in microtubule assembly, stability and protofilament numbers (Ti et al., 2018).

The second element of the tubulin code are PTMs (Figure 1.5). Axonemal tubulins are the substrates of many PTMs including acetylation, (poly)glycylation, (de)tyrosination and (poly)glutamylation (Janke & Magiera, 2020). Most PTMs occur on the C-terminal tail of tubulin that is located on the external surface of the microtubule doublets, with the exception of acetylation which occurs inside the microtubule lumen (Figure 1.5). Higher levels of PTMs are found on stable microtubules, previously it was unclear whether this is due to stable microtubules having more time to accumulate PTMs or

whether PTMs have stabilising effects (Piperno et al., 1987). It is now thought that PTMs play a role in actively stabilising microtubules (Janke & Magiera, 2020). Tubulin PTMs are also involved in regulating microtubule dynamics, organisation and interacting with associated motors (Wloga et al., 2017).

Acetylation was one of the first PTMs to be described and is strongly associated with microtubule stability. In *Chlamydomonas,* α 1-tubulin is found in the cell body, before its integration into the flagellar axoneme it undergoes acetylation to become α 3-tubulin (L'Hernault & Rosenbaum, 1983). During induced flagellar resorption, α 3-tubulin is de-acetylated beginning from the distal tip (L'Hernault & Rosenbaum, 1985). This de-acetylation permits disassembly, suggesting acetylation has stabilising effects on microtubules. Unlike *Chlamydomonas,* in *T. brucei* acetylated tubulin is not organelle specific and is instead found on microtubules throughout the parasite including in the subpellicular microtubules and mitotic spindles (Sasse & Gull, 1988; A. Schneider et al., 1987). The microtubule spindles are a highly dynamic structure, suggesting that in this case acetylation may not only be associated with stable microtubules.

A detyrosination/re-tyrosination cycle occurs on tubulin (Figure 1.5). Most α tubulin genes encode a C-terminal tyrosine residue making the natural state of tubulin tyrosinated (Sanyal et al., 2021). This tyrosine can be cleaved to leave a detyrosinated state and then may be re-tyrosinated by ligases. Detyrosination is sometimes used as a marker for stable microtubules as detyrosinated tubulin is only found on long-lived microtubules, such as those in the flagellum. In *T. brucei,* antibodies against tyrosinated α tubulin (YL 1/2) can differentiate the new and the old flagellum in diving cells (Sasse & Gull, 1988a). During assembly, the flagellum is enriched with tyrosinated tubulin and when the flagellum reaches its full length the tubulin becomes de-tyrosinated and the antibody signal is lost. The new flagellum had a bright signal due to the presence of tyrosinated tubulin whilst the old flagellum remains detyrosinated. This differential staining has led to the YL1/2 antibody being considered a marker of tubulin array growth during the cell cycle (Sinclair et al., 2021). In *Chlamydomonas,* both detyrosinated and tyrosinated tubulin is found along the length of the flagellum but tyrosinated tubulin is concentrated at the tip (Johnson, 1998). Immuno-electron microscopy showed that the central pair and the A tubule of the outer doublets are tyrosinated. During assembly the B tubules of the outer doublets start as tyrosinated tubulin, then about midway through the assembly point they start to become de-tyrosinated.

Previous research suggests that the differential modifications to the A and B tubules could be involved in regulating dynein activity to impact flagellum beating(Chaya & Furukawa, 2021; Wloga, 2017). Notably the A and B tubules of the doublets also play different roles in IFT. In *Chlamydomonas* dynein-1b, the retrograde motor, travels exclusively along the A tubule, whilst the anterograde motor, kinesin-2, is restricted to the B tubules (Stepanek & Pigino, 2016). Yet in *T. brucei,* which to date has shown no difference in de/tyrosination patterns between the A and B tubules, both IFT motors travel

on both A/B tubules of a restricted set of doublets (Bertiaux et al., 2018) (see section 1.4.3). This suggests that PTMs could be important in localising IFT trains to specific microtubules tracks.

Polyglutamylation and polyglycylation are common PTMs found on axonemal tubulins (Figure 1.5). These PTMs are concentrated at the proximal end of the axoneme and gradually reduce in density towards to distal tip, and again show an association with stable microtubules (Prigent et al., 1996). Both these PTMs are suggested to have similar roles potentially in flagellum beating, axoneme stability and cross-regulating each other (Rogowski et al., 2009; Wloga et al., 2009; Xia et al., 2000). Glycylation is essential in many eukaryotes, including in early branching species such as *Giardia* but surprisingly is absent in *T. brucei* (Schneider et al., 1997). As the *T. brucei* axoneme is unusually heavily polyglutamylated and glutamylation and glycylation perform similar roles, it may mean that glycylation is redundant in *T. brucei*. As *Leishmania* are close relatives of *T. brucei,* it is reasonable to assume glycylation is also not a major PTM in the *Leishmania* flagellum. Therefore, in the present study, polyglycylation was not analysed (see section 2.2)

1.7.1 Do PTMs play a role in regulating IFT?

Based on the abundance of PTMs in the flagellum and their influence over both microtubule-based motors and microtubule stability, it may be reasonable to assume PTMs could play a role in regulating IFT.

PTMs such as acetylation are strongly associated with stability. When deacetylases (enzymes that remove acetyl group) are knocked down, this can have effects on flagellum length (Sasse & Gull, 1988b; Wloga, 2017). In mammals, knockdown of deacetylases results in longer flagella and overexpression of the deacetylases can lead to significantly shorter flagella (Wloga, 2017). This change of length could be due to the loss of acetylation and therefore the loss of the microtubule's stability. Alternatively, by removing the acetyl group it allows other PTMs such as polyubiquitination, a PTM associated with degradation, to bind to the tubulin and facilitate disassembly (Huang et al., 2009).

PTMs have also been associated with microtubule motor regulation. For, example in mammalian neuronal microtubules both kinesin-1 and 2, have increased velocity when microtubules are polyglutamylated compared to an unmodified axoneme (Regnard et al., 1999). The levels of polyglutamylation can also act as a 'molecular traffic sign', ensuring correct localisation of neuronal axoneme proteins, such as kinesin-3 and synaptic cargo (Ikegami et al., 2007). In *C. elegans,* the protein CCPP-1 acts as a regulator of polyglutamylation on male specific cilia (O'Hagan et al., 2011a). CCPP-1 is thought to regulate OSM-3, the anterograde transport motor for *C. elegans,* velocity and localisation(O'Hagan et al., 2011). Loss of CCPP-1 results in defects in the localisation and abundance of IFT motors and their cargo in cilia. However, these mutants have different phenotype than IFT mutants in *C. elegans* and unlike IFT mutants that have defects in assembling a

flagellum, CCPP-1 mutants have defects in ciliary maintenance due to the mis-regulation of polyglutamylation (O'Hagan et al., 2011). These findings, suggest that PTMs may play a role in the regulation in IFT or in flagellum length.

1.8 An introduction to the *Leishmania* parasite

Leishmania are flagellated, unicellular parasites and the causative agent of leishmaniasis (CDC, 2020a). Leishmaniasis is present in over 100 countries worldwide and major risk factors include poverty, malnutrition, climate change and population mobility (Burza et al., 2018). The disease presents itself in three clinical forms: visceral leishmaniasis where the parasite affects the visceral organs and if left untreated 95% of cases result in death; mucocutaneous leishmaniasis which can lead to complete destruction of the mucosal tissue around the nose and throat and cutaneous leishmaniasis which is the most common type and can lead to permanent scaring and disability (WHO, 2022). There are over 53 recorded *Leishmania* species, 20 of which are known to infect humans (Bates, 2008). The parasites are transmitted to mammals via the bite of an infected *Phlebotomus* or *Lutzomyia* female sand fly.

1.8.1 The *Leishmania* life cycle

Leishmania is a vector borne disease that infects both the sand fly vector and is an intracellular parasite of mammals (CDC, 2020b). Throughout the two hosts the parasites are exposed to drastically different environments, so the parasites have evolved to differentiate into different life cycle stages, each with distinct morphologies in order to survive (CDC, 2020a). One of the most striking changes is the structural changes to the flagellum during the life cycle. The two main forms of the parasites are the highly motile promastigotes present in the sand fly and the sensory amastigotes present in the macrophages of the mammalian hosts (Figure 1.6a).

When a female sand fly takes a blood meal from an infected mammal they ingest amastigotes into the midgut. Amastigotes are defined by a spherical cell body and a flagellum that barely extends out of the flagellar pocket (Figure 1.6a). Within 24-48 hours, amastigote parasites undergo differentiation to procyclic promastigotes (Figure 1.6a-b) (Kamhawi, 2006). The cell body of procyclic promastigotes is between 6-11 μm long and their flagellum is shorter than their body (Figure 1.6a) (Sunter & Gull, 2017). Procyclics parasites divide more rapidly than amastigotes and are more resistant to digestive enzymes so build up large numbers inside the insect midgut (da Silva et al., 2013; Kamhawi, 2006). Then, within 72 hours post feeding, parasites further differentiate into long slender nectomonads, which have an elongated cell body (>12 μm) and flagellum of variable length (Sunter & Gull, 2017). The role of the nectomonads is to escape the peritrophic matrix and insert the flagellum tip between the flies epithelial to anchor the parasite to avoid excretion (Figure 1.6b) (Bates, 2008; Kamhawi, 2006). After four to seven days, nectomonads start to differentiate into leptomonads, which are characterised by a cell body which is 6-11 μm long, with a flagellum longer than the cell body (Sunter

& Gull, 2017). These forms are thought to be responsible for increasing parasites numbers prior to infection due to increased capability to divide (Gossage et al., 2003). Leptomonads can differentiate to haptomonads or metacyclic forms after 5-7 days (Figure 1.6a-b) (Kamhawi, 2006). Haptomonads have an expanded flagellum base and adhere to the stomodeal valve via hemidesmosomes like structures to form a plug. The haptomonads cause damage to the stomodeal valve, interfere with feeding and may facilitate reflux of parasites into the host when the fly is feeding (Dostálová & Volf, 2012). The metacyclic form is the infective form and has a cell body of ~8 μm long and ~ 1 μm wide with a flagellum longer than the body (Sunter & Gull, 2017). The small cell body with elongate flagellum allows rapid movement in the mammalian host and these parasites are known to be resistant to lysis by complement (Kamhawi, 2006). Once inside the mammalian host cell, parasites are engulfed by immune cells and encapsulates in parasitophorous vacuole (PV) where they differentiate to amastigotes and the cycle repeats.

The many different lifecycle stages of these parasites allow it to become highly adapted to its changing environment. These striking changes to the flagellum require extensive remodelling, yet the processes behind the remodelling required to generate these specialised flagella remains unclear.
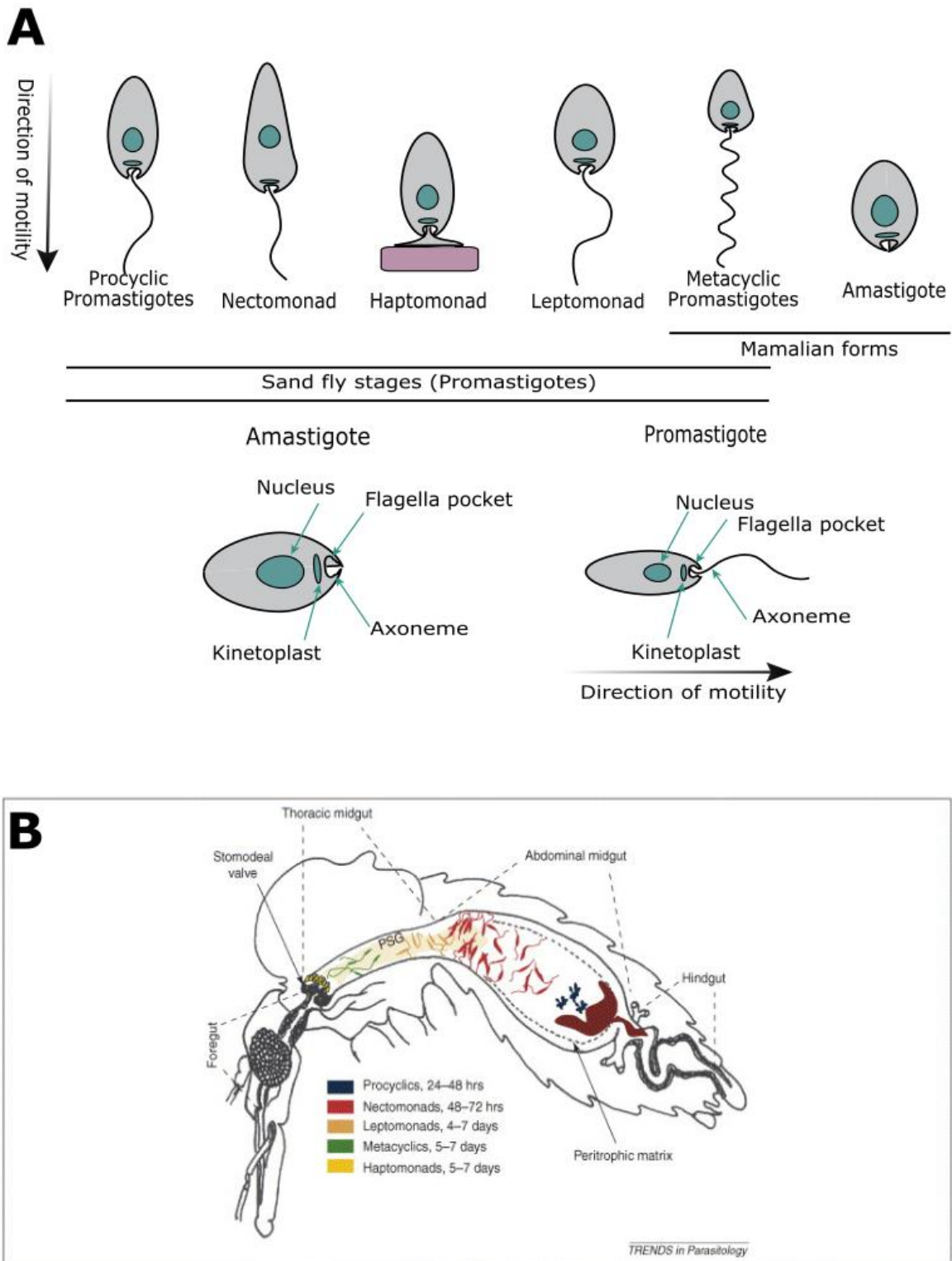
Figure 1.6 The different life cycles stages *Leishmania* displays whilst inside the sand fly vector and mammalian macrophages. **A**. Schematic displaying the life cycle stages of *Leishmania*. Note the major changes in flagellum morphology. **B.** The progression of parasite infection through the sand fly. Starting from the initial blood meal amastigotes are ingested into the midgut where they must escape the peritrophic matrix. They continue through the life cycle differentiating into nectomonads, leptomonads and haptomonads. They finally differentiate into the infective form, metacyclic promastigotes that will be transmitted to a mammal when the sand fly takes the next blood meal (Kamhawi, 2006)

1.8.2 The amastigote flagellum

Whilst inside the PV amastigote parasites can hijack the host's immune response and modulate their intracellular environment (Batista et al., 2020). Historically, the amastigote flagellum was considered to be non-functional, however the current hypothesis is that it plays important roles in signalling (Gluenz et al., 2010).

Working with macrophages and intracellular amastigotes can be challenging. Therefore *in vitro* forms of amastigotes known as axenic amastigotes, can be generated by a decrease in pH and an increase in temperature. Axenic and intracellular parasites are generally considered comparable as less than 1% of all genes significantly differ from one another transcriptionally (Fiebig et al., 2015). Therefore, many of the experiments use axenic amastigotes as a proxy for intracellular amastigotes.
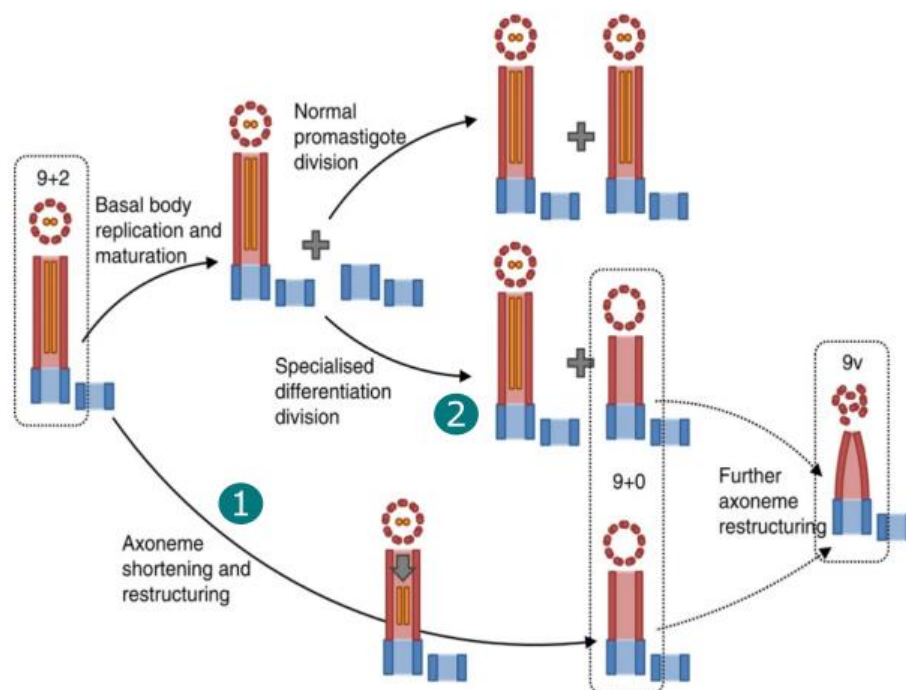
Figure 1.7 The generation of the amastigote flagellum in *Leishmania*. The generation of the amastigote flagellum occurs via two routes, (1) axoneme shortening and restructuring or (2) specialised differentiation. (1) When differentiation is initiated, full length 9+2 flagella undergo shortening of the axoneme to a 9+0 axoneme, which collapses further to generate a 9v structure. (2) When cells divide during differentiation they can assemble a new 9+0 flagellum de novo but will further collapse to generate a 9v axoneme structure (Wheeler et al.,2015).

Differentiation from a 9+2 promastigote flagellum to a 9v amastigote flagellum, occurs by two potential routes (Figure 1.7). The first is axoneme disassembly, the second is a specialised differentiation division (Wheeler et al., 2015). Axoneme disassembly occurs within 16 hours after differentiation and happens in two steps. The first step is the disassembly of structures such as the paraflagellar rod (PFR), central pair projections and PF16 (a protein that stabilises the central pair). These structures are additional to the 9 microtubule doublets, showing that the flagellum first 'strips

back' to a 9+0 before it can begin shortening. Then the flagellum gradually decreases in length resulting in a short, 9+0 flagellum. The second step is the collapse of the 9+0 flagellum to a 9*v*. In *9v* flagellum, the outer microtubule doublets have collapsed on themselves (Figure 1.7). Structures such as the outer-dynein arm, radial spoke, and dynein complexes are lost which likely trigger the axoneme collapse.

Specialised division can also generate a 9*v* flagellum. After differentiation, dividing parasites have a long, old flagellum (~15 μm) and a new, short flagellum (~4 μm). After four hours into differentiation, the old flagellum gradually shortens (~4 μm) with a short new flagellum (<1 μm) beginning to appear and after 10 hours, most dividing cells had the very short new flagellum. These short new flagella were assembled without the central pair, demonstrating that differentiating *Leishmania* can possess both a 9+2 and a 9+0 flagellum, simultaneously. At this stage, the short flagellum still has 9+0 radial symmetry, meaning that the flagellum must first be assembled with a 9+0 axoneme, then undergo further collapse to generate a 9*v* flagellum.

2. Justification and aims.

During the lifecycle of *Leishmania,* the parasites must navigate and survive in a range of environments across two hosts. Parasites differentiate into multiple lifecycle stages, each with its own unique adaptations to maximise its survival across different environments. One of the most striking changes, is the remodelling of the flagellum.

These natural changes in flagellum morphology, along with a well-established gene editing toolkit, makes *Leishmania* an excellent system to study flagellum disassembly and modification. As discussed, the well-studied model, *Chlamydomonas* provides invaluable insight into the IFT system but may not be applicable to other systems. Here, the aim is not to provide another model of flagellum biology but instead focus on how the remodelling of the *Leishmania* flagellum suits the parasite's unique biology.

The theme of this work is to look at the ways that *Leishmania* disassembles and remodels its flagellum. Within this the following questions will be investigated:

2.1 Does the intraflagellar transport system play a role in *L. mexicana* flagellum disassembly and if so, how?

Previous research by Wheeler, showed that during early differentiation there was a significant reduction in IFT material as flagella disassembled (Wheeler et al., 2015). However, the timing of the IFT reduction and if this reduction solely accounts for flagellum disassembly is unclear. Chapter 4 aims to address this question with a number of objectives.

First, *L. mexicana* mutants will be generated that express the individual IFT proteins endogenously fused with fluorescent proteins. These mutants will be then used to track IFT movement along the flagellum in both promastigotes and differentiating parasites. IFT velocity and numbers will be quantified from these tracks. By generating multiple *L. mexicana* mutants expressing different IFT proteins, these can be used to determine whether IFT velocity and numbers remain consistent across the different IFT proteins.

2.2 Are additional factors involved in regulating flagellum disassembly?

Based on the findings from Chapter 4, it is likely that other factors may be regulating IFT disassembly. Previous research shows that PTMs are involved in both microtubule stability, and regulation of some microtubule-based motors (Huang et al., 2009; Regnard et al., 1999). Therefore, it is possible that PTMs could have a role in the regulation of flagella disassembly.

The findings from Chapter 4 also demonstrated that IFT was active throughout flagellum disassembly. Although IFT was active, it was not clear whether the trains were transporting cargo. Chapter 5 will aim to address these questions with a number of objectives.

First, various tubulin PTMs will be antibody labelled in the flagellum of *L. mexicana* at various stages of differentiation from promastigotes to amastigotes. Additionally, in order to attempt to capture cargo trafficking, *L. mexicana* mutants expressing putative IFT cargoes (namely RSP4/6 and PF16) fused to fluorescent proteins will be generated. The flagellum of these mutants will undergo FRAP analyses during stages of growth, maintenance and disassembly.

2.3 Naturally occurring dysflagellar mutants from patient isolates – an IFT defect?

A paper by Zauli and colleagues, describes a strain of *L. braziliensis* isolated from a patient lesion that did not assemble a full length flagellum (Zauli et al., 2012). Instead, a disorganised collection of material was present at the exit of the flagellar pocket. From what is known about flagellum assembly, it was hypothesised that mutations in the IFT system could lead to severe flagellum defects. Therefore, gDNA was kindly supplied from the authors and the underlying cause of this defect was investigated. The results were intriguing as a large deletion was identified that contained four genes including serine kinases, this deletion was further analysed.

In Chapter 6, we aim to describe the mutation of the dysflagellar parasite and to replicate the phenotype *in vitro*. To achieve this, the four *L. braziliensis* genomes (one mutant, three with normal morphology from the same region) will be sequenced and the genomes assembled. The mutant sequences will be compared to the wild-type to identify any major deletions. Then the individual gene deletions observed in the mutants, will be replicated in *L. mexicana.* The genes will be then reintroduced into the deletion mutants to document whether the phenotype is rescued.

3. Methods

3.1 Protein identification and selection

IFT proteins are well documented in species such as *T. brucei* and *C. reinhardtii.* Gene IDs of the 24 IFT protein orthologues in *L. mexicana* were extracted from TryTrypDB to be used in downstream analyses (Aslett et al., 2009) (see Table 4.1).

The protein sequence identity of IFT proteins from *T. brucei, T. cruzi, L. major, L. braziliensis* and *L. donovani* were compared to *L. mexicana* using NCBI Blast (Sayers et al., 2022). Heap maps were generated using the R package pheatmap (version 1.0.12) (Figure 4.1). The PFAM domains and secondary structures of the IFT proteins were annotated onto the protein sequences using the InterPro and PFAM online databases. Images of the secondary structures were self-generated.

3.2 Sequencing of the *L. braziliensis* dysflagellar mutant

3.2.1 Sample background

Zauli and colleagues obtained *L. braziliensis* parasites from patient isolates collected from hospitals in the state of Goiás, Brazil (Zauli et al., 2012). Four samples were collected from the same region, three with normal morphology (BE5, DMO8, JBC8) and the dysflagellar mutant EFSF6. The gDNA extracted from these samples were kindly donated by Silvia RB Uliana.

3.2.2 Sequencing of the Goiás samples

Sequencing was performed commercially by BGI Tech Solutions (HongKong.Ltd) using short-read Illlumnia sequencing. The normal flagellum samples had low scores on BGI quality assessment and were further processed with a NEB ultra-library prep kit. The dysflagellar mutant (EFSF6) passed the quality check and was processed without the extra step. Samples were sequenced with BGI's proprietary next-generation sequencing platform DNBSEQ™ at 50x coverage, 100 bp read length.

3.2.3 Read mapping and identification of deletions.

All sequencing files from the paired end runs were stored as two zipped .fq files and all reference sequences were downloaded from NIH genome library as .fna/.fasta files.

Bowtie2 software (Langmead & Salzberg, 2013) was used to map the reads of the *L. braziliensis* samples to the reference sequence (strain MHOM/BR/75/M2903) to generate the SAM output files. Samtools was used to convert the SAM files to sorted BAM files (an indexed output) (R. Li & Zhu, 2022). Variants, namely single/multi-nucleotide polymorphism, insertions and deletions were called samples using the FreeBayes software (Richter et al., 2020).

3.3 Parasite culture and cell line generation

3.3.1 Parasite culture

Parasite strains used in this work were *L. mexicana* (MNYC/BZ/62/M379), which contain a construct encoding T7 RNA polymerase and Cas9 nuclease (C9/T7) to facilitate CRISPR-Cas9 mediated genome modification (Beneke et al., 2017). *L. mexicana* promastigotes were grown at 28°C in M199 medium with Earle's salts, L-glutamine, 10% FBS, 40 mM HEPES-NaOH (pH 7.4), 26 mM NaHCO$_3$, and 5 μg/mL hemin. Axenic amastigotes were generated by sub-culturing promastigotes into Schneider's *Drosophila* medium with 20% FBS (pH 5.5) at 34°C.

3.3.2 Generation of endogenously tagged parasites.

Primers for the N-terminal endogenous tagging of proteins in *L. mexicana* were designed using the LeishGEdit software (Beneke et al., 2017) (Tagging primers are listed in Apendix 1a). Using the previously described protocol (Dean et al., 2015), constructs for endogenous tagging, containing flanking ORFs of the protein on interest, the mNeonGreen (mNG) protein and Blasticidin resistance were generated by PCR (Appendix 1b and 1c details template PCR reagents and thermocycler conditions). To complement each tagging template a single guide RNA containing the T7 promotor was amplified (Appendix 1d and 1e details guide PCR reagents and thermocycler conditions).

PCR products were run on a 1% agarose gel to verify product size. If correct, the template and guide for individual genes were combined and ethanol precipitated to concentrate and sterilise the DNA and then suspended in 20 μl of ddH$_2$0. The constructs were added to 1×10^7 log culture of *L. mexicana* C9/T7, which were resuspended in 1x Roditi buffer (Burkard et al., 2007). Cells were then electroporated using the programme X-001 on a Nucleofector 2b (Lonza). Cells were recovered in 10 mL of M199 media with selection drug blasticidin (5μg/mL) added after 6 hours.

3.3.3 Generation of knockout cell lines

Primers for the knockout of proteins in *L. mexicana* were designed with LeishGEdit (Beneke et al., 2017) (Tagging primers are listed in Apendix 2a). The pT plasmids (Beneke et al., 2017) formed the template for the deletion constructs and encoded a drug resistance marker; either resistance to blasticidin or G418. Two plasmids each encoding a different resistance marker were used to knockout the two copies of the gene and generate deletion mutants with resistance to both drugs.

The constructs were amplified by PCR using the previously described protocol and reagents and thermocycler conditions are detailed in Appendix 2b-2c (Dean et al., 2015). Single guide RNAs were used to introduce a double stranded break, both upstream and downstream of the gene of interest. Both these guides were generated by PCR and details of regents are detailed in Appendix 2d-2e. The size of the PCR products was assessed by running on a 1% agarose gel, and the two corresponding template and two guide products were combined, and ethanol precipitated and resuspended in 20 μl of sterile ddH$_2$0.

The constructs were added to 1×10^7 log culture of *L. mexicana* C9/T7, which were resuspended in 1x Roditi buffer. Cells were then electroporated programme X-001 on a Nucleofector 2b (Lonza). Cells were recovered in 20 mL of M199 media with selection drug Blasticidin and G418 (5µg/mL and 20 µg/mL respectively) added after 6 hours. The cells were plated in a 96 well plate to allow selection of cones. These parasites were recovered at 28°C with CO_2 for up to 14 days.

3.3.4 PCR Confirmation of successful knockout generation

Genomic DNA from the suspected knockout cell lines along with the parental C9/T7 was extracted with DNAeasy Blood and Tissue kit (Qiagen), according to the manufacturer's instructions.

Primers were designed to target the coding region of the gene of interest and amplify a 500 bp fragment (Appendix 3a). PCR reactions were performed, with suitable positive and negative controls and PCR products were ran on 1% agarose gels to determine if bands were absent for the knockout parasites. (Appendix 3b-3c for details of reagents and thermocycler conditions).

3.3.5 Generation of addback plasmids for *Δ36.1520*

Plasmid pJ1364 (generated by Jack Sunter) was digested to generate a linearized plasmid with overhangs at the end to act as the addback backbone. To create N-terminal addbacks, reactions were performed with 1 µl each of BamHI and Xbal restriction enzymes (NEB), 5 µl of 10X CutSmart (NEB), 5 µl of pJ1364 plasmid, made up to 50 µl with ddH_2O. The digests were incubated at 37°C for 1.5 hours. Digests were run on a 1% agarose gel and a gel extraction kit (NEB) was used to purify the linearized plasmid (~5 kb). PCR was used to amplify the LmxM.36.1520 gene from the parental parasite's gDNA. (Primer's appendix 4a). PCR reagents and conditions are listed in Appendix 4b-4c. PCR products were run on a 1% agarose gel and bands of the correct size (1.5kb) were cut out and DNA extracted from the gel using a gel extraction kit (NEB).

To digest the PCR product, 10 µl of PCR product, 5 µl CutSmart buffer (NEB), 1 µl each of the appropriate restriction enzymes made to a final volume of 50 µl of ddH_2O and incubated at 37°C for 1.5 hours. The digested insert was purified (PCR & DNA Cleanup Kit, Monarch). The linearized plasmid and DNA insert were ligated with 1 µl of 10X T4 ligase buffer, 0.5 µl of DNA ligase made up to 10 µl with ddH_2O and ligations were incubated at 4°C overnight.

3.3.6 Bacterial transformations

The ligated plasmid-insert was combined with 25 µl of *E. coli* SURE 2 competent cells (Agilent technologies) left for 15 minutes on ice then transformed by heat shock at 42°C for 1 minute then immediately placed back on ice. Transformed bacteria were plated on ampicillin agar plates (100 µl/mL) and grown at 37°C for 12-16 hours. Individual colonies were picked and grown in overnight cultures of 4 mL LB medium with 100 µl/mL ampicillin at 37°C for 12-16 hours. Plasmids were extracted from cultures with MiniPrep Kit to reach a final concentration of 10 µg of plasmid (NEB). Plasmids were digested in a 200 µl volume with 3 µl of PacI (Neb). The digest was ethanol

precipitated and resuspended in 20 µl of sterile water then transfected into knockout cell lines (see section 3.3.2).

3.4 Light microscopy

3.4.1 Live cell microscopy

1 mL of cell culture, density $1x10^6$-$1x10^7$ cells/ml, were washed three times (for 3 minutes at 1000 g) in M199 media without FBS. On the second wash 1 µg/mL Hoechst 33342 was added to the wash buffer to stain the nucleus and kinetoplast. After the washes, parasites were resuspended in the wash buffer and 2.3 µl of suspension was added to a glass slide and mounted with a #0 mm coverslip.

Cells were imaged immediately post slide preparation using an x 63, oil-immersion, NA 1.4 lens, Axio Imager Z2 (Zeiss) wide-field microscope with an ORCA-Flash 4.0 (Hamamatsu) camera. Images were captured in phase, and at the appropriate wavelength for the fluorescently tagged protein (mNeonGreen excitation 506 nm, emission 517 nm/mCherry excitation 587 nm, emission 610nm) and nuclear stain. Images were captured using Zen Blue software and saved as .czi files.

3.4.2 Cytoskeleton preparation

For cytoskeleton preparation, 1 mL of parasite culture was washed three times in vPBS and resuspended to a final concentration of roughly $1x10^7$. 1 x 1 cm wells were drawn onto clean glass slides using a PAP-pen (Merck) and allowed to dry completely. The cell suspension was settled onto the wells for 8-12 minutes, until the parasites had adhered to the slides. The suspension was removed and replaced with 0.5% IGEPAL CA-63 detergent in 1x PEME (100 mM PIPES-NaOH pH 6.9, 1 mM MgSO4, 2 mM EGTA, 0.1 mM EDTA) for 10 seconds followed by immediate fixation in -20°C methanol for 20 minutes. Cells were rehydrated in PBS three times at room temperature.

3.4.3 Immunofluorescence staining of parasites.

Slides with the fixed parasites were blocked with 0.1% BSA in 1x PBS for a minimum of one hour inside a humidity chamber. Slides were then washed for 5 minutes in 1X PBS for three times. Primary antibodies were diluted in 0.1% BSA in 1X PBS and were added to the cells and incubated inside a humidity chamber for 1 hour (see Appendix 4d for antibody concentrations). Slides were washed three times for 5 minutes per wash in 1X PBS before adding the appropriate secondary antibody conjugated to Fluorescein (FITC) (1:200 in 0.1% BSA) and incubating inside the humidity chamber for 1 hour. Cells were washed three times for 5 minutes in 1X PBS, on the second to last wash Hoechst 33342 (1 µg/mL) was added to the wash buffer. Slides were mounted with 3 µl of anti-fade mounting media and a #0 coverslip was secured with nail varnish (see section 3.4.1 for imaging details)

3.4.4 Live cell microscopy of IFT transit

Cells were imaged at 0, 2, 4, 6 and 8 hours post initiation of differentiation. 1 mL of cell culture was centrifuged at 1000 g for 3 minutes and washed three times with M199, without FBS (the buffers were pH 7 for promastigotes, pH 5.5 for amastigotes) and resuspended in the appropriate wash buffer. Cells were transferred to a glass slide and the flagellum laid flat against the slide so the IFT transit could be imaged. Cells were imaged immediately post slide preparation using an x63, oil-immersion, NA 1.4 lens, Axio Imager Z2 (Zeiss) wide-field microscope with an ORCA-Flash 4.0 camera (Hamamatsu). IFT videos were recorded for 100 frames (4.04 fps), at 175 ms exposure time with the shutter remaining open (mNeonGreen excitation 506 nm, emission 517 nm/mCherry excitation 587 nm, emission 610nm). Images were saved as .czi files.

3.4.5 IFT cargo analysis

Based on previous research we selected RSP4/6 and PF16 as putative cargos (Lechtreck et al., 2018a; Wheeler et al., 2015). In cell lines expressing endogenously tagged IFT74::mNG and either RSP4/6 or PF16::mCherry (mCh), following the tagging protocol, as described in section 3.3. In order to generate parasites expressing a very bright signal for the endogenously tagged cargo, cell lines expressing PF16, or RSP4/6 endogenously tagged with three copies of mNeonGreen (3mNG) were also created. After verifying the expression of the fluorescently tagged proteins, the cell lines were used for FRAP analysis.

For FRAP analyses, Zeiss LSM800 upright microscope with an x100/1.4 NA oil immersion objective, GaAsp-PMT detector was used. Promastigotes were maintained at 28°C and amastigotes at 32°C during imaging. ROIs of various sizes dependant on the flagellum length were photobleached using the 590nm (mCh) or 405nm (3mNG) laser at 80% power for 2 pulses at various points along the flagellum. In the case of dividing parasites both flagella were bleached. Due to the exploratory nature of this experiment the ROI size and location were not consistent intentionally. After photobleaching, time-lapse videos were captured for at least 90 seconds (exposure time of 0.73s). Images and time-lapse were captured using Zen Blue software and saved as .czi files.

Fluorescence recovery curves were generated with metadata from the experiments. Utilising the ImageJ plugin package from Stowers University FRAP analysis FRAP recovery curves of the bleached regions and unbleached IFT pool and section of flagella.
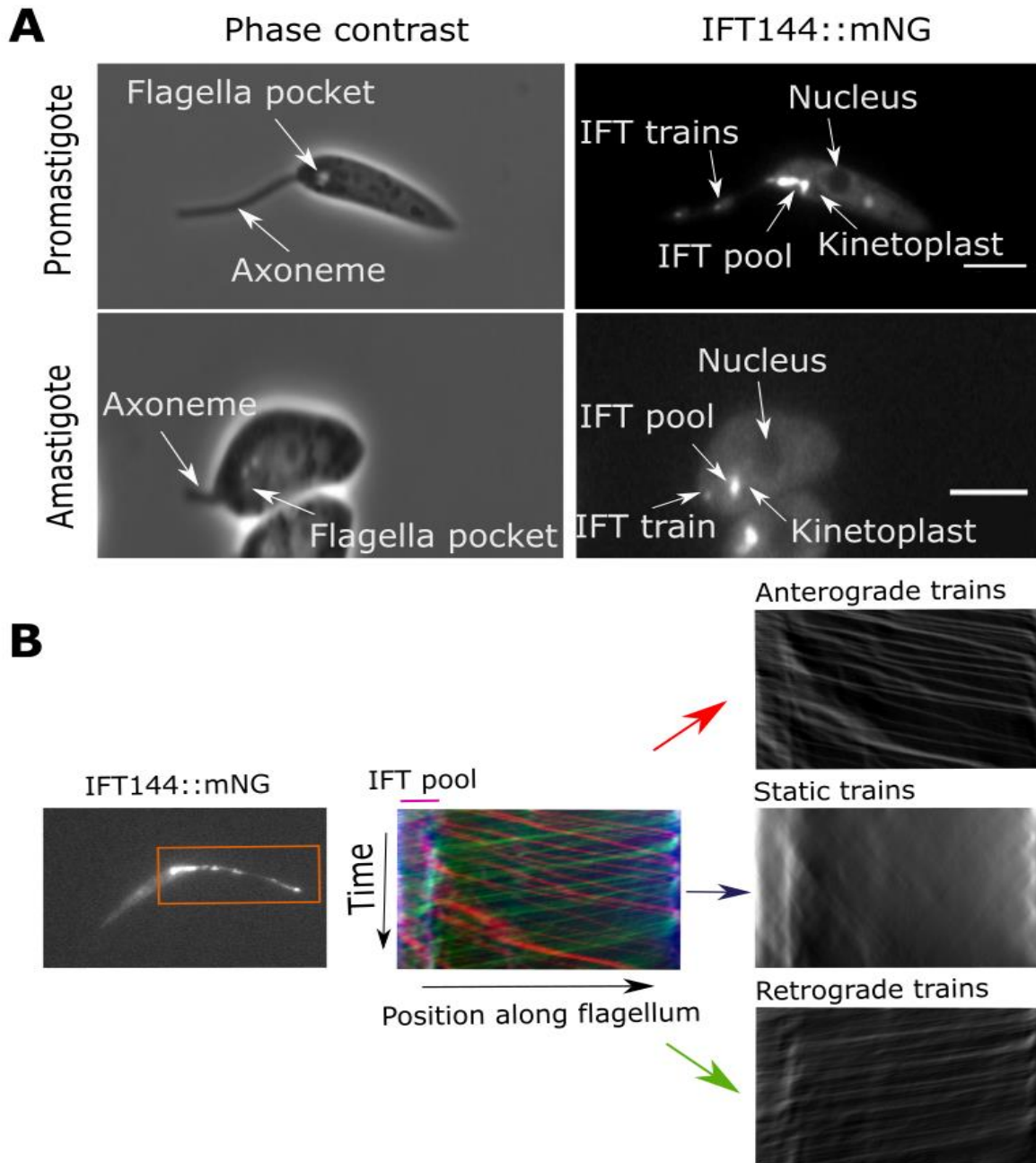
Figure 3.1. Morphology and key structures of *L. mexicana* during differentiation A. Example of a *L. mexicana* promastigote and an eight hour axenic amastigote expressing an IFT 144::mNG. Relevant structures are labelled (Scale bar= 5 µm)**. B.** Example Kymograph, a graphical representation of IFT particle movement in a cell line expressing IFT56::mNG. On the left a still image, taken from a video capturing IFT. From the videos, individual IFT proteins were tracked, and the middle plot shows IFT movement as a function of time (y axis) and the x axis shows the movement from proximal (flagellum base) to distal (flagellum tip). This graph can then be separated into static movement, seen here as clustered around the IFT pool and flagellum tip, the anterograde trains moving from the pool to the tip and retrograde trains moving from the tip to the pool. Graphs were generated with KymographDirect v2.

3.5 Image and statistical analysis

From the .czi videos from data obtained from method 3.4.4, still images of each of the 100 frames were extracted and saved as individual .TIFF files in the same folder. Each cell line and time point were saved in a separate folder for downstream processing. Kymographs, displaying the IFT movement along the flagellum over time, were extracted from the IFT videos using ImageJ plugin KymographClear (Mangeol et al., 2016). Figure 3.1b shows an example kymograph with the IFT proteins from the anterograde, retrograde, and static direction with their position along the flagellum tracked against the time. KymographClear generated a composite image of the cell over the course of the time series which the flagellum was manually annotated onto. Velocity and the distance of the IFT trains were extracted with the KymographDirect programme (Mangeol et al., 2016). Number of IFT trains were manually counted from the generated kymographs and normalised for flagellum length.

Mean velocities of IFT anterograde and retrograde trains between different time points, were subject to separate unequal variance t-tests and z tests to compare proportions (significance $p<0.05$) (R, V.3.6.1).

3.6 Electron Microscopy

3.6.1 Parasite fixation, embedding, and infiltration.

Parasites (at a cell density of $1x10^7$ cells/ml) were fixed inside the culture flask by the addition of 1:10 of 25% glutaraldehyde. Cultures were washed twice with a buffer fixative comprised of 0.1% tannic acid, 2.5% glutaraldehyde in 0.1 PIPES pH7.2. Cells were transferred to a 1.5 mL Eppendorf and fixed for one hour at room temperature. After incubation, cells were washed three times for five minutes in 0.1 M PIPES buffer, between washes cells were centrifuged for 2 minutes at 1000 g.

After washing, cells were stained with 1% osmium tetroxide and 1.5% potassium ferricyanide in 0.1M PIPES buffer for one hour in the dark. After incubation, cells were washed three times for five minutes each in 0.1 M PIPES buffer with a two minute spin between washes. Post washing, cells were embedded into 4% agarose in 20 mL of 0.1 PIPES buffer and refrigerated for 15 minutes. Agarose pellets were cut into small pieces that were dense with stained parasites and placed in small glass vials and washed three times for five minutes in ddH$_2$O and centrifuged at 1000 g for two minutes between washes. The agarose pellets were incubated overnight, in the dark at 4°C with 1% uranyl acetate in ddH$_2$O.

Pellets were washed three times for five minutes each in ddH$_2$O. Then pellets were dehydrated in increasing stepwise concentrations of ethanol (in ddH$_2$O) for 10 minutes per step. Ethanol concentrations started at 30%, 50%, 70%, 90%, 100% followed by 2 steps at absolute ethanol. Fully dehydrated cells were infiltrated with 50% TAAB 812 HARD resin in absolute ethanol for 4 hours with gentle agitation. Pellets were then transferred to 100% for overnight infiltration, with gentle agitation. After overnight infiltration, cells were transferred to fresh 100% resin for 5-6 hours then

pellets were transferred to BEEM capsules (BEEM®Embedding Capsule size 00) and set overnight at 60 °C.

3.6.2 Thin sectioning and imaging

Hardened samples were removed from the BEEM capsule and manually trimmed using with a glass knife to create a trapezium, which contained the sample (PowerTome PT-PC, Boeckeler). Serial thin sections were sliced using a diamond knife (DiATOME®). Sections were collected and settled onto copper grids (TAAB G200). One step staining was undertaken with Reynolds lead citrate (0.4%) for 5 minutes and washed four times with ddH$_2$O. Random sections on grids were imaged with Joel-1400 flash TEM with Gatan One View camera.

4. Analysis of IFT during *Leishmania mexicana* flagellum remodelling

4.1 Introduction

When *Leishmania* is transmitted from the sand fly vector to the mammalian host, it differentiates from the promastigote to the amastigote form (see section 1.7, Figure 1.6a). During this differentiation, the long, motile 9+2 flagellum is remodelled to a short, sensory 9v flagellum (Gluenz et al., 2010). The precise mechanisms underlying this remodelling is unclear.

The IFT system orchestrates flagellum assembly and maintenance. There is emerging evidence that IFT also plays a role in disassembly. Previous work demonstrated that during flagellum shortening, the IFT signal within the flagellum decreases (Wheeler et al., 2015). Within four hours into differentiation, there was over a threefold reduction in IFT signal in the anterograde direction and almost tenfold reduction in the retrograde direction. Previously, the balance-point model has demonstrated that the flagellum tip is the site of continued turnover, thereby the continued influx of IFT is required to maintain the concentration of axonemal proteins at the flagellum tip. Therefore, the huge reduction in IFT, as observed in differentiating *L. mexicana* parasites, could reduce the influx of axonemal proteins to the tip, meaning that there is no new material to replace the disassembled units of the axoneme, and ultimately drive flagellum disassembly.

Other ways IFT could impact the rate of disassembly is via the velocity of the trains. There seems to be a correlation between longer flagella and faster IFT and vice versa with shorter flagella and slower IFT (Table 1.1). In *Leishmania,* IFT trains (indicated by IFT52::mNG) had an average velocity of 1.6 μm/s and 1.5 μm/s for anterograde and retrograde tracks, respectively (Wheeler et al, 2015). These velocities are slightly slower than those reported from other flagellates such as *T. brucei* and *Chlamydomonas.* Unusually, unlike other organisms the retrograde train velocities were also slower than the anterograde trains.

This chapter builds upon the idea that a large reduction if IFT may contribute to flagellum disassembly and will document IFT in detail across the early differentiation in *L. mexicana.* During differentiation, the IFT train numbers for a range of IFT proteins (from both IFT-A and IFT-B subgroups) will be quantified. Velocities of anterograde and retrograde trains across the time course will be tracked to determine whether the velocities change during flagellum shortening.

4.2 IFT structure and sequence is highly conserved across trypanosomatids species.

IFT proteins are highly conserved across eukaryotes (Taschner & Lorentzen, 2016). There are slight variations in the numbers of proteins across species, but the core of at least six IFT-A and 16 IFT-B proteins are conserved. There are a minimum of 25 IFT proteins in *L. mexicana* - six IFT-A proteins, 16 IFT-B proteins, and three motor proteins. Here, we focused on 22 IFT proteins for analyses and excluded the IFT motor proteins.

A key step in both *Leishmania* and *T. cruzi* life cycles is the ability to disassemble or lose their flagellum in the mammalian host (Kurup & Tarleton, 2014). In contrast, *T. brucei* does not disassemble its flagellum at any point. The first step was to rule out the possibility that IFT protein sequences differed significantly between the species. Species such as *L. braziliensis* and *L. donovani* were included to compare with even the most divergent *Leishmania* species.

First, IFT protein sequences from *L. mexicana* were compared with the IFT orthologs across the selected subset of trypanosomatids. All IFT proteins were present in all the species examined. As expected, the sequence similarity of the proteins mirrored the overall relatedness of a species. The highest similarities were observed between the *Leishmania* species, with most proteins showing around 80-90% sequence similarity (Figure 4.1). Whereas *L. braziliensis* shows slightly more divergence than the other species with similarity between 70-80%. *L. braziliensis* was expected to show slightly higher dissimilarity due to its divergence from *Leishmania* species (Rogers et al., 2011). In the separate, but closely related, *Trypanosoma* genus the similarities were below 75%, although this is slightly lower this is still generally considered well conserved. The high similarities of IFT proteins between species suggests that differences in IFT sequences is unlikely to be contributing to the ability to disassemble the flagellum.

Secondly, the functional domains of *L. mexicana* IFT proteins were analysed to infer some of the functionality of *Leishmania* IFT proteins. It was clear that the functional domains of *L. mexicana* proteins were remarkably similar to those reported in *Chlamydomonas,* again demonstrating the remarkable conservation between IFT proteins (Taschner et al., 2012). The structures of IFT proteins of *L. mexicana* were enriched with WD40, coiled-coils and TPR domains, these are all domains associated with protein-protein interactions and co-ordinating multi-protein assemblies (Figure 4.2).
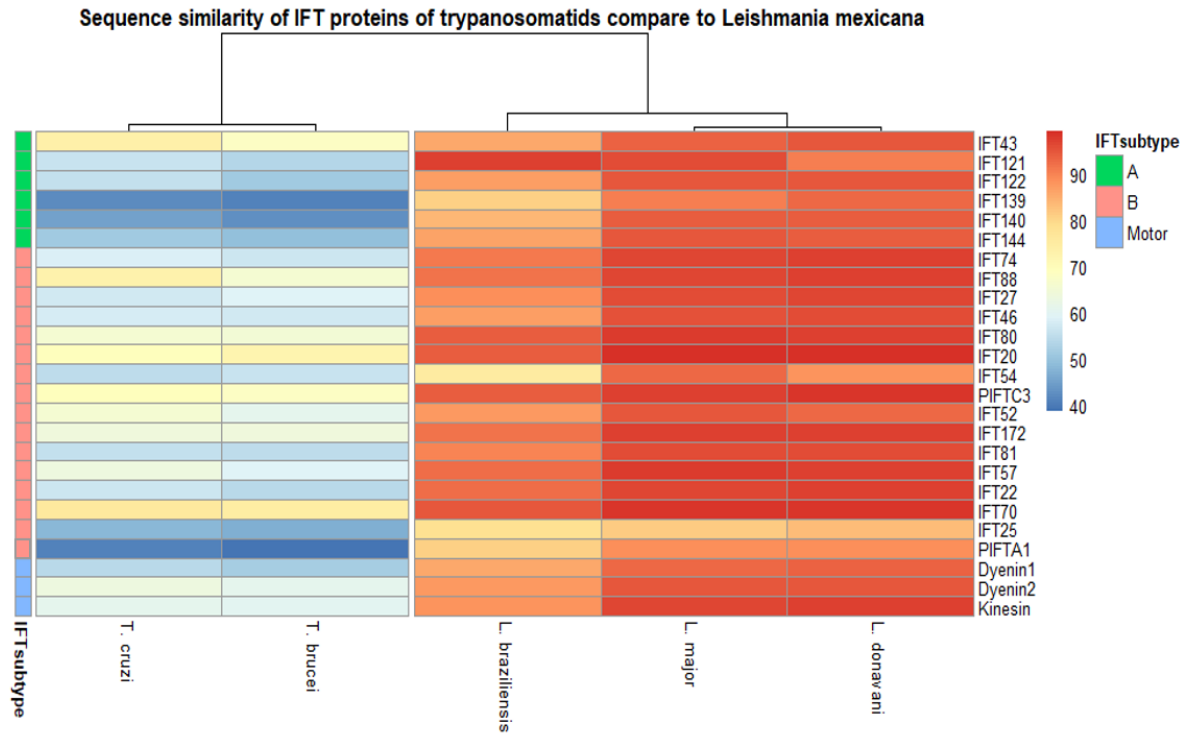
Figure 4.1 - Sequence similarity of IFT proteins and motors across *Leishmania* and *Trypanosoma* species. Sequence similarity of IFT proteins in *Leishmania braziliensis, L. major, L. donovani*, *Trypanosoma cruzi* and *T. brucei*. Scale for similarity is shown to the right with the high 90% shown in reds and low similarity <50% in blues. The high similarity suggests that IFT proteins are highly conserved within trypanosomatids. Figure generated with R package, pheatmap (version 1.0.12).
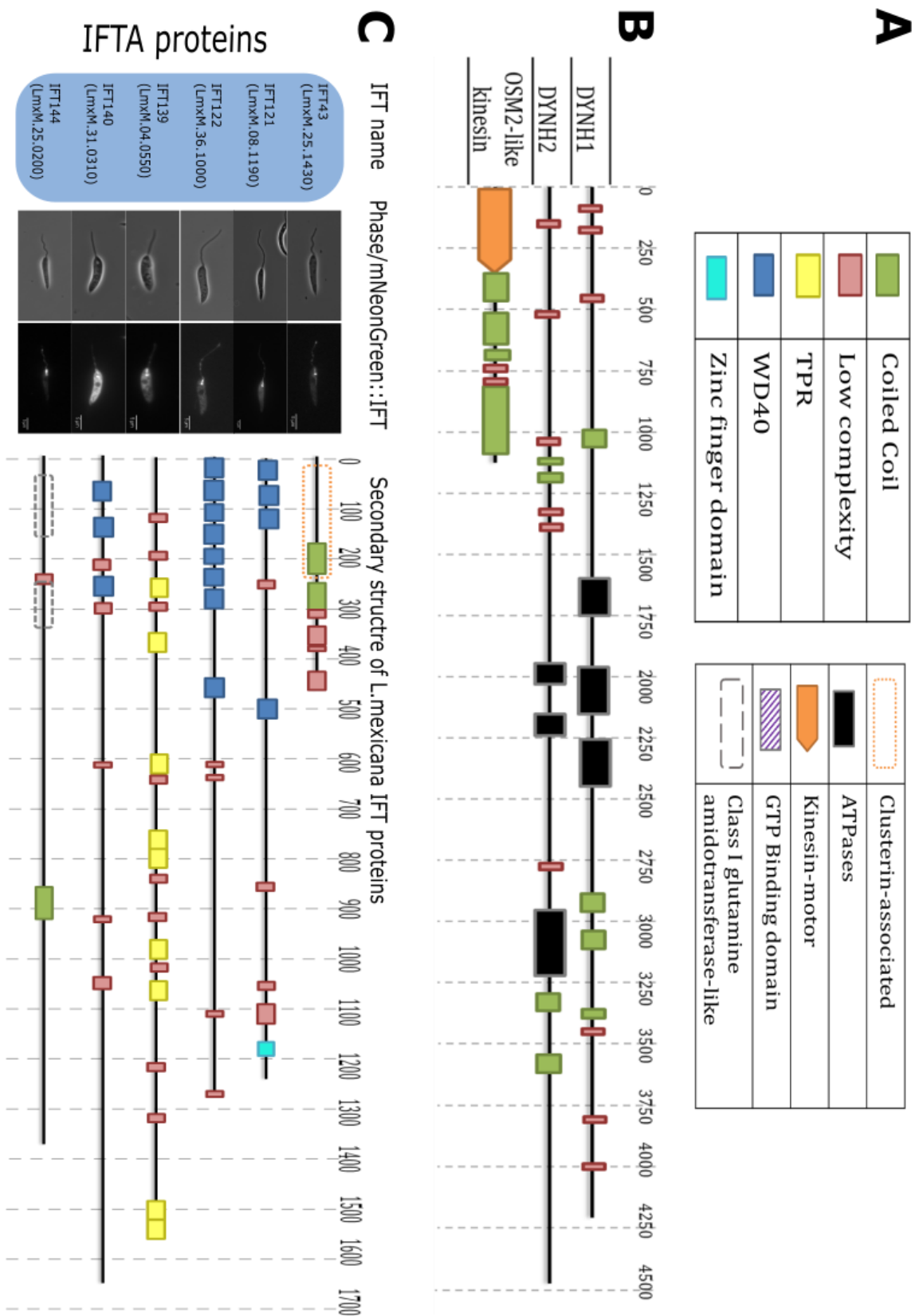
Figure 4.2. Endogenously tagged IFT proteins with functional domains annotated. 21/22 of the IFT proteins (excluding motors) in *L. mexicana* promastigotes were endogenously tagged with mNeonGreen. Images captured in the phase and fluorescence channels (scale = 5 μm). Schematics of the associated secondary structures, labelled with PFAM domains are shown next to these. **A.** Key to PFAM domains **B**. the motor proteins **C.** IFT-A proteins **D**. IFT-B proteins. Figures were created based on the PFAM domains.

IFTB proteins

D

IFT25 (LmxM.09.1140)
IFT70 (LmxM.08_29.0510)
IFT22 (LmxM.31.3210)
IFT57 (LmxM.32.0620)
IFT81 (LmxM.33.0230)
IFT172 (LmxM.21.0980)
IFT52 (LmxM.19.0230)
PIFTC3 (LmxM.08_29.2760)
IFT54 (LmxM.21.1566)
IFT20 (LmxM.29.2000)
IFT80 (LmxM.19.0330)
IFT46 (LmxM.29.1170)
IFT27 (LmxM.08_29.0090)
IFT88 (LmxM.27.1130)
IFT74 (LmxM.22.1370)

Extends to 1800 aa
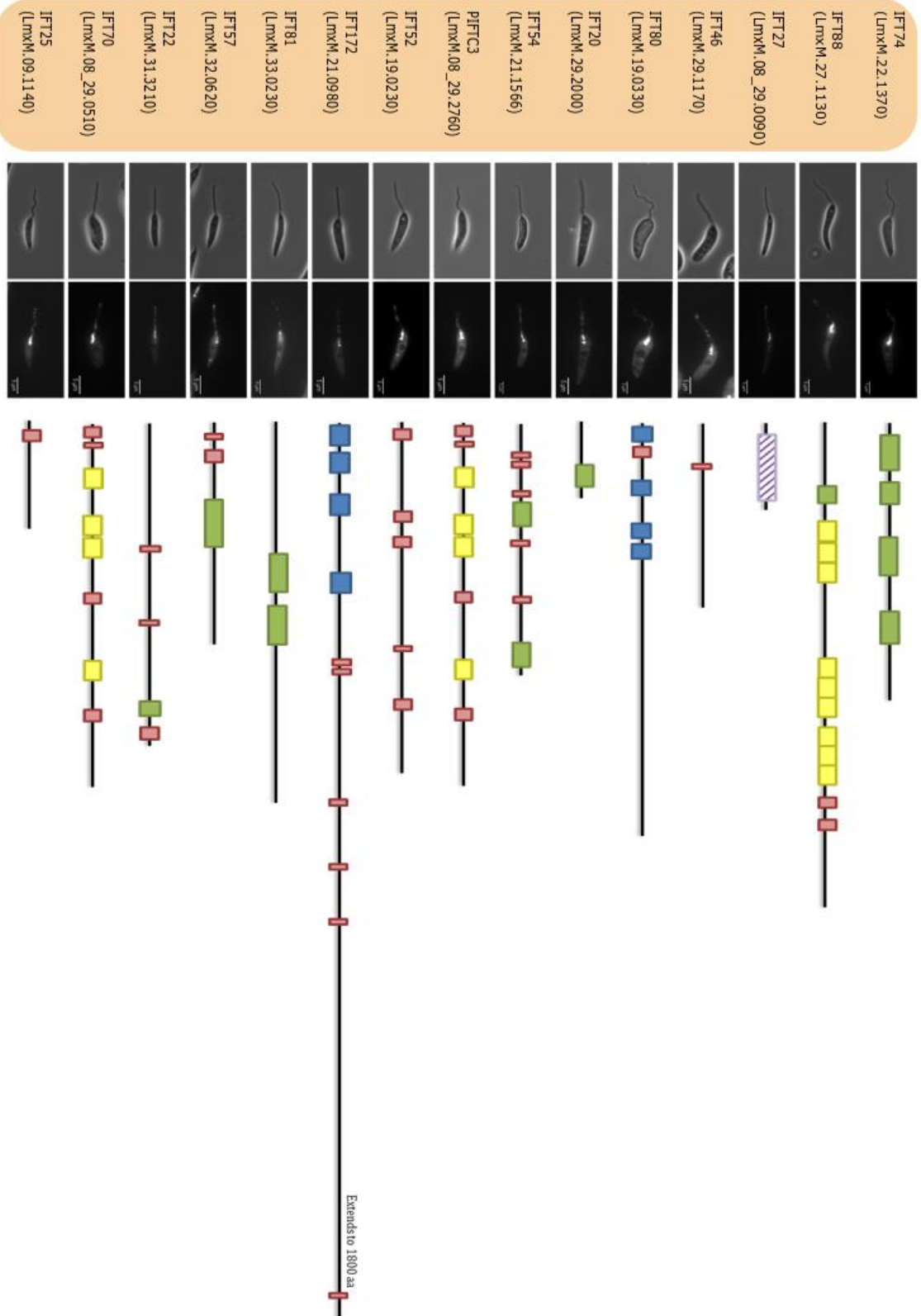
4.3 IFT proteins could be successfully tagged and tracked along the flagellum.

IFT trains are comprised of multiple protein components. To examine the changes in velocity and train numbers during differentiation, cell lines expressing various IFT proteins fused to mNeonGreen were generated. In total, 21/22 proteins fused to mNeonGreen were successfully expressed in *L. mexicana* promastigotes, the localisation of these proteins is shown in Figure 4.2. The majority of the cell lines displayed a typical IFT localisation, characterised by a strong signal in the IFT pool with trains travelling along the flagellum. 2/21 proteins had a weak, secondary lysosome signal and 2/21 had a weak, secondary cytoplasm signal (Halliday et al., 2019). IFT motors were not tagged as previous reports show that they have unusual IFT dynamics such as different speeds along the flagellum and they may diffuse, rather than travel via IFT in the retrograde direction (Douglas et al., 2020; Luo et al., 2017; X. Pan et al., 2006). From these 22 proteins, seven were selected for downstream analyses (selected proteins highlighted in Table 4.1). The seven selected proteins showed the brightest IFT signal and did not have a secondary signal, as increased background fluorescence made IFT tracking less accurate. Both IFT-A and IFT-B proteins were selected as they are associated with retrograde and anterograde transport, respectively.

4.4 Early axenic amastigotes were successfully generated in eight hours.

To define the morphological changes that occur during the early stages of amastigote differentiation, we generated axenic amastigotes. It is difficult to achieve a synchronous *Leishmania* culture (Minocha et al., 2011), so parasites were asynchronous when differentiation began. All parasites were imaged during log phase in attempts to mitigate the impact of asynchronous culture. Promastigote parasites (zero hours) had a slender cell body and elongated flagellum (Figure 4.3a) and over the eight-hour differentiation period, parasites became shorter and more spherical. The length of the flagellum was reduced by over 50% from an average of 12.5 μm at zero hours to ~5.5 μm at eight hours (Figure 4.3b). At this point, the flagellum still extended out of the flagellar pocket. These results demonstrated that in eight hours of differentiation, early stages of flagellum disassembly could be captured.

Table 4.1 IFT proteins in *L. mexicana*. The gene ID corresponds to the TriTrypDB database. The different IFT genes are labelled whether they are IFTA or B, whether they could be successfully tagged and the location in *L. mexicana* promastigotes. The seven proteins that were used in further experiments are highlighted in the table.

Gene ID *L. mexicana*	IFT NAME	A/B	tagged	Localisation	Secondary localisation
LmxM.25.1430	IFT43	A	yes	IFT	Weak lysosome
LmxM.08.1190	IFT121	A	yes	IFT	
LmxM.36.1000	IFT122	A	yes	IFT	
LmxM.04.0550	IFT139	A	yes	IFT	
LmxM.31.0310	IFT140	A	yes	IFT	
LmxM.25.0200	IFT144	A	yes	IFT	
LmxM.18.1460	IFT38	A	no (3 failures)		
LmxM.22.1370	IFT74	B	yes	IFT	
LmxM.27.1130	IFT88	B	yes	IFT	Weak cytoplasm
LmxM.08_29.0090	IFT27	B	yes	IFT	
LmxM.29.1770	IFT46	B	yes	IFT	Weak cytoplasm
LmxM.19.0330	IFT80	B	yes	IFT	
LmxM.29.2000	IFT20	B	yes	IFT	
LmxM.21.1566	IFT54	B	yes	IFT	
LmxM.08_29.2760	IFT56	B	yes	IFT	
LmxM.19.0320	IFT52	B	yes	IFT	
LmxM.21.0980	IFT172	B	yes	IFT	
LmxM.33.0230	IFT81	B	yes	IFT	
LmxM.32.0620	IFT57	B	yes	IFT	Weak lysosome
LmxM.31.3210	IFT22	B	yes	IFT	
LmxM.08_29.0150	IFT70	B	yes	IFT	
LmxM.09.1140	IFT25	B	yes	IFT	
LmxM.27.1750	Dyenin	Motor	Not attempted		
LmxM.33.4160	Dyenin	Motor	Not attempted		
LmxM.31.0680	Kinesin	Motor	Not attempted		
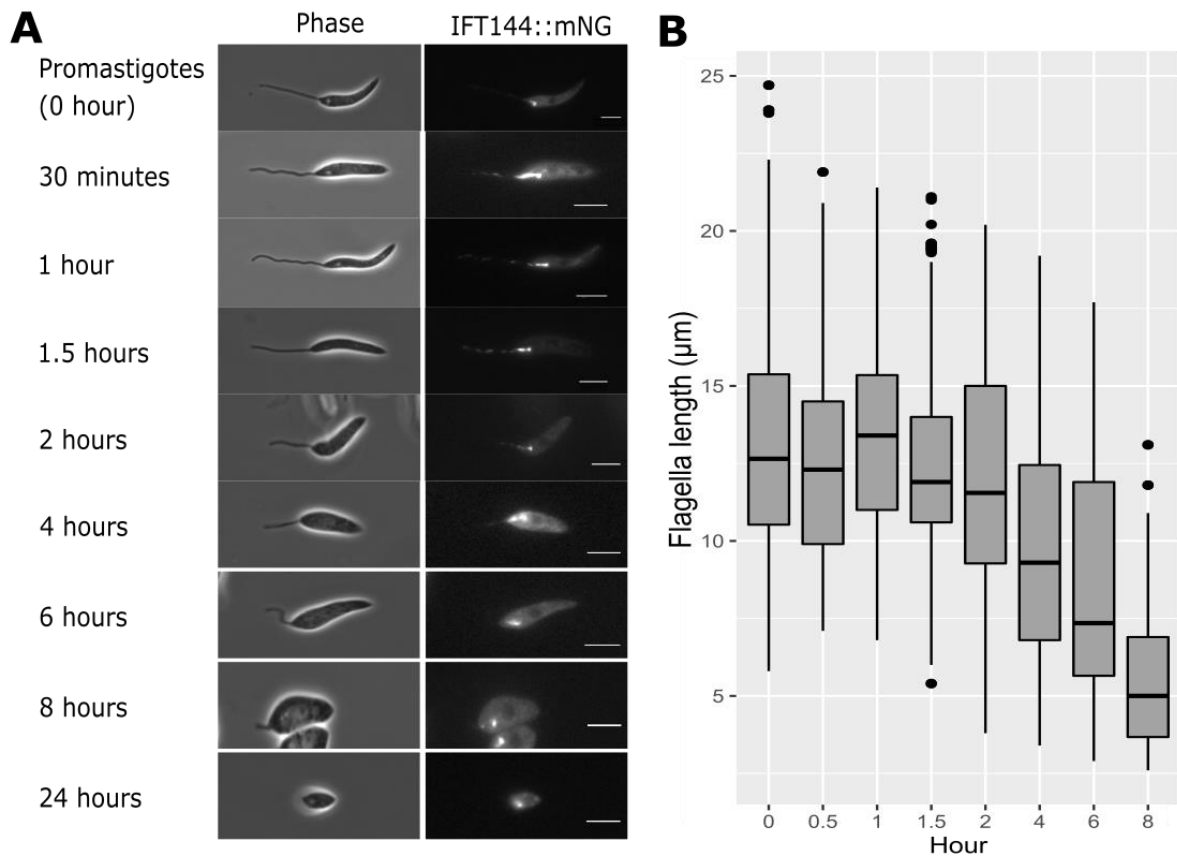
Figure 4.3 *L*. mexicana morphology throughout early amastigotes differentiation. A. Morphology of parasites during axenic amastigote generation. Parasites are shown during differentiation at various time points from 0-24 hours. Images of phase and IFT144 endogenously tagged with mNeonGreen are shown (Scale bar = 5 μm). **B**. The average flagellum length of parasites during early differentiation (0-8 hours), measured in μm.

4.5 IFT velocity decreases throughout parasite differentiation.

IFT proteins were tracked across early differentiation of *L. mexicana* parasites. Videos were taken at two-hour intervals from zero to eight hours. An IFT signal was inferred as a IFT train and will be referred as train throughout this chapter. Figure 4.4 highlights examples of kymographs extracted from these videos. These kymographs show that as the flagellum length decreases the number of traces on the kymographs also decrease. Showing the reduction of IFT trains over parasite differentiation.
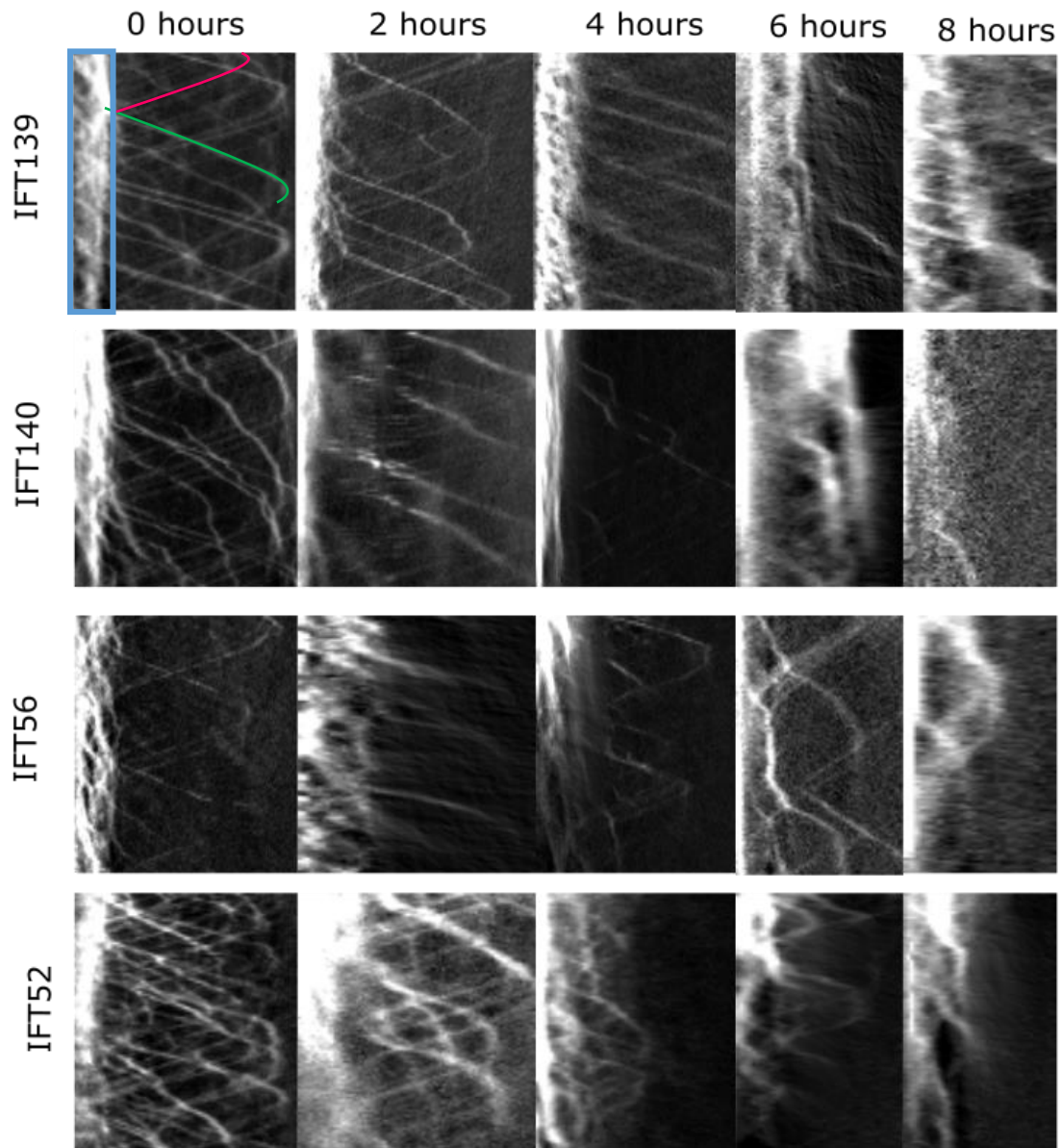
Figure 4.4. Examples of Kymographs extracted from *L. mexicana* parasites undergoing differentiation. The first kymograph has been annotated with a green line indicating anterograde trafficking and the pink line indicating retrograde trafficking. The blue box indicates the IFT pool, which across all kymographs, regardless of stage of differentiation, remains bright. This is due to the static IFT proteins within the IFT pool.

From the microscopy videos, IFT proteins from every flagellum in the field of view that remained stationary and in focus, were tracked. However, as the cell body started to get more spherical at the later stages of differentiation, it became difficult to clearly visualise some flagella. This reduced the sample size for cells at later time points, mainly six and eight hours. Throughout differentiation the IFT::mNG retained a strong signal in the IFT pool (Figure 4.4 and 4.5) and trains could be visualised traversing along the flagellum in both anterograde and retrograde directions. Figure 4.5 shows examples of IFT train movement in IFT140 and IFT20 during promastigotes and eight-hour axenic amastigotes. Individual trains were tracked moving along the flagellum in the anterograde direction briefly pausing at the tip, where they are presumably remodelling into retrograde trains, then moving back down the flagellum to the IFT pool (protein tracks for IFT122, IFT139, IFT80, IFT52 and IFT56 are shown in supplemental 4a-4h).
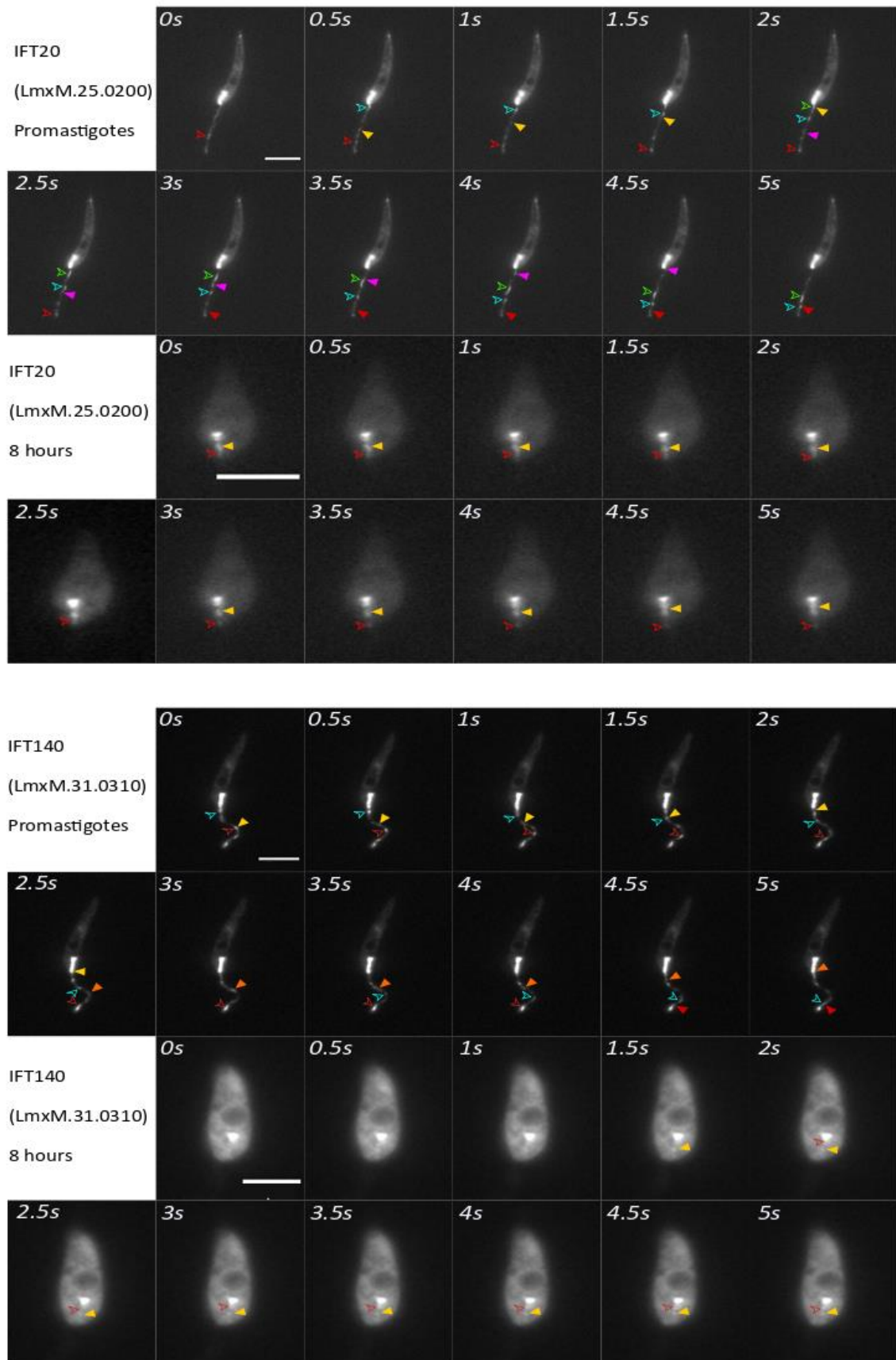
Figure 4.5. IFT140 and IFT20 transport in promastigotes and early amastigotes. Tracking of IFT140::mNG and IFT20::mNG in promastigotes and early amastigote at eight hours into differentiation are shown. The tracks are shown for 5 seconds of the videos, full videos are shown in supplemental videos 4a-4n. Unfilled arrows represent anterograde trains, filled arrows represent retrograde trains. The same train is tracked with the same coloured arrows throughout the time series (Scale bar = 5 μm)

Kymographs were extracted from the 24 second microscopy videos (supplemental videos 4a-4n) Using KymoClear software, kymographs were separated into anterograde and retrograde directions and the tracked velocities were exported (n=19894 tracks). Across cell lines at zero hours, the average velocity of IFT trains ranged from 2.5-3 μm/s in the anterograde direction, and slightly higher in retrograde direction of 2.7-3.4 μm/s (Figure 4.6). These findings also reflect the trend that the retrograde trains are generally quicker than anterograde trains (Buisson et al., 2013; Chien et al., 2017; Williams et al., 2014).

However, across all cell lines, the IFT velocities were highly variable with large fluctuations seen between the cell lines (Figure 4.6). In cell lines such as IFT139 and IFT20 this is more apparent. For example, the median velocity of IFT139 proteins at zero hours was 2.75 μm/s and 3 μm/s for anterograde and retrograde directions, respectively. Then there was a large dip in velocity at two hours into differentiation where the train speeds dropped to 1.25 μm/s and 2 μm/s for anterograde and retrograde directions, but at four hours the speeds in both directions had increased to similar speeds as seen in the promastigotes. At six hours, the speeds dropped again to 2.5 μm/s and 2.6 μm/m for anterograde and retrograde and they remained here at eight hours. Aside from the general fluctuations and variability between the cell lines, there was also an unusual pattern observed in the IFT-B cell lines (IFT52, IFT56, IFT80 and IFT20), where the retrograde velocity consistently increased between four and six hours (Figure 4.6).

Despite the variability across cell lines there was a general small reduction in the median IFT velocity across the differentiation process. In all cell lines, the average velocity in the eight hour early amastigotes was reduced compared to the promastigotes, showing that there is a small reduction in IFT velocity during flagellum disassembly.
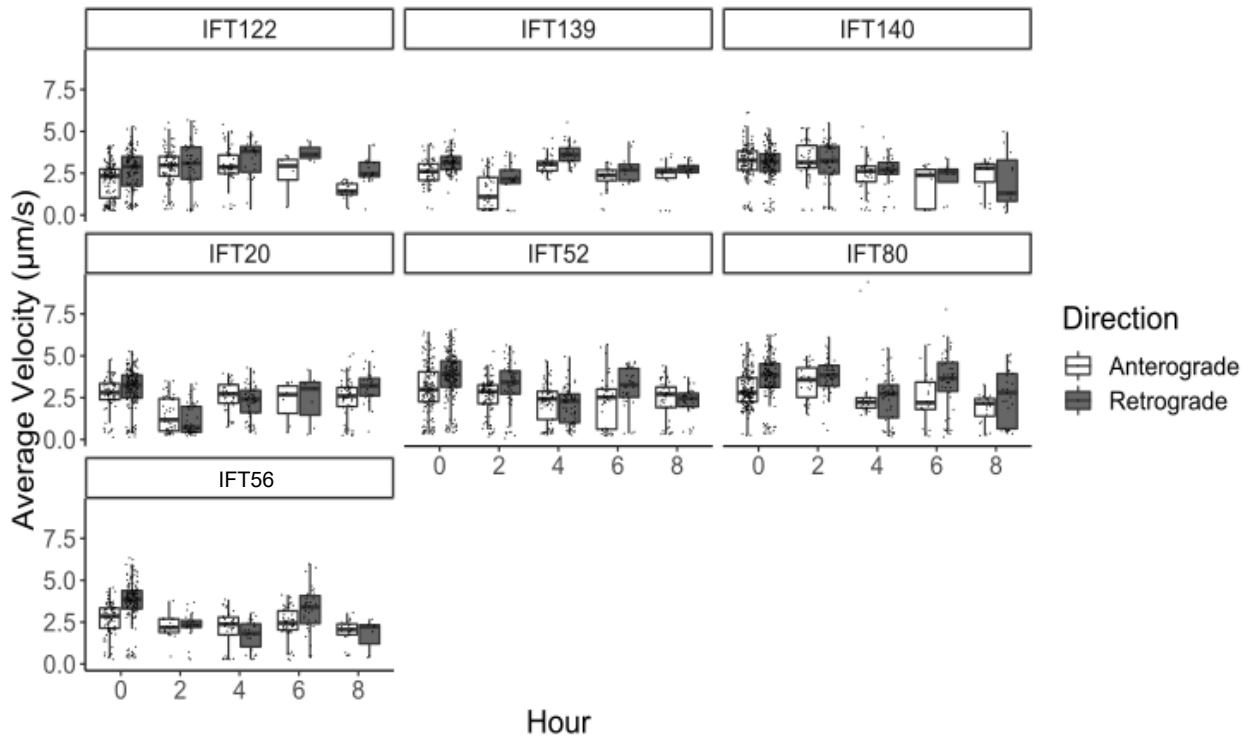
Figure 4.6 Average IFT velocities across the seven individual IFT cell lines. Velocities of IFT trains (μm/s) collected across early differentiation to axenic amastigotes (0-8 hours). Anterograde and retrograde directions are shown separated. Graphs are shown as box and whisker with the midpoint representing the median.

4.5.1 IFT-A and IFT-B proteins had different reported velocities during differentiation.

IFT-A and IFT-B proteins are associated with retrograde and anterograde transport, respectively. However, both IFT-A and IFT-B proteins are present on the same IFT trains (Jordan et al., 2018a). The next steps were to compare IFT velocity between IFT-A and IFT-B proteins.

In promastigotes, in both directions, IFT-B proteins displayed a slighter higher velocity than the IFT-A proteins (median of IFT-A=2.6 μm/s, IFT-B=2.7 μm/s for anterograde and IFT-A=2.8 μm/s, IFT-B=3 μm/s for retrograde, $p=<0.001$) (Figure 4.7). At two hours, in both directions, the velocities dropped but were not significantly different between the IFT-A and IFT-B groups. Yet, at four hours into differentiation, IFT-A proteins were now significantly faster than IFT-B proteins (median of IFT-A=2.7 μm/s, IFT-B=2.5 μm/s for anterograde and IFT-A=3 μm/s and IFT-B= 2.4 μm/s for retrograde, $p=<0.001$). Between four to eight hours, in the anterograde direction there were no significant differences observed between the IFT-A and IFT-B proteins. However, in the retrograde direction there was an increase in velocity seen only in the IFT-B proteins group at six hours, reflecting the increase reported in the individual cell lines (median IFT-A=2.5 μm/s, IFT-B= 3.5 μm/s, $p=<0.05$). This increase at six hours appears unusual but is seen consistently across cell lines, suggesting a true increase rather than a technical error.
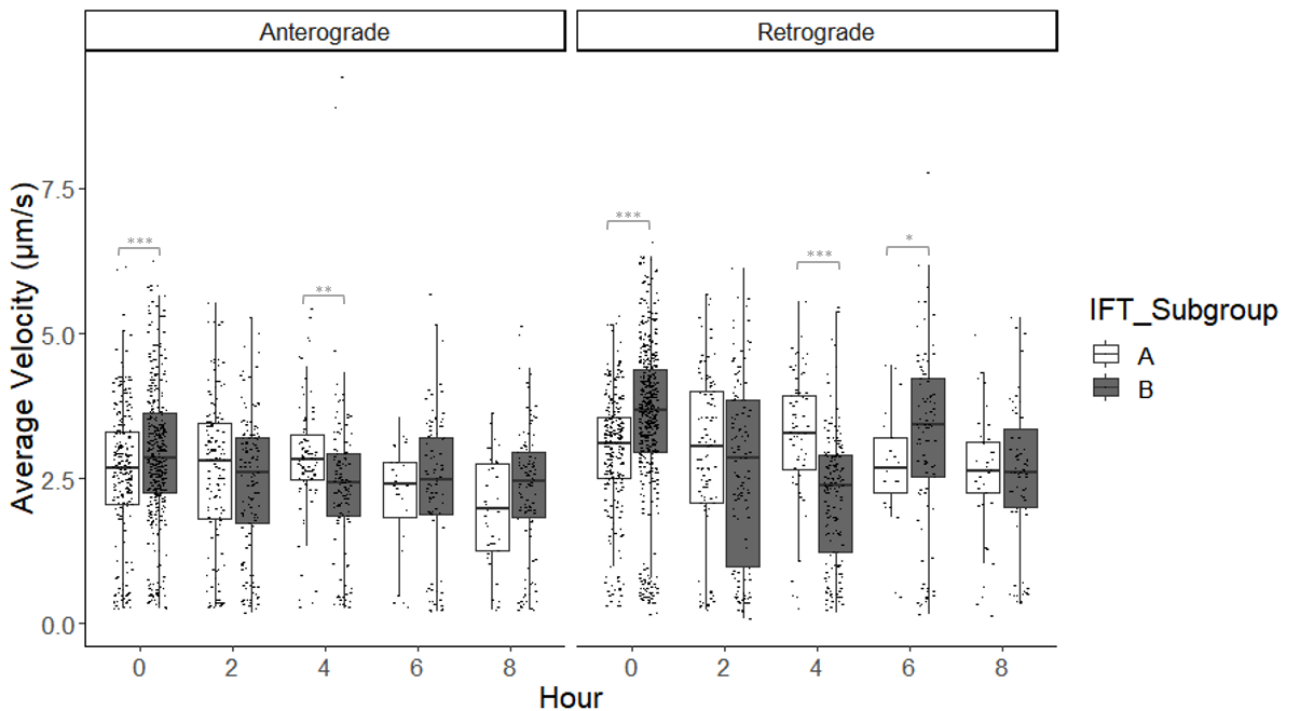
Figure 4.7. Average IFT velocities reflected across IFT-A and IFT-B proteins. The data from the 3 IFT-A and 4 IFT-B protein velocities (μm/s) were combined to show the average across between IFT-A and IFT-B. Welches t-test comparing IFT-A vs IFT-B from the same time point *(*** = p<0.001, ** = p<0.01, * = p<0.05)*. Graphs are shown as box and whisker with the midpoint representing the median. Individual points are representative of an average velocity for one track i.e., one IFT train recorded from the video.

4.5.2 Combined velocities can act as biological replicates.

IFT proteins travel as multi-protein complexes, with one train composed of many different proteins. Therefore, each cell line may act as an independent replicate of one another. Although there was a lot of variability of IFT velocities in the individual cell lines, when results are combined the trends in IFT velocity are clear and the multiple repeats increase the reliability of the findings. Data collated from all the cell lines, separated into anterograde and retrograde directions, are shown in Figure 4.8.

In the anterograde direction there was a significant drop in velocity between zero and two hours (2.8 μm/s to 2.5 μm/s, $p=< 0.001$). For the remainder of the differentiation, the average velocity remained between 2.3-2.5 μm/s. The retrograde direction showed more variation in average velocity. In promastigotes the average IFT velocity started at 3.3 μm/s, then at two hours into differentiation it dropped to 2.7 μm/s ($p=<0.001$), followed by a further drop in velocity at four hours to 2.5 μm/s ($p=<0.05$). At six hours the velocity increased to an average of 3.1 μm/s ($p = 0.001$) then a reduction in velocity again at 8 hours to 2.5 μm/s ($p = 0.001$).

Overall, these findings suggest that differentiation results in a slight reduction in IFT train velocity in both directions but with the significant reduction between zero and two hours. However, this small reduction in IFT velocity alone cannot explain the *Leishmania* flagellum shortening.
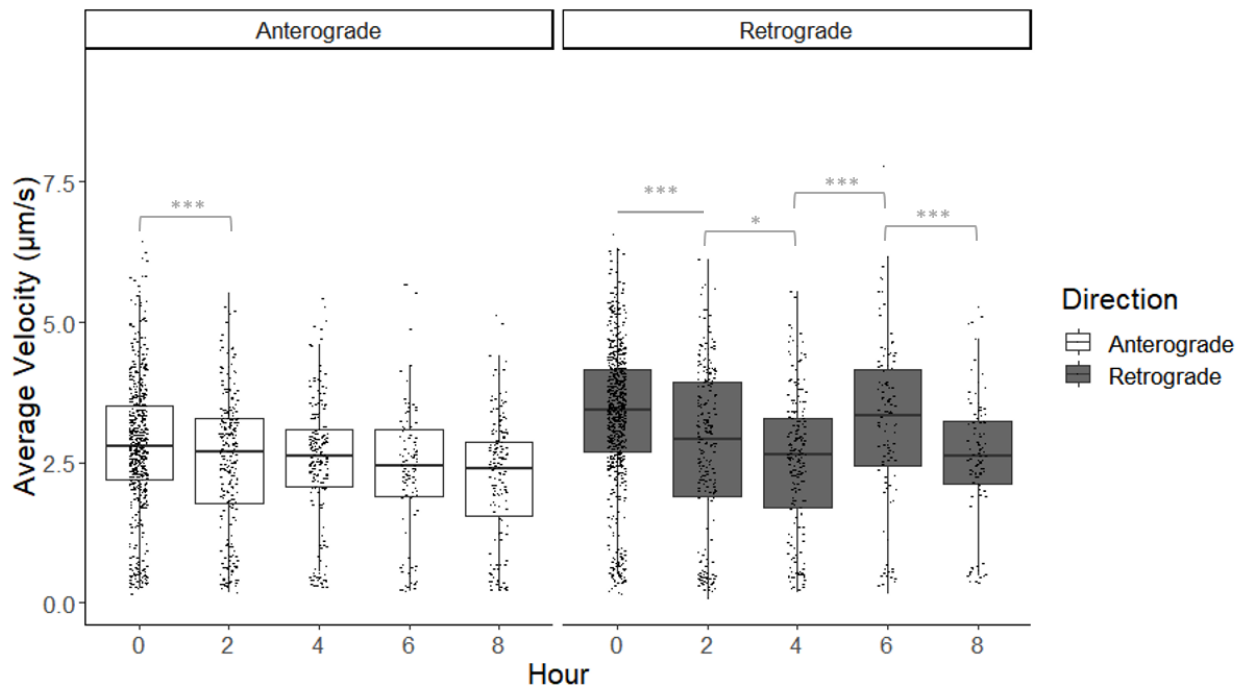
Figure 4.8. Average IFT velocities combined across all seven tagged cell lines. Combined velocities across all cell lines (μm/s). Velocities split into anterograde and retrograde directions. Welches t test comparing average between the subsequent time points *(*** = p<0.001, ** = p<0.01, * = p<0.05).* Graphs are shown as box and whisker with the midpoint representing the median.

4.6 Train numbers significantly reduce in differentiating parasites.

The slight reduction in IFT velocity may account for a small reduction in flagellum length but it is unlikely to fully explain the flagellum shortening during differentiation. Therefore, the next step was to analyse the number of IFT trains throughout early differentiation (n=1135).

In promastigotes, the number of trains ranged from 0.28-0.61 trains s^{-1} in the anterograde direction and 0.3-0.77 trains s^{-1} in the retrograde direction (Figure 4.9). There were lots of fluctuations in the numbers of trains across the cell lines, however, they all showed the highest number of trains in promastigotes and the lowest number of trains eight hours into differentiation.
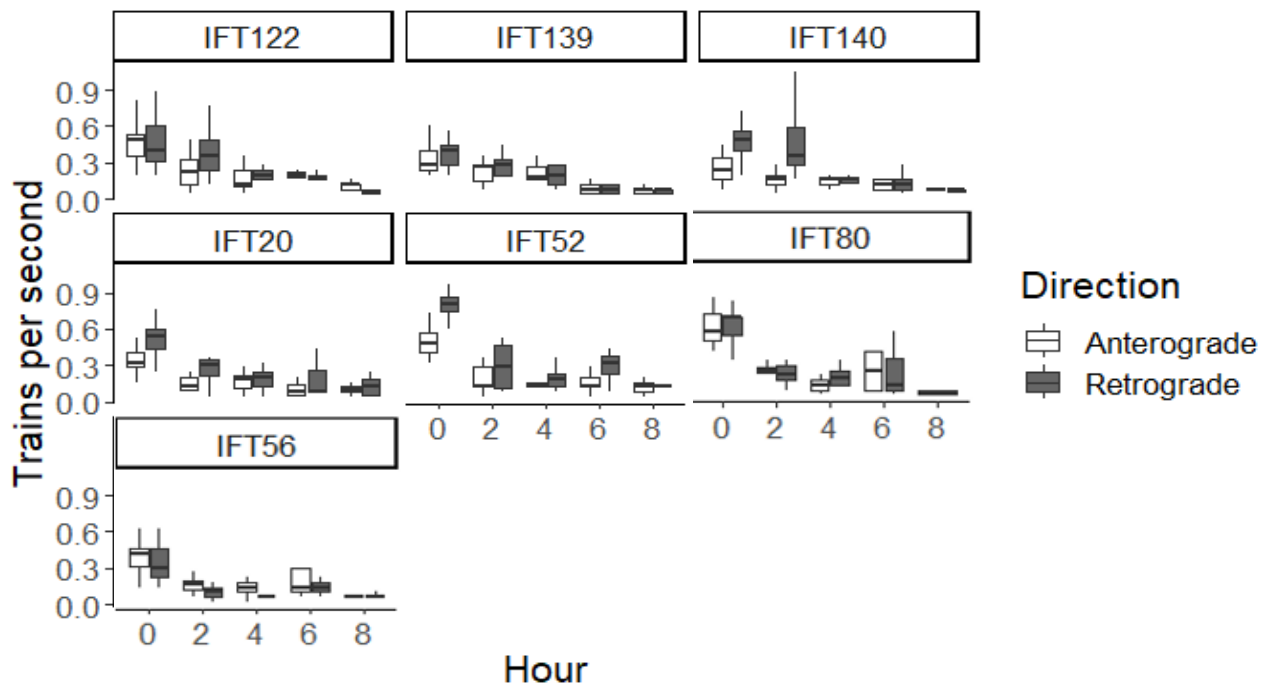
Figure 4.9 Average IFT number across different endogenously tagged IFT lines. Average number of IFT trains (per second) collected across early differentiation to axenic amastigotes (0-8 hours). Anterograde and retrograde directions are presented separately. Graphs are shown as box and whisker with the midpoint representing the median.

As small differences in IFT velocities were observed between IFT-A and IFT-B proteins (Section 4.5.1), potential differences between IFT numbers were also compared. In the anterograde direction IFT-A/B proteins had comparable average numbers of trains s^{-1} throughout the differentiation process (Figure 4.10). In the anterograde direction, throughout differentiation, the IFT numbers remained similar between IFT-A and IFT-B proteins. In the retrograde direction, there were slightly different number of trains between IFT-A and IFT-B groups. In promastigotes, IFT-B proteins had slightly higher trains s^{-1} than IFT-A (IFT-A= 0.45 trains s^{-1}, IFT-B=5.8 trains s^{-1}, *p=<0.05)* but at two hours this had switched with IFT-A having higher numbers than IFT-B (IFT-A= 3.2 trains s^{-1}, IFT-B = 2 trains s^{-1}, *p=<0.01*). From four to six hours the IFT numbers between A and B proteins were at similar levels to one another.

IFT-A/B subunits are present on the same trains; therefore, it is not clear why there are discrepancies in both the number of trains and the velocities, particularly in the retrograde direction.
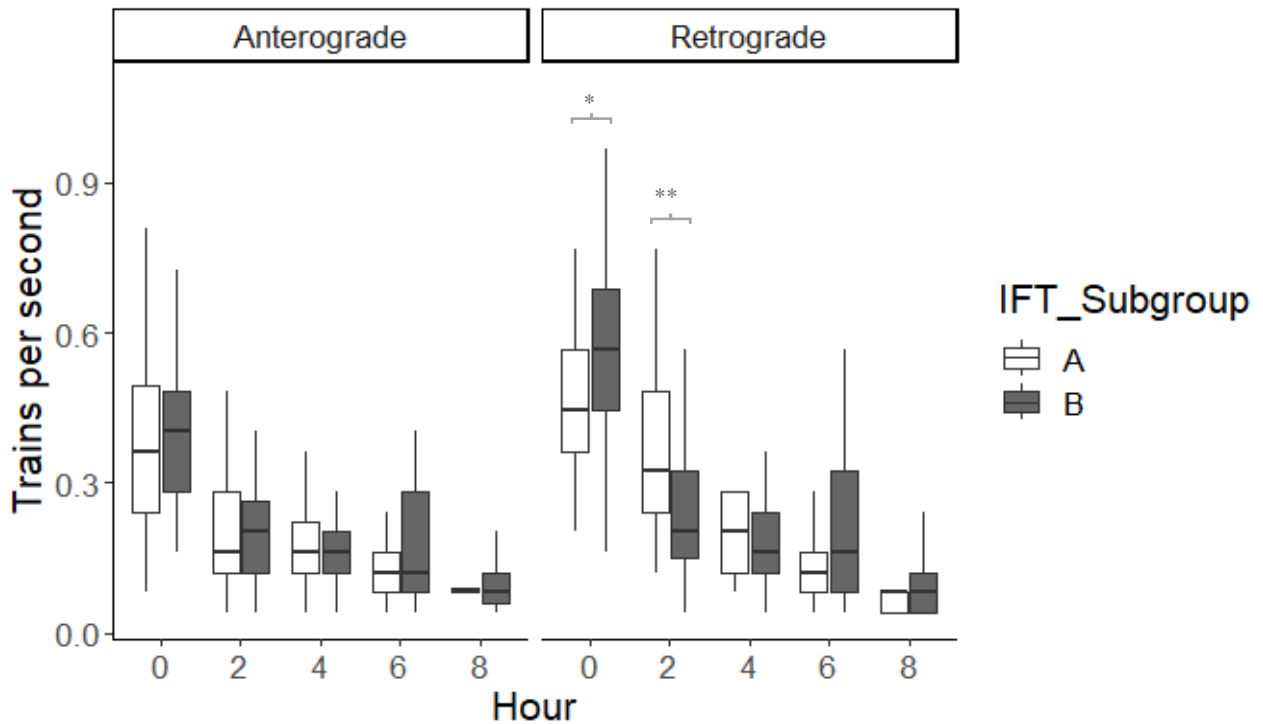
Figure 4.10 Average IFT train numbers grouped into IFT-A and IFT-B proteins. The data from the 3 IFT-A and 4 IFT-B average IFT train numbers were combined to show the average across between IFT-A and IFT-B. Welches t-test comparing IFT-A vs IFT-B from the same time point *(*** = p<0.001, ** = p<0.01, * = p<0.05).* Graphs are shown as box and whisker with the midpoint representing the median.

Next, data was combined from all the individual IFT proteins to highlight the overall trends for the number of trains throughout differentiation. Combined data showed a distinct drop in IFT numbers within two hours, in both directions. In the anterograde direction train number dropped by over 50%, from 0.42 trains s^{-1} to 0.2 trains s^{-1} *(p=<0.001)* (Figure 4.11). From two to eight hours, the train numbers remained between 0.1-0.2 trains s^{-1}. In the retrograde direction, there was also a significant drop in train numbers within two hours, from 0.47-0.29 trains s^{-1}. There was a further drop between two and four hours to 0.17 trains s^{-1}. For the remainder of the differentiation, trains numbers remained under 1.5 trains s^{-1}.

In both directions there was a large drop in IFT numbers, within two hours of differentiation. Whilst anterograde train numbers plateau after two hours, trains numbers in the retrograde direction dropped over the first four hours then slightly drop again at eight hours. This large drop in train number between zero and two hours (as shown in Figure 4.11) is likely to be important for flagellum disassembly particularly the drop in anterograde trains.
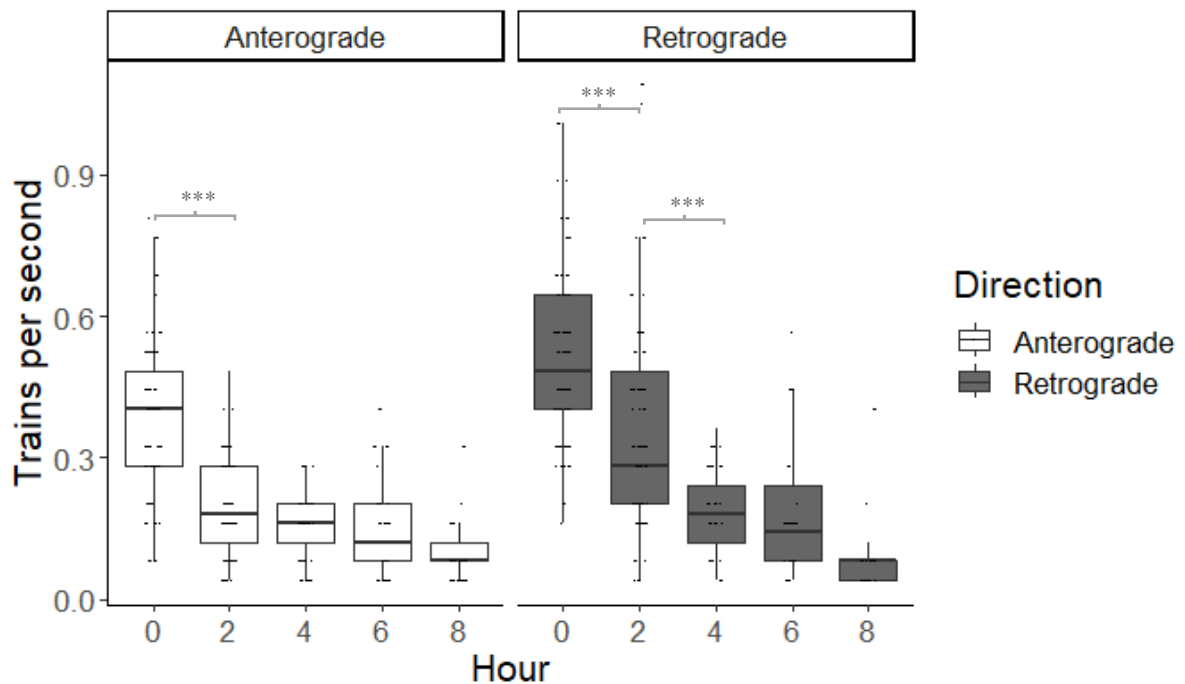
Figure 4.11 Average IFT train numbers combined across all seven tagged cell lines. Combined average train numbers across all cell lines (trains per second). Split into anterograde and retrograde directions. Welches t test comparing average between the subsequent time points *(*** = p<0.001, ** = p<0.001, * = p<0.05)*. Graphs are shown as box and whisker with the midpoint representing the median.

4.7 The ratio of very slow trains increased significantly between with two hours of differentiation.

Previous studies in *T. brucei* have reported a clear subset of 'slow' and 'very slow' trains in procyclic forms (Buisson et al., 2013). In our study there were also clear subsets of slow trains throughout *Leishmania* differentiation. We followed the criteria set by Buisson for 'normal' trains above 1.5 μm/s, 'slow' trains between 1 and 1.5 μm/s and 'very slow' under 1 μm/s. The 'normal' speed trains made up over 90% of tracks collected, slow trains 3.9% (n= 139) and very slow 5.8% (n=207) (Figure 4.12).

Although the slow and very slow trains made up a small proportion of tracks, the proportions changed throughout the time course. In both directions the very slow trains increased significantly between zero and two hours. In the retrograde direction the very slow trains at zero hours made up 3.8% of total tracks and jumped to 12.7% of trains at two hours (z= 6.6, *p=<0.001*). In the anterograde direction, at zero hours very slow trains made up 3% of total tracks whereas at two hours this jumped to 8.6% of tracks (z=4.1, *p=<0.001*). After the proportional increase at two hours observed in both directions, the proportion of slow and very slow trains then decreased. In retrograde trafficking, both categories decreased slightly between two and four hours then remained similar throughout the

remainder of differentiation. In anterograde trains, there was a reduction in the proportion of slow and very slow trains between two and four hours, then a further increase between six and eight hours.

Similar to Bussion, we observed a subset of slow and very slow IFT trains. These trains were small in relative proportion to the overall number of trains, the slow and very slow trains both significantly increased in proportion between zero and two hours in both directions.
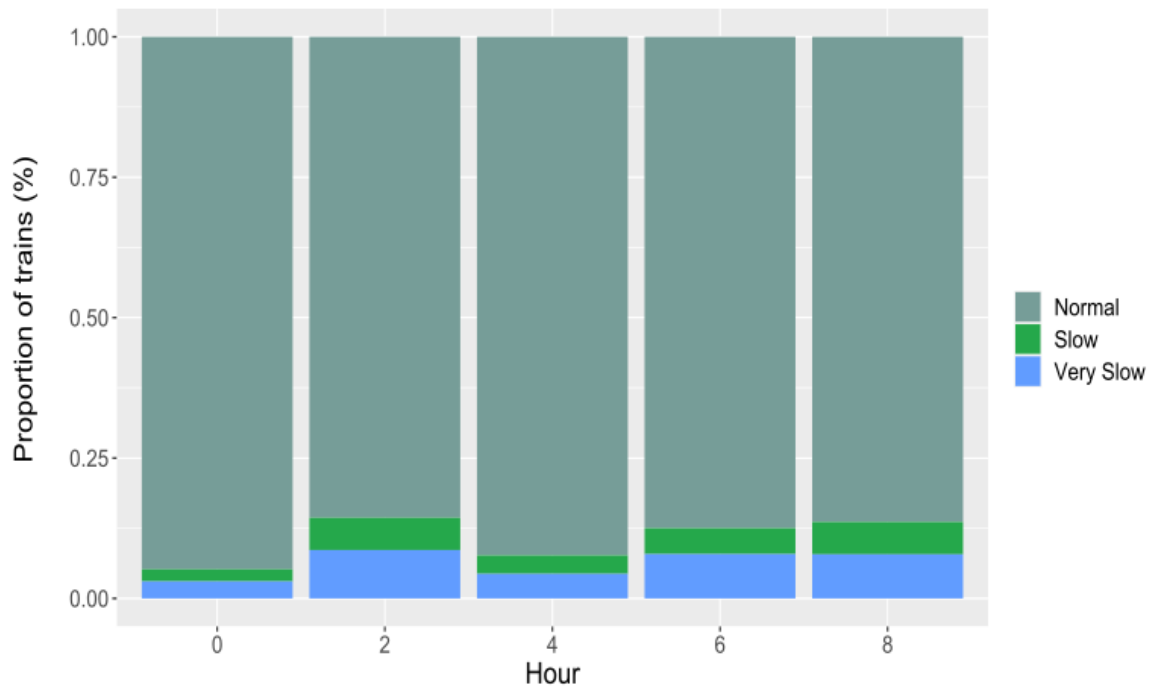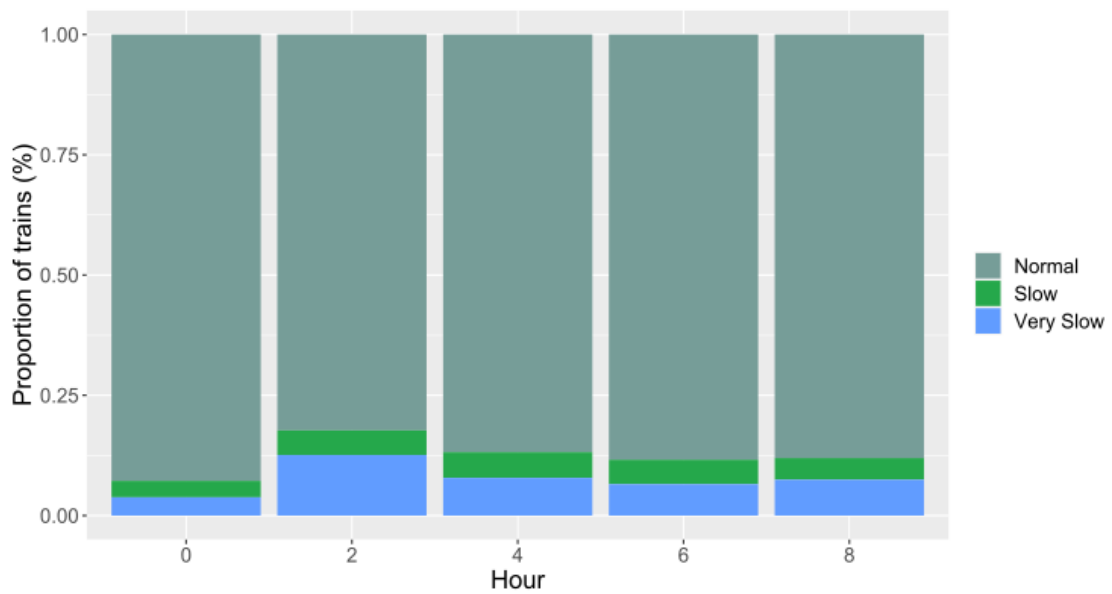
Figure 4.12. Trains can be categorised into different velocity subtypes across early differentiation. IFT trains were classified as either 'Very slow' (< 1 µm/s), 'Slow' (between 1 and 1.5 µm/s) and 'Normal' (> 1.5 µm/s) Significance determined by z-test. Train velocity categories were defined by (Buisson et al., 2013).

4.8 The drop in velocity and train numbers started immediately after differentiation was initiated.

The previous experiments showed that both train number and velocity dropped within the first two hours of differentiation. To pinpoint when this drop occurred, the IFT numbers and velocity in differentiating parasites were analysed in more detail between zero and two hours. From zero to two hours the parasites were imaged every thirty minutes. Along with providing information about the early time points, this extra set of data provided repeats for some of the time points (i.e., zero and two hours) on alternative days and cultures. Here, the data is presented as a combination of all the cell lines.

The drop in IFT velocity happened immediately. In the anterograde direction, the drop in velocity occurred within 30 minutes (Figure 4.13a). The promastigote velocity was 2.8 μm/s, and this dropped at 30 minutes to under 2 μm/s. At the one hour time point there was a slight increase to a little over 2 μm/s and this average velocity remained the same throughout early differentiation. In the retrograde direction a similar drop in train velocity at 30 minutes from 3.4 μm/s to 2.4 μm/s was observed. At the one hour timepoint there was a slight increase to 2.9 μm/s, until the six hour time point the velocity remained around 2.6 μm/s. Then at six hours, the increase in velocity was reported (as reported in section 4.5.1), then a further drop at eight hours.

A similar immediate drop was observed for IFT numbers. In the anterograde direction, the train numbers dropped from 0.32 trains s^{-1} to 0.27 trains s^{-1} within 30 minutes of differentiation (Figure 4.13b). The anterograde IFT numbers remained at a similar level throughout the remainder of the time series. In the retrograde direction the reduction occurred more gradually. Within 30 minutes, train numbers decreased from 0.47 trains s^{-1} to 0.35 trains s^{-1}. These average numbers of trains remain at a similarly low level until two hours, here the train numbers slowly began to decrease over differentiation, until at eight hours the average numbers were 1 trains s^{-1}.

By analysing these early time points we were able to detect the immediate drop in IFT numbers seen in the anterograde direction and the gradual decrease in numbers from zero to two hours in the retrograde direction.
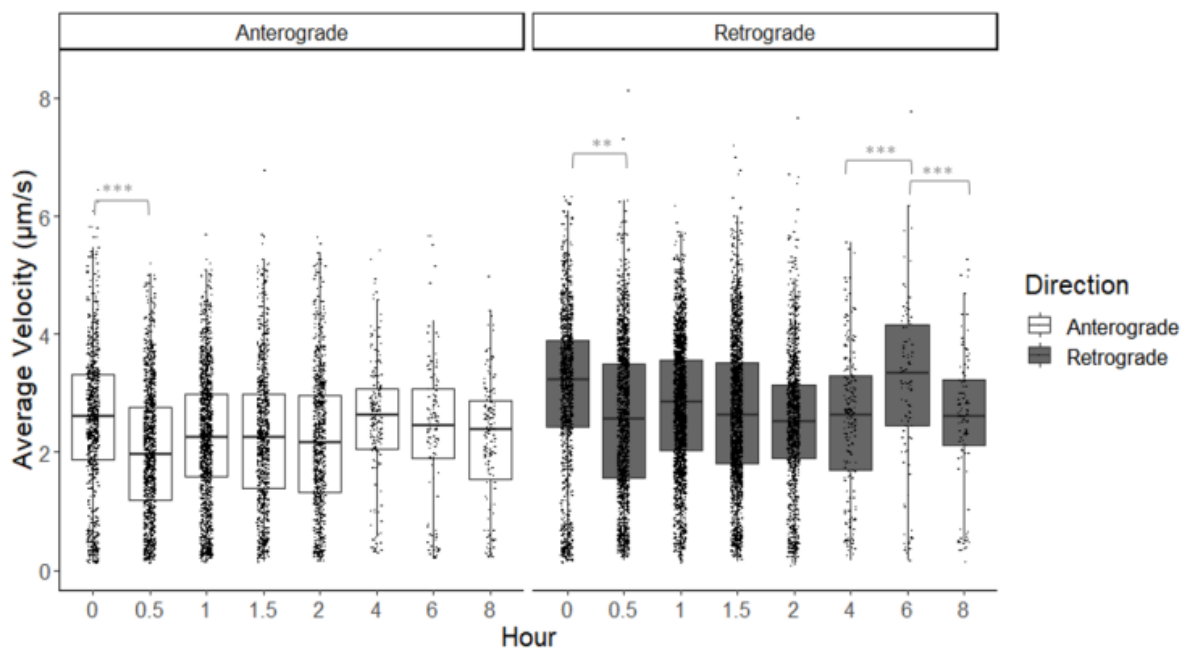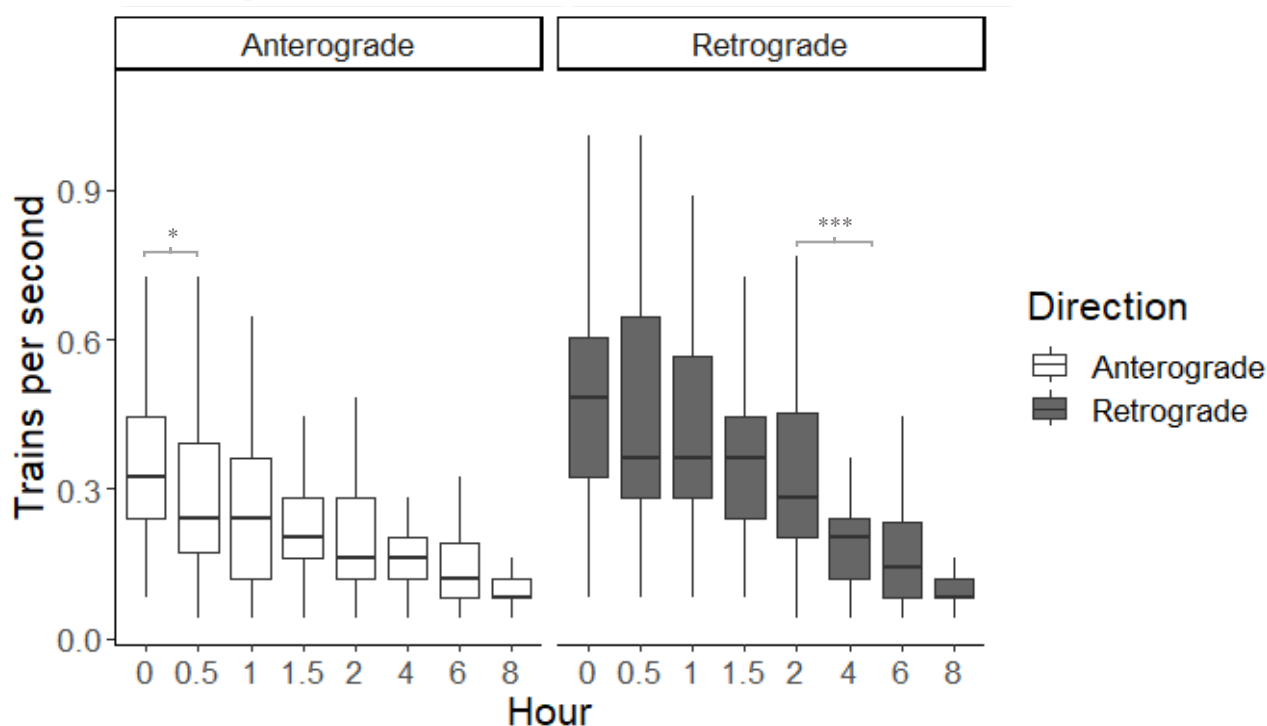
Figure 4.13. Average IFT velocities and train numbers combined across early differentiation time points A. Combined average velocities across all cell lines (μm/s) in the early stages of differentiation to amastigotes 0-8 hours. Split into anterograde and retrograde directions. **B.** Combined average train numbers across all cell lines (trains per micron) in the early stages of differentiation to amastigotes 0-8 hours. Split into anterograde and retrograde directions. Graphs are shown as box and whisker with the midpoint representing the median. Welches t test comparing average between the subsequent time points *(*** = p<0.001, ** = p<0.001, * = p<0.05*).

4.9 The relationship between frequency, velocity, and flagellum length.

Previous sections have demonstrated the how flagella length, train velocity and train numbers all decrease during differentiation. Figure 4.14 shows the relationship between the three variables, grouped by the time of differentiation. There appears to be no clear relationship between all three, and instead a stronger relationship between the time of differentiation and each of the variables. A cluster of eight hour time points (indicated by yellow points Figure 4.14c) is observed with low train numbers, velocity, and short length. The subset of trains with a slow and very slow velocity can also be visualised. Flagella with an average slow velocity (<1 μm/s) show a distinct cluster, but these flagella exhibit a range of train frequencies and lengths (Figure 4.14b). Although not definitive, this suggests that there may be other factors during differentiation that is impacting IFT velocity and numbers beside from just flagellum length.
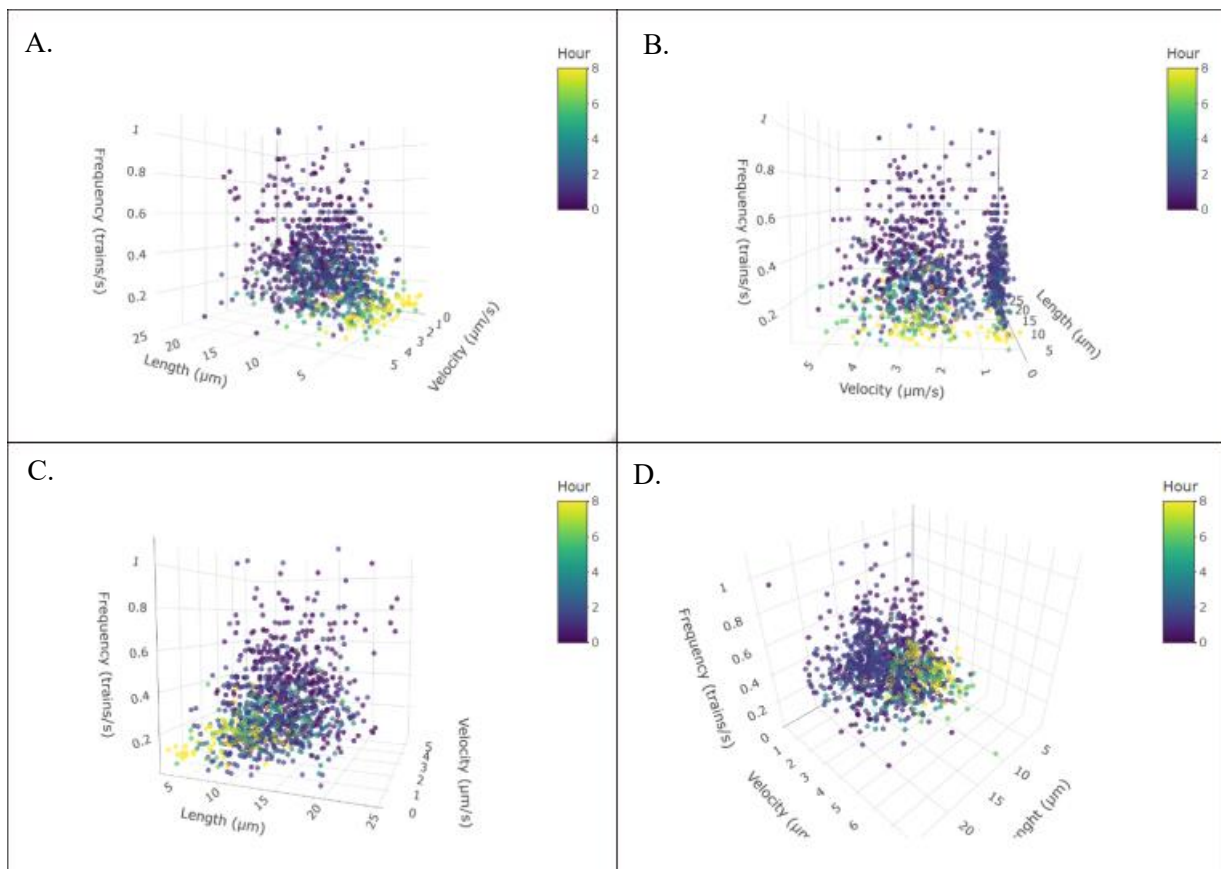
Figure 4.14. The relationship between train frequency, velocity, and flagellum length over parasite differentiation. Individual points represent the average velocity and frequency per flagellum. Four orientations of the same plot are shown. 3D scatterplot created with R package Plotly.

4.10 IFT is still present in both the old and new flagellum.

Dividing *Leishmania* parasites have two flagella; the old that will be disassembling and the new which will likely be synthesising the 9v flagellum *de novo*. Unfortunately, there were very few dividing (2F) parasites observed during these experiments and not enough dividing cells with both flagella in focus were present in order to effectively compare the IFT velocity and numbers between the two flagella. There were extremely few 2F cells in the later stages of the differentiation (i.e., four-eight hours). Figure 4.15 shows examples of various cell lines expressing fluorescently tagged IFT proteins in dividing cells at different stages of early differentiation. Both flagella had an IFT signal around the pool and randomly distributed along the flagellum suggesting that IFT is operating during both maintenance and assembly, a similar distribution was also seen in *T. brucei* (Absalon et al., 2008a). During differentiation, in the few parasites that were captured where the cell remained still and in focus, there is evidence of IFT movement particularly close to the IFT pool in both flagella also (see supplemental vidoes 4o-4r). This shows that IFT was present in the old and new flagellum during flagellum disassembly however, here it was not possible to accurately track the IFT trains.
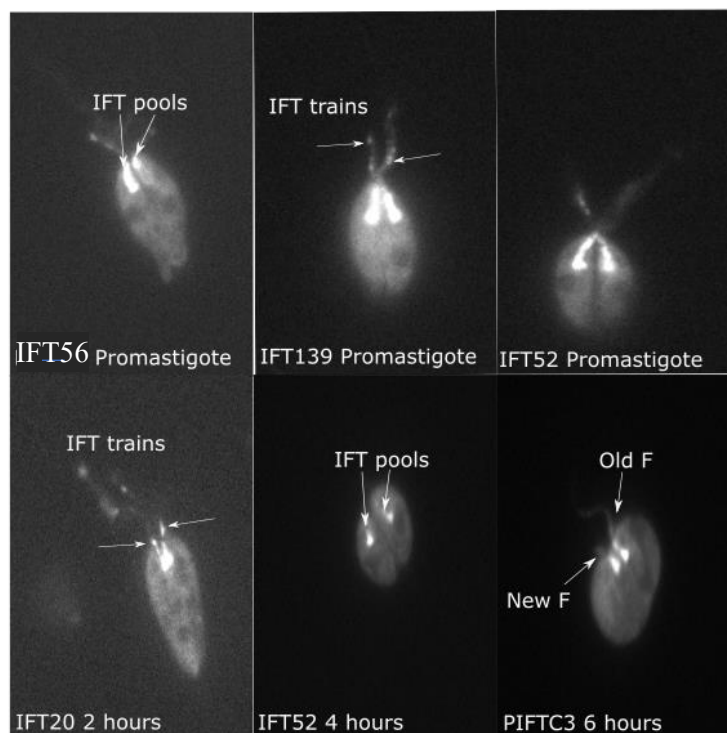
Figure 4.15 Dividing *L. mexicana* parasites retain an IFT signal in both the old and new flagellum. Examples of dividing parasites with various endogenously tagged IFT signals are shown. The IFT is present in both the new and the old flagellum and in parasites during late division there are two IFT pools present.

4.11 IFT pool was present in attached forms, but IFT trafficking was rarely seen.

The results from the previous sections focused upon differentiation to amastigotes. However, *Leishmania* parasites can also differentiate to a range of life cycle stages, including the attached haptomonad forms (Figure 1.6a). Haptomonads have a modified flagellum, which facilitates attachment to the sand fly stomedal valve. In the present study, *in vitro* attached *Leishmania* parasites were generated by plating dense cultures on glass, gridded coverslips for 24 hours. Parasites adhered to the surface of the coverslips with their flagellum but due to the orientation and movement of the parasites it was difficult to track IFT proteins in the flagellum. However, the presence and localisation of IFT proteins in the parasite's flagellum could be determined with this method.

Parasites readily adhered within 12 hours and tended to adhere in large clusters (Figure 4.16a). A recent paper described the attachment plaque and the parasite attachment process (Yanase et al., 2022). First parasites undergo localised attachment with the flagellum, this then progresses to stable attachment, sometimes with the formation of a looped flagellum. The flagellum then shortens and finally, late-stage attachment results in the formation of a dense attachment plaque. Figure 4.16b shows parasites in the loop stage and also at later attached forms with the dense attachment plaque.

Promastigotes, expressing IFT74::mNG were plated onto coverslips and parasites at different stages of attachment were imaged. Figure 4.16b depicts early attached forms with the looped flagellum, IFT proteins were seen in the IFT pool and moving along the flagellum however, proteins appeared to not enter the loop region (also shown in supplemental videos 4u-4v). The low IFT protein signal in the flagellum loop suggests that IFT may not be entering the loop or entering at greatly reduced levels.

In parasites that were further along in the attachment process, there was a bright signal at the IFT pool and a very faint signal in the plaque (Figure 4.14b-c, supplemental videos 4s,4t, 4w). The videos do not show evidence of IFT movement in these later attached parasites, suggesting that there is little IFT trafficking in these attached forms, but an IFT signal is still present.
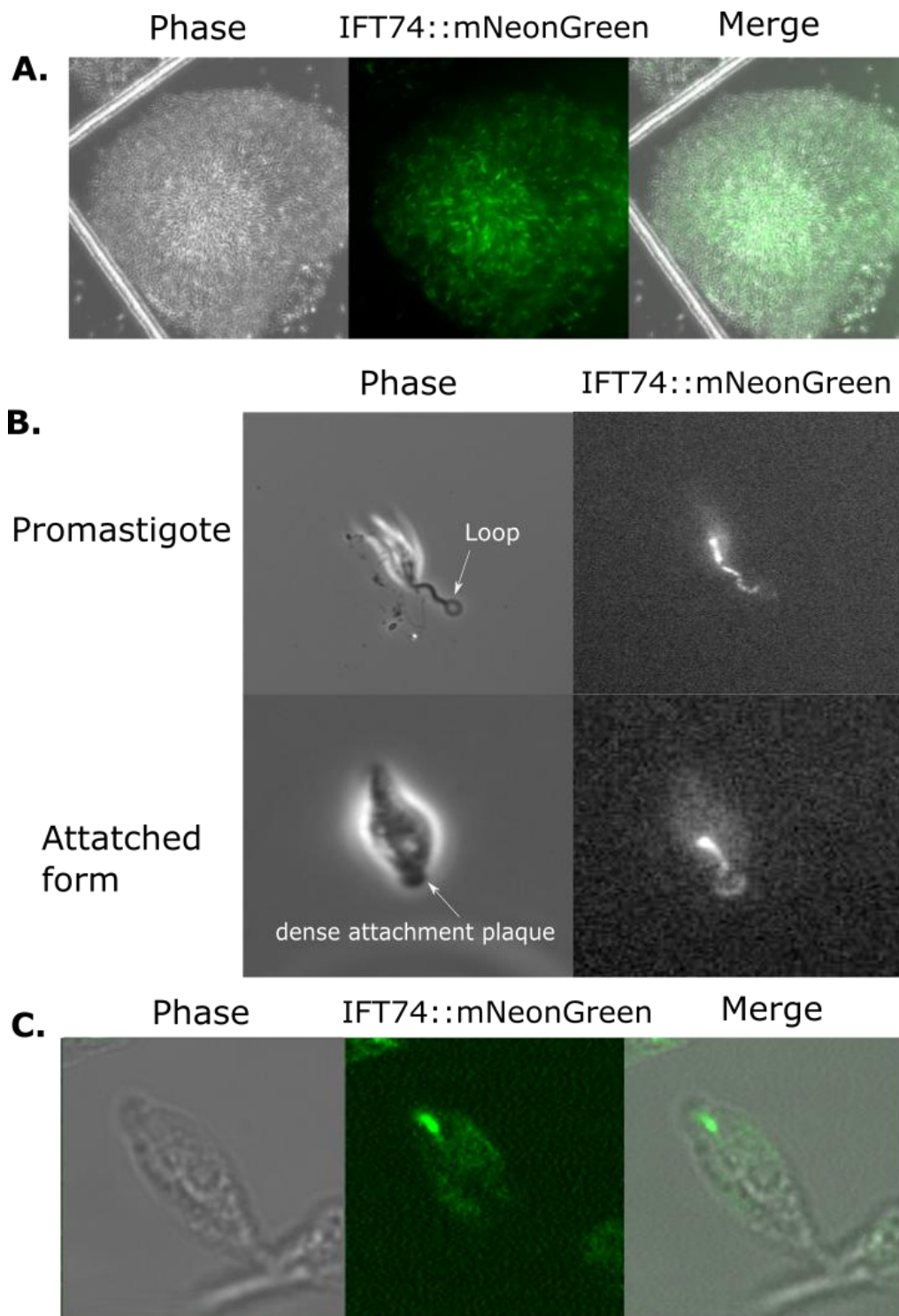
Figure 4.16 _L. mexicana in vitro_ generation of haptomonads A. Large aggregates of attached haptomonads are commonly observed. **B.** When initiating attachment, the distal portion of the flagellum forms a loop. Inside the loop there is a reduced IFT74::mNG signal in comparison to the rest of the flagellum. The later attached forms have a bright IFT signal in the IFT and very little in the plaque. In this example there is some evidence of a faint signal that forms a loop inside the plaque **C**. The majority of attached forms showed a concentrated IFT signal around the IFT pool and little to none in the plaque.

4.12 Discussion

Within eight hours of differentiation, the *Leishmania* flagella had decreased in length by at least 50%. This was correlated with a large drop in both IFT numbers and velocity within thirty minutes of differentiation, this occurred much quicker than previously reported (Wheeler, 2015). How these reductions in IFT relate to the parasite's biology will be discussed.

4.12.1 IFT velocity and train numbers are highly variable.

In the current study, the velocities and IFT train numbers from the individual cell lines were highly variable yet, the overall trend showed that both the velocity and numbers decreased over differentiation. Efforts were made to ensure imaging conditions remained consistent i.e., all parasites were taken from growing cultures at a density of $1x10^6$ - $1x10^7$ cells mL and were imaged within ten minutes of being placed on the slide. However, due to timing constraints, these cell lines had to be imaged across different days. Therefore, factors such as cell line growth, different batches of media/buffers, the age of the flagellum, and sample preparation could account for some differences in velocities and numbers. In fact, other studies have also reported variable IFT numbers and velocities even between the same cell lines and even between different flagella of the same cell (Jiang et al., 2015).

Another important note is the asynchronicity of the cultures. Although a similar density of parasites was used, we did not control for the cell cycle stage nor age of the flagellum. IFT proteins have been associated with non-IFT roles during cell division and the localisation and accumulation of IFT proteins varies during the cell cycle, however these roles have yet to be shown to occur in *Leishmania* or *T. brucei* (Vitre et al., 2020; Wood et al., 2012). Factors such as these could affect the IFT velocities and numbers in the flagellum, depending on the cell cycle stage. The cell cycle stage, culture media and temperature can also influence when the parasites initiate differentiation (Barak et al., 2005; Dagger et al., 2018; Leon et al., 1995). For example, in *L. donovani,* parasites were synchronised at the G1 stage and then exposed to the differentiation signal (i.e., change of pH and temperature). G1 parasites started expressing an amastigote marker, A2, within one hour whereas parasites arrested at G2 stage took up to six hours to express A2 (Barak et al., 2005) .The authors propose that parasites begin to undergo differentiation during G1. As over 80% of *L, mexicana* parasites are at the G1 phase in growing cultures, this is unlikely to solely account for the high variability seen in the present study (Wheeler et al., 2011b). Although, the cell cycle stage proportions have yet to be recorded in parasites undergoing differentiation. However, with the smaller samples in the individual cell lines, the effect of the 20% of parasites not in G1 could be amplified and potentially account for some of the IFT number and velocity variation seen in the later stages of differentiation.

Synchronisation of parasites can be achieved with low doses of the anti-cancer drug hydroxyurea (Martinez-Rojano et al., 2008). However, higher doses are toxic to *Leishmania* and the effect of the drug on IFT is unknown. The aim of the present study was to determine how IFT functions throughout differentiation; therefore, set out to complete the experiment drug free to avoid drug-toxicity effects.

The present study also did not take flagellum age into account. Previous studies have shown that the old and new flagellum of *T. brucei* have different IFT properties (Absalon et al., 2008b). *Leishmania,* species also possess a new and an old flagellum during cell division. We showed that IFT was present in both the new and the old flagellum (Figure 4.15) but due to the low number of dividing parasites we were not able to quantify IFT velocities or numbers. However, the *Leishmania* flagellum grows differently to *T. brucei.* The flagellum of *T. brucei* will grow until a certain length, then 'lock' the length throughout cell division cycles (Bertiaux, Morga, Blisnick, Rotureau, & Bastin, 2018b). On the other hand, the flagellum of *L. mexicana* continues to grow over multiple cell division cycles (Wheeler et al., 2011b). In fact, there was little association between flagellum length and cell cycle progression. Therefore, a direct comparison between the old and new flagellum cannot be interpreted as the maintaining and growing flagellum. This large variation in flagellum length and therefore flagellum age could account for the high degree of variability observed withing the cell lines. However, when flagellum length was compared to IFT velocity and numbers, there appeared to be no correlation (Figure 4.14).

Overall, by combining the velocities from multiple cell lines we increased the power of our findings and also the individual cell lines may act as biological replicates. Therefore, although the individual cell lines show large variability, when combined they become adequately powered to address the question. Ultimately, although variable, the numbers and velocity of IFT generally decreased rapidly after differentiation began and were lower in the early amastigotes compared to promastigotes.

4.12.2 IFT velocities of *L. mexicana* were quicker than previously recorded.

In this report we show that IFT velocities were quicker than previously reported. Wheeler showed that *L. mexicana* promastigotes had velocities of 1.6 μm/s for anterograde trains and 1.5 μm/s for retrograde trains, whilst this study reported 2.8 μm/s and 3.3 μm/s for anterograde and retrograde velocities, respectively. It is not clear why there are discrepancies between the IFT velocities reported in this study and those reported in Wheeler's study. One factor could be differences in analysis methods. For instance, in our analyses if an IFT train moved less than 0.5 μm during the video the velocity was not recorded. It is unclear if the Wheeler paper has similar inclusion criteria. Ultimately, this highlights the limitations of measuring values such as velocity and IFT numbers as the analysis methods can differ vastly between groups. Therefore, emphasis on the changes in velocities during the

differentiation rather than the actual numbers may be more important.It is also interesting to highlight that when compared with other reported IFT velocities, the Wheeler numbers are comparably lower. For example, in *Chlamydomonas* IFT velocities were ~2 μm/s and 3 μm/s for antegrade and retrograde trains and *T. brucei* was 2.4 μm/s and 5.6 μm/s (Buisson et al., 2013; Kozminski et al., 1993). This again could be differences in the analysis methods between studies.

Across a wide array of species there appears to be a positive correlation between flagellum length and IFT velocity. Organisms with longer flagella (+10 μm) such as *Chlamydomonas* and *T. brucei* tend to have faster IFT velocities (~2-3 μm/s) whereas shorter flagella such as those in *C. elegans* and mammalian primary cilia tend to have slower IFT velocities (~0.5 μm/s) (Table 1.1). In *Chlamydomonas,* as flagellum length increases there is an almost linear increase in IFT velocity (Engel et al., 2009). In other systems length does not appear to influence IFT velocity, or vice versa. This can be seen in the parasite *Giardia* as there were no reported differences in IFT rates, number, or size of trains between its four sets of flagella (McInally et al., 2019).

In the present study, we found that during differentiation there was a decrease in velocity observed in the shorter flagellum of the eight-hour amastigotes. Although the IFT velocity decreased as the flagellum shortened, these slower velocities were lower than those reported from flagella of comparable lengths across different species. For example, the eight hour differentiating parasites had an average flagellum length of ~5 μm and had average velocities of 2.2 and 2.5 μm/s (anterograde and retrograde, respectively). Whilst *Tetrahymena* have an average flagellum length of 4.7 μm and show a much slower IFT velocity of 0.98 -1.43 μm/s (anterograde and retrograde, respectively) (Jiang et al., 2015; Rajagopalan et al., 2009). This could imply that IFT train velocity may be correlated with flagellum length, but other factors perhaps the rate of flagellum turnover or the biological role of the flagellum (sensory vs motility) may be important.

4.12.3 IFT trains are composed of IFT-A and IFT-B – so why are there differences in the IFT numbers?

IFT trains travel as multi-protein complexes; composed of rows of IFT-A and IFT-B sub-complexes (Van Den Hoek et al., 2021). However, we report some differences between IFT-A and IFT-B numbers and velocity. The variability seen in the individual cell lines is likely the underlying cause of the differences in IFT velocity and numbers between IFT-A and B proteins. Factors mentioned previously such as cell line variability, growth media, and imaging across multiple days are likely at play.

Yet, there is a consistent increase in velocity observed at six hours with IFT-B proteins, travelling in the retrograde direction. These cell lines were imaged across multiple days and the order of imaging of IFT-A/B proteins was random. Therefore, this increase could be attributed to IFT variability but as this occurred across multiple cell lines, this could be the result of a true increase in velocity at six

hours. The true reason for this increase cannot be inferred from only these experiments. However, many factors could be contributing to the peak in velocity at six hours.

Firstly, as previously mentioned there is a large range of flagellum lengths across parasites. Figure 4.3 shows the large range of flagellum lengths, particularly at six hours. At six hours flagellum length is positively skewed towards shorter flagellum, meaning that most parasites had a short flagellum, although parasites with longer flagella still remains. Longer flagella tend to have faster IFT velocities, meaning that the IFT speeds from parasites with long flagella at six hours are likely contributing to increase in IFT velocity seen at this time point.

However, this does not explain why the velocities only increased in the IFT-B and not the IFT-A proteins. Retrograde IFT-B proteins at six hours did show a very large range of train velocities, suggesting there are still IFT trains present that have faster velocities. As the data is not skewed at this time point, it suggests that the range of velocities is not caused by a subset of fast or slow IFT trains, but instead a normal distribution of velocities is present. This could suggest there are some unusual IFT dynamics occurring with at six hours within the flagellum that our data does not capture.

We can begin to explore non-conventional hypotheses here. For example, the non-uniformity of the flagellum could be contributing to the small peak in velocity observed at six hours. Along the length of the flagellum, various proteins are positioned asymmetrically. For example, there is a proximal/distal segregation in the outer dynein arm complex (B. F. L. Edwards et al., 2018). This means that as the flagellum disassembles, the assembly of different flagellar structures within different sections of the flagellum are encountered. Hypothetically, this could impact the rates of assembly and therefore loading of IFT trains. For example, regions of high complexity could disassemble more slowly than more simple structures. In the case of *Leishmania,* as the flagellum disassembles if there is a less complex region at the point of six hours into disassembly then perhaps this would enable quicker axoneme disassembly and perhaps faster IFT trains. However, at this stage this is speculative and further knowledge of the dynamics of individual axoneme components rate of assembly and disassembly is required.

Another factor that could influence IFT velocity could be the potential changes in train composition. Structural analyses of IFT trains showed that they were composed of rows of IFT-A and IFT-B proteins (Jordan et al., 2018a). These trains then unfold at the flagellum tip and are restructured to retrograde trains (Van Den Hoek et al., 2021). Let us consider that as IFT trains reach the flagellum tip and disassemble, they could reorganise themselves into retrograde trains with a varying composition of IFT proteins. Some trains could be larger than others and with different numbers of particular proteins on each train. These claims are conjectural but raises and important question whether retrograde IFT trains share a similar structure, a question that could be addressed by detailed structural analyses of IFT trains from a range of organisms.

However, these claims alone cannot explain the increase only in retrograde IFT trains at six hours. Therefore, the varying flagellum length coupled with large variability in IFT velocities recorded across cell lines is a likely explanation.

4.12.4 The ratio of anterograde to retrograde numbers is lower than previously reported.

Here, we showed that that retrograde trains were more abundant than anterograde trains. Older reports showed a 1:1 ratio between anterograde and retrograde trains (McInally et al., 2019). However, with the introduction of higher resolution imaging methods, there is now believed to be a 1:3 ratio of anterograde to retrograde trains(Chien et al., 2017). Retrograde trains are roughly three times shorter than their anterograde counterparts and experimentally three-fold more retrograde trains can be detected in kymographs (Pigino et al., 2009). In our findings, in promastigotes, retrograde trains were on average 1.3 times more abundant than anterograde trains. At eight hours into differentiation, this dropped to a 1:1 ratio of anterograde to retrograde trains. In procyclic *T. brucei,* retrograde trains were 2.8 times more abundant than anterograde trains (Buisson et al., 2013). Although the average numbers of anterograde trains were comparable between the two studies (the present =0.8, Buisson= 0.86), the retrograde train numbers were substantially higher in the Buisson study (the present=1, Buisson=2.5).

One explanation for the differences between the ratio of anterograde and retrograde trains between the present study and Buisson's could be the imaging method. As retrograde trains are smaller in size, they often have a lower signal intensity in microscopy experiments than anterograde trains (Lechtreck et al., 2009b). Therefore, in the present study, the imaging method may not have accurately detected all of the retrograde trains in the flagellum.

Additionally, there are distinct differences between the flagellum structure of *Leishmania* and *T. brucei,* which could impact how IFT is imaged between the two species. If we assume that both parasite species have a restricted set of microtubule doublets that IFT trains can travel along, then IFT trains may not be as visible in some orientations (Bertiaux et al., 2018). The Trypanosome flagellum is mostly connected to the cell body; therefore, the attached region of the flagellum will be more likely to be orientated the same way across different parasites. However, the *Leishmania* flagellum is mostly unattached to the cell body and the flagellum can orientate in multiple ways. These differences in orientation could impact the number of IFT trains that were visualised and partially explain why there are reduced numbers of retrograde trains visualised in the present study.

However, it could be the case that the ratio seen between anterograde and retrograde trains is a true ratio and not due to technical issues. However, further high resolution imaging strategies to capture the smaller retrograde trains are needed to address this issue. For example, capturing the structure of the smaller retrograde trains from TEM, CLEM, or expansion microscopy would allow more accurate predictions to the shape and size of retrograde trains in trypanosomatids. Utilising super resolution techniques to capture IFT trains *in vivo* could be achieved via methods such as high speed super

resolution microscopy (SPEED) would not only enable higher resolution imaging to capture the smaller retrograde trains but also address the spatial distribution of anterograde and retrograde trains within the flagellum (Ruba et al., 2018).

4.12.5 IFT is present in the attached forms.

We showed that throughout early differentiation from promastigotes to amastigotes, IFT remained active. But was this the case with other *Leishmania* life cycle stages? Figure 1.6a details the many different life cycle stages of the parasite, each with different flagellum morphology. In the present study, we began to observe how IFT functions in the attached forms, also known as haptomonads.

Until recently, relatively little was known about the formation or structure of haptomonads. However, a recent study detailed the structure of the attached flagellum and how haptomonads form *in vitro* (Yanase et al, 2022)*. In vitro,* the promastigotes first begin to probe the surface with their flagellum and form a localised flagellum attachment. In some cases, a flagellum loop is formed, and the parasites undergo subsequent stable attachment and flagellum disassembly to form mature attachment. Haptomonads have an expanded flagellum membrane, which encapsulates a short 9+2 axoneme. From the experiments presented in this chapter, the attached forms retained a strong signal in the IFT pool.

In parasites in early stages of attachment, we observed the formation of a 'loop' (Figure 4.16). Notably, IFT can be seen traversing along the length of the flagellum but when the trains reach the loop they appear to become stationary and not enter. Inside the loop formation, IFT is much more infrequent or not present at all. One explanation is that the loop was slightly out of focus, so it was difficult to capture the IFT movement.

An alternative, intriguing explanation could be that the formation of the loop could be blocking IFT entry/exit from the loop. In *C. elegans,* researchers demonstrated that applying external pressure on points along the flagellum could successfully block IFT from passing (Nievergelt et al., 2022). This also demonstrated the intrinsic ability of *C. elegans* anterograde IFT trains to convert to retrograde trains at various points along the flagellum. The conversion was triggered by applying an external force to the flagellum membrane to block IFT passing that point and triggering IFT conversion. In the present study, the loop seen in the early attachment stages of haptomonads could potentially be applying pressure at that point of the flagellum; thereby, blocking IFT passage and potentially triggering IFT train conversion. Further experiments may aim to optimise IFT tracking in attached forms and potentially quantify turnaround at the entrance to the flagellum. For example, TEM analysis detailing the IFT train structure both in and out of the loop may provide insight into the structural differences. As a proof of concept, replicating the Nievergelt study with *Leishmania* to show that external pressure can block IFT movement would be beneficial. From there, the loop formation could be a useful too to study this phenomenon is a naturally occurring setting (with the

caveat that currently the loop has only been observed in *in vitro* haptomonad formation (Yanase et al., 2022).

4.12.6 Can the balance point model explain flagellum shortening in *Leishmania*?

The balance point model is one of the most widely accepted models of flagellum growth. The model was first described by Marshall and Rosenbaum and states that flagellum length is a balancing act between assembly and disassembly (Marshall and Rosenbaum, 2001). If assembly is favoured the flagellum grows, if disassembly is favoured the flagellum shortens.

In the present study, a large drop in IFT train numbers occurred within 30 minutes of the initiation of differentiation. In the anterograde direction, IFT numbers dropped immediately, whilst in the retrograde direction IFT numbers gradually decreased over the first four hours of differentiation (Figure 4.13b). The large drop in IFT trains numbers may also reduce the capacity for flagellar components to be transported into the flagellum. In this case, the balance point model would suggest that the reduction of IFT would reduce axoneme assembly, shift the balance to favour axoneme disassembly and ultimately drive flagellum shortening.

However, the balance point model may be oversimplistic to explain flagellum shortening during *Leishmania* differentiation. Firstly, there are at least two known ways that *Leishmania* flagella shortens during differentiation; disassembly of full length flagellum or *de novo* construction of a short flagellum after cell division (see Figure 1.7) (Wheeler et al, 2015). In the present study, based on Wheelers previous analyses, we can assume that the majority of flagella observed during the first 0-2 hours of differentiation are undergoing disassembly. It is possible that by the later stages of differentiation, 4-8 hours, a larger proportion of short flagellum have been constructed *de novo.* Therefore, in the first few hours of differentiation, flagellum shortening could be explained by the balance point model, i.e., a reduction in IFT is driving flagellum shortening. However, the *de novo* construction of short flagella cannot be explained by this model. The fact that there are at least two distinct flagellum types in the parasite cultures makes it difficult to compare how they are disassembled or assembled. Although experimentally challenging, it could be useful to separate the *de novo* constructed flagella to the disassembling flagella as the flagellum construction of these two types are achieved by different mechanisms.

The balance point model also suggests that the overall quantity of IFT material remains the same, regardless of the length of the flagellum. The models suggests that IFT trains in shorter flagella are longer (more IFT proteins in one train) and as flagella grow the trains break up and become shorter and more dispersed (Engel et al., 2009). However, this is not the case in *Leishmania* as it has been shown that during flagellum shortening the amount quantity of IFT reduces. Previously, Wheeler determined the total amount of IFT by quantifying total fluorescence in the *Leishmania* flagellum and found that there was a huge reduction in amount the tagged IFT52 as the flagellum shortened

(Wheeler et al., 2015). Quantification of fluorescence inside the flagellum would not be impacted by the size of IFT trains, only the total amount of IFT. This reduction is also reflected in the reduction in counts of IFT trains shown in the experiments presented in this chapter. Therefore, in the *Leishmania* disassembling flagellum the balance point model may not be applicable.

4.12.7. Alternative explanation for flagella shortening in the *Leishmania* flagella.

In the experiments presented in this chapter, we demonstrate that a drop in IFT velocity and number were associated with flagellum shortening. As discussed in section 4.12.6, the balance point model may not be applicable to *Leishmania* during differentiation. Therefore, what alternative models/mechanism could impact flagellum disassembly.

Before alternative models can be discussed, it is important to note an important limitation of the experiments in this chapter; they do not address whether the drop in IFT led to flagellum shortening or whether the drop in flagellum shortening led to a reduction in IFT. However, it could be argued that due to the rapid reduction in IFT numbers within 30 minutes, it is likely that this drop in IFT is driving flagellum shortening.

However, to definitely state that this is the case further experiments should be conducted. For example, the use of microtubule stabilising agents would prevent the axoneme from disassembling and therefore shortening (Wordeman & Vicente, 2021). If parasites with stabilised flagella were exposed to differentiation factors they would not be able to shorten the flagellum, but the IFT from these stabilised flagella could be analysed to determine if a drop was still observed. If this was the case, this may suggest that the drop in IFT preceded flagella shortening. Alternatively, if mutations were introduced into either the kinesin or dynein, rendering them non-functional, this would prevent IFT trafficking. If these mutants were exposed to differentiation factors and were able to successfully shorten the flagella this would suggest that flagella shortening occurs independently of IFT.

4.12.8. IFT may function differently across different organisms.

Throughout this report we have made assumptions about the *Leishmania* flagellum based upon findings from other flagellates such as *Chlamydomonas* and *T. brucei*. Granted, IFT proteins share remarkably similarity; however, the distinct flagellum biology of these organisms should not be overlooked.

In the algae *Chlamydomonas,* the flagellum is important in motility, mating, and sensing (Cross & Umen, 2015; Ringo, 1967b). During mating *Chlamydomonas* gametes fuse together to form a zygote with four flagella, then all flagella shorten simultaneously over the course of around 2 hours (J. Pan & Snell, 2005). In these shortening flagella (either triggered by mating or a shortening inducing agent), IFT proteins and motors are stimulated. Within 30 minutes of shortening, the entry of IFT-A and IFT-B trains and motors into the flagellum increased 4-fold, when compared to wild type cells. Additionally, the rate of putative IFT cargo (in this case radial spoke proteins) did not increase in the shortening

flagellum, despite the large influx of IFT trains entering the flagellum. These findings suggest that IFT trains may are actively involved in flagellum disassembly in *Chlamydomonas.* The fact that putative cargoes do not increase at the same rate of IFT proteins may even suggest that the influx of IFT is to carry 'empty trains' to the tip to enable disassembly.

In comparison, *Leishmania* parasites have a significantly slower period of flagellum shortening; over 24 hours to achieve full amastigote differentiation and around 8 hours for early amastigotes. In the *Leishmania* shortening flagellum, it has been shown that there is a huge drop in IFT in the flagellum after 4 hours suggesting it is the lack of IFT rather than the influx of it that facilitates disassembly (Wheeler et al, 2015). The authors suggest that the differences in time taken to shorten the flagellum between the species may account for the differences in IFT dynamics. The results presented in this chapter also corroborate that a large drop in IFT proteins is correlated with flagella shortening. However, we found that there were still trafficking of IFT trains in the flagellum of early amastigotes and the sudden drop in anterograde IFT numbers occurs within 30 minutes of differentiation (Figure 4.13b).

There are also structural differences in flagellum organisation between different species, which may impact disassembly dynamics. There are distinct differences in the tip organisation between *Chlamydomonas* and kinetoplastids parasites (Gluenz et al., 2010; Morga & Cilia, 2013). *Chlamydomonas* builds its flagella by simultaneously assembling the axoneme, securing the growing axoneme with 'anchors' connecting it to the flagellum membrane (Höög et al., 2014). At the flagellum tip is an electron dense central pair cap is present. Whilst *T. brucei* (a close relative of *Leishmania*), grows its flagellum by extending it's the axoneme in a disordered manner then stabilising with proteins such as radial spokes. *T. brucei* do not have anchors or a central pair cap.

These differences in assembly and flagellum structure could explain how *Chlamydomonas* is able to assemble its flagellum at 24 μm/hour and 9 μm/hour for short and long flagellum respectively, whilst the flagellum in *T. brucei* grows more slowly at a constant rate of 4 μm/hour (Höög et al., 2014). Therefore, this may also be the case for the reverse process. If disassembly occurs in a similar disordered manner rather than simultaneous and controlled, this will inevitably take longer and would not require the huge influx of IFT trains, but rather a reduced number of IFT trains would be needed continuously over the disassembly period.

4.13 Summary

The data presented here gives a clear indication that *Leishmania* flagellum disassembly is triggered within 30 minutes. The biggest driver for this change seems to be the large reduction in IFT numbers and a small reduction in IFT velocity. In terms of the parasite's biology, the ability to differentiate whilst inside the parasitophorous vacuole is key to its survival. During differentiation the flagellum must be rapidly disassembled. The beating promastigote flagellum has the potential to cause damage

to the host cell and the short amastigote flagellum also has important sensory and signalling roles that modify the vacuole, thereby disassembling the flagellum allows the parasite to preserve its intracellular environment (Gluenz et al., 2010). The host cellular environment provides both environmental pressure from low pH, elevated temperature, and nutrient resources in addition to the selective pressure of immune detection (Khan et al., 2018; Zilberstein & Shapira, 1994). *In vitro,* the axenic amastigotes do not have this selection pressure therefore the physiological 'shock' of the drop in pH and increase in temperature is likely the trigger of the sudden drop in IFT numbers and enable the disassembly of the flagellum. In Chapter 5, potential drivers of this drop in IFT train numbers and cargo trafficking will be explored.

5. In search of molecular triggers of flagellum disassembly

5.1 Introduction

The results of Chapter 4 demonstrated that a small decrease in IFT velocity and a large drop in IFT numbers, occurs immediately during differentiation. This drop in train numbers may account for some of the flagellum reduction; however, other factors are likely contributing to the flagella shortening. In addition, there are also key questions that remained to be answered surrounding IFT regulation, such as: i) How the reduction in IFT train numbers is regulated? ii) Are trains still actively transporting cargo in either direction iii) is diffusion playing a role in flagella disassembly? This chapter will aim to address these questions by the analysis of flagellar PTM and putative IFTcargoes.

Tubulin based microtubules are highly conserved structures across eukaryotes yet, they can fulfil a wide range of biological functions, which requires tubulin diversity (Figure 1.5). One way of achieving diversity is via the tubulin code, which encompasses different α/β tubulin isotypes and various PTMs of tubulin to (Gadadhar et al., 2017). Different elements of this code may have functions in microtubule organisation, stability, and dynamics.

PTMs allow the dynamic, reversible fine tuning of microtubules spatially (i.e., along different regions of the flagellum) and temporally (i.e., during different periods of growth) therefore may be associated with flagellum disassembly regulation (Edwards et al., 2014). In flagella PTMs have been strongly associated with microtubule stability and interactions with motor-proteins, including kinesin-2 (Regnard et al., 1999; Wloga, 2017). As PTMs may have important roles in microtubule stability and possible associations with motors, this chapter aims to document potential changes in PTMs in the disassembling flagellum.

5.2 Major changes in PTM distribution were not detected in differentiating parasites.

5.2.1 Acetylation

The anti-acetylation antibody, C3B9, detects α tubulin acetylation on the K40 residue (Woods et al., 1989). In promastigotes, a bright signal with a strong edge effect was associated with the cell body, indicating that the antibody was detecting the cortical cytoskeleton (Figure 5.1). There was a continuous signal along the length of the flagellum, and in the case of parasites with two flagella, the signal was present on both.

As parasites began to differentiate between two and four hours the cell body signal remained (Figure 5.1). However, the distinct edge effect observed in promastigotes was no longer present. Instead, a striated signal was observed within the cell body. This suggests that the antibody associated with the cortical cytoskeleton. The flagellum retained the continuous signal at two and four hours into differentiation. By 24 hours, the parasite flagellum had dissembled so that it barely extended past the flagellar pocket. The cell cytoskeleton has a bright signal, and a very strong signal was observed along the length of the internalised amastigote flagellum, which could be visualised from inside the cell body (Figure 5.1, white arrow).

Throughout differentiation, the flagellum axoneme remained heavily acetylated even whilst inside the amastigotes (Figure 5.1). Overall, the acetylation patterns in the parasites did not change significantly during differentiation.

5.2.2 Tyrosination

YL1/2 is an antibody against tyrosinated α tubulin. The IFT pool contains tyrosination tubulin that is integrated into the flagellum axoneme, after its integration tubulin undergoes modification to its detyrosinated state (Bonhivers et al., 2008).

In promastigotes, there was a strong signal in the IFT pool, indicative of tyrosination tubulin (Figure 5.1, white arrow). The YL1/2 antibody also detects the transition fibre protein, RP2, which is likely contributing to the bright signal. The rest of the flagellum, particular in the distal region, had a weak signal and in a subset of cells there was a weak accumulation of signal in the posterior cell body tip.

At two and four hours into differentiation, the signal from the cell body had increased in comparison to promastigotes (Figure 5.1). The differentiating parasites retained the brightest signal around the IFT pool and at the posterior cell tip. At 24 hours, there was a strong signal throughout the parasite with no distinct regions of brightness.
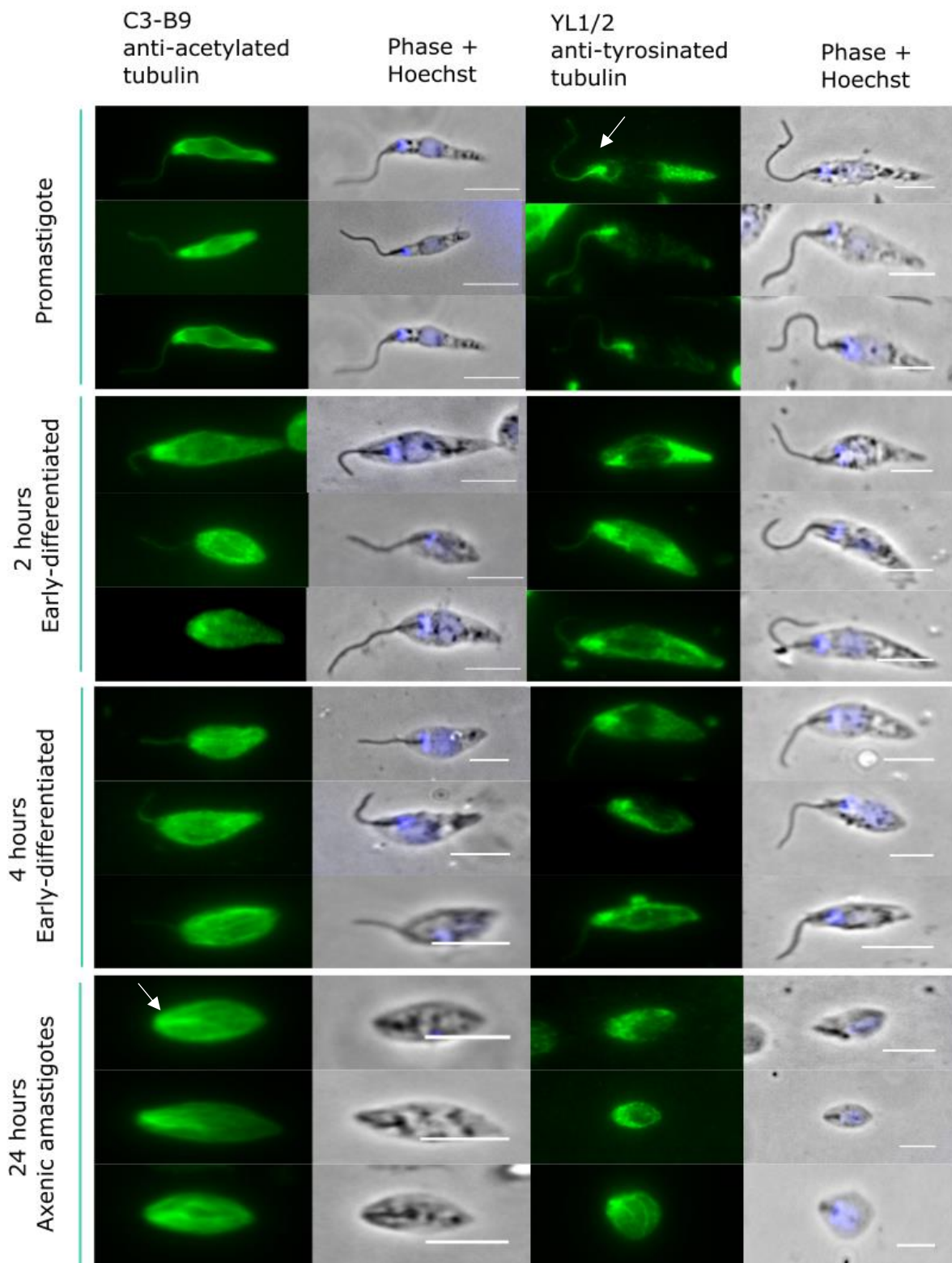
Figure 5.1 Differentiating parasites treated with anti-acetylated tubulin and anti-acetylated tyrosinated tubulin antibodies. Extracted cytoskeletons of *L. mexicana* parasites undergoing differentiation were treated with various anti-post translational modification antibodies and imaged in the appropriate channel along with phase and DNA stain. Parasites are shown in the promastigote stage, two and four hours into differentiation and 24 hour differentiated parasites. (Scale bar = 5 μm).

5.2.3 Polyglutamylation

Polyglutamylation is a common PTM of flagella. Here we used three different anti-polyglutamylation antibodies. PolyE recognises long glutamate side chains of four or more residues, whilst GT335 recognises glutamate chains of various lengths. Therefore, when the PolyE signal is absent but GT335 is present this suggests that there are only short chains in the area (Rogowski et al., 2010; Wolff et al., 1992). T9822 is also an antibody against polyglutamylation but is reported to have specificity to bi-polyglutamylation tubulins (Gagnon et al., 1996; Ikegami et al., 2007).

In promastigotes stained with GT335, there was a bright signal with an edge effect that correlates with the cortical cytoskeleton (Figure 5.2). The flagellum, in comparison had a weak signal that stopped ~1 µm before the end of the flagellum tip (Figure 5.2). In the early differentiating parasites, the cell body retained a bright signal and the flagellum signal extended to the tip, likely due to the disassembly of the unstained region. By 24 hours, the entire cell body had a bright signal with some distinct striations.

Parasites labelled with PolyE had a speckled staining, potentially suggesting that parasites were poorly extracted. Parasites had a bright signal in the cell body with an edge effect, indictive of the cortical cytoskeleton. In promastigotes there was a bright signal along the flagellum that stopped (<1 µm) before the flagellum tip, similar to the pattern seen in GT335 treated parasites (Figure 5.2). In the early differentiating parasites, the bright signal along the edge of the cell body remained.

Promastigotes treated with T9882 had bright signal across the cell body and along the flagellum; similar staining is seen on the new and old flagellum (Figure 5.2). Throughout two and four hours the flagellum maintained its bright signal, indicative of polyglutamylated tubulin.

Although the three antibodies had slightly different substrates, the general pattern of polyglutamylation was similar between the different antibodies. However, GT335 and Poly-E staining stopped <1 µm the end of the flagellum tip, whilst T9882 continued until the flagellum tip.
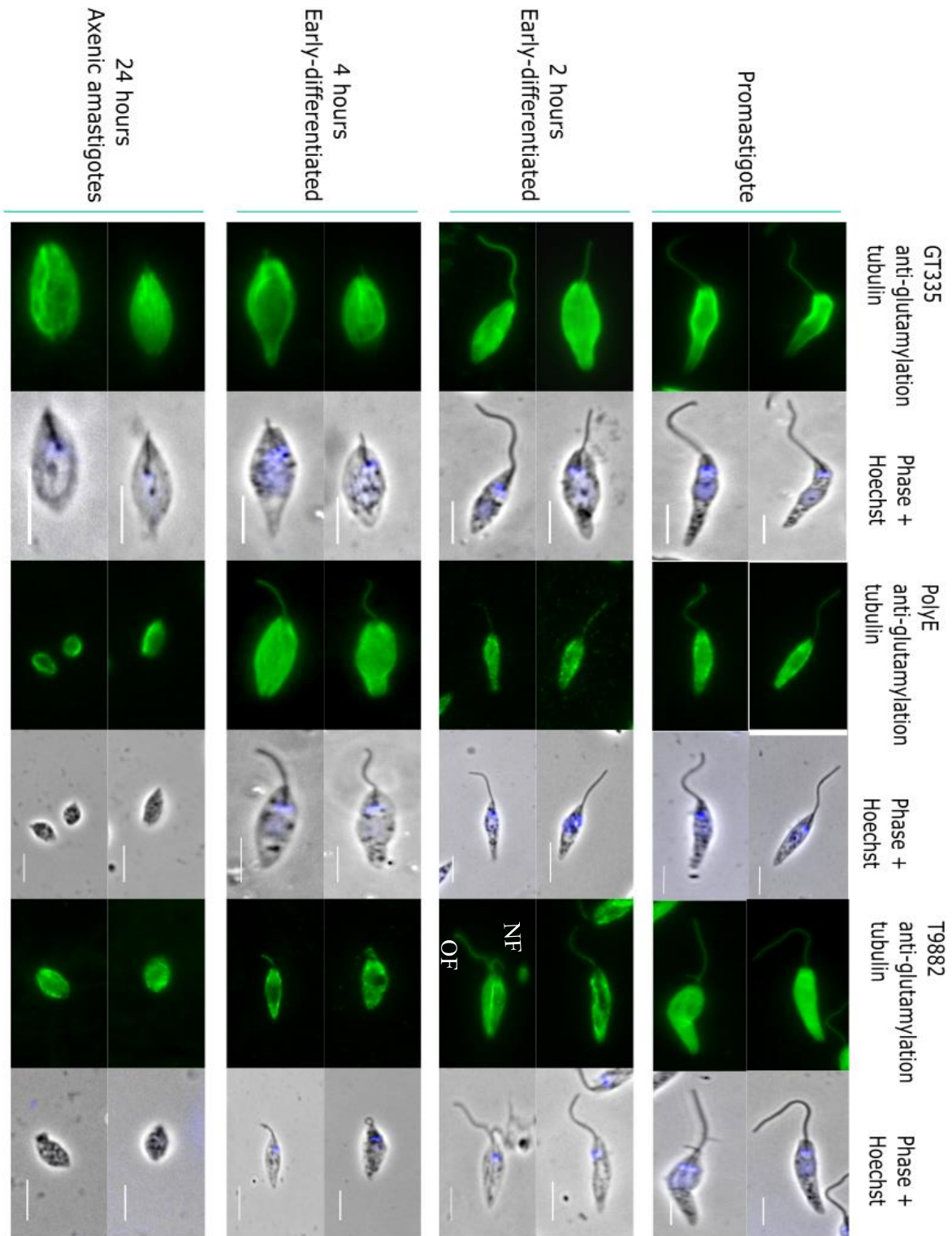
Figure 5.2. Differentiating parasites treated with various anti-polyglutamylated tubulin antibodies. Extracted cytoskeletons of L. mexicana parasites undergoing differentiation were treated with various anti-polyglutamylation antibodies and imaged in the appropriate channel along with phase and DNA stain.. Parasites are shown in the promastigote stage, two and our hours into differentiation and 24 hours into differentiation. (Figure rotated landscape, scale bar = 5 μm). OF = old flagellum, NF = new flagellum

5.3 Does IFT continue to transport cargo during flagellum disassembly?

In Chapter 4, it was shown that IFT trains remained active in both directions throughout the differentiation from promastigotes to early amastigotes, but it was not clear whether these trains were transporting flagellum material or were empty. This raises questions such as i) were the anterograde trains still transporting cargo? ii) could we visualise flagellum components that had been disassembled being transported back to the cell body.

5.3.1 Estimation of cargo abundance in the flagellum

IFT cargo has been visualised in other systems such as *Chlamydomonas.* PF16 and RSP4/6 were selected as putative cargo due to their abundance within the flagellum. This ensured that there was a higher likelihood of capturing protein movement throughout the disassembly process. Additionally, these two proteins had also been previously identified as cargo in *Chlamydomonas* (Lechtreck et al., 2018; Wren et al., 2013). PF16 is an axonemal component of the central pair and RSP4/6 is part of the radial spoke protein complex. The flagellar axonemes contains a conserved 96 nm repeat region. Within this region there are two/three repeating radial spokes in *Chlamydomonas* and three in *T. brucei* (Langousis and Hill, 2014). There is no measurement of radial spoke repeats in *Leishmania,* therefore it is assumed that *Leishmania* also have three radial spokes in the repeated unit. RSP4/6 proteins are present in the head of the radial spokes, which are attached to the A tubule of the nine microtubule doublets via a neck region. Therefore in 12 μm of flagellum (the average flagellum length for both *Chlamydomonas* and *Leishmania)* there will be ~126 repeating units and therefore ~2268 radial spokes in *Chlamydomonas* and ~3402 in *Leishmania.*

Lechtreck concluded that *Chlamydomonas* RSP4/6 was transported by IFT during flagellum maintenance and recorded 0.6 transports per minute (Lechtreck et al., 2018). When *Chlamydomonas* undergo induced deflagellation they can regenerate a full-length flagellum (~10-12 μm) within 60 minutes. During this regeneration period, RSP4/6 was transported by IFT up to 30 times per minute (Lechtreck et al., 2018). Anterograde transport happened at a normal rate, but very little retrograde transport was observed throughout the flagellum regeneration.

The rate of turnover in steady state *Chlamydomonas* is roughly 1 μm per hour, therefore roughly 0.3 transports per minute would be theoretically expected (~0.016 μm per minute = six minutes per 1 repeating unit, two radial spokes per unit) even though this is lower than the experimentally recorded of 0.6 per minute (Lechtreck et al., 2018; Marshall & Rosenbaum, 2001). If the same logic is applied to *Leishmania* that has three radial spokes per unit, a conservative, theoretical estimate of 0.5 transports per minute in maintaining flagellum would be expected. During flagellum disassembly, the *Leishmania* flagellum disassembles ~1.5 μm on average in the first two hours of differentiation. ~425 radial spokes would be in this region, so we would expect ~0.4 transport events per minute in disassembling flagellum within this initial two-hour period.

PF16 is a component of the C1 microtubule of the central pair. In *Chlamydomonas* PF16 dimers form polymers that form spirals that wrap around the C1 microtubules; although the exact number of molecules in one polymer is unknown, these spirals overlap at least every 16 nm (Han et al., 2022). Based upon these estimates, the number of PF16 molecules is at least two molecules per 16 nm of the central pair. In *Chlamydomonas* the central pair slightly extends past the nine microtubule doublets at the flagellum tip, but in *Leishmania* and *T. brucei* the central pair form a blunt end and stop in roughly the same place as the nine microtubule doublets. Therefore, in the 12 μm of the flagellum there would be at minimum 1500 repeating PF16 units. Although this is not the most abundant protein in the flagellum it is a good candidate for looking at early differentiation as the central pair is one of the first structures to disassemble during the differentiation process (Wheeler et al., 2015).

5.4 Cargo could not be detected in promastigotes or differentiating parasites.

In order to capture transit of putative cargoes, cell lines were generated that expressed IFT74 endogenously tagged with mNeonGreen and PF16 or RSP4/6 endogenously tagged with mCherry (Figure 5.3 and 5.4). Live microscopy showed that, the RSP4/6::mCh signal extended from the basal body along the flagellum axoneme and the PF16::mCh signal extended from the distal tip of the flagellum and stopped 1-2 μm from the IFT pool, reflecting the structure of the central pair and suggesting the correct structures were labelled.

To investigate cargo transit, FRAP analyses were conducted on parasite flagella. Parasites from log phase cultures were imaged (n=50 with 1 flagellum (1F) and 2 flagellum (2F)). In 1F parasites the flagellum was bleached along the middle of the flagellum, as we expected these cells to be in a maintaining phase. In 2F parasites both flagella were bleached simultaneously, with the old flagellum (characterised by it being longer in length) being bleached at in the middle of the flagellum. The new flagellum (defined as the shorter one) was bleached at the most distal region of the flagellum as these cells were expected to be assembling. Previous studies have documented more trafficking events in assembling flagellum, therefore 2F parasites were included in the analyses (Lechtreck et al., 2018).

In 1F promastigotes, expressing RSP4/6::mCh, there was no detectable cargo trafficking. In Figure 5.3, (supplementary video 5a) there was continued transit of the IFT74::mNG (Figure 5.3, white arrows) after the photobleaching event, suggesting that the parasites did not suffer major damage during the bleaching event and that IFT was still active. Post-bleaching, there was no evidence of RSP4/6 movement, and IFT did not appear to colocalise with any cargo (as indicated by the IFT remaining green (Figure 5.3, supplementary video 5a)). The FRAP recovery curves showed no evidence of fluorescence recovery (Figure 5.8).

In 2F promastigotes there was also no detectable cargo movement in either the old or new flagellum (Figure 5.4, Figure 5.8, supplementary video 5d-e). IFT74::mNG remained active in the old and new flagellum post-bleaching, but no transport of RSP4/6 could be visualised in either flagellum. This

experiment was repeated with parasites expressing IFT74::mNG and PF16::mCh promastigotes and although IFT74 remained active again, transit of PF16 was not detected (Figure 5.4).

Differentiating parasites, undergoing flagellum disassembly were also analysed. Two and six hour differentiating parasites expressing IFT74::mNG and RSP4/6::mCh were imaged (Figure 5.5 supplementary video 5f-g)). In these parasites, the middle of the flagellum was photobleached, to capture cargo moving in a retrograde direction either by IFT or possibly via diffusion. In differentiating parasites there were a reduced number of trains compared to the promastigotes (Chapter 4 showed that after two hours the total number of IFT drastically drops). However, there was no evidence of cargo trafficking in these differentiating parasites (Figure 5.8 shows no recovery in the FRAP recovery curves). This was also attempted in the parasites expressing IFT144::mNG and PF16::mCh (Figure 5.6) there was no recorded transit of the cargo (Figure 5.8).
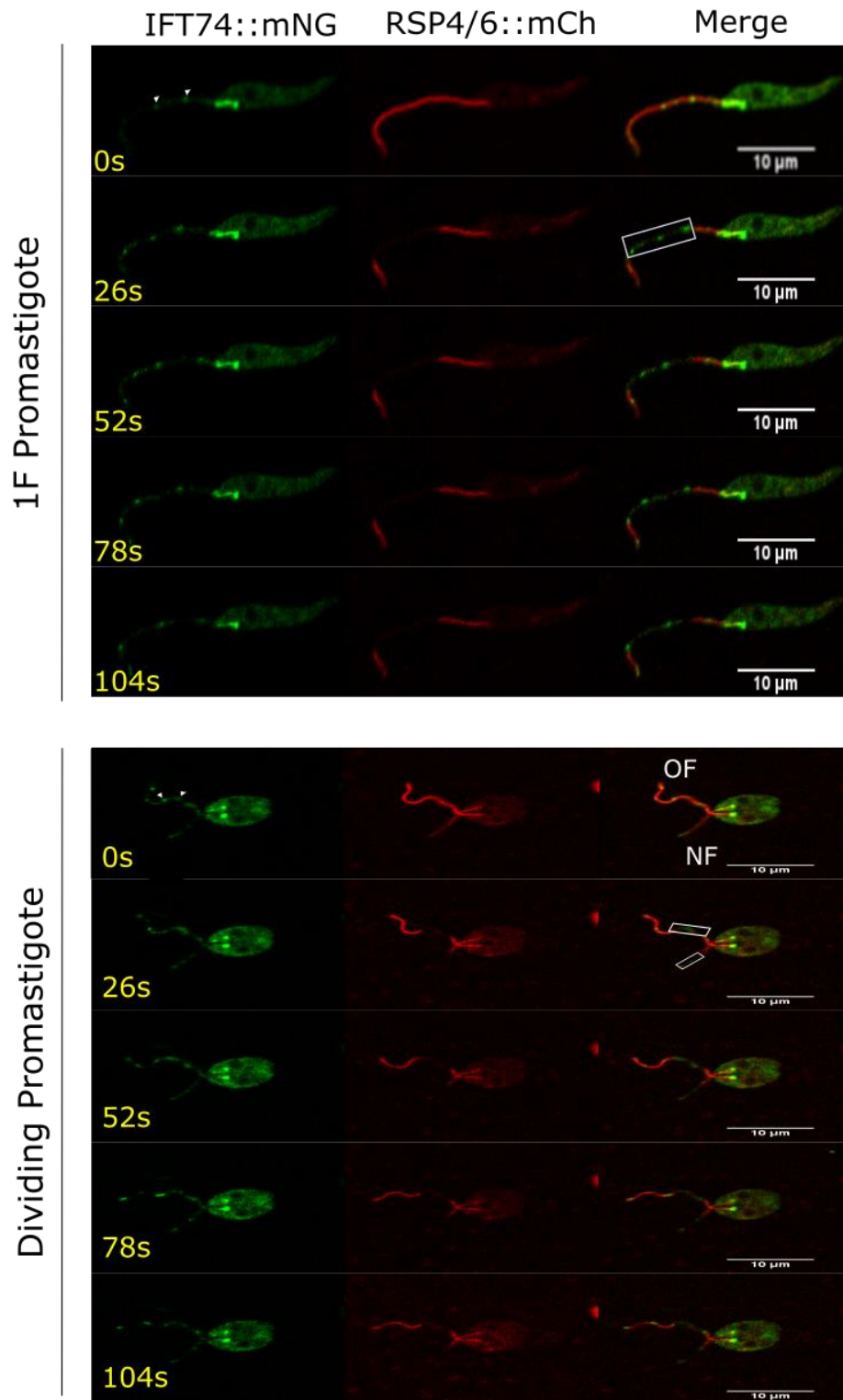
Figure 5.3. FRAP analysis of live *L. mexicana* promastigotes and dividing parasites expressing RSP4/6::mCh and IFT74::mNG. The flagellum was photobleached (indicated by the white rectangle) and parasites were imaged for 100 frames, timings shown in yellow text. IFT trains are indicated by white arrows (scale bar = 10 μm). For the dividing parasites both flagella were photobleached, the middle of the old flagellum and the end of the new flagellum.
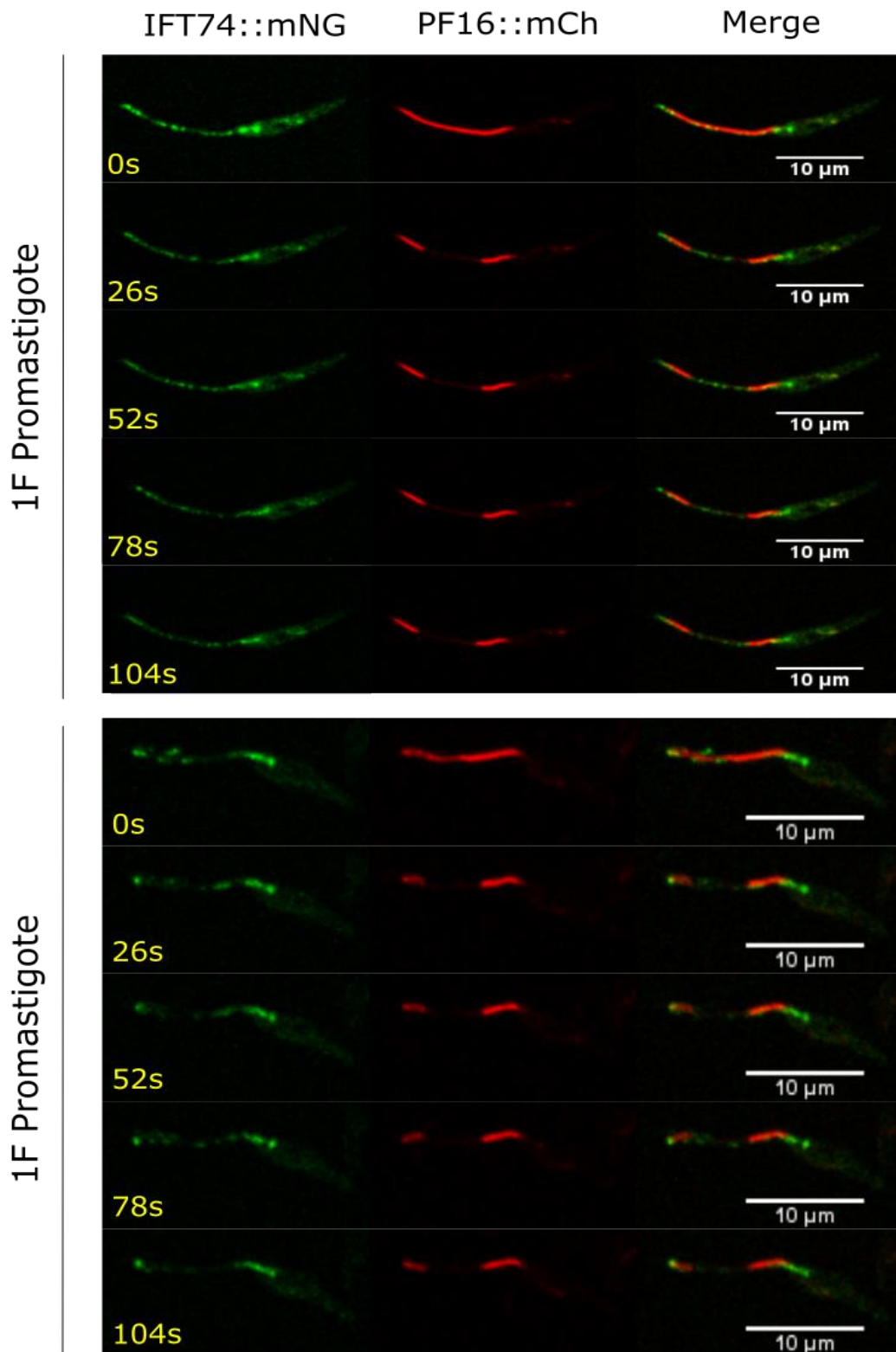
Figure 5.4. FRAP analysis of live *L. mexicana* promastigotes expressing PF16::mCh and IFT74::mNG. The flagellum was photobleached (indicated by the white rectangle) and parasites were imaged for 100 frames, timings shown in yellow text (scale bar = 10 μm).
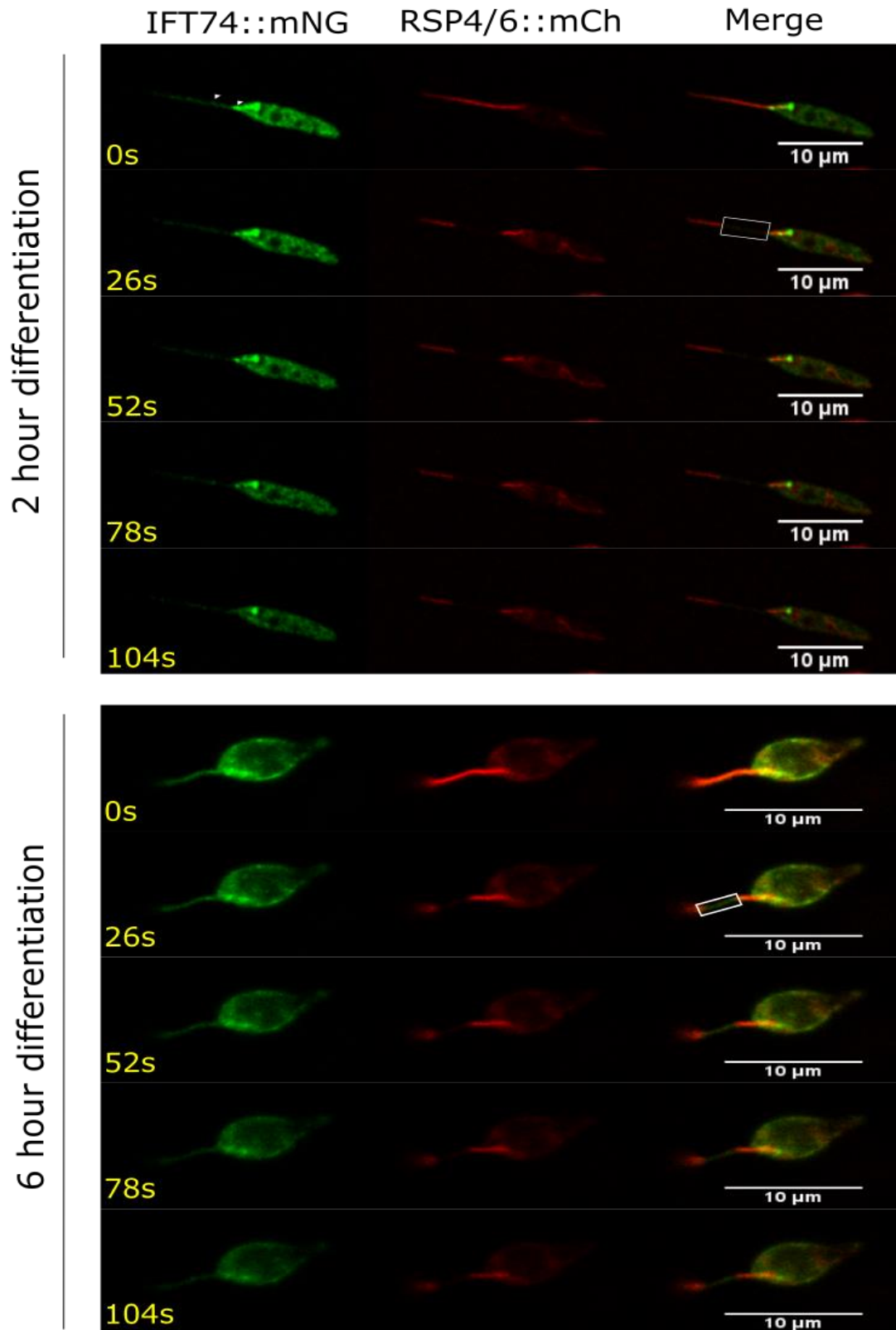
Figure 5.5. FRAP analysis of live *L. mexicana* at two and six hours into differentiation expressing RSP4/6::mCh and IFT74::mNG. The flagellum was photobleached (indicated by the white rectangle) and parasites were imaged for 100 frames, timings shown in yellow text (scale bar = 10 μm).
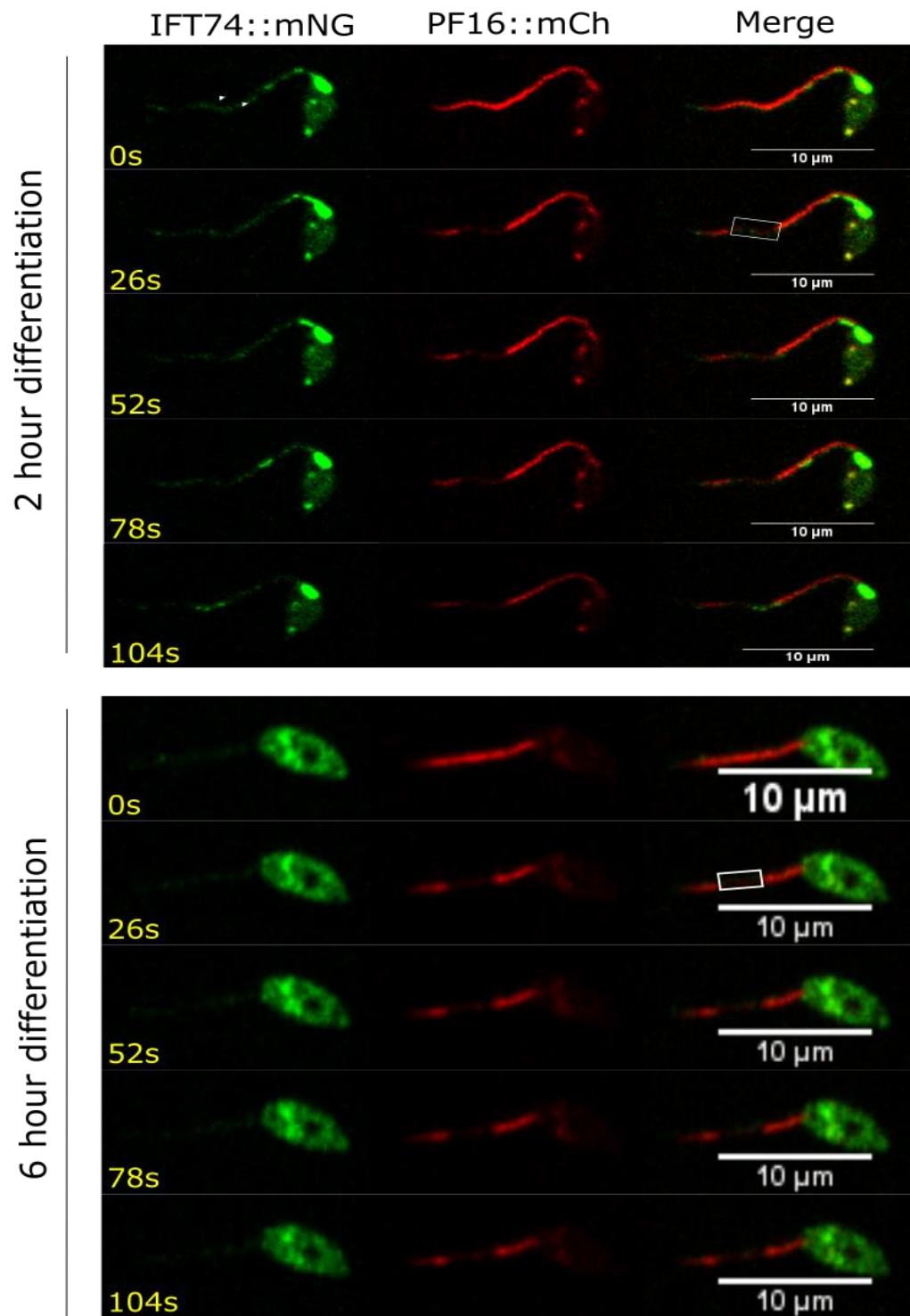
Figure 5.6 FRAP analysis of live *L. mexicana* at two and six hours into differentiation expressing PF16::mCh and IFT74::mNG. The flagellum was photobleached (indicated by the white rectangle) and parasites were imaged for 100 frames, timings shown in yellow text. (Scale bar = 10 μm).

5.4.1 Brightness was not a limiting factor for the detection of cargo.

From the previous cargo tracking there were concerns that we were attempting to track a single fluorescent protein tag, and this would be difficult, especially with the high background. Therefore, the photo-bleaching experiment was repeated in cell lines expressing cargos tagged with a triple mNeonGreen as this is more photo stable and brighter, which should aid detection. Attempts were made to generate cell lines expressing both a cargo tagged with three copies of mNeonGreen and an IFT protein tagged with mCherry, but these cells were not viable, therefore experiments were conducted on parasites only expressing tagged cargoes. The triple mNeonGreen signal from the flagellum was much brighter and more photostable allowing clear imaging of the flagellum. Yet, there was still no evidence of transit of cargo in these parasites. Figure 5.7 (supplementary video 5h) shows promastigotes expressing fluorescently tagged PF16 with bright signal present along the axoneme, the middle section of the flagellum was photobleached and there was no movement of cargo detected in the bleached region of the flagellum (Figure 5.8). There appeared to be some loss of fluorescence from the adjacent regions to the bleached flagellum, but this is likely due to the movement of the flagellum coming in and out of focus as these parasites were very motile (Figure 5.7).
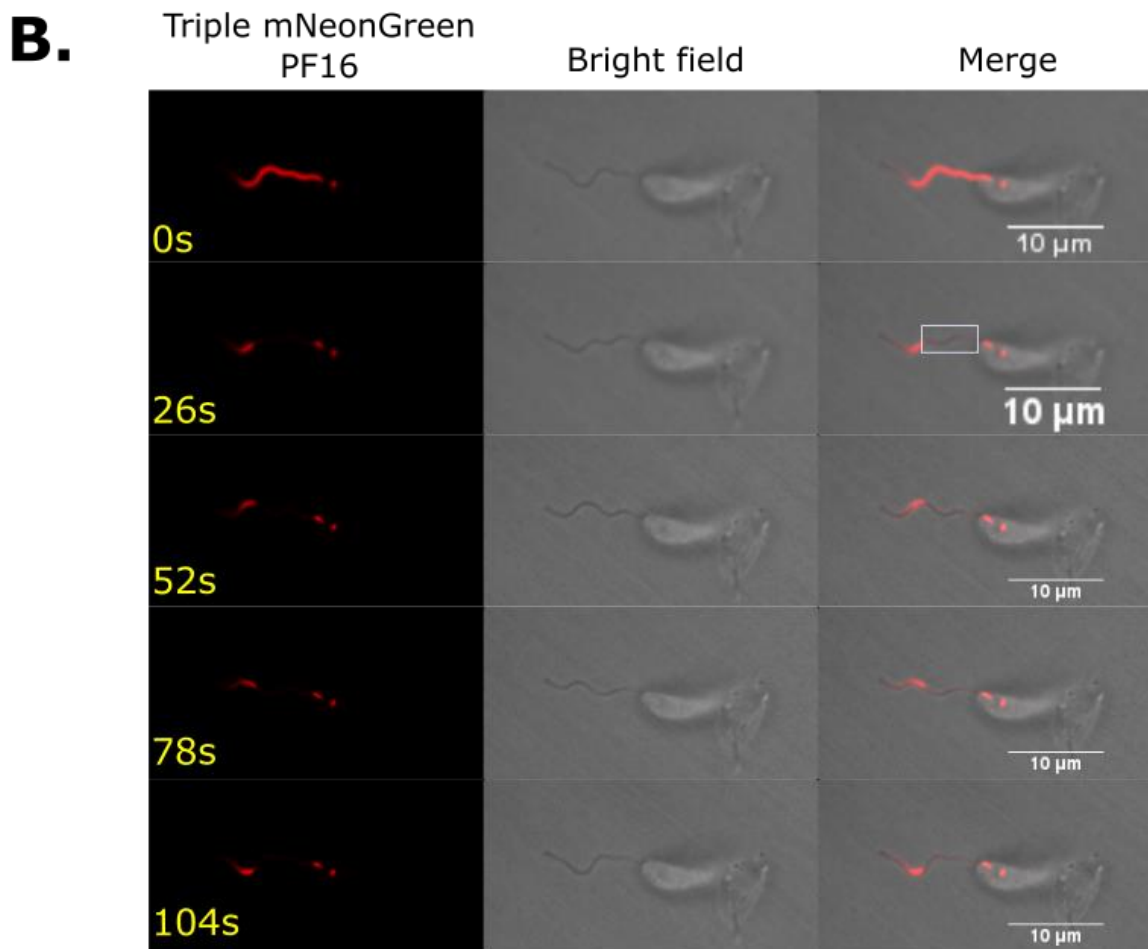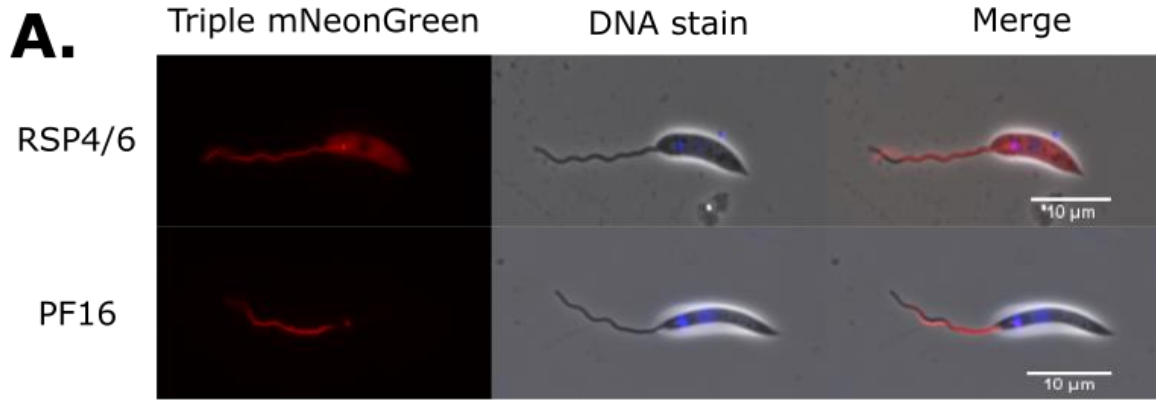
Figure 5.7. Promastigotes expressing putative cargoes endogenously tagged with three copies of mNeongreen. A. Still images of the parasites expressing PF16/RSP4/6::3mNG. The RSP4/6 had <30% of cells with a signal and PF16 had >70% with a signal. **B**. FRAP analysis of live *L. mexicana* at two and six hours into differentiation expressing PF16::3mNG. The flagellum was photobleached (indicated by the white rectangle) and parasites were imaged for 100 frames, timings shown in yellow text. IFT trains are indicated by white arrows (scale bar = 10 μm).
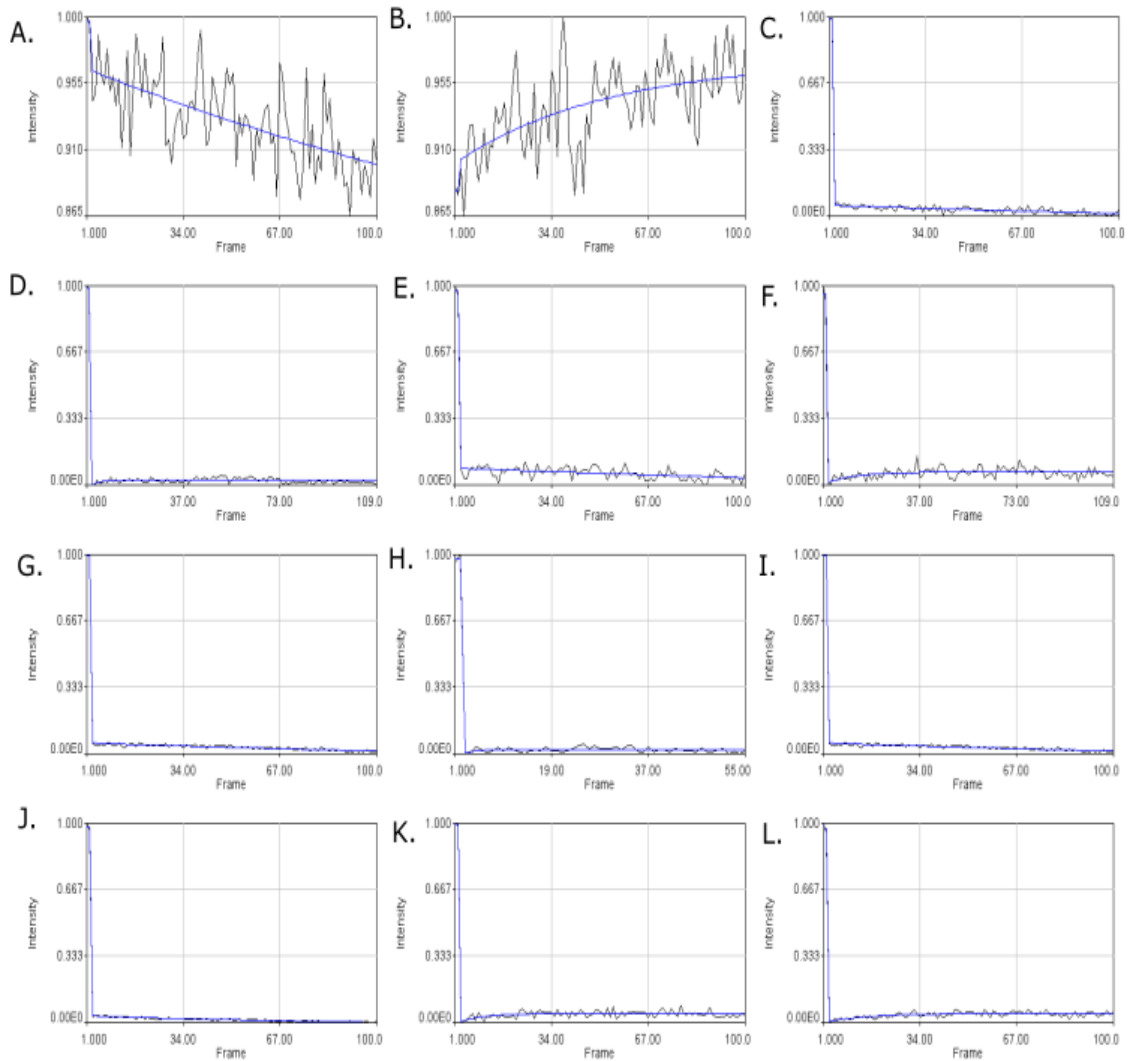
Figure 5.8. FRAP recovery curves. Normalised recovery curves from the bleached regions along the flagellum, Graphs correspond to the previous figures. A. Unbleached region of the IFT pool in promastigotes. **B.** Unlbleached region of the flagellum in promastigotes. **C.** Bleached region of promastigote flagellum (RSP4/6::mNG, Figure 5.3). **D.** Bleached region of the promastigote flagellum (PF16::mNG, Figure 5.4). **E.** Bleached region of the flagellum of a dividing cell (RSP4/6::mNG, Figure 5.3). **F.** Bleached region of the second flagellum of a dividing cell (RSP4/6::mNG, Figure 5.3). **G.** Bleached region of the flagellum of a 2 hour differentiating parasite (RSP4/6::mNG, Figure 5.5). **H.** Bleached region of the flagellum of a 6 hour differentiating parasite (RSP4/6::mNG, Figure 5.5). **I.** Bleached region of the flagellum of a 2 hour differentiating parasite (PF16::mNG, Figure 5.6). **J.** Bleached region of the flagellum of a 6 hour differentiating parasite (PF16::mNG, Figure 5.6). **K-L.** Bleached region of the flagellum of a promastigote (PF16::mnG, Figure 5.7).

5.5 Discussion

Chapter 4 demonstrated that IFT train numbers and velocity dropped within 30 minutes of differentiation – but what was driving these reductions? In this chapter, we attempted to identify the molecular triggers of the reduction in IFT and flagellum shortening.

The findings from Chapter Four also showed that IFT was active throughout flagellum disassembly. Although IFT was active, it was not clear whether the trains were transporting cargo. Therefore, we analysed whether the transit of two putative cargoes, PF16 and RSP4/6, could be captured during flagellum assembly, maintenance, and disassembly.

5.5.1 IF did not have the resolution to detect the subtle changes in PTM levels.

It was predicted that PTMs may play a role in regulating flagellum disassembly. PTMs are highly abundant in the flagellum, and they are known to finetune microtubule properties (Wloga, 2017). Multiple PTMs were analysed throughout the differentiation to axenic amastigotes. Some of the antibodies against PTMs highlighted differences in the PTM distribution across the parasites, but most were unable to detect the subtle changes in the flagellum that we were hoping to capture (Figure 5.1-5.2).

Of the PTMs analysed, the largest change was seen in the tyrosination levels. The anti-tyrosination antibody showed a strong signal in the IFT pool (a combination of the RP2 transition fibre protein and the tyrosinated tubulin (Andre et al., 2014)). During differentiation, the signal in the cell body signal increased and the IFT pool/RP2 protein signal remained. As tyrosinated tubulin is typically considered a marker of tubulin array growth, the increased signal in the cell body is likely a reflection of axenic amastigotes cell body remodelling (Gluenz et al., 2010; Sinclair et al., 2021). As amastigotes become more spherical and shorter than promastigotes, tyrosinated tubulin is incorporated into the remodelled cytoskeleton, hence the increased signal. Early differentiating parasites also retained a strong signal at the IFT pool, suggesting an accumulation of tyrosinated tubulin at the base of the flagellum. Previous research suggests tyrosinated tubulin is abundant in the IFT pool and only undergoes the modification to its detyrosinated state once integrated into the axoneme (Sasse & Gull, 1988a). It is not clear whether these tyrosinated tubulins are at the pool awaiting the to be transported into the flagellum, or have been recently disassembled, re-tyrosinated and delivered back to the IFT pool. As YL1/2 also binds to a transition fibre protein, it is difficult to distinguish how much signal is from the tubulin compared to the RP2. There is the additional issue that the cell body signal was very bright, making it difficult to distinguish the location of the basal bodies. However, the anti-tubulin antibody TAT1 (supplemental 5a) also detected a strong signal around the IFT pool, hence it is likely that the signal is a combination of both tyrosinated tubulin and RP2. Nonetheless, to truly distinguish between the RP2 protein and the tyrosinated tubulin, an RP2 marker should have been endogenously tagged.

Most of the antibodies did not detect changes in PTM levels in the flagellum throughout differentiation. There were some technical issues with poorly extracted parasites seen across the images. Early differentiating parasites seemed particularly susceptible to damage during cytoskeleton extraction, therefore many were over/under extracted, which may have impacted antibody staining. Ultimately it was likely that the microscopy set up that was used was not able to detect the subtle changes in PTMs during differentiation. Firstly, the levels of antibody signal were very high. In order to visual the signal in the flagellum, the cell body signal was oversaturated, which created a high background. Potential methods to overcome this oversaturation from the cell body could be to isolate the flagellum or purify the tubulin (Beneke et al., 2020; Orbach & Howard, 2019). Previously, tubulin purification has resulted in very low yields or damage to the tubulin, however due to gentler purification methods, it is now possible to purify and then distinguish tubulin PTMs along a single microtubule (Orbach & Howard, 2019). This could allow the tubulin from the cell body and the flagellum to be treated and analysed independently and improve the sensitivity of PTM detection.

Secondly, the main issue is likely that IF is not suitable to detect low levels of PTM variation. The most abundant protein in the flagellum is tubulin, which is known to be extensively modified, resulting in lot of PTMs occurring along the axoneme. This means that detecting a small sub-population of modified tubulin would require a sensitive method.

predict the level of subtle PTM changes we must consider the parasites structure and biology. *Leishmania,* similarly to *T. brucei,* presumably have a restricted set of microtubule doublets that IFT trains can travel along (Bertiaux et al., 2018). Therefore, changes in PTM levesl could be happening on these restricted microtubule doublets, again making detection of PTM changes difficult. Alternative methods have also been used to detect PTMs. For example, immunogold electron microscopy has generated detailed location data regarding the asymmetry of polyglutamylated sites along the axoneme in green flagellates (Lechtreck & Geimer, 2000). To the best of my knowledge, this has not been repeated in *T. brucei* or *Leishmania* species, and with optimisation could provide greater insight to the PTM sites along the flagellum.

Here, subtle changes in the PTM organisation in differentiating parasites were not detected, likely due to insufficient resolution. Prior evidence has shown that tubulin PTMs are highly abundant in the flagellum and may have roles in microtubule stability and interactions with motor proteins (Regnard et al., 1999; Wloga, 2017). Therefore, it would be surprising if PTMs did not play a role in flagellum stability or elongation and shortening. Due to time constraints, it was not possible to trial alternative detection methods. However, if possible, future research attempting to document PTM changes in *Leishmania* may wish to try a combination of high-resolution techniques, such as electron microscopy and mass-spectrometry.

5.5.2 Flagellum stability in Leishmania

The results from Chapter 4 and Chapter 5 suggest that the flagellum disassembled throughout *Leishmania* differentiation, that the reduction in IFT alone cannot account the axoneme shortening and that PTMs were not shown to change drastically during flagellum shortening. Flagellum length control is complex and highly variable between species. In fact, even between the evolutionarily closely related trypanosomatids, there are stark differences in the ability to alter the length of the flagellum.

Throughout the lifecycle of *T. brucei* the mature flagellum stays at a similar length, however in *Leishmania* the flagellum length and morphology drastically change (Figure 1.6). This may be due in part to the differences in axoneme stability observed between the species. In *T. brucei,* very little tyrosinated tubulin (a marker for tubulin array growth (Sinclair et al., 2021)) is observed in the old flagellum (Fort et al., 2016). However, the results show that in the mature flagellum of *L. mexicana,* tyrosinated tubulin was present along the length of the mature flagellum (Figure 5.1). This could suggest that tubulin turnover may be occurring in mature *Leishmania* flagella. These differences between the two species could suggest that *T. brucei,* have higher levels of microtubule stability compared to *L. mexicana.* The reduced axoneme stability observed in *L. mexicana* could be contributing to its ability to disassemble its flagellum. Moreover, this could mean that the reduction in IFT numbers during differentiation could be partly responsible for the reduction in IFT length due to the lack of replacement of IFT components as the axoneme undergoes turnover.

However, in the closely related *T. brucei,* tubulin turnaround does not occur in full length flagellum (Fort et al., 2016). Instead IFT is only required for flagellum growth and maintaining the distribution of flagellar proteins along the axoneme. When the flagellum elongates to a set point the axoneme locks and the flagellum does not extend any further (Bertiaux et al., 2018). When IFT components were knocked down, the new flagellum was significantly shorter, but the length of the old flagellum was unaffected. In *T. brucei* the old flagellum is considered extremely stable. In fact, in species with a high flagellum turnover, such as *Chlamydomonas,* a capping structure is present at the flagellum tip, which is believed to be involved in axoneme stability (Croft et al., 2018). *T. brucei* lack this capping structure potentially due its axonemes inherent stability, therefore capping is unnecessary.

However, there are a number of potential factors that have been associated with flagellum stability. Another factor not discussed here, is the role of microtubule associated proteins. For example, in *Leishmania* and *Giardia* kinesin-13, a microtubule depolymerising kinesin, was found to be associated with flagellum length control (Blaineau et al., 2007; Dawson et al., 2007). When mutations were introduced in these enzymes, there was significant elongation of the flagellar axonemes, and in *Leishmania,* overexpression of kinesin-13 lead to shortened flagella. These findings may suggest that kinesin-13 can maintain and potentially could have roles in disassembly. However, in *T. brucei* kinesin-13 had no measurable effect on flagellum length, again highlighting the differences in the

microtubule stability between the species (Chan & Ersfeld, 2010). Future studies could quantify the levels of enzymes from the kinesin-13 family (MCAK/KIF2 in *Leishmania* (Blaineau et al., 2007)) via western blot during the differentiation process.

5.5.2 Cargo trafficking was not detected in the Leishmania flagellum.

IFT trains carry cargo to the flagellum tip to be integrated into the axoneme (Qin et al., 2004). In Chapter 4, trains were recorded moving in both directions throughout early differentiation; this raised multiple explanations. One hypothesis was that the anterograde trains could be 'empty' and not transporting cargo. Instead, empty trains could be transported to the flagellum tip, loaded with disassembled axoneme proteins, and transport proteins back to the IFT pool via retrograde transport. An alternative thought was that cargo could be disassembled then diffuse back to the pool, independently of IFT. Therefore, these experiments aimed to capture transit of putative IFT cargoes during disassembly.

Unfortunately, no transport events or diffusion was detected. First, full length flagellum and growing flagellum (as defined by the short flagellum of 2F parasites) were analysed. Both putative cargoes showed a bright signal along the axoneme, suggesting successful incorporation of the endogenous tag, and that the fluorescent protein did not interfere with axoneme assembly. However, after photobleaching, IFT trafficking appeared normal but there was no evidence of cargo trafficking either via IFT or diffusion (Figure 5.3-5.7). The recovery curves showed no evidence of fluorescence recovery in the bleached regions of the flagella (Figure 5.8). It was speculated that the detection of essentially a single protein being transported would be challenging. Therefore, parasites were generated that expressed three copies of mNeonGreen in order to increase the fluorescent signal. Although the signal was extremely bright, there were no detectable transport events.

Cargo trafficking has been previously detected in *Chlamydomonas* and *C. elegans* (Craft et al., 2015; Dai et al., 2018; Hao et al., 2011; Lechtreck et al., 2018; Wren et al., 2013). To date, most instances of cargo trafficking has been captured in *Chlamydomonas,* with the majority originating from the Lechtrek laboratory. In the examples listed, cargo trafficking was captured using spinning-disk confocal or TIRF microscopy. When compared to traditional confocal microscopy, TIRF and spinning disk tend to have a faster acquisition time (e.g., Wren *et al* captured at 31 fps), a much lower background and improved signal-to-noise ratio (Ross & Schwartz, 2022). Therefore, perhaps our microscopy set up did not have the resolution or sensitivity to capture the cargo transit.

However, in *T. brucei* capture of the transit of the putative cargoes: DRC, RSP, PF16 and the dynein arm complex was not possible (Vincensini et al., 2018). The authors could not distinguish whether the transport of DRC was via an alternative pathway or due to technical issues such as the fluorescent protein was not bright enough or the train had interfered with the ability of the GFP to fluoresce. The protocol used here was similar to the Vincensini paper. Both used similar fluorescent proteins, a comparable microscope set up for FRAP analyses and closely related organism of interest. It is not

clear if there is some difficulty in capturing the cargo movement in trypanosomatids or like other aspects of their flagellum biology there is another level of regulation here.

However, it is also possible that cargo trafficking in *Leishmania* and *T. brucei* is lower than predicted. In *Chlamydomonas* IFT is required for the maintenance of the flagellum length but in *T. brucei* IFT is either not present or severely reduced in mature flagellum and is not required for maintaining flagellum length (Fort et al., 2016; Lechtreck et al., 2018) . The difference in the role of IFT in mature flagella of the two species is thought to be due to the high level of stability of the *T. brucei* axoneme (Discussed in section 5.5.2). If the rate of axoneme turnover is lower than expected, perhaps the frequency of cargo transport is much lower than expected, therefore we are missing transport events.

There is also the possibility that IFT trains are not always required to carry the cargo to the flagellum tip. Studies have repeatedly shown that IFT passes through the ciliary gate barrier into the flagellum compartment (Lechtreck, 2015; Szymanska & Johnson, 2012; Vieillard et al., 2016; Wei et al., 2013). However, there is the possibility that the cargo could dissociate with the IFT trains once inside the flagellum. Diffusion has been shown to have a role in the trafficking of certain components, such as tubulin, in certain species (Luo et al., 2017; Van de Weghe et al., 2021). In fact, in *Chlamydomonas,* IFT is required for tubulin to pass through the ciliary gate but not for transport to the tip. Therefore, IFT could be facilitating the entry of axoneme components into the flagellum to allow the establishment of a gradient of components. Logically, then these components could diffuse along the gradient from a high concentration at the base to a low concentration at the tip. The IFT trains could be acting as only a regulator for maintaining this diffusion gradient. Perhaps the bleaching of a site closer to the IFT pool/gate would allow the visualisation of diffucison occurring.

Future research may wish to focus upon i) attempting to capture transit of a wider array of putative cargoes ii) the utilisation of higher resolution imaging methods iii) developing methods that would allow substantially longer time periods longer for tracking cargo.

5.5.4 There could be multiple levels of IFT control.

In this study we analysed two potential factors that could drive flagellum disassembly. However, there many different ways that flagellum disassembly could occur.

For example, regulation at the ciliary gate could contribute to changes in flagellum length. The gate (the transition zone and transition fibres) acts as a selective barrier for IFT proteins into the flagellum (Lechtreck, 2015). When mutations were introduced into transition zone proteins, the accumulation of IFT proteins around the pool decreased, which led to a reduced number of IFT trains entering the flagellum (Fort et al., 2016) . However, this observation was more severe at 48 hours post induction. As shown in Chapter 4, this drop in IFT numbers occurs rapidly, therefore reduced IFT accumulation in the IFT pool cannot be the sole factor driving the reduction in IFT trafficking and flagellum shortening.

The flagellum tip could also play a role in axoneme disassembly. Croft and colleagues demonstrated that protein composition of the flagellum tip and the tip structure itself varies between species (Croft et al., 2018). For example, the presence of a 'capping structure' at the flagellum tip is present in species such as *Chlamydomonas* and *Tetrahymena* but is not present in species such as *T. brucei, Leishmania* and human sperm. Whether these structures and protein differences are due to biological requirements of the flagellum (e.g., do they need to disassemble/how stable are they/are they sensory?) or they are evolutionarily conserved between groups is unclear. Nonetheless, these differences in proteins and structures at the tip could aid with facilitating disassembly of the flagellum.

Although we have suggested potential mechanisms of flagellum disassembly during differentiation, it is likely that multiple mechanisms drive the disassembly. The disassembly process is organised; it is a stepwise process where structures like the PFR are disassembled prior to the axoneme (Wheeler et al., 2015). The process is also triggered rapidly after the start of differentiation, likely due to the drop in pH and increase in temperature. Therefore, potential mechanisms, whether they act alone or in unison must occur rapidly and be tightly regulated. Hopefully future research can aim to address these questions.

6. The naturally occurring *L. braziliensis* dysflagellar mutant

6.1 Introduction.

During the life cycle of *Leishmania,* the parasite undergoes drastic morphological changes, the most striking being the changes to the flagellum. The flagellum remodels across the multiple life cycle stages, allowing the parasite to fulfil different biological adaptations. For example, in promastigotes the flagellum is crucial for motility inside the sand fly host, the flagellum of haptomonads, leptomonads, and nectomonads is important for attachment in the insect, whilst even the short flagellum of amastigotes have sensory roles inside macrophages (Gluenz et al., 2010; Pimenta et al., 1992).

In culture, parasites without a flagellum can be generated and maintained by deleting a variety of genes including IFT-B proteins and protein kinases (Baker et al., 2021; Beneke et al., 2019; Sunter et al., 2018). The culture conditions provide a nutrient dense, temperature stable environment without the challenges of host immunity or the movement of blood or fluid to contend with. These conditions create an artificial selection pressure where parasites that would not be viable in the host are viable in culture, such parasites without a flagellum.

As the flagellum is integral for infection and persistence, parasites that fail to assemble a functional flagellum, in theory, should be at a major evolutionary disadvantage. However, surprisingly there is a documented example of parasites collected from patient samples that fail to form a full length flagellum; these were characterised as 'dysflagellar mutants' (Zauli et al., 2012). The mutant parasites, referred to as strain EFSF6, were collected from lesions of patients in Brazil. These parasites were frozen down soon after collection and the gDNA was extracted within a maximum of seven passages. In culture, only 2-3% of EFSF6 promastigotes had a visible short flagellum but otherwise appeared normal. The majority of parasites had a very short but otherwise normal axoneme, but the flagellum formed a disordered bulge at the exit of the flagellar pocket (Figure 6.1a-b). The bulge formed contained a mass of electron dense material of unknown origin. Despite the loss of a full length flagellum, EFSF6 promastigotes showed no significant reductions in growth rate or parasite density.

In wild-type *Leishmania*, the flagellum plays critical roles in macrophage infection by triggering phagocytosis (species dependent), and flagellum-mediated orientation inside the parasitophorous vacuole (Forestier et al., 2011). Given the multiple ways that the flagellum plays a role in macrophage infection, it was surprising that in mouse models, EFSF6 parasites managed to successfully infect and maintain high parasitaemia (Figure 6.1c). Suggesting that the dysflagellar mutants can successfully differentiate into amastigotes.

During the sandfly infection, *Leishmania* utilises the flagellum for motility and attachment (Bates, 2008). The dysflagellar mutants were able to persist inside the sand fly for at least 96 hours post-

infection and showed similar infection load to the wild-type parasites (Zauli et al., 2012). The peritrophic matrix (PM) of *Lu. Longipalpis* (the vector used in Zauli study) develops one hour after feeding and is a fully matured barrier within 24 hours. To avoid excretion from the sandfly, parasites must escape the PM within two to three days post feeding (Ramalho-Ortigao et al., 2010; Secundino et al., 2005). Therefore, by 96 hours the dysflagellar mutants should have escaped the PM, despite the mutant's immobility. Unfortunately, the progression of parasites throughout the sand fly and the morphology of the parasites during sandfly infection was not shown in the study. Hence, it remains unclear whether the dysflagellar parasite managed to migrate out of the midgut or if they are able to successfully differentiate to other lifecycle stages such as leptomonads and haptomonads.

The flagellum is considered key to many aspects of the parasite's life cycle, so the fact that the dysflagellar mutant can infect and persist inside the host and vector is unusual. This chapter will focus on the characterisation of EFSF6 mutants. Firstly, by the analysis of its genome, is there an underlying genetic cause to the dysflagellar phenotype? Secondly, by replicating the phenotype in the closely related *L. mexicana* and using bioimaging techniques to further characterise the mutants.
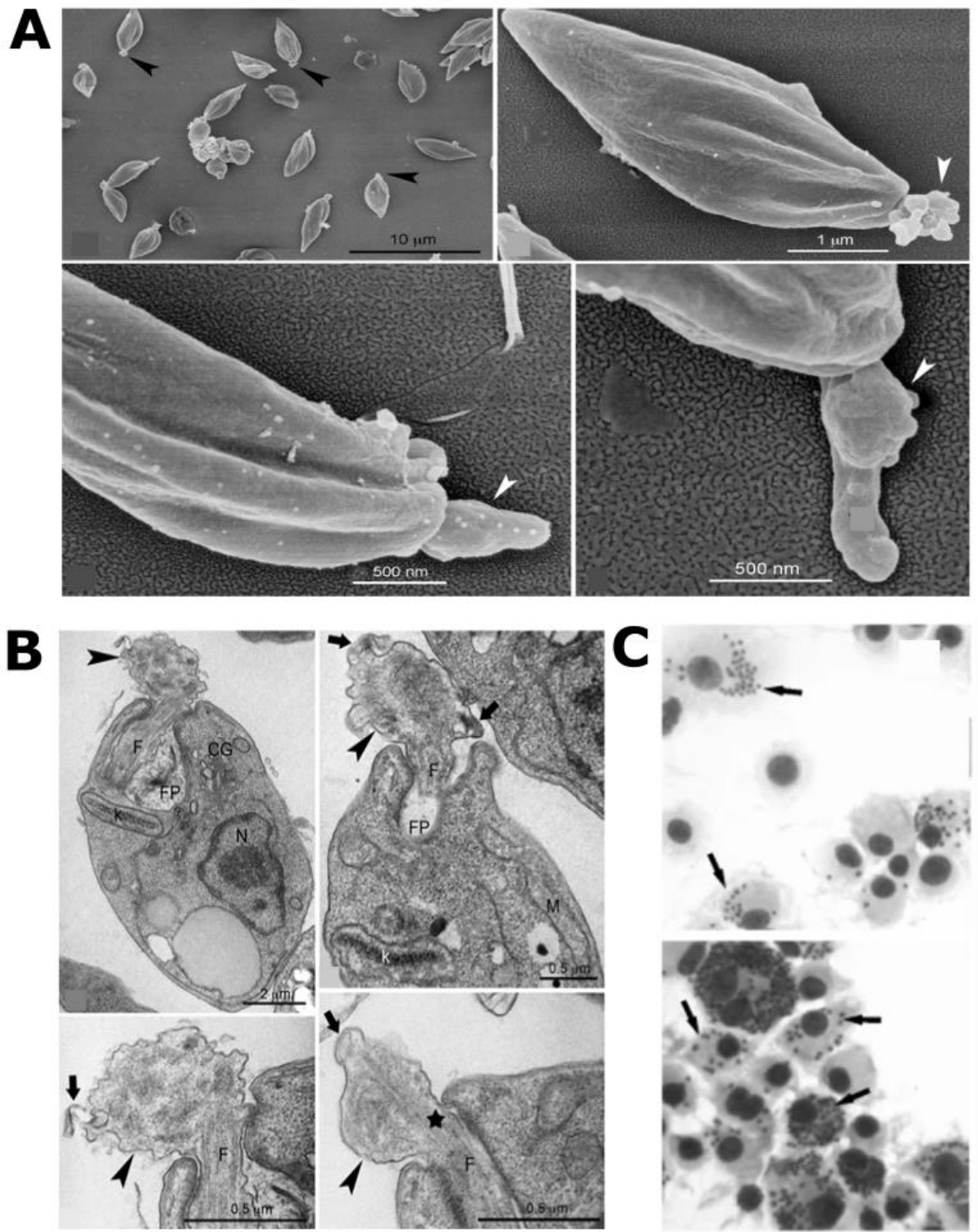
Figure 6.1. The dysflagellar mutant (EFSF6) morphology, isolated from patient lesions. A-B SEM/TEM analyses of the mutant. The disordered material at the exit of the flagellar pocket is indicated by arrows in both. **C.** The mutants can establish heavy infection inside mouse macrophages (Zauli et al., 2012)

6.2 Results

6.2.1. A 27 kb deletion was identified in the dysflagellar mutant.

The first step was to sequence and detect potential mutations that could lead to the dysflagellar phenotype. Whole genome sequencing of 50x coverage was performed on the EFSF6 mutant and three other *L. braziliensis* strains, that showed normal morphology and were collected from a similar area. The sequencing statistics are shown in Table 6.1.

Table 6.1 Sequencing statistics for the *L. braziliensis* genomes collected from patient samples.

Sample Name	Clean Reads	Clean Bases	Read Length (bp)	Q20(%)	GC(%)
BE5	23,959,432	2,395,943,200	100	96.07	55.01
DMO8	19,994,486	1,999,448,600	100	95.68	55.67
EFSF6	20,629,874	2,062,987,400	100	94.49	56.31
JBC8	23,982190	2,398,219,000	100	95.60	53.53

The sequences from the four *L. braziliensis* parasite isolates were aligned to the *L. braziliensis* reference sequence (strain MHOM/BR/75/M2903). Isolates were mapped to the 35 chromosomes of the reference genome. The alignment statistics are detailed in Table 6.2. All isolates showed a high mean coverage (>91%) and a high percentage of mapped reads to the reference sequence (>85%).

Table 6.2 Alignment statistics for the *L. braziliensis* genomes collected from patient samples.

Strain	Total number of reads	Number of mapped reads	Mapped reads (%)	number of properly paired	Properly paired (%)	Mean coverage (%)
EF5F6	20629874	18535778	89.85	15917614	77.16	91.41
BE5	23959432	20416192	85.21	18751878	78.27	91.47
DMO8	23146895	20056894	86.65	18732718	78.14	91.46
JBC8	22987654	19563902	85.1	18678493	79.97	91.43

The sequences from the four isolates were then examined for genetic variation. In comparison to the reference strain, the levels of genome variation (indels/SNPs etc) in the patient derived parasites were relatively high (Figure 6.2). However, the dysflagellar mutant EFSF6 did not show any substantial variation when compared to other patient isolates. In fact, EFSF6 showed lower counts of most types of variation of the patient isolated strains. This could be due to the lower number of reads of EFSF6 when compared to the other isolates.
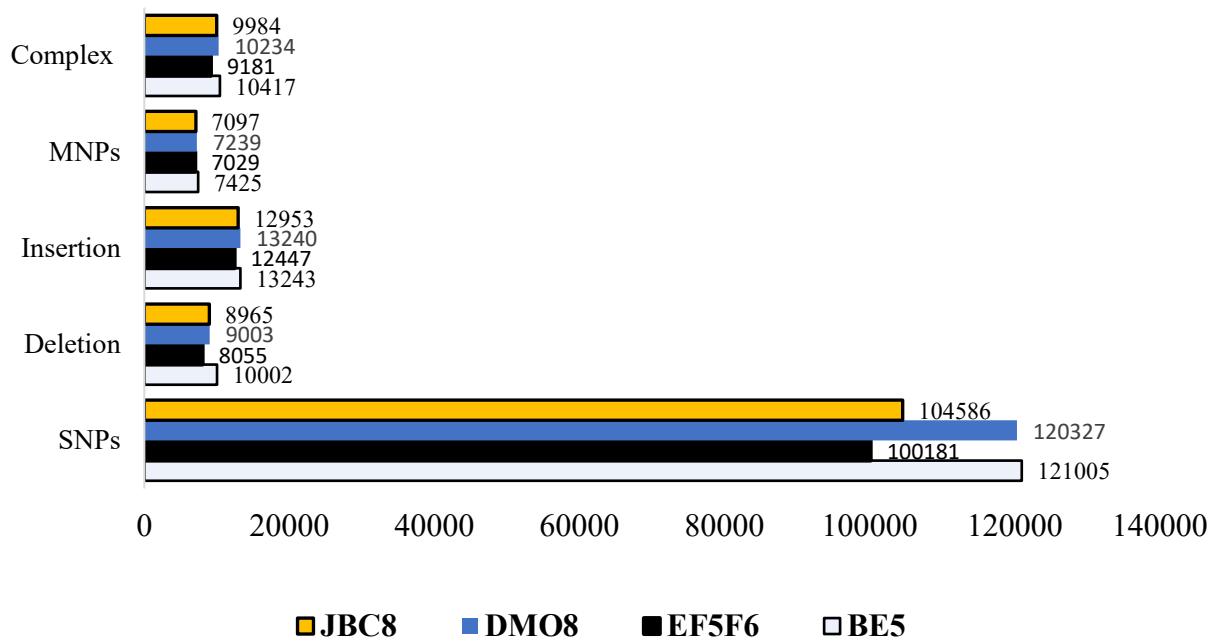
Figure 6.2. Variant data from the dysflagellar mutant and three locally collected strains compared to the _L. braziliensis_ reference genome (strain MHOM/BR/75/M2903). The numbers of the recorded variations are shown in the figure. Variants were called with FreeBayes

However, in EFSF6 there was a large deletion of ~27 kb detected on chromosome 35 (604,400 kb-631,100 kb). Figure 6.3 highlights the deleted region, with two small segments of DNA remaining. These two segments appear highly variable with the first containing many SNPs and the second segment is a predicted site of inversion or duplication.

The large deletion contained four genes; LbrM.35.1660, 70, 80, 90. Functional predictions, based on orthologs from other species, suggest that LbrM.35.1660 and LbrM.35.1670 are both serine/theorine kinases, LbrM.35.1680 contains a predicted engulfment and motility domain and LbrM.35.1690 is a hypothetical conserved protein, without a predicted function (Figure 6.4b). LbrM.35.1660 was conserved across kinetoplastids including _T. brucei_ and _Bodo saltans_ (a free living kinetoplast), whilst the other three genes were conserved in a restricted cluster of organisms including _Leishmania spp, Crithidia_ and _Leptomonas_ (Figure 6.4a).
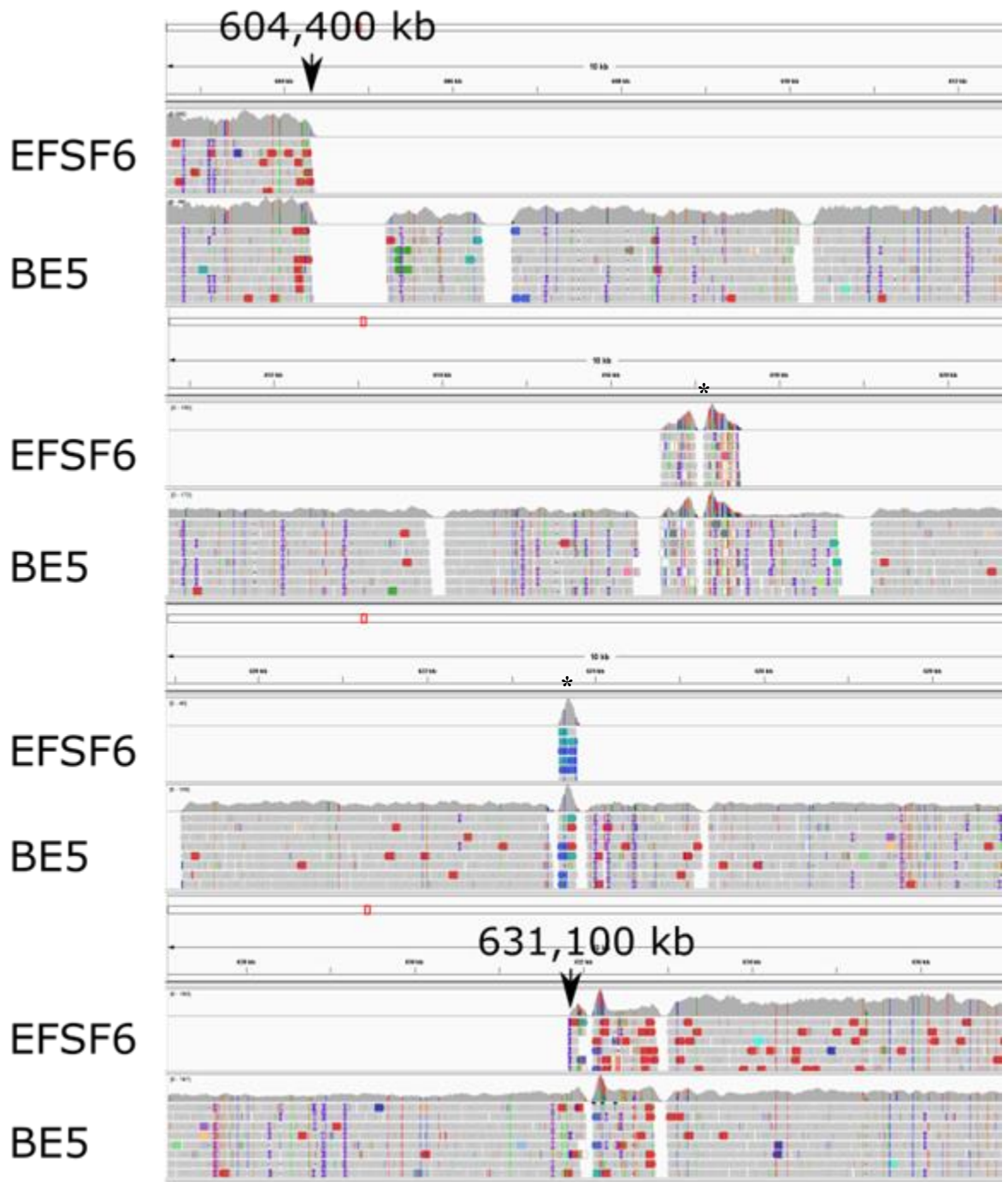
Figure 6.3. IGV screenshot of the dysflagellar mutant (EFSF6) compared to a local *L. braziliensis* strain (BE5). The 27 kb deletion is present on Chromosome 35 from 604400 kb – 631100 kb. Within this deletion, there are two small regions of DNA that remain (highlighted with *).
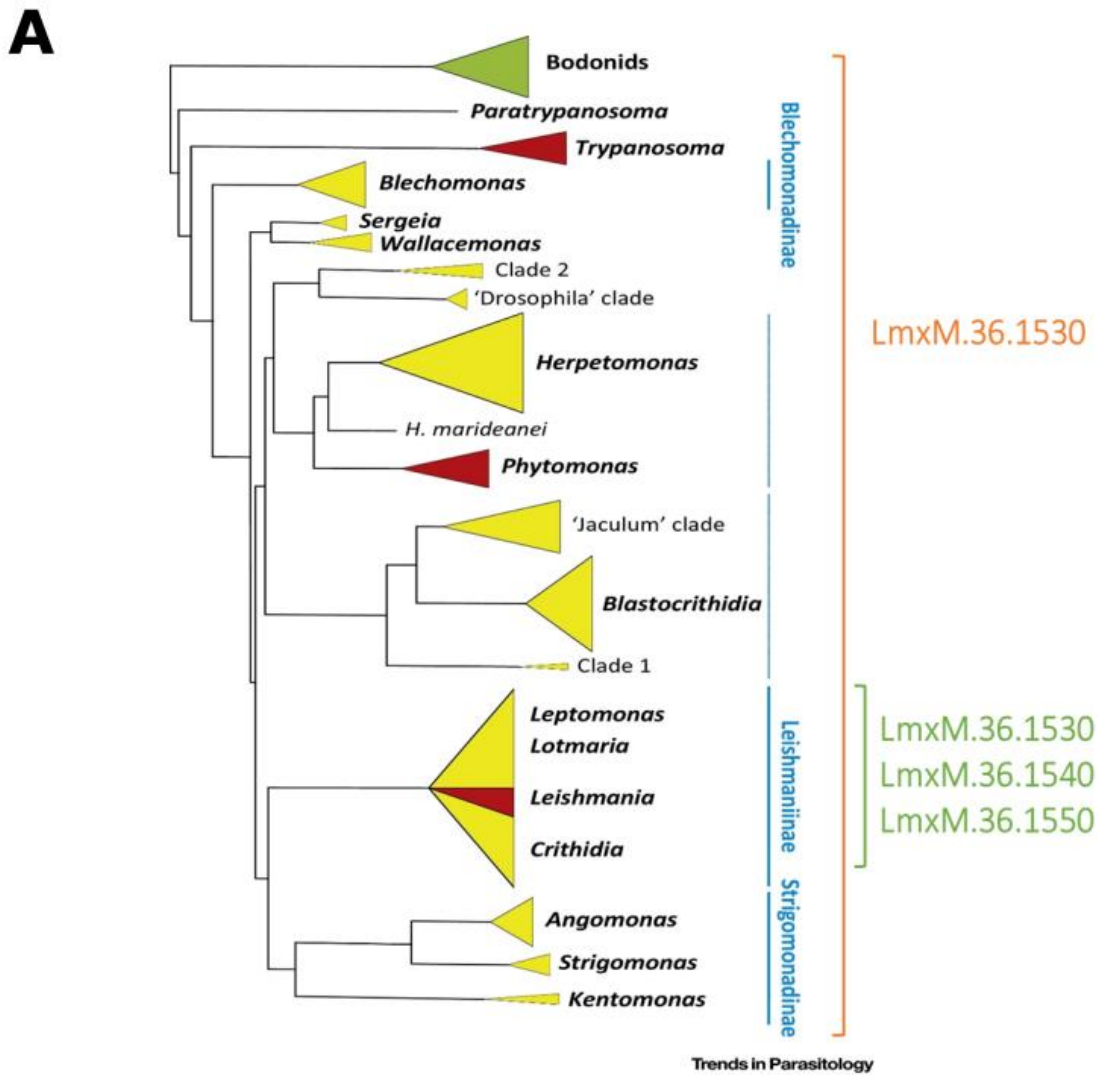
Figure 6.4 Genetic descriptions and phylogeny of the deleted genes. A. Shows the conservation of the deleted genes across the trypanosomatid family. The NEK17 like serine/threonine protein kinase was conserved throughout the family and the other three deleted genes were present only in a restricted set of parasites (Votýpka et al., 2015) **B.** Table showing the four deleted gene IDs in the dysflagellar mutant, the orthologues in *L. mexicana* and the annotation describing the predicted function of the genes.

6.2.2 The deletion contained four genes.

Due to logistical constraints (licence restrictions, lack of efficient genetic editing tools), it was not possible to carry out the experiments in *L. braziliensis* therefore, subsequent analysis was conducted on *L. mexicana,* the using a different *Leishmania* species will be discussed later in the chapter. The gene ID orthologues for *L. mexicana* are shown in Figure 6.4b. A point of clarity, the genome of *L. braziliensis* has 35 chromosomes due to the independent fusion of chromosomes 8 and 29 and 20 and 36 whilst other *Leishmania* species have 36 chromosomes (Britto et al., 1998).

These genes were endogenously tagged, and the localisations are shown in Figure 6.5. The localisations appeared random and there is no association to specific structures of organelles. The localisations included, nuclear, flagellar pocket, kinetoplast, basal body and cytosol (see Figure 6.5).

6.2.3 Replicating the deletions in *L. mexicana* generated 'bulge' flagella.

Orthologs of the deleted genes in the dysflagellar mutant were identified in *L. mexicana* (Figure 6.4b). In *L. mexicana* promastigotes the four genes were endogenously tagged with mNeonGreen to determine the protein localisation (Figure 6.5). LmxM.36.1520::mNG promastigotes showed a bright signal in the nucleus and basal body, with a reduced signal in the cytoplasm and flagellum. In dividing parasites, the nucleus and basal body signal remained but the cytoplasm and flagellum signal were greatly reduced. LmxM.36.1530::mNG promastigotes exhibited a bright signal in the cytoplasm in addition to a lysosome signal, which in dividing parasites became diffused. LmxM.36.1540::mNG promastigotes had a very bright signal in the flagellar pocket, which extended into flagellar 'streamers' (frayed sections of flagellum membrane that extend from the flagellum). Dividing parasites retained the flagellar pocket signal in both flagella. Both LmxM.36.1550::mNG promastigotes and dividing parasites had a cytoplasm signal along with a bright basal body signal (Figure 6.5, white arrows). The four tagged proteins showed various localisations in *L. mexicana* with no clear pattern of localisation. Some of the proteins showed associations with flagellum related structures including the flagellar pocket and basal body.

Both alleles of each of the four genes LmxM.36.1520-1550 were then deleted in *L. mexicana* promastigotes using CRISPR/Cas9 (Figure 6.6a). Parasites were seeded onto clonal plates, clones selected and cultured in a larger volume for further analyses. The mutants did not show any significant growth defects in comparison to the parental parasites (Figure 6.7a). PCR was used to verify to the gene had been successfully deleted, with loss of the ORF confirmed (Figure 6.6b). Across the four knockouts similar phenotypes were observed: Normal flagellum (the external flagellum was more than half the length of the cell body), Short flagellum (external flagellum was less than half the length of the cell body), flagellum bulge (the flagellum was very short, barely extending from the flagellar pocket, it could be rounded, frayed or straight) or no visible flagellum (Figure 6.7b, 6.8a).

The proportions of these different morphologies varied between the mutants. For example, the majority of *Δ36.1520* and *Δ36.1530* cells had a 'flagellum bulge'. The cells with a flagellum bulge, were not motile i.e., there was no directional movement, but instead the bulge appeared to show some form of beat from side to side (supplemental video 6a-6c). This bulge morphology was also present in *Δ36.1540* and *Δ36.1550* but at a much lower proportion (Figure 6.8b). In the *Δ36.1540* and *Δ36.154*0 mutants, most parasites had a normal length flagellum (Figure 6.8b) or had cells with a short flagellum, where the length of the flagellum was less than half that of the cell body.

There were a very small proportion of parasites with no visible flagellum in all deletion cell lines. Other than the differences in flagellum morphology there appeared to no other visible changes to the parasites.

From light microscopy analyses, the flagellum bulge morphology appeared similar to the dysflagellar mutants. They showed very limited motility and retained the collection of material at the exit of the pocket, as described by Zauli (Zauli et al., 2012). However, further analysis by TEM was required to determine if the ultrastructure of the flagellum bulge reflected that of the dysflagellar mutant.
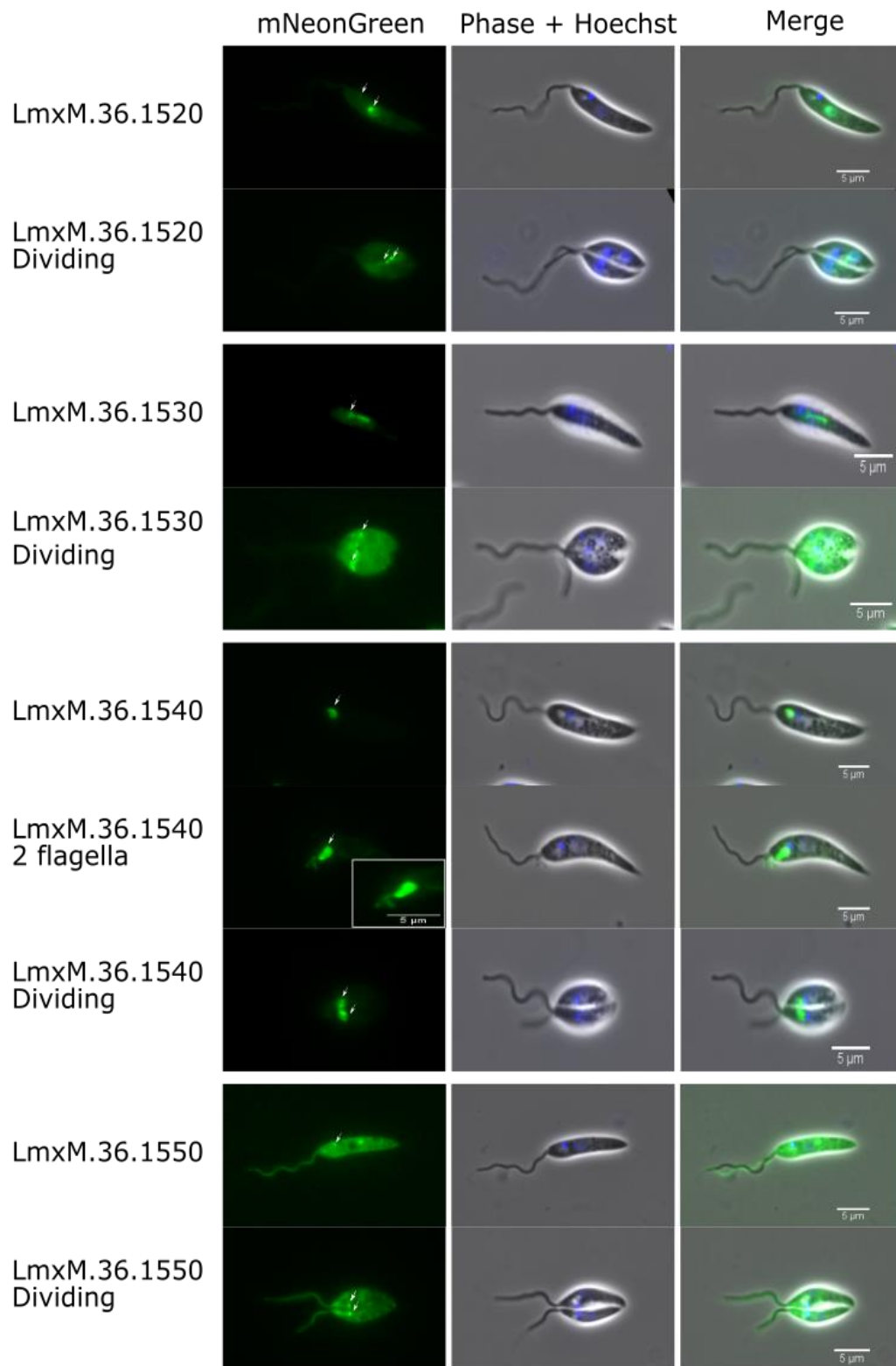
Figure 6.5 Localisation of the four genes found to be deleted in the dysflagellar mutants (EFSF6). Orthologues of the deleted genes from the dysflagellar mutant were identified and localisations were replicated in. *L. mexicana* promastigotes. Parasites are shown expressing LmxM36.1520-50 with mNeonGreen are (scale bar = 5 μm). Individual parasites with either one flagellum, two flagellum or dividing are shown. White arrows highlight the signal in the mNeonGreen channel.

116
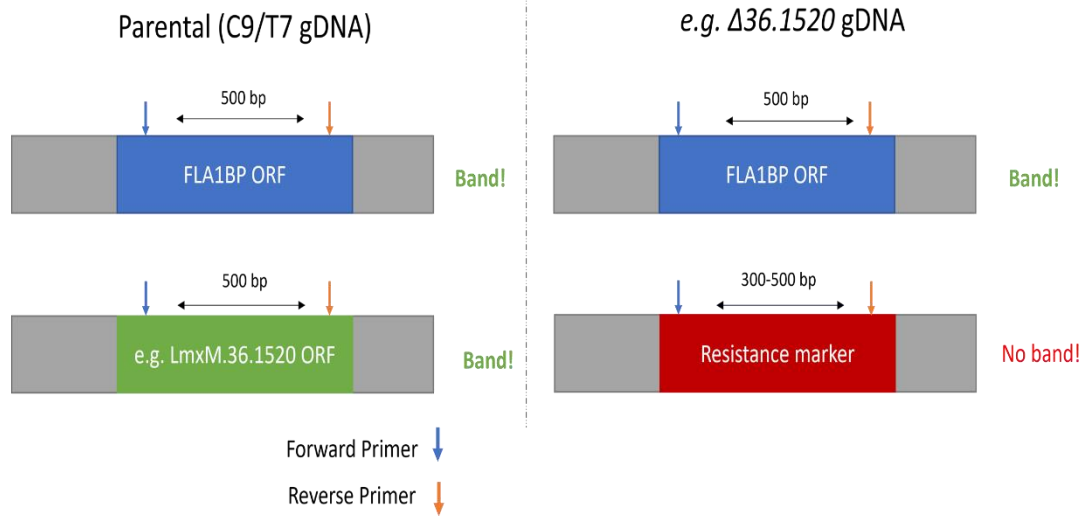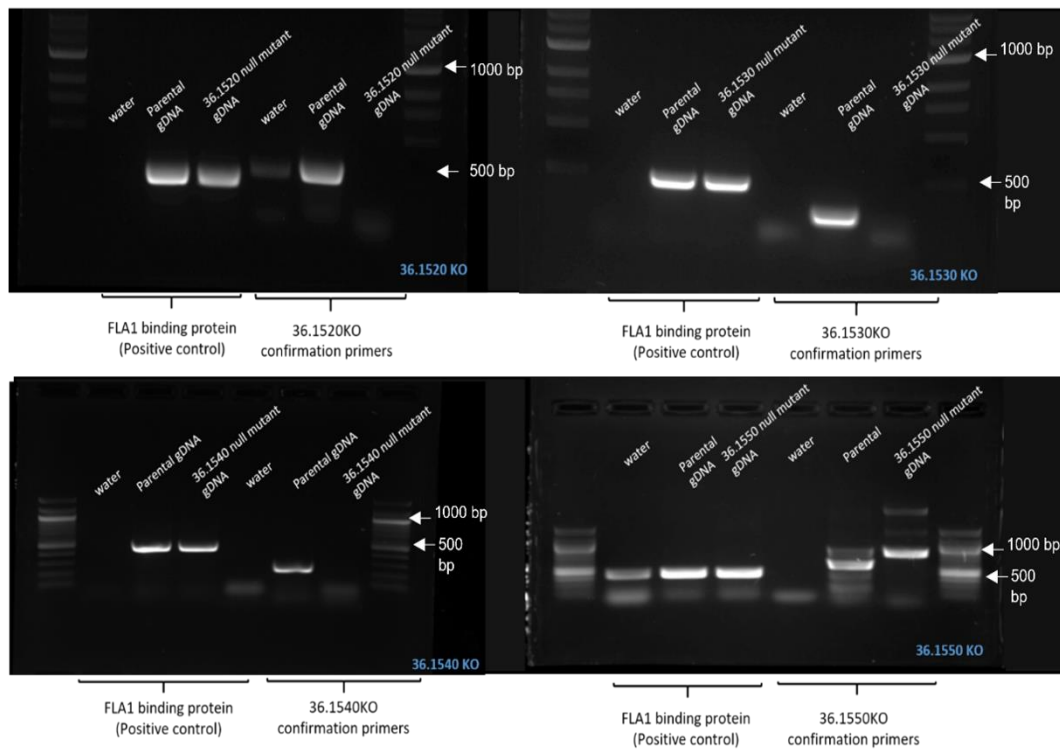
Figure 6.6. Diagnostic PCR confirmed the individual gene deletions of LmxM36.1520-50 in *L. mexicana*. A. Schematic showing the primer binding sites and the outcome of the PCR with those conditions i.e., the expectation of a band. **B.** FLA1 binding protein and the parental C9/T7 gDNA acts as a positive control, water acts as the negative control. The primers were designed to produce a 500 bp gene product. The PCR products were run on a 1% agarose gel with NEB 100 bp DNA ladder.
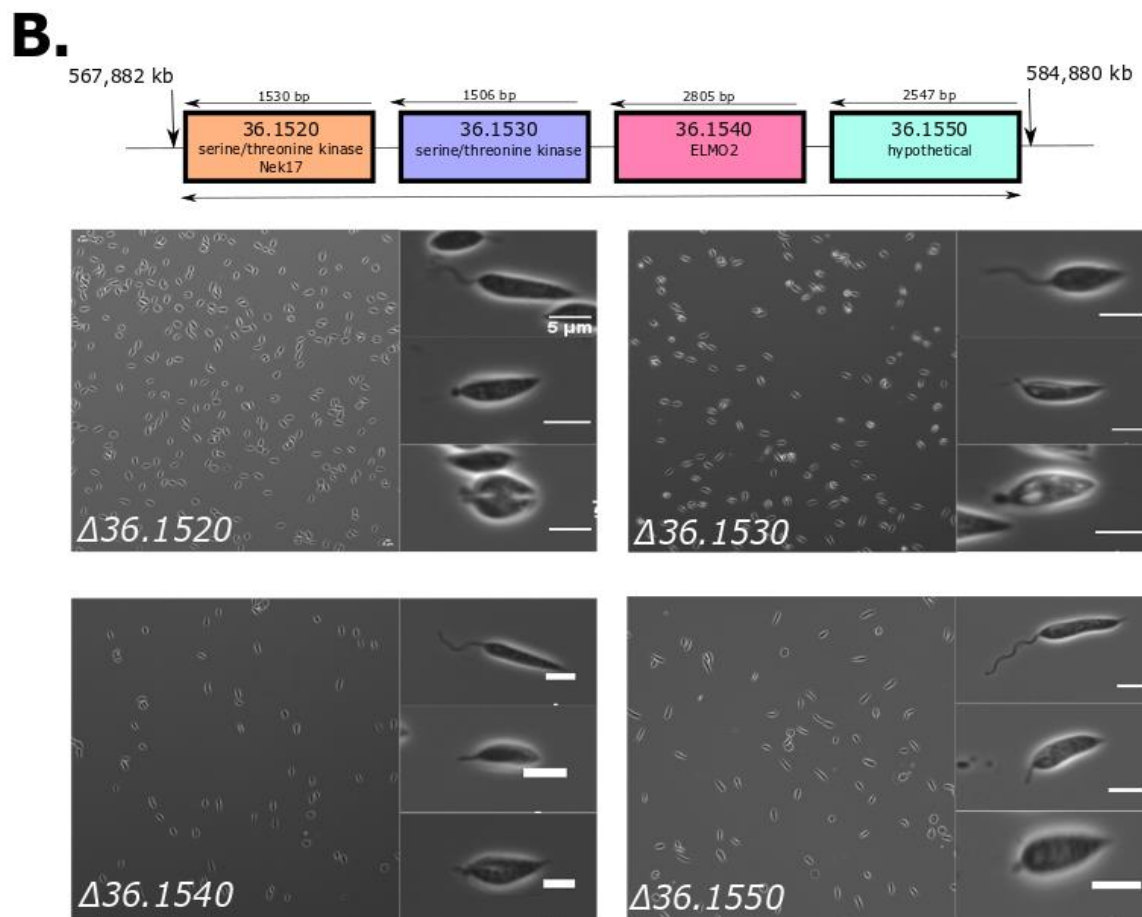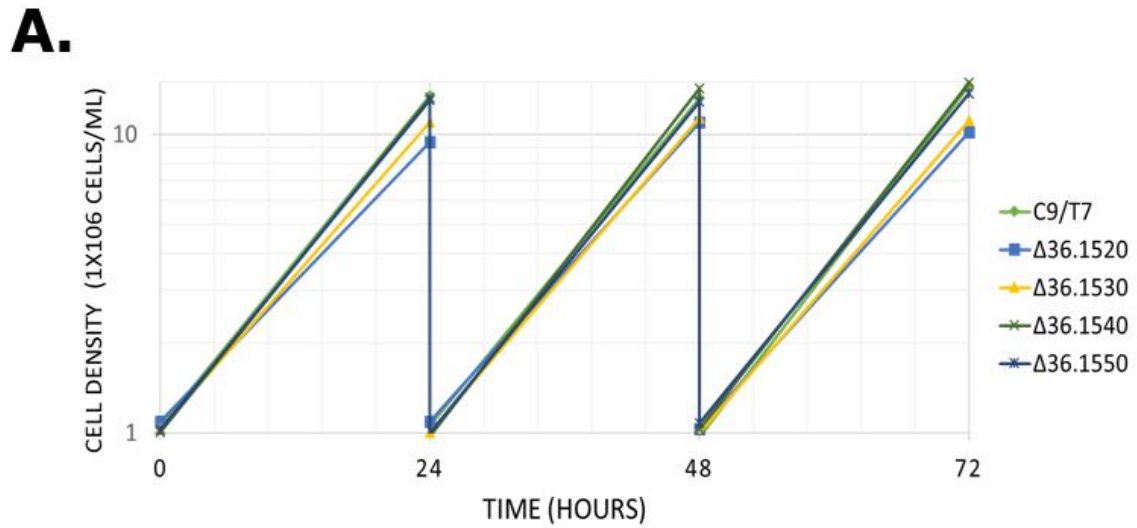
Figure 6.7. Growth curve and flagellum morphologies of the deletion mutants. A. Growth curves for the four deletion mutants plus the parental strain C9/T7 were generated over 72 hours. No significant growth defects were observed **B.** Schematic showing order and gene IDs of the deleted genes in EFSF6 in L. mexicana. Mutants were generated for each of the four genes in L. mexicana and the morphologies are shown.
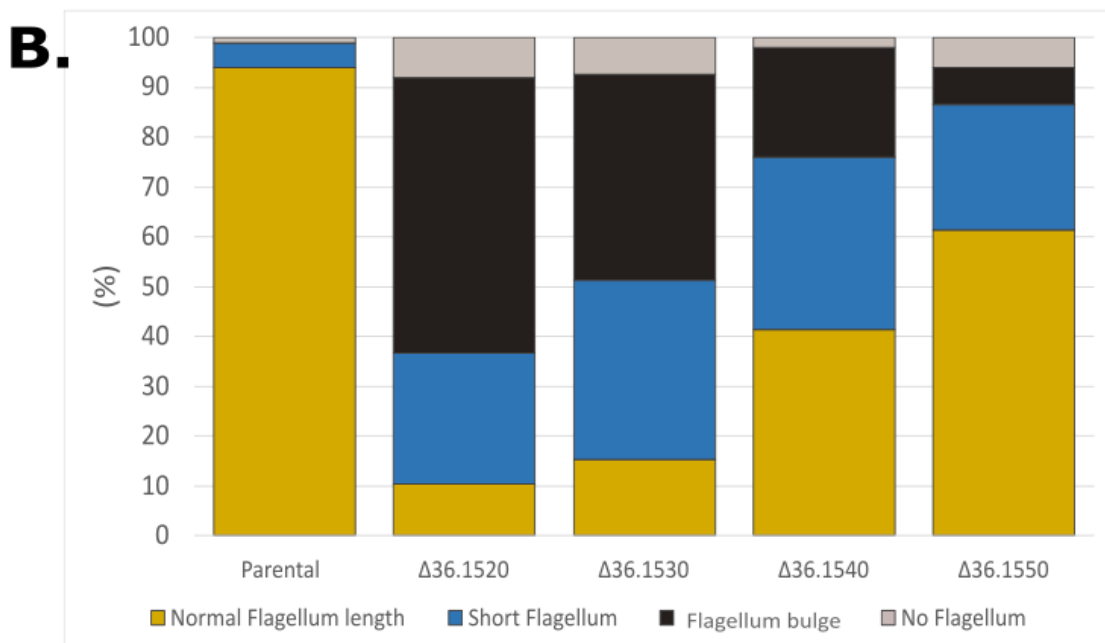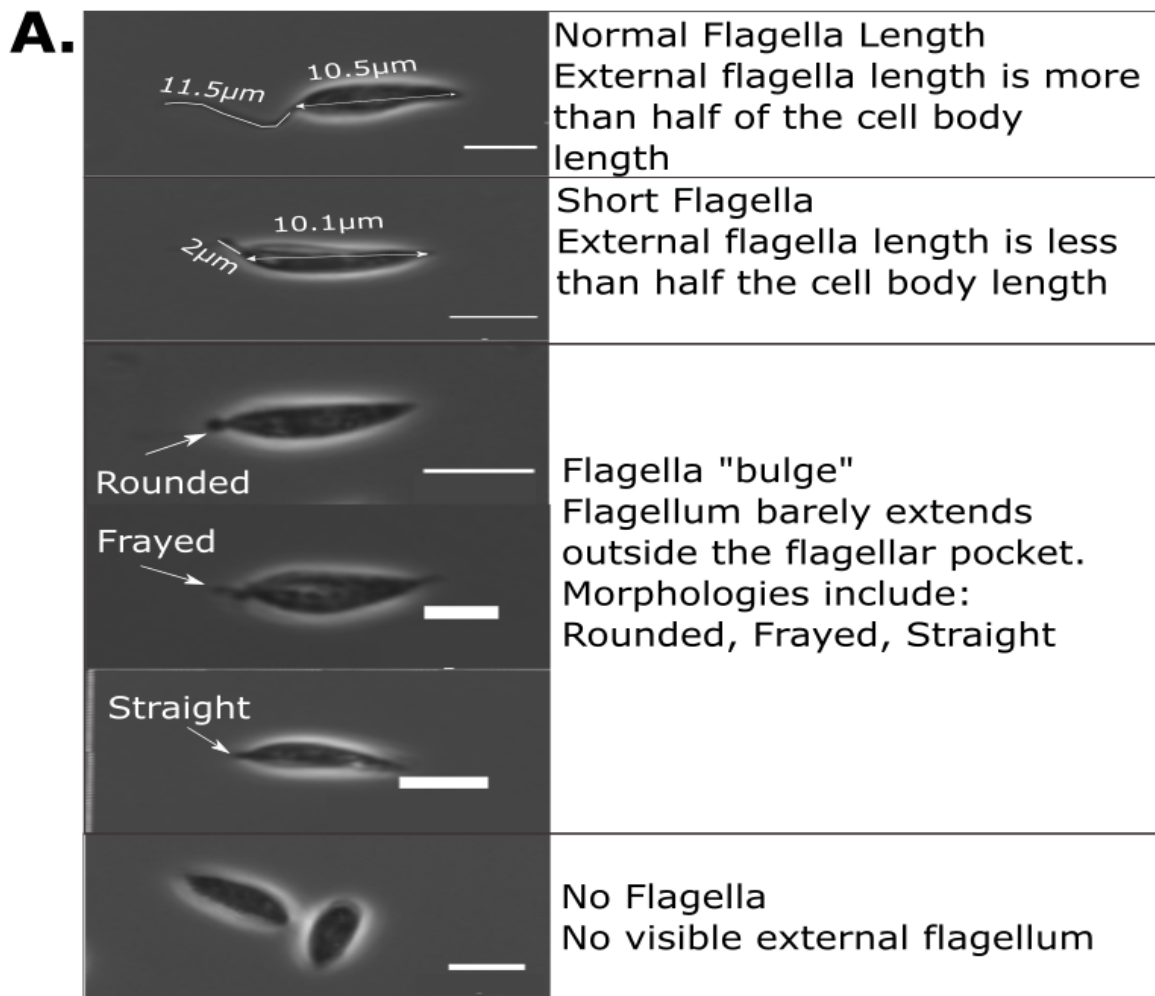
Figure 6.8 The knockout morphologies and proportions of the phenotypes observed across the deletion mutants. A. Main flagellum morphology categories observed across the mutants. Scale bar = 5 μm. **B.** Percentage of morphologies present across the different mutants *(n=300).*

6.2.4 The deletion mutants resembled the dysflagellar phenotype.

TEM analysis was used to examine the flagellum bulge in further detail. The normal ultrastructure of *L. mexicana* parasites is shown in Figure 6.9. In the parental parasites, most flagella extend out of the pocket and there are many cross sections of flagella indicating the presence of many flagella. The longitudinal and cross sections of an assembled axoneme show the lattice structure of the PFR. If the flagellum extends out of the pocket the cross section will show the microtubule doublets and central pair and sometimes the presence of PFR (Figure 6.9c). When the flagellum is located inside the pocket, the cell body can be seen surrounding the flagellum cross section (Figure 6.9d). The proportion of flagellum cross sections either located inside or outside the pocket (compared to the parental) will give an indication of the length of the flagellum i.e., longer flagellum means more external cross sections.

Almost 80% of *Δ36.1520* parasites had flagellum cross sections located inside the flagellar pocket (Figure 6.10) and very few external flagellum cross sections were seen, reflecting that the majority of these parasites in culture had a short or a bulge flagellum. Flagella had a 9+2 axoneme that seemed to assemble normally until the exit of the pocket where it appeared to stop. All microtubule doublets stopped at the same length, giving a 'blunt end' appearance (Figure 6.11b, f). At the exit of the pocket was the most striking feature of these cells; a large, rounded mass of unorganised material (Figure 6.11a-g). In this bulge lots of electron dense material was present and, in some cases, numerous vesicles around the bulge (Figure 6.11d). In many of the flagellum cross sections, instead of the organised PFR structure seen in the parental parasites a disordered electron dense, material was present, suggesting a failure to assemble an organised PFR.

Surprisingly, *Δ36.1530* parasites had only 30% of flagellum cross sections located inside the pocket (Figure 6.12). In culture, many parasites had either a short or a 'bulge' flagellum (Figure 6.12b), however TEM analyses showed that most of the flagellum extended past the exit of the pocket. The mutant parasites had a shorter cell body and most cross sections showed a typical 9+2 axoneme with assembled PFR. However, many of these cells had lots of disordered material around the flagellum and many contained multiple vesicles. The presence of a smaller rounded structure at the exit of the pocket was observed in some parasites and in some cases the axoneme extended past the bulge (Figure 6.12b). In other parasites, the axoneme extended out of the pocket by ~1 μm then a collection of vesicles at the flagellum tip created a rounded end (Figure 6.12e-f). From the cross sections, most flagella maintained a typical structure, a 9+2 axoneme and a clearly assembled and structured PFR (Figure 6.12h-k). However, in some examples, there was electron dense collection of highly disordered material that may have led to flagellar membrane distortion (Figure 6.12g).

Most *Δ36.1540* parasites showed a normal morphology (Figure 6.13). They maintained the elongated cell body shape and long flagella with a 9+2 axoneme. Most flagellum longitudinal and cross sections showed a highly structured PFR (Figure 6.13h-k) unlike the *Δ36.1520* and *Δ36.1520* mutants.

However, in a subset of cross sections the axoneme and PFR were present but there was also disordered material alongside the axoneme directly opposite the PFR (Figure 6.13h-k). The presence of this disordered material was found in cross sections both internal and external to the flagellar pocket. *Δ36.1550* parasites were poorly infiltrated and due to limited time could not be repeated, therefore are not included in these analyses.

The TEM images, particularly of *Δ36.1520* parasites, show disordered electron dense material in the flagellum that is gathered at the exit of the flagellar pocket. These images reflect the dysflagellar mutants' morphology, therefore we can assume that deletion of LxmM.36.1520 and to some extent LxmM.36.1530 generates a similar phenotype (Zauli et al., 2012).
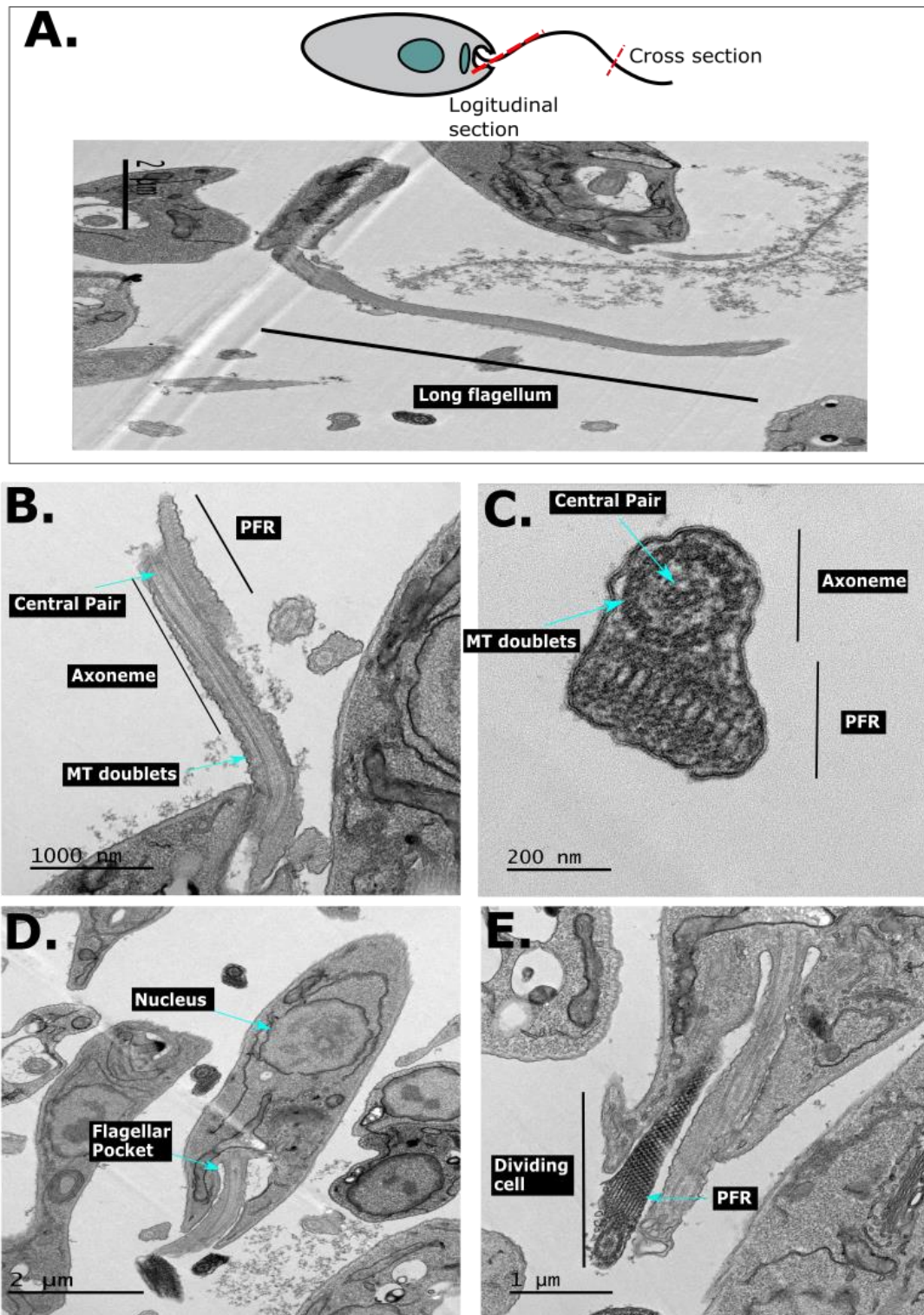
Figure 6.9. The normal structures observed in the parental promastigotes by TEM. A. Cartoon of *L. mexicana* parasite and example of a longitudinal section of a long flagellum. **B**. Longitudinal cross section of the flagellum highlighting axoneme structures. **C.** Cross section of an axoneme with 9+2 axoneme structure and highly structured PFR. **D.** Cell body morphology. **E.** longitudinal section of the PFR
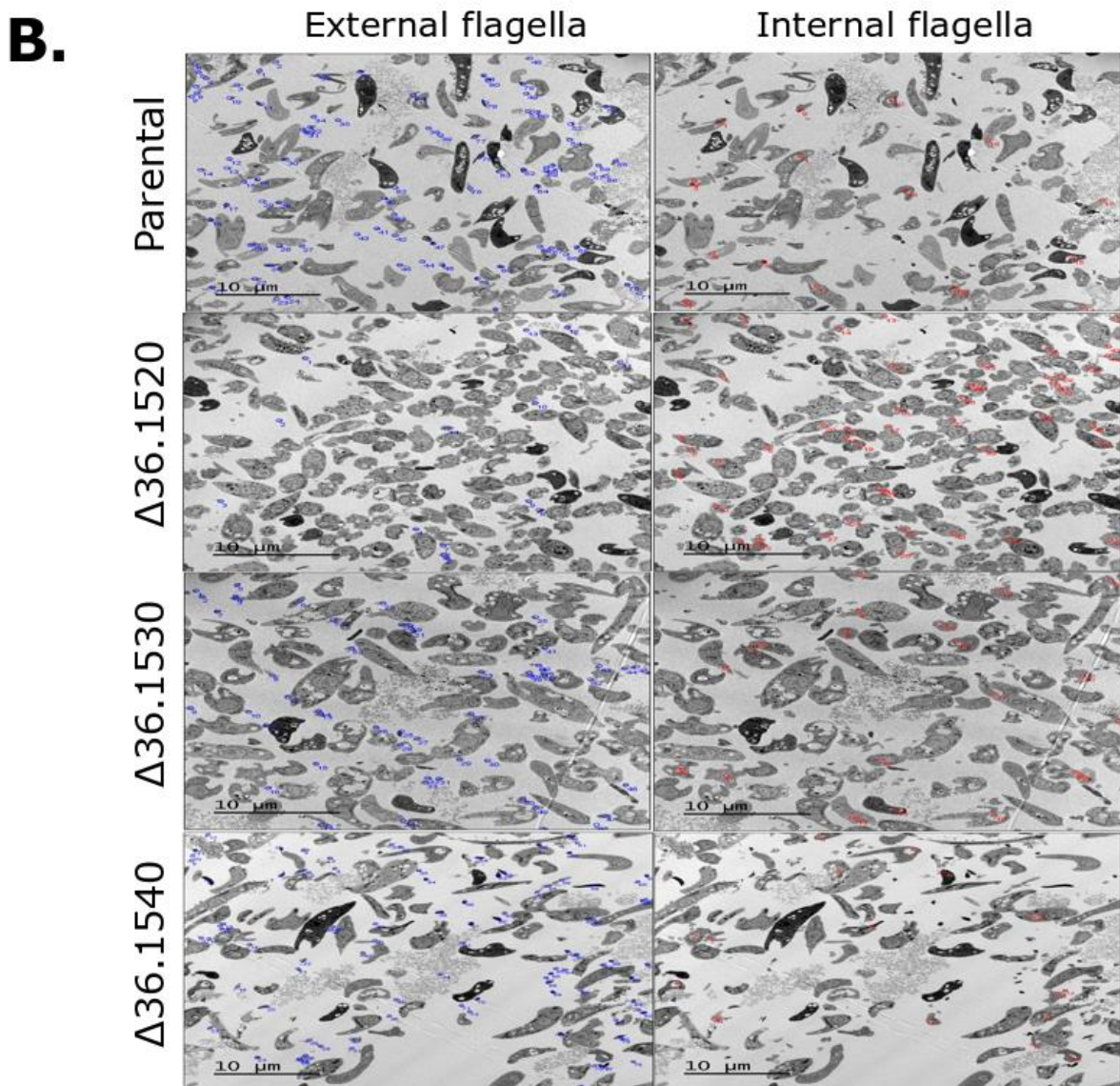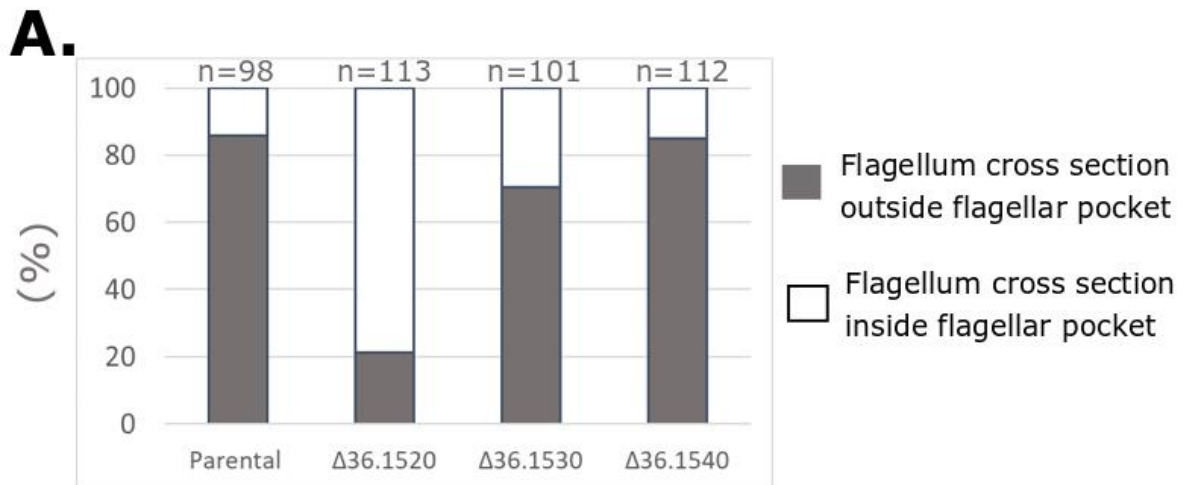
Figure 6.10. 'External' vs 'Internal' of the flagellar pocket flagellum cross section counts. Many external cross sections indicate long flagellum that extend past the flagellar pocket whilst many internal cross sections suggest the flagellum is very short. **A.** Ratios across the deletion mutants for internal vs external. **B.** Examples of TEM slices with labelled interval vs external flagellum cross sections.

ΔLmxM.36.1520
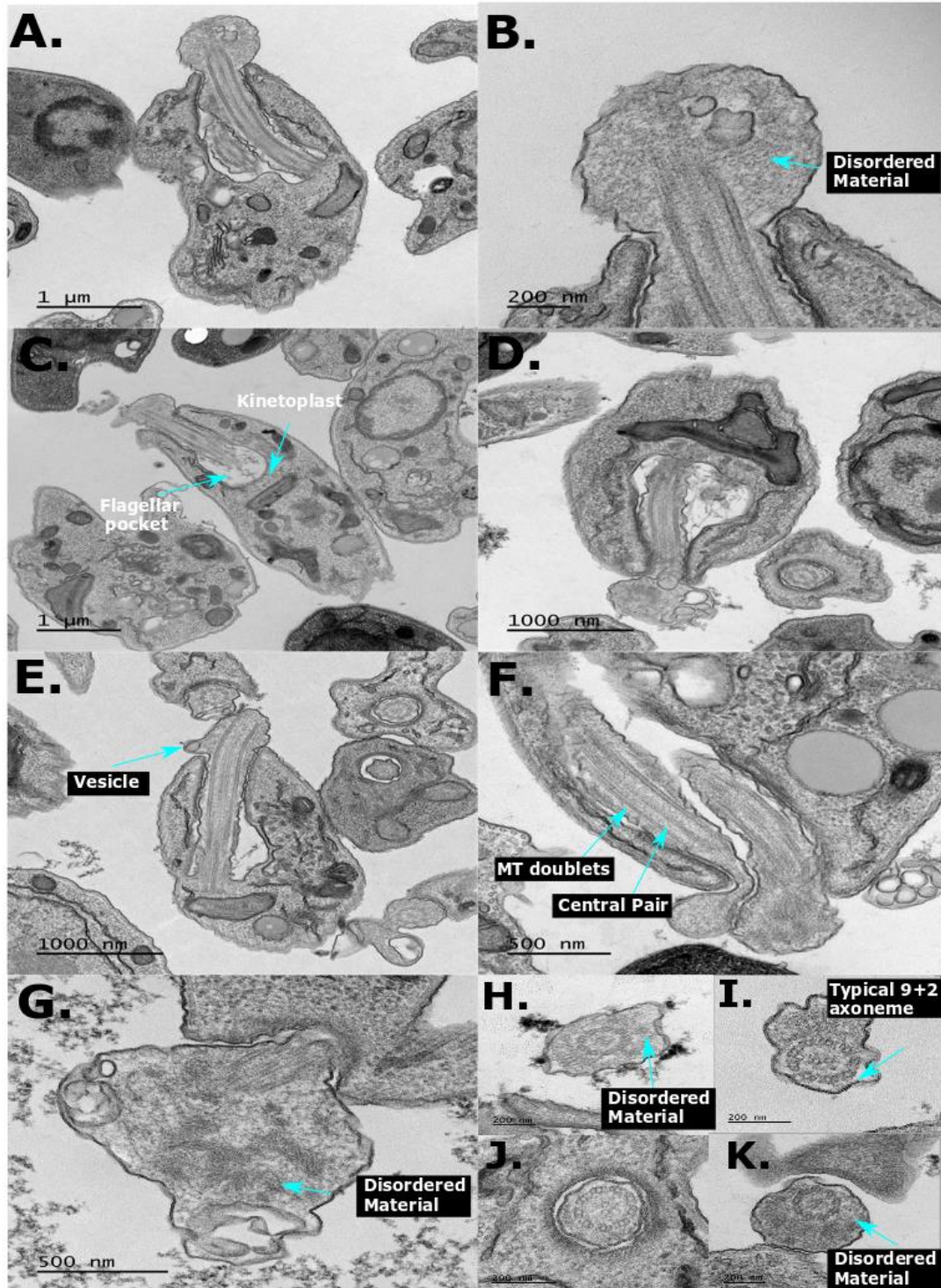
Figure 6.11. TEM analyses of the 36.1520 deletion mutant. A-G Examples of the disordered electron dense material in the bulge at the exit of the flagellar pocket. Key structures are labelled. **H-K** flagella cross sections showing a normal 9+2 microtubule doublet axoneme. Some cross sections show the electron dense disorganised material surrounding the axoneme.

ΔLmxM.36.1530
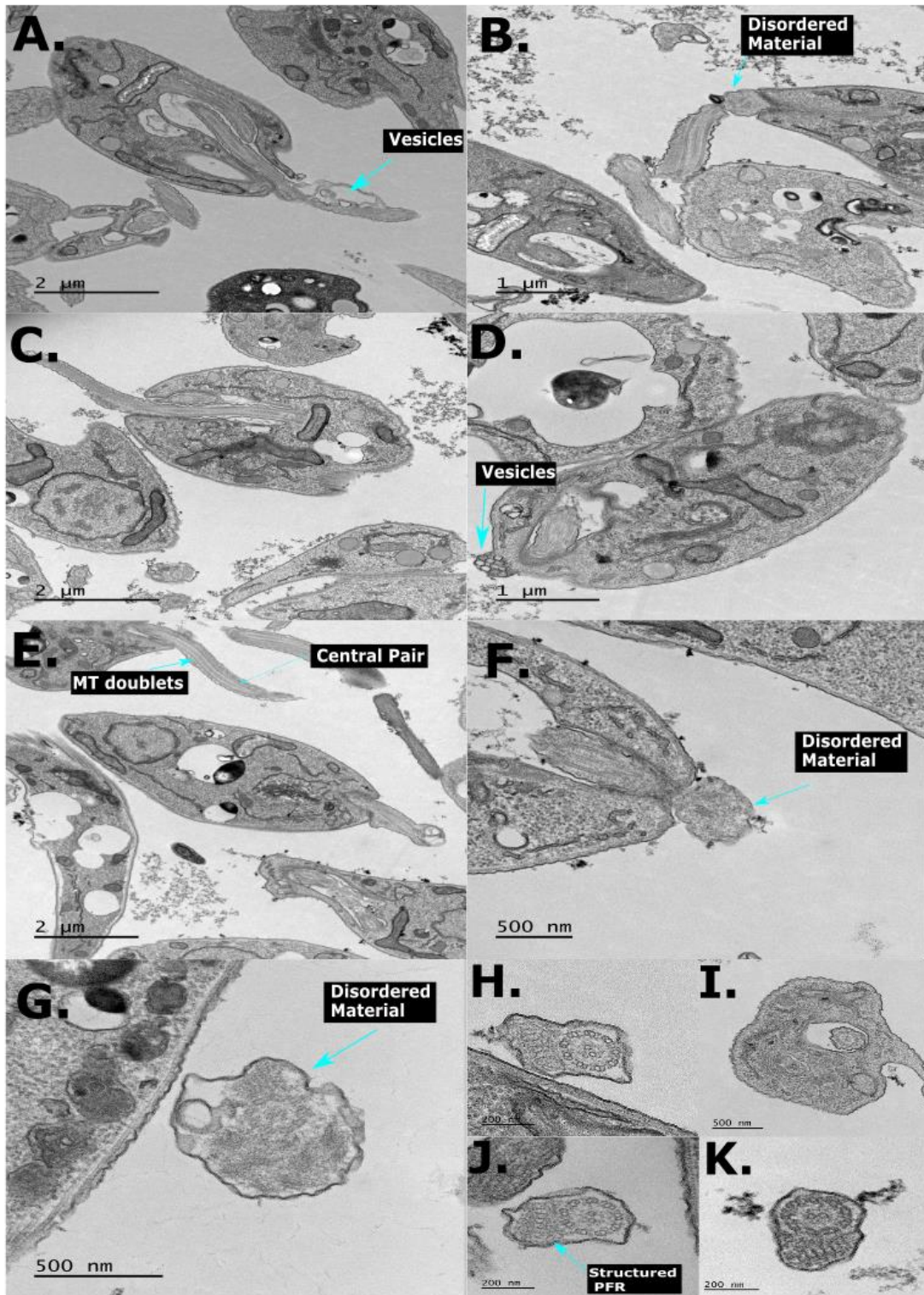
Figure 6.12. TEM analyses of the 36.1530 deletion mutant. A-G Examples of parasites with longer flagella. Many have vesicles along the length of the flagellum and gathered at the tip. Some examples of the disordered bulge can be seen. Key structures are labelled. H-K flagella cross sections showing a normal 9+2 microtubule doublet axoneme with most cross sections showing a structured PFR.

ΔLmxM.36.1540
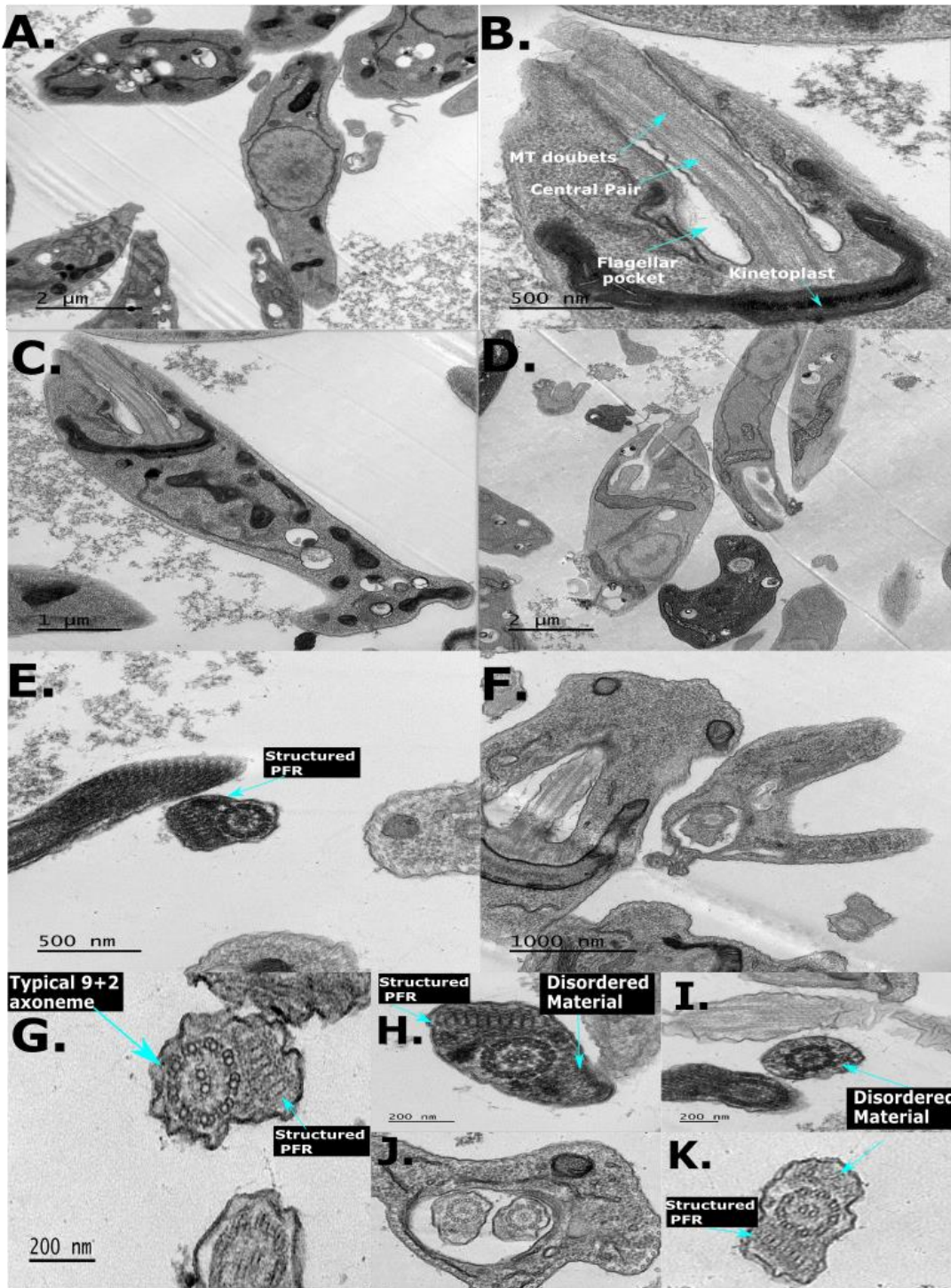
Figure 6.13. TEM analyses of the 36.1540 deletion mutant. A-G Show examples of parasites with a mostly normal cell body and flagella structure. Key structures are highlighted. H-K Most flagella cross sections had structured PFR material. Some had additional disordered material on the opposite site of the axoneme than the PFR and some showed disordered material alongside the axoneme.

6.2.5 Mutants retained an IFT pool and could differentiate into axenic amastigotes but failed to form attached forms.

The dysflagellar mutants were shown to survive both in mammalian macrophages and in sand flies. As *in vivo* experiments are not possible in our laboratory, the *in* vitro forms of amastigotes and haptomonads were used. These act as a simplified way of analysing the abilities of the mutant parasites to successfully differentiate.

IFT is required to assemble a full-length flagellum in *Leishmania (*Sunter et al., 2018). Therefore, as these mutants failed to assemble a flagellum, IFT was analysed to determine its location and functionality in the mutants. IFT139 was endogenously tagged with mNeonGreen in *Δ36.1520* and *Δ36.1530* mutants as these mutants had the most severe phenotypes (Figure 6.14a). In parasites with a large, disordered bulge, IFT139 had a very bright signal at the base of the flagellum where the IFT pool is located, but a signal was not present inside the bulge. In parasites with a very short flagellum but without a bulge there was a bright IFT signal along the short flagellum, with the brightest signal concentrated in the distal region of the flagellum. Supplemental video 6d shows IFT movement in the *Δ36.1530* mutant.

To assess the mutant's ability to differentiate into axenic amastigotes, *Δ36.1520* and *Δ36.1530* parasites were placed into differentiation media and incubated at 34°C for 48 hours. The mutants successfully differentiated to axenic amastigotes (Figure 6.14b). The parasites showed similar morphology to typical axenic amastigotes with a smaller, spherical cell body and no external flagellum. In addition, to assess the ability to differentiate to attached forms, mutants were seeded onto gridded culture dishes for 24 hours and left to form attachment. Compared to the parental line, the mutants showed little attachment to the coverslip (Figure 6.15a). The *Δ36.1530* mutant formed around 40% less attached forms than the parental parasites. Most of these were defined as plaque forms, a stage that typically occurs later in attachment. Whilst the majority of the parental attached forms were at the looped flagellum stage, associated with earlier attachment (Yanase et al., 2022). However, for *Δ36.1520* mutant remarkably low levels of attachment were observed, in fact only one attached form was observed. The inability of these deletion parasites to form attachment is not surprising as these parasites are lacking a full-length flagellum, however this raises questions as to whether the dysflagellar parasites would be able to form a true infection in the sand fly if they could not adhere.

When the dysflagellar mutant was originally documented, the authors proposed that the material at the tip of the flagellum could be a collection of PFR components, which had failed to assemble a structured PFR (Zauli et al., 2012). In order to attempt to classify the material in the 'bulge', the parental parasites and the two most severe deletion mutant parasites *Δ36.1520* and *Δ36.1530* were stained with the antibody L8C4, which recognises PFR2, a key competent of PFR. Counts were taken

from five fields of view. The parental parasites had a bright signal that extended along the flagellum from the basal body and stopped roughly <2 μm from the flagellum tip (Figure 6.16a-b). All parasites in the field of view had a flagellum signal suggesting normal PFR assembly. In contrast, very few *Δ36.1520* mutants had a signal in the flagellum (Figure 6.16a). In the small number that retained a signal, it was a linear signal along the axoneme that stopped just before the end of the flagellum (Figure 6.16b). The signal was not observed in the disordered bulge of the mutants (Figure 6.16b). In *Δ36.1530* mutants, a higher proportion of parasites had a L8C4 signal in the flagellum (Figure 6.16a). The majority of parasites with the L8C4 signal were those with normal length flagela. In the few shorter/bulge flagellum that retained the signal, it was present from the base of the flagellum and extended, linearly, to just before the end of the flagellum. Similarity to the *Δ36.1520* mutants, *Δ36.1530* bulge parasites did not have a signal in the bulge. This suggests that in the mutants, PFR is at least partially assembled in some of the parasites. When PFR is present it is in the typical location along the flagellum and PFR material was not detected in the bulge. If the disordered material in the bulge was PFR material, we would expect an amorphous pattern of staining. However, as there was no detectable signal in the bulge it is likely that this is not PFR material or PFR2 protein at the least.
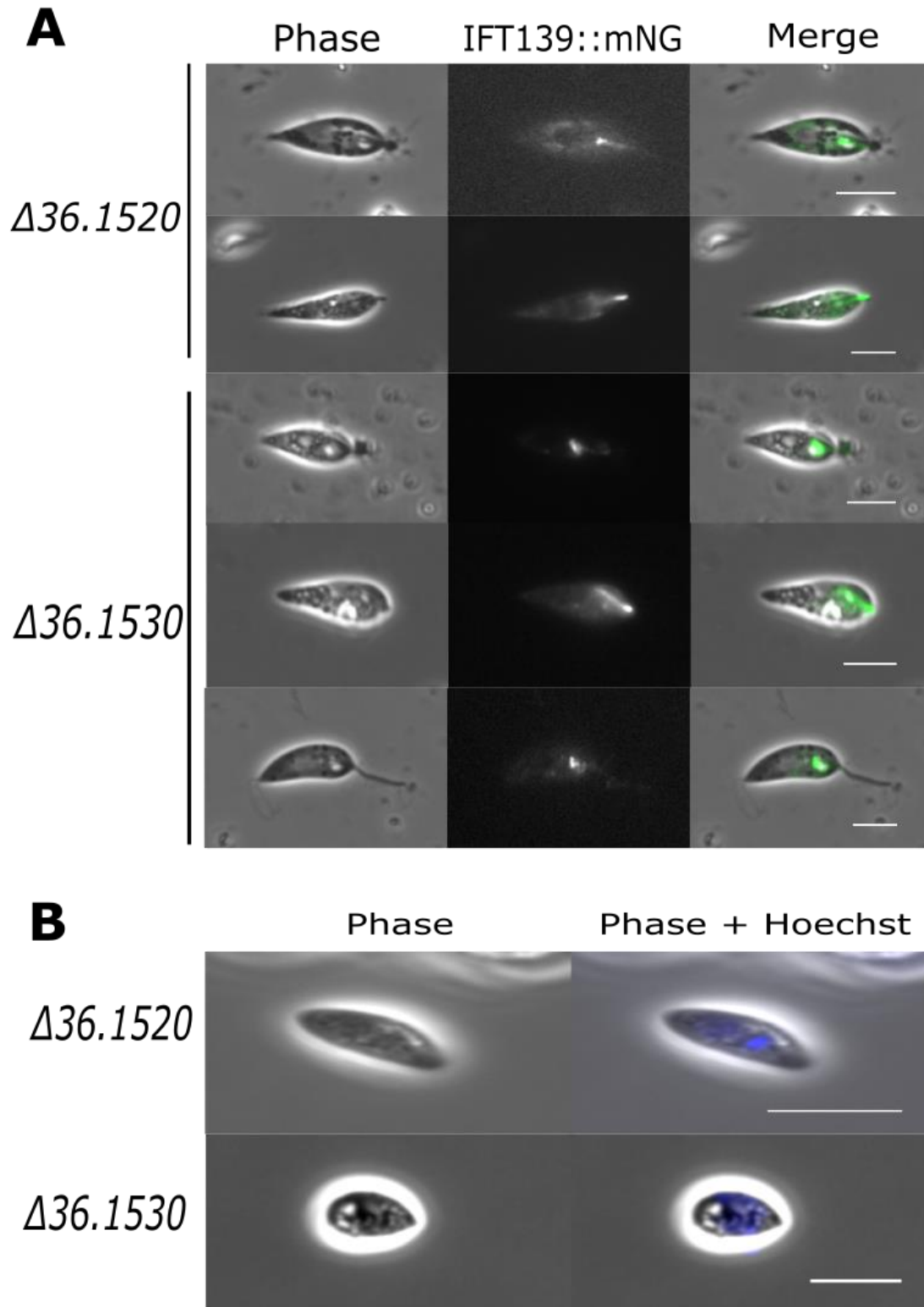
Figure 6.14. Deletion mutants have an IFT signal and can differentiate to amastigotes. A Deletion mutants, *Δ36.1520 Δ36.1530*, expressing IFT139::mNG. IFT can be seen in at the base on the flagellum and along the axoneme but not in the bulge. **B**. Deletion mutants could differentiation to axenic amastigotes. Parasites are shown at 48 hours into differentiation. (Scale bar = 5 μm)
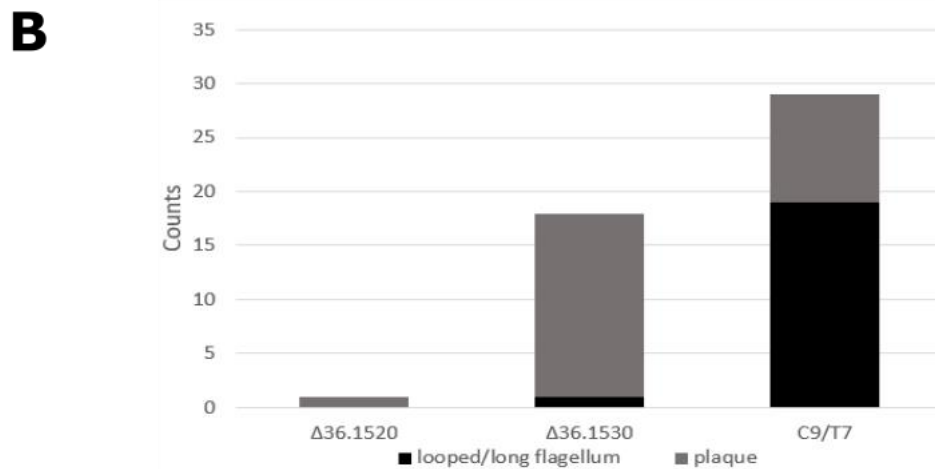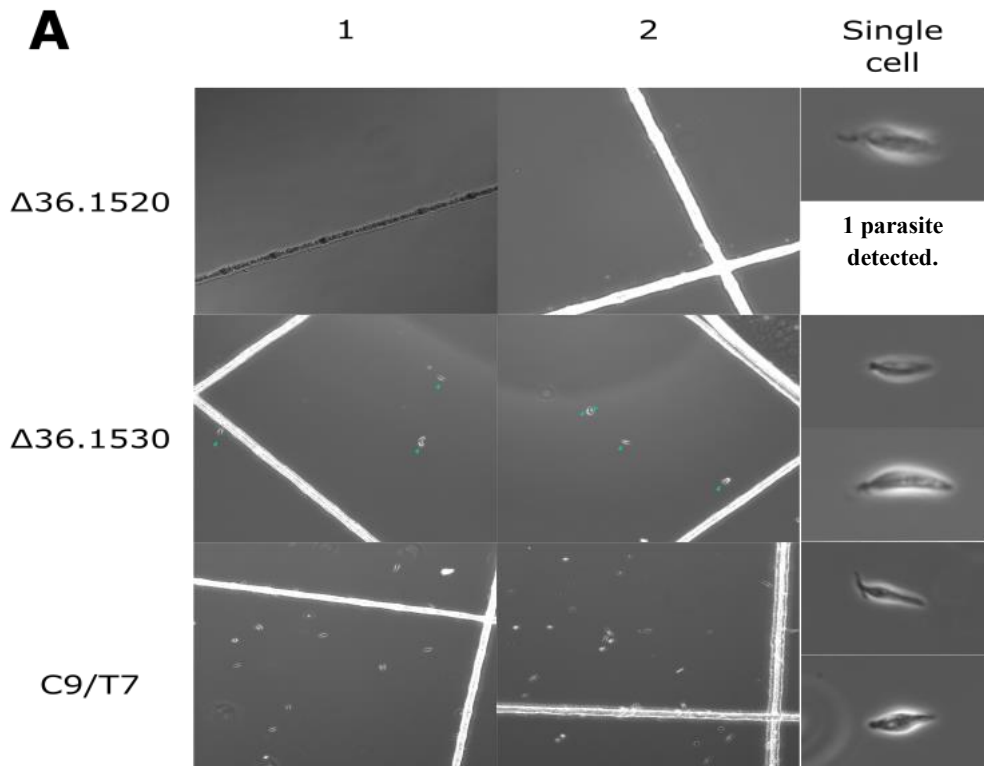
Figure 6.15. Deletion mutants struggle to form attachment. A. Parasites were left to attach to plates for 24 hours. Two examples of the field of view of the plates, for the *Δ36.1520, Δ36.1530* mutants and the parental strain C9/T7, are shown. Attached parasites are highlighted with cyan arrows. Examples of the morphologies across the cell lines are shown. **B.** Counts of the different types of attached parasites from five of the gridded sections of the parental C9/T7 parasites and the deletion mutants. (One replicate, counts collected from 5 fields of view).
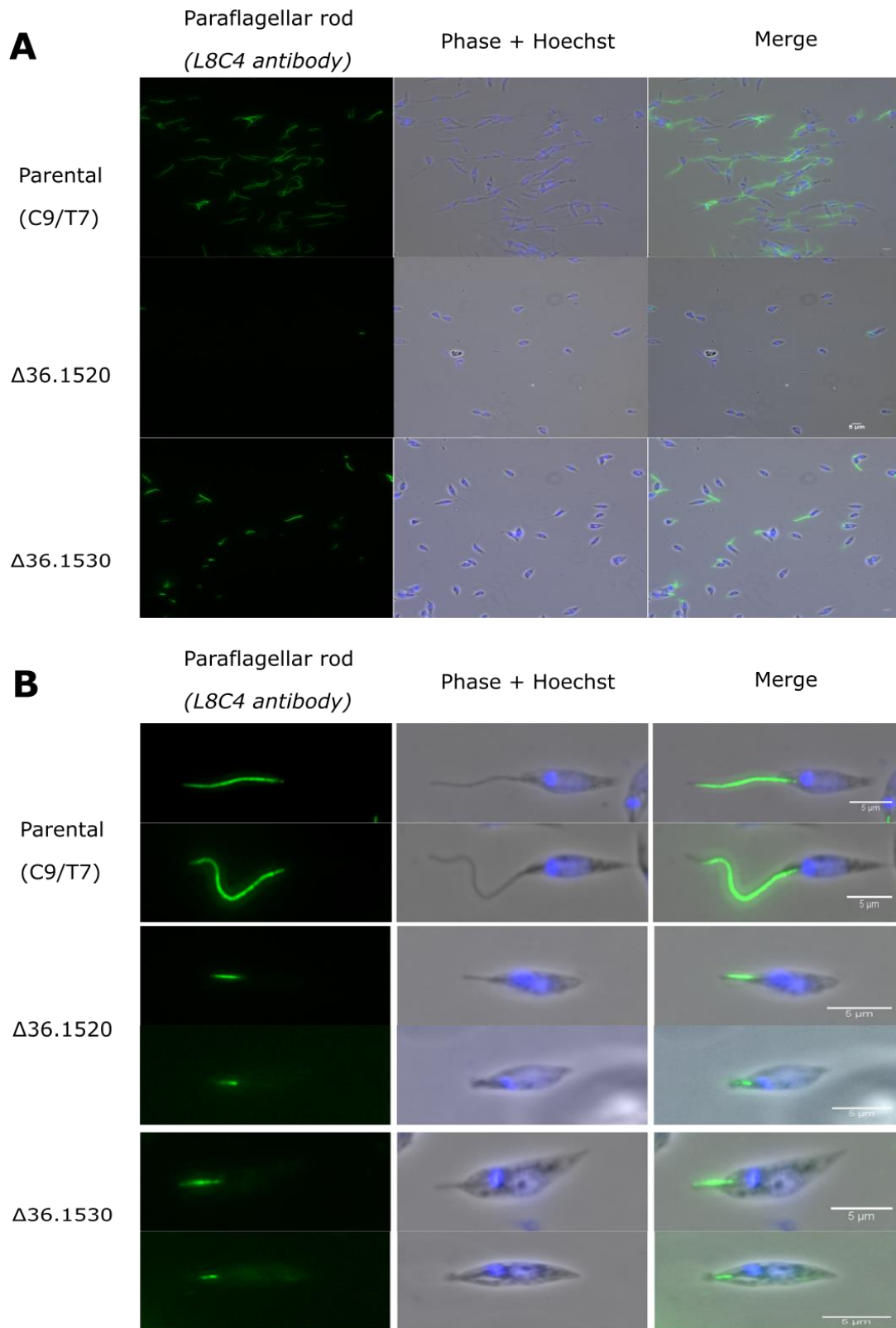
Figure 6.16. Parasites were stained with the L8C4 anti-PFR2 antibody. PFR2 is a component of the PFR. **A**. Field of view captured for parental and the *Δ36.1520 Δ36.1530* deletion mutants (40x). **B**. Examples of the parasites with the L8C4 signal shown in green (100x). (Scale bar = 5 μm)

6.2.6 The addback of the serine kinase rescued the 'bulge' phenotype.

To confirm that the bulge was the result of deletion of the serine/theorine kinase (LmxM.36.1520), add back cell lines were generated, addbacks or the other mutants were not generated due to time constraints. Addbacks expressed the serine/theorine kinase tagged with mNeonGreen at the N-terminus (Figure 6.17). These parasites were analysed by light microscopy and showed a bright signal at the basal body and the cytoplasm. This signal was similar to the endogenously tagged 36.1520 (Figure 6.5), confirming expressing of the addback gene. The addback parasites showed a full-length flagellum. Suggesting that the addback of the gene could successfully rescue the disordered flagellum phenotype.
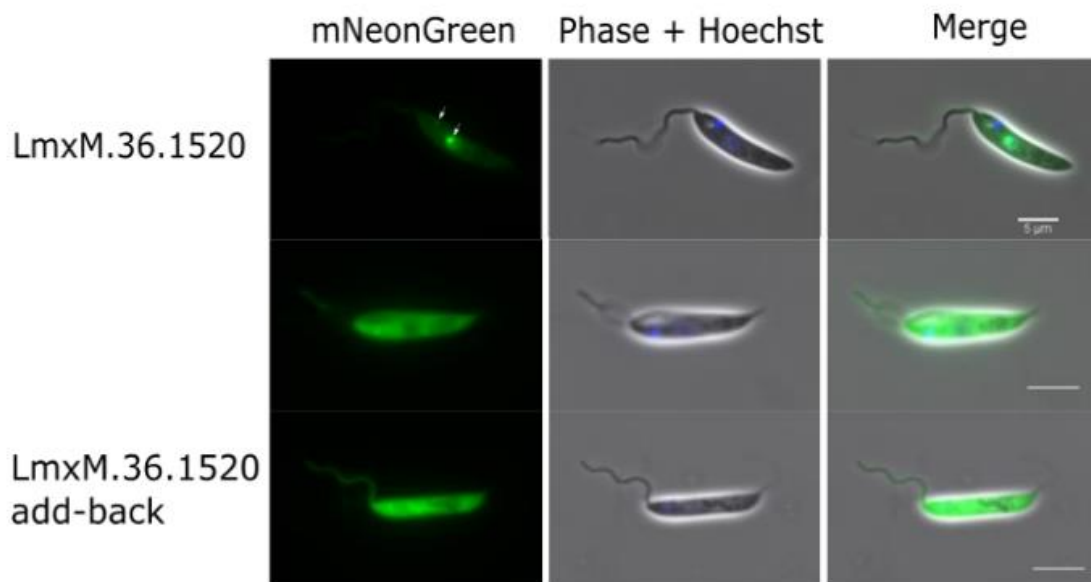
Figure 6.17. Add back of the 36.1520 gene to *Δ36.1520* deletion mutants restored the full length flagella. The green signal can be seen within the cytoplasm and flagellum. LmxM.36.1520 localisation is shown as the positive control. Scale bar = 5 μm

6.3 Discussion

The flagellum is considered vital for *Leishmania's* survival and transmission (Sunter & Gull, 2017). However, the detection of the dysflagellar mutant collected from patient samples challenges this idea. How can an immotile parasite infect and persist in the host?

6.3.1 A large deletion was detected on chromosome 35 in the dysflagellar mutant.

A large ~27 kb deletion on chromosome 35 in the dysflagellar mutant was detected. This deletion contained four genes with predicted functions including serine/kinases, one gene that contained an engulfment and motility domain and protein with no functional predictions. Deletion mutants of each of the four genes were replicated in *L. mexicana. L. mexicana* was used in these experiments rather than *L. braziliensis,* mainly due to logistical reasons (i.e., the license restrictions in using these parasites) but also due to the genetic editing tools readily available in *L. mexicana.*

All of the mutants showed no noticeable growth defects in comparison to the parental parasites. The severity of the flagellum morphology varied between the mutants. In *Δ36.1540* and *Δ36.1550* around 75-85% of parasites retained a normal length or a short flagellum but a small percentage (<25%) of parasites had a bulge or no visible flagellum. The TEM analyses of *Δ36.1540* showed mostly long flagella but in some cross sections there was a collection of disordered material on the opposite side of the axoneme to a structured PFR. Whilst *Δ36.1520* and *Δ36.1530* parasites show a more serve flagellar phenotype. Both showed ~50% of parasites had a bulge, or no visible flagellum and TEM analyses showed a large mass of disordered material at the exit of the flagellar pocket. In particular, the flagellum bulge of *Δ36.1520* was remarkably similar to the morphology described in the dysflagellar mutant (Zauli *et al.,*2012). The phenotype of *Δ36.1520* was rescued when a copy of the gene was reintroduced in the mutant. Therefore, we propose that the main underlying cause of the dysflagellar mutant was the loss of the Nek17 kinase (LbrM.35.1660).

However, the dysflagellar mutant was originally reported to have only 2-3% of parasites with flagellum (Zauli et al., 2012). From our study we found that in the *Δ36.1520* mutants, around 35% of parasites still maintained a long or short flagellum. Despite, multiple attempts to clone the bulge phenotype from the population the presence of parasites with a flagellum remained. Unsuccessful attempts were made to delete all the four consecutive genes. At most generated partial knockouts were generated, where at maximum the LmxM.36.1520 and LmxM.36.1550 were deleted and the middle two genes remained. Perhaps if the full knockout was achieved, we may have reported much lower percentages of parasites that retained a flagellum however, to date this has not been possible.

6.3.2 Could the dysflagellar mutants successfully complete the Leishmania lifecycle?

The dysflagellar mutants reportedly were successfully able to differentiate to amastigotes and persist in the sand fly vector for at least 96 hours (Zauli et al., 2012). To analyse the mutant's ability to differentiate, attempts were made to generate axenic amastigotes and attached forms. The mutants

could successfully differentiate into axenic amastigotes but showed low numbers of attached forms when compared to the parental parasites. In fact, only one attached form of *Δ36.1520* was detected.

Whilst *Δ36.1530* managed to form attachment to the coverslips the type of the attachment differed from the parental. Over 90% of attached forms of *Δ36.1530* formed attachment via an attachment plaque, typically an indication of a later stage of attachment (Yanase et al., 2022). Yet, the majority of the parental parasites were attached via a looped flagellum, indicative of an earlier stage of attachment (Yanase et al., 2022). This disparity in the attachment types could suggest that i) there could be a different attachment process in parasites with the flagellum defects one that potentially skips the loop stage ii) the attachment occurs faster in the shorter flagellum; therefore, we did not capture the early loops. However, without further evidence this is currently speculation.

Yet, the severe reduced ability of the *Δ36.1520* mutant to attach to the coverslip, raises questions regarding how did the dysflagellar mutant persist in the sand fly? As discussed, attachment is key during sand fly infection, for parasites not to be excreted (Bates, 2008; Wakid & Bates, 2004). As the parasite load in the sandfly was only tracked for 96 hours, any reduced capacity attach may not have been captured at leptomonads form within 4-7 days and haptomonads even later (Bates, 2008). Therefore, it would be useful to determine if the dysflagellar mutants could persist in the sand fly for longer and go through the complete cycle (i.e., from ingestion to transmission) and if so capture the morphologies at these various stages to determine how a parasite survives without a flagellum.

6.3.3 What is the material in the flagellum bulge?

TEM analyses showed that, in some mutants, inside flagellum at the exit of the flagellar pocket there was a collection of disordered electron dense material. The axoneme 9+2 ultrastructure appeared typical but in a number of mutants a structured PFR was not present. In the *Δ36.1540* mutants, the PFR was present but an additional disordered material on the opposite side of the axoneme was observed.

Zauli, originally speculated that the material was misassembled PFR. However, in *Δ36.1520* mutants staining with an anti-PFR antibody showed that most parasites lacked a PFR signal but in some mutants a short linear signal was present along the axoneme, but no signal was detected in the bulge of any parasites. If the material was PFR, or at least PFR2 (the component that L8C4 antibody detects) an amorphous signal in the bulge would be expected but the lack of a signal suggests that the material does is not PFR but in the mutants PFR assembly is affected. However, we did not include a marker such as a flagellar pocket or neck region protein therefore it is difficult to determine the exact location of this staining.

In the mutants the axoneme appears normal and has the characteristic 'blunt end' structure of *L. mexicana* (Croft et al., 2018). This suggests that the mutants are able to assemble a shorter version of an axoneme and that the role of the serine kinases could include the further elongation of the

flagellum in order to reach its full length. In line with this, IFT (indicated by IFT139) is still recruited to the base of the flagellum and enters the axoneme and some parasites had a bright signal at the distal segment of the flagellum, which could possibly indicate the presence of an aggregation of IFT in this distal region? How and if the IFT could transit through the disordered material is unclear. No IFT trains were detected during TEM analyses.

One interesting note is that there is some resemblance between dysflagellar mutant, the deletion mutants described in the present study with amastigotes that are undergoing differentiation to promastigotes (Gadelha et al., 2013). In *L. amazonensis,* as amastigotes are starting to reassemble a flagellum during differentiation. At this stage the flagellum is very short, thick and lacks a PFR. The reassembling flagellum also has the presence of a bulge at the exit of the flagellar pocket (Figure 6.18). This may also suggest that the parasites likely were arrested during flagella elongation rather than assembling a full length flagellum and then collapsing it. The evidence that very few long flagella were observed in the serve deletion mutants also supports this claim (Figure 6.8).

One that account, it may be possible that the dysflagellar parasites could have lost the 27 kb region of DNA whilst amastigotes residing in the human host, here, they were not under any selective pressure to retain a long flagellum and therefore survived. However, when attempting to differentiate back into the promastigotes whilst in culture, the flagellum became arrested at this intermediate stage and as the culture conditions presented no real selection pressure, the dysflagellar mutants survived and replicated. In fact, assembling a flagellum is so energetically costly these parasites may be at an advantage not having to assemble one.

Ultimately, at this stage we cannot conclude what the material is in this flagellar bulge or how the bulge phenotype came to be. However, it could be reasonable to suggest that this mass is a collection of assorted flagellar material that failed to be assembled. It has been shown that *T. brucei* assembles its flagellum in a disordered manner and then stabilises it with accessory structures such as radial spokes (Höög et al., 2014). Perhaps this mutant is arrested during the flagellum elongation stage as a similar phenotype is observed in the intermediate stages of development of other *Leishmania* species. Although at this stage we cannot definitely state what this material is, this mutant could be used to further understand flagellum length control in *Leishmania* due to its ability to assemble a short, typical axoneme and then just stop at a fixed point.
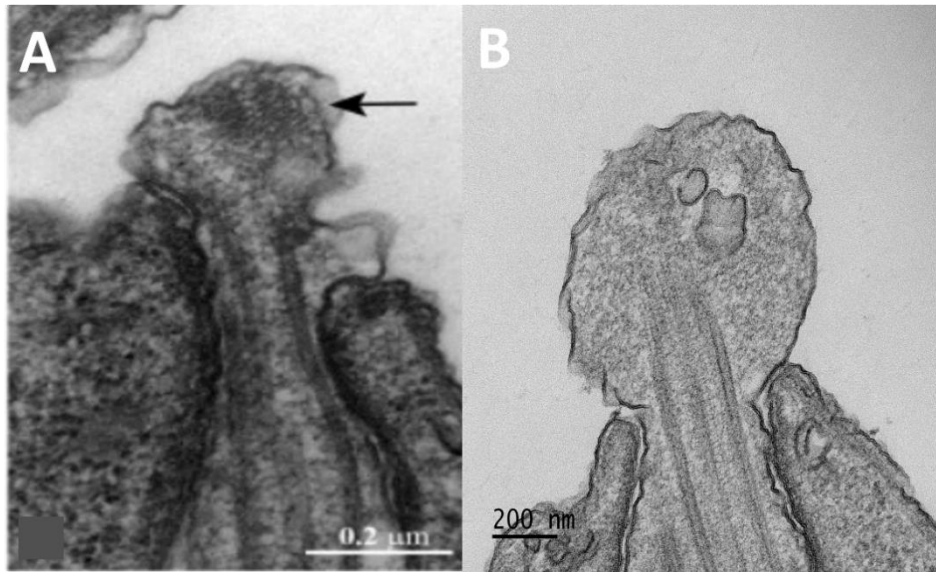
Figure 6.18 The bulge morphology observed in the EFSF6 dysflagellar mutants is similar to that in parasites differentiating from amastigotes to promastigotes. A. An intermediate stage of a *L. amazonensis* amastigote differentiating to a promastigote (Gadelha et al., 2013) **B.** TEM of the EFSF6 mutant with the characteristic flagellar bulge.

6.3.4. Consecutive related genes are uncommon in *Leishmania.*

One unusual thing to note in the present study is that the four deleted genes shared a similar function as demonstrated by the morphology of the deletion mutants (Figures 6.7-6.13). The protein localisation of the four genes appeared unrelated (Figure 6.5) but the deletions showed a similar flagella phenotype with a bulge of material at the exit of the pocket or at least, the failure to assemble a full length flagella.

Leishmania parasites typically have large polycistronic transcription units of functionally unrelated genes (Grünebast & Clos, 2020). These units are all transcribed together, regardless of function. Therefore, to observed four adjacent genes with a similar function all deleted is uncommon. It is not clear how these genes interact, as mentioned, they all have different localisations. Perhaps they are involved in a protein trafficking pathway of proteins into the flagellum with LmxM36.1520-30 being the most important ones as they have the most severe knockout phenotype. Perhaps the 36.1540 has some redundancy with proteins of a similar function. Further studies may wish to explore this in more detail.

6.3.5 Culture adaption may drive gene loss.

During the analyses of the dysflagellar mutant, a paper detailing the culture adaptation of *L. donovani* was published (Bussotti et al. 2021). The study focused upon culture adaptation and showed that mutants arose during the adaptation from splenic amastigotes to cultured promastigotes. These mutants arose independently of each other and showed a similar phenotype to the dysflagellar mutant;

a short flagellum, very low motility, and no noticeable growth defect. They found that a 10.3 kb deletion on chromosome 36 that contained a NIMA kinase homolog (ortholog to LdBPK_361580.1 in *L. donovani)* was present in the mutants. However, they were not able to replicate this deletion by gene editing. In the mutants, they found no evidence of genetic compensation but did show evidence RNA compensatory mechanisms including post-translationally stabilising an orthologous kinase.

This NIMA-kinase deletion is syntenic to the deletion seen in the dysflagellar mutant. Whilst the *L. donovani* NIMA-kinase mutant has ~10 kb deletion, which encompassed one gene, the *L. braziliensis* dysflagellar mutant has a larger in deletion of ~27 kb in its syntenic region, which encompasses four genes in total. It is not clear whether the dysflagellar mutant arose very early in culture or was present in the patient isolates therefore, this phenotype could be due to culture adaptation also. What is evident is that this locus and the genes contained within it are not essential for survival in culture. In all instances the NIMA-kinase, the dysflagellar and the *Δ36.1520* mutants, proliferated at a normal rate and had no noticeable growth defects.
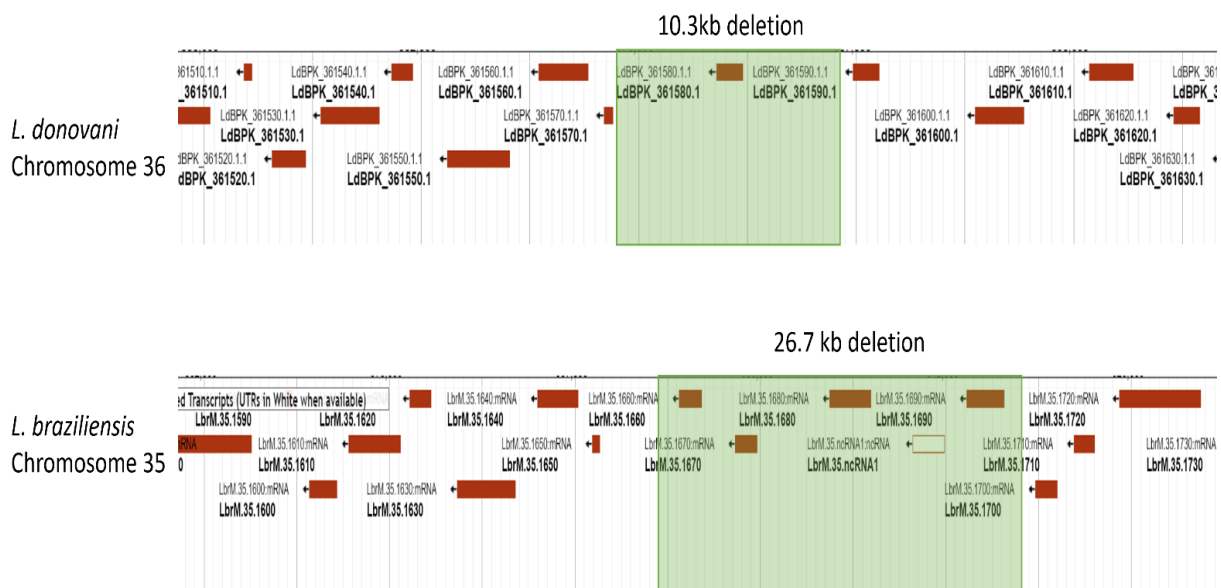
Figure 6.19. The deleted regions between the *L. braziliensis* dysflagellar mutant and the *L.donavani* NIMA-kinase mutant occur at a similar locus. Screenshots from the deleted regions form each region with the annotated genes (FromTryTrypDB) (Bussotti et al., 2021; Zauli et al., 2012)

The fact that two completely independent *Leishmania* species lost this gene may suggest that this locus is particularly susceptible to deletion. Overall, the *Leishmania* genome is highly plastic and diverse. Like other trypanosomatids, *Leishmania spp,* the genome is arranged is large polycistronic units of functionally unrelated genes, which are constantly transcribed into precursor RNAs (Clayton, 2019). Gene regulation occurs post-transcriptionally by mechanisms such as translationally regulation and RNA and protein degradation (Salloum et al., 2021). This posttranslational RNA compensation

was observed in the NIMA-kinase, (Bussotti et al., 2021). In the genome copy number variations of chromosomes and genes such as aneuploidy and gene duplications and deletions are also commonly utilised for expression regulation (Santi & Murta, 2022). In fact, there is little difference in individual genes between *Leishmania* species, but variation occurs from copy number of genes or chromosomes (Rogers et al., 2011). Instances of large gene deletions have also been documented in patient derived L*eishmania* samples (Schwabl et al., 2021). As this is the case, in the present study we should have examined the potential for compensatory mechanisms, such as those detailed in the NIMA-kinase. Future studies may wish to build upon this.

The highly variable nature of the genome means that profiling -omics from culture adapted forms could result in findings that are not representative of the species. Presumably, against the turbulence of blood and fluid flow across host and vector, an un-flagellated *Leishmania* would struggle to survive. One of the ongoing debates across biological research is the applicableness of findings from *in vitro,* highly adapted cultured pathogens to those found in real-world settings. If a deletion that results in flagellum loss can occur within 20 passages, such as that in the NIMA-kinase mutant, how adapted are parasites that been in culture for many decades? It is routine to occasionally passage parasites through a mammalian model to limit the levels of culture adaptation but i) these rodent models are also often not representative of the biological pressures such as co-infections and drug pressures of the parasites natural hosts ii) goes against the 3R principles: replacement, reduction, and refinement (Akhtar, 2015). One thought would be the introduction of cell culture systems that imitate the hemodynamic properties of blood. Systems such as these are common in some mammalian endothelial system. If we were to apply a similar principle for culturing promastigotes, a sandfly environment would have to be replicated that captured the formation of a peritrophic membrane, mimicked excretion and challenged the parasites to attach. Understandably, this a difficult and probably costly system to setup. However, continued improvements to cell culture models that address even small aspects of parasites life cycles could make findings more representative of that species.

6.4 Summary

Overall, we propose that the deletion of LmxM.36.1520 is the main underlying cause of the dysflagellar mutant. It is likely that full deletion of all the four genes, or at least partial deletion of both the kinase (LmxM.36.1520 and LmxM.36.15230) could replicate the dysflagellar phenotype fully. This locus also seems susceptible to deletion during culture adaptation and has the unusual phenotype of adjacent genes with a similar phenotype. t would be interesting to document why this region is susceptible and if there are other mechanisms of compensation seen in the dysflagellar mutant.

7. Conclusions and future outlooks

This thesis has documented a number of aspects of flagellum remodelling in the *Leishmania* parasite, including – i) the changes that occur in the IFT system during flagellum disassembly and attachment, ii) attempting to identify potential triggers for these changes and iii) determining the underlying cause of the naturally occurring dysflagellar mutant.

7.1 Conclusions and unanswered questions

Previously it was shown that flagellum shortening during differentiation was associated with a large drop in IFT numbers (Wheeler et al., 2015). In Chapter Four this idea was developed to show that IFT numbers drop immediately after differentiation was initiated (<30 minutes) and a small decrease in IFT velocity in both directions occurred. This reduction in IFT numbers in the flagellum is likely resulting in reduced cargo trafficking along the flagellum and in turn reduces protein integration at the flagellum tip then ultimately shifts the balances in favour of flagellum disassembly. As this changed occurred so quickly the environmental shock of the pH and temperature change may be triggering flagellum disassembly. Moreover, as the drop in IFT numbers and velocity occurred so quickly, the mechanism driving this reduction must also occur rapidly.

This led us to attempting to find the driver of the drop in IFT numbers and velocity. PTMs are known to occur quickly, are highly abundant in the flagellum and are associated with regulating motor proteins (Chaya & Furukawa, 2021; Wloga, 2017). Unfortunately, we were not able to detect major changes to PTMs during amastigote development. As these modifications are potentially only occurring on a small subset of microtubules, it was likely that our experimental procedures were not sensitive enough to detect these modifications. In Chapter Five, attempts were made to image putative cargo trafficking in both growing, maintaining, and disassembling flagella. However, we were not able to capture cargo movement. Although this may have been unsuccessful due to the imaging set up, it also raises the possibility for an IFT independent, or at least semi-independent, cargo trafficking mechanism.

Finally, Chapter Six detailed the analyses of the patient derived *Leishmania* dysflagellar mutant. This mutant had a seemingly normal 9+2 axoneme structure that stopped just after the exit from the flagellar pocket (Zauli et al., 2012). It also has a large bulge of unidentified electron dense material inside the flagellum at the tip. The cause of this mutant was deletion of a 27 kb locus, which contained four genes. When these genes were deleted, a serine kinase was shown to have the most severe phenotype and TEM analyses showed that the deletion mutant resembled the dysflagellar mutant. When the serine kinase gene was reintroduced, the phenotype was rescued confirming that the loss of the serine kinase led to the flagellum bulge phenotype.

Overall, we hoped to have provided initial observations regarding flagellum remodelling of *Leishmania* that can be used to address unanswered questions such as what is controlling flagellum disassembly and is cargo actually transported by IFT. However, a number of questions still remained unanswered. For example:

Although we see a drop in IFT during amastigote generation – what is driving this reduction? We have determined it must be fast acting and reversible (as differentiating parasites transferred back to promastigote culture conditions revert back to promastigotes). However, the underlying cause is still undetermined. Cargo trafficking, both in the present study and previous work in *T. brucei,* was not detected (Fort et al., 2016). Therefore, this raises the questions of, does protein turnover in trypanosomatids similar to *Chlamydomonas* and if so can cargo be trafficking be captured? What started with an investigation into the potential loss of IFT in the dysflagellar mutant, led to many more questions being raised about culture adaption and the plasticity of the *Leishmania* genome. For example, how to flagellum mutants survive without this key organelle.

These are just a few questions that future research may wish to explore.

7.2 Is IFT *actually* conserved?

Throughout this thesis, many of these results have been interpreted based upon findings and models from other organisms. Although these models have provided key knowledge regarding IFT function can these models help to explain *Leishmania* flagellum biology?

One of the ongoing debates throughout biological research is how useful are model organisms. Models are often easy to genetically manipulate, have fast generation times and can be maintained in culture, thus have improved our understanding of many biological processes. However, how applicable are these findings to other species?

In terms of flagellum biology, the flagellum is considered a highly conserved organelle found throughout the eukaryotic kingdom. Aspects such as the axoneme ultrastructure and the IFT system, is present across ciliated species (Rosenbaum & Witman, 2002). Early research on flagella biology focused upon flagella evolution, the biophysics and the diversity of flagella (Holwill, 1977; Marchese-Ragona & Holwill, 1980; Phillips, 1969; Piperno et al., 1977; Prensier et al., 1980; Renzaglia & Garbary, 2001). This work was often carried out in a variety of organisms, though commonly in protists likely due to ease of manipulation.

However, after the discovery of IFT in the early 90's, flagellum research started to focus on *Chlamydomonas* (Kozminski et al., 1993). As the major players in the IFT and flagellum biology fields such as Kozminksi, Whitman, Rosembaum and Dentler studied and, consequently developed genetic tools, mutant cell line and imaging techniques focusing on *Chlamydomonas,* it quickly became a popular model organism for flagellum biology. Hence many of the key principles and models for flagellum growth are based on data from *Chlamydomonas.*

It is logical to make very detailed models of flagellum assembly in species such as *Chlamydomonas* due to its wide and frequent use. Therefore, understanding the exact mechanism of flagellum assembly is important for guiding further work. For example, important findings in *Chlamydomonas* such as the principle of an open IFT pool, the fact that IFT trains run along the A and B tubule in different directions and that the size of the IFT trains vary in relation to the flagellum length (Engel et al., 2009; Stepanek & Pigino, 2016; Wingfield et al., 2017). These findings can then further guide predictions and allow future research to build upon and develop these models within *Chlamydomonas*.

However, issues can arise when these models are applied to different species. For example, in another flagellum model, *T. brucei,* the IFT pool is closed, IFT happens bidirectionally on a restricted set of microtubules and the anterograde and retrograde trains are different lengths(Bertiaux et al., 2018; Buisson et al., 2013) . These findings are in direct contrast to those in *Chlamydomonas.* In addition, organisms such a *C. elegans* are often considered 'unusual' due to the differences, particular in the IFT motor dynamics, observed in their sensory cilia. In fact, they just oppose the traditional working model of IFT generated from *Chlamydomonas*. I would argue that if flagellum assembly was observed in a larger number of species, more of these 'unusual' examples would appear therefore, not be considered that unusual.

Hypocritically, the exact same thing has been done in this thesis. There have been numerous assumptions based on IFT research from other species. Most of these assumptions with extrapolated from *T. brucei*. Although *T. brucei* and *Leishmania* are closely related, their flagellum biology is completely different. *T. brucei* maintains a flagellum, which does slightly change length throughout its lifecycle but remains long and retains its 9+2 axoneme structure throughout (Gluenz et al., 2010). Conversely, the *Leishmania* flagellum undergoes extensive remodelling both during the differentiation to the amastigote stage or to facilitate attachment. The axoneme itself also must switch from a 9+2 to a *9v* during amastigote differentiation. It would be almost surprising to assume that the flagellum of *Leishmania* would then have the exact control mechanisms as seen in *T. brucei* or *Chlamydomonas.* However, due to the gaps in IFT knowledge surrounding *Leishmania,* we have interpreted the findings in relation to generally accepted IFT models but have tried to highlight the potential caveats with making these assumptions and hopefully have attempted to continuously focus on how the findings can apply to *Leishmania* biology.

Models such as *Chlamydomonas* have provided key information regarding the basic principles of IFT biology, such as more material in results in a longer flagellum more material out leads to a shorter flagellum (Engel et al., 2009). In addition to highly detailed structural data of IFT trains from cryo-EM (Jordan et al., 2018). These principles and structures are useful across many organisms. However, to understand differences in flagellum biology utilising the same set of models cannot address all of the questions. For example, *Chlamydomonas* has two flagellum that are the same length. To study flagellum length control many mutants of *Chlamydomonas* have been created. However, an organism

such as *Giardia* naturally has four sets of flagella, each set with different lengths. A ground-breaking study by McInally demonstrated that disassembly was the main driver of flagellum length and features that we considered conserved, such as the transition zone, were not present in *Giardia* (McInally et al., 2019). Therefore, alternative systems to study length control could provide useful data.

This principle can also be applied to flagellum disassembly. In *Chlamydomonas* disassembly is often triggered by external factors such as drugs. In our study, we hoped to replicate a naturally occurring disassembly step in the *Leishmania* life cycle (albeit a cultured form) that may provide a more biologically relevant answer to how flagellum disassembly occurs.

Overall, striking a balance between the usefulness of using model organisms and the applicability of these findings to other species is incredible complex. However, as flagella functions is so diverse, expanding our set of models may allow us to order to address interesting biological questions throughout eukaryotes.

8. References

Absalon, S., Blisnick, T., Kohl, L., Toutirais, G., Doré, G., Julkowska, D., Tavenet, A., & Bastin, P. (2008). Intraflagellar transport and functional analysis of genes required for flagellum formation in trypanosomes. Molecular Biology of the Cell, 19(3), 929–944. https://doi.org/10.1091/mbc.E07-08-0749

Adhiambo, C., Forney, J. D., Asai, D. J., & LeBowitz, J. H. (2005). The two cytoplasmic dynein-2 isoforms in Leishmania mexicana perform separate functions. Molecular and Biochemical Parasitology, 143(2). https://doi.org/10.1016/j.molbiopara.2005.04.017

Ahmed, N. T., Gao, C., Lucker, B. F., Cole, D. G., & Mitchell, D. R. (2008). ODA16 aids axonemal outer row dynein assembly through an interaction with the intraflagellar transport machinery. Journal of Cell Biology, 183(2). https://doi.org/10.1083/jcb.200802025

Akhtar, A. (2015). The Flaws and Human Harms of Animal Experimentation. Cambridge Quarterly of Healthcare Ethics, 24(4). https://doi.org/10.1017/S0963180115000079

Andre, J., Kerry, L., Qi, X., Hawkins, E., Drižyte, K., Ginger, M. L., & McKean, P. G. (2014). An alternative model for the role of RP2 protein in flagellum assembly in the African trypanosome. Journal of Biological Chemistry, 289(1). https://doi.org/10.1074/jbc.M113.509521

Aslett, M., Aurrecoechea, C., Berriman, M., Brestelli, J., Brunk, B. P., Carrington, M., Depledge, D. P., Fischer, S., Gajria, B., Gao, X., Gardner, M. J., Gingle, A., Grant, G., Harb, O. S., Heiges, M., Hertz-Fowler, C., Houston, R., Innamorato, F., Iodice, J., … Wang, H. (2009). TriTrypDB: A functional genomic resource for the Trypanosomatidae. Nucleic Acids Research, 38(SUPPL.1). https://doi.org/10.1093/nar/gkp851

Baker, N., Catta-Preta, C. M. C., Neish, R., Sadlova, J., Powell, B., Alves-Ferreira, E. V. C., Geoghegan, V., Carnielli, J. B. T., Newling, K., Hughes, C., Vojtkova, B., Anand, J., Mihut, A., Walrad, P. B., Wilson, L. G., Pitchford, J. W., Volf, P., & Mottram, J. C. (2021). Systematic functional analysis of Leishmania protein kinases identifies regulators of differentiation or survival. Nature Communications, 12(1). https://doi.org/10.1038/s41467-021-21360-8

Barak, E., Amin-Spector, S., Gerliak, E., Goyard, S., Holland, N., & Zilberstein, D. (2005). Differentiation of Leishmania donovani in host-free system: Analysis of signal perception and response. Molecular and Biochemical Parasitology, 141(1). https://doi.org/10.1016/j.molbiopara.2005.02.004

Bates, P. A. (2008). Leishmania sand fly interaction: progress and challenges. In Current Opinion in Microbiology (Vol. 11, Issue 4). https://doi.org/10.1016/j.mib.2008.06.003

Batista, M. F., Nájera, C. A., Meneghelli, I., & Bahia, D. (2020). The Parasitic Intracellular Lifestyle of Trypanosomatids: Parasitophorous Vacuole Development and Survival. In Frontiers in Cell and Developmental Biology (Vol. 8). https://doi.org/10.3389/fcell.2020.00396

Beneke, T., Demay, F., Hookway, E., Ashman, N., Jeffery, H., Smith, J., Valli, J., Becvar, T., Myskova, J., Lestinova, T., Shafiq, S., Sadlova, J., Volf, P., Wheeler, R. J., & Gluenz, E. (2019). Genetic dissection of a Leishmania flagellar proteome demonstrates requirement for directional motility in sand fly infections. PLOS Pathogens, 15(6), e1007828. https://doi.org/10.1371/journal.ppat.1007828

Beneke, T., Demay, F., Wheeler, R. J., & Gluenz, E. (2020). Isolation of Leishmania Promastigote Flagella. In Methods in Molecular Biology (Vol. 2116). https://doi.org/10.1007/978-1-0716-0294-2_29

Beneke, T., Madden, R., Makin, L., Valli, J., Sunter, J., & Gluenz, E. (2017). A CRISPR Cas9 high-throughput genome editing toolkit for kinetoplastids. Royal Society Open Science, 4(5). https://doi.org/10.1098/rsos.170095

Bertiaux, E., & Bastin, P. (2020). Dealing with several flagella in the same cell. Cellular Microbiology. https://doi.org/10.1111/cmi.13162

Bertiaux, E., Mallet, A., Fort, C., Blisnick, T., Bonnefoy, S., Jung, J., Lemos, M., Marco, S., Vaughan, S., Trépout, S., Tinevez, J. Y., & Bastin, P. (2018). Bidirectional intraflagellar transport is restricted to two sets of microtubule doublets in the trypanosome flagellum. Journal of Cell Biology, 217(12), 4284–4297. https://doi.org/10.1083/jcb.201805030

Bertiaux, E., Morga, B., Blisnick, T., Rotureau, B., & Bastin, P. (2018). A Grow-and-Lock Model for the Control of Flagellum Length in Trypanosomes. Current Biology, 28(23). https://doi.org/10.1016/j.cub.2018.10.031

Bhogaraju, S., Cajanek, L., Fort, C., Blisnick, T., Weber, K., Taschner, M., Mizuno, N., Lamla, S., Bastin, P., Nigg, E. A., & Lorentzen, E. (2013). Molecular basis of tubulin transport within the cilium by IFT74 and IFT81. Science, 341(6149), 1009–1012. https://doi.org/10.1126/science.1240985

Bhowmick, R., Li, M., Sun, J., Baker, S. A., Insinna, C., & Besharse, J. C. (2009). Photoreceptor IFT complexes containing chaperones, guanylyl cyclase 1 and rhodopsin. Traffic, 10(6). https://doi.org/10.1111/j.1600-0854.2009.00896.x

Blaineau, C., Tessier, M., Dubessay, P., Tasse, L., Crobu, L., Pagès, M., & Bastien, P. (2007). A Novel Microtubule-Depolymerizing Kinesin Involved in Length Control of a Eukaryotic Flagellum. Current Biology, 17(9). https://doi.org/10.1016/j.cub.2007.03.048

Bonhivers, M., Landrein, N., Decossas, M., & Robinson, D. R. (2008). A monoclonal antibody marker for the exclusion-zone filaments of Trypanosoma brucei. Parasites and Vectors, 1(1). https://doi.org/10.1186/1756-3305-1-21

Breslow, D. K., Koslover, E. F., Seydel, F., Spakowitz, A. J., & Nachury, M. v. (2013). An in vitro assay for entry into cilia reveals unique properties of the soluble diffusion barrier. Journal of Cell Biology, 203(1). https://doi.org/10.1083/jcb.201212024

Briggs, L. J., Davidge, J. A., Wickstead, B., Ginger, M. L., & Gull, K. (2004). More than one way to build a flagellum: comparative genomics of parasitic protozoa. http://users.path.ox.ac.uk/~kgull/

Brunke, K. J., Young, E. E., Buchbinder, B. U., & Weeks, D. P. (1982). Coordinate regulation of the four tubulin genes of chlamydomonas reinhardi. Nucleic Acids Research, 10(4). https://doi.org/10.1093/nar/10.4.1295

Buisson, J., Chenouard, N., Lagache, T., Blisnick, T., Olivo-Marin, J. C., & Bastin, P. (2013). Intraflagellar transport proteins cycle between the flagellum and its base. Journal of Cell Science, 126(1), 327–338. https://doi.org/10.1242/jcs.117069

Burkard, G., Fragoso, C. M., & Roditi, I. (2007). Highly efficient stable transformation of bloodstream forms of Trypanosoma brucei. Molecular and Biochemical Parasitology, 153(2). https://doi.org/10.1016/j.molbiopara.2007.02.008

Burza, S., Croft, S., & Boelaert, M. (2018). Leishmaniasis. The Lancet .

Bussotti, G., Piel, L., Pescher, P., Domagalska, M. A., Rajan, K. S., Cohen-Chalamish, S., Doniger, T., Hiregange, D. G., Myler, P. J., Unger, R., Michaeli, S., & Spath, G. F. (2021). Genome instability drives epistatic adaptation in the human pathogen Leishmania. Proceedings of the National Academy of Sciences of the United States of America, 118(51). https://doi.org/10.1073/pnas.2113744118

Carvalho-Santos, Z., Azimzadeh, J., Pereira-Leal, J. B., & Bettencourt-Dias, M. (2011). Tracing the origins of centrioles, cilia, and flagella. In Journal of Cell Biology (Vol. 194, Issue 2). https://doi.org/10.1083/jcb.201011152

CDC. (2020). Parasites - Leishmaniasis. https://www.cdc.gov/parasites/leishmaniasis/index.html

Chan, K. Y., & Ersfeld, K. (2010). The role of the Kinesin-13 family protein TbKif13-2 in flagellar length control of Trypanosoma brucei. Molecular and Biochemical Parasitology, 174(2). https://doi.org/10.1016/j.molbiopara.2010.08.001

Chaya, T., & Furukawa, T. (2021). Post-translational modification enzymes as key regulators of ciliary protein trafficking. In Journal of Biochemistry (Vol. 169, Issue 6). https://doi.org/10.1093/jb/mvab024

Chien, A., Shih, S. M., Bower, R., Tritschler, D., Porter, M. E., & Yildiz, A. (2017). Dynamics of the IFT machinery at the ciliary tip. ELife, 6, e28606. https://doi.org/10.7554/eLife.28606

Clayton, C. (2019). Regulation of gene expression in trypanosomatids: Living with polycistronic transcription. Open Biology, 9(6). https://doi.org/10.1098/rsob.190072

Cole, D. G. (2003). The intraflagellar transport machinery of Chlamydomonas reinhardtii. In Traffic (Vol. 4, Issue 7). https://doi.org/10.1034/j.1600-0854.2003.t01-1-00103.x

Cole, D. G., Chinn, S. W., Wedaman, K. P., Hall, K., Vuong, T., & Scholey, J. M. (1993). Novel heterotrimeric kinesin-related protein purified from sea urchin eggs. Nature, 366(6452). https://doi.org/10.1038/366268a0

Craft, J. M., Harris, J. A., Hyman, S., Kner, P., & Lechtreck, K. F. (2015). Tubulin transport by IFT is upregulated during ciliary growth by a cilium-autonomous mechanism. Journal of Cell Biology, 208(2). https://doi.org/10.1083/jcb.201409036

Croft, J. T., Zabeo, D., Subramanian, R., & Höög, J. L. (2018). Composition, structure and function of the eukaryotic flagellum distal tip. In Essays in Biochemistry (Vol. 62, Issue 6). https://doi.org/10.1042/EBC20180032

Cross, F. R., & Umen, J. G. (2015). The Chlamydomonas cell cycle. Plant Journal, 82(3). https://doi.org/10.1111/tpj.12795

Da Silva, M. S., Monteiro, J. P., Nunes, V. S., Vasconcelos, E. J., Perez, A. M., Freitas, L. D. H., Elias, M. C., & Cano, M. I. N. (2013). Leishmania amazonensis promastigotes present two distinct modes of nucleus and kinetoplast segregation during cell cycle. PLoS ONE, 8(11). https://doi.org/10.1371/journal.pone.0081397

Dagger, F., Bengio, C., Martinez, A., & Ayesta, C. (2018). Leishmania mexicana differentiation involves a selective plasma membrane autophagic-like process. Cell Stress and Chaperones, 23(4). https://doi.org/10.1007/s12192-017-0864-z

Dai, J., Barbieri, F., Mitchell, D. R., & Lechtreck, K. F. (2018). In vivo analysis of outer arm dynein transport reveals cargo-specific intraflagellar transport properties. Molecular Biology of the Cell, 29(21). https://doi.org/10.1091/mbc.E18-05-0291

Dawson, S. C., Sagolla, M. S., Mancuso, J. J., Woessner, D. J., House, S. A., Fritz-Laylin, L., & Cande, W. Z. (2007). Kinesin-13 regulates flagellar, interphase, and mitotic microtubule dynamics in Giardia intestinalis. Eukaryotic Cell, 6(12). https://doi.org/10.1128/EC.00128-07

Dean, S., Sunter, J. D., & Wheeler, R. J. (2017). TrypTag.org: A Trypanosome Genome-wide Protein Localisation Resource. In Trends in Parasitology (Vol. 33, Issue 2). https://doi.org/10.1016/j.pt.2016.10.009

Dean, S., Sunter, J., Wheeler, R. J., Hodkinson, I., Gluenz, E., & Gull, K. (2015). A toolkit enabling efficient, scalable and reproducible gene tagging in trypanosomatids. Open Biology, 5(1). https://doi.org/10.1098/rsob.140197

Deane, J. A., Cole, D. G., Seeley, E. S., Diener, D. R., & Rosenbaum, J. L. (2001). Localization of intraflagellar transport protein IFT52 identifies basal body transitional fibers as the docking site for IFT particles. Current Biology, 11(20). https://doi.org/10.1016/S0960-9822(01)00484-5

Deflorin, J., Rudolf, M., & Seebeck, T. (1994). The major components of the paraflagellar rod of Trypanosoma brucei are two similar, but distinct proteins which are encoded by two different gene loci. Journal of Biological Chemistry, 269(46). https://doi.org/10.1016/s0021-9258(19)61968-x

Dentler, W. (2005). Intraflagellar transport (IFT) during assembly and disassembly of Chlamydomonas flagella. Journal of Cell Biology, 170(4), 649–659. https://doi.org/10.1083/jcb.200412021

Dentler, W. L., & Rosenbaum, J. L. (1977). Flagellar elongation and shortening in chlamydomonas. III. Structures attached to the tips of flagellar microtubules and their relationship to the directionality of flagellar microtubule assembly. Journal of Cell Biology, 74(3). https://doi.org/10.1083/jcb.74.3.747

Diniz, M., Carolina L. Pacheco, A., M. Farias, K., & M. de Oliveira, D. (2012). The Eukaryotic Flagellum Makes the Day: Novel and Unforeseen Roles Uncovered After Post-Genomics and Proteomics Data. Current Protein & Peptide Science, 13(6). https://doi.org/10.2174/138920312803582951

Dostálová, A., & Volf, P. (2012). Leishmania development in sand flies: Parasite-vector interactions overview. In Parasites and Vectors (Vol. 5, Issue 1). https://doi.org/10.1186/1756-3305-5-276

Douglas, R. L., Haltiwanger, B. M., Albisetti, A., Wu, H., Jeng, R. L., Mancuso, J., Cande, W. Z., & Welch, M. D. (2020). Trypanosomes have divergent kinesin-2 proteins that function differentially in flagellum biosynthesis and cell viability. Journal of Cell Science, 133(13). https://doi.org/10.1242/jcs.129213

Edwards, A. V. G., Edwards, G. J., Schwämmle, V., Saxtorph, H., & Larsen, M. R. (2014). Spatial and temporal effects in protein post-translational modification distributions in the developing mouse brain. Journal of Proteome Research, 13(1). https://doi.org/10.1021/pr4002977

Edwards, B. F. L., Wheeler, R. J., Barker, A. R., Moreira-Leite, F. F., Gull, K., & Sunter, J. D. (2018). Direction of flagellum beat propagation is controlled by proximal/distal outer dynein arm asymmetry. Proceedings of the National Academy of Sciences of the United States of America, 115(31). https://doi.org/10.1073/pnas.1805827115

Einarsson, E., & Svärd, S. G. (2015). Encystation of Giardia intestinalis—a Journey from the Duodenum to the Colon. In Current Tropical Medicine Reports (Vol. 2, Issue 3). https://doi.org/10.1007/s40475-015-0048-9

Engel, B. D., Ludington, W. B., & Marshall, W. F. (2009). Intraflagellar transport particle size scales inversely with flagellar length: Revisiting the balance-point length control model. Journal of Cell Biology, 187(1). https://doi.org/10.1083/jcb.200812084

Engelke, M. F., Waas, B., Kearns, S. E., Suber, A., Boss, A., Allen, B. L., & Verhey, K. J. (2019). Acute Inhibition of Heterotrimeric Kinesin-2 Function Reveals Mechanisms of Intraflagellar Transport in Mammalian Cilia. Current Biology, 29(7). https://doi.org/10.1016/j.cub.2019.02.043

Ezratty, E. J., Stokes, N., Chai, S., Shah, A. S., Williams, S. E., & Fuchs, E. (2011). A role for the primary cilium in notch signaling and epidermal differentiation during skin development. Cell, 145(7). https://doi.org/10.1016/j.cell.2011.05.030

Fiebig, M., Kelly, S., & Gluenz, E. (2015). Comparative Life Cycle Transcriptomics Revises Leishmania mexicana Genome Annotation and Links a Chromosome Duplication with Parasitism of Vertebrates. PLoS Pathogens, 11(10). https://doi.org/10.1371/journal.ppat.1005186

Forestier, C. L., MacHu, C., Loussert, C., Pescher, P., & Späth, G. F. (2011). Imaging host cell-leishmania interaction dynamics implicates parasite motility, lysosome recruitment, and host cell wounding in the infection process. Cell Host and Microbe, 9(4). https://doi.org/10.1016/j.chom.2011.03.011

Fort, C., Bonnefoy, S., Kohl, L., & Bastin, P. (2016). Intraflagellar transport is required for the maintenance of the trypanosome flagellum composition but not its length. Journal of Cell Science, 129(15), 3026–3041. https://doi.org/10.1242/jcs.188227

Fowlkes-Comninellis, T., & Beverley, S. (2015). Leishmania IFT140 mutants show normal viability but lack external flagella: A tool for the study of flagellar function through the infectious cycle. Cilia, SUPPLEMENT 1. https://doi.org/10.1186/2046-2530-4-S1-P49

Funabashi, T., Katoh, Y., Michisaka, S., Terada, M., Sugawa, M., & Nakayama, K. (2017). Ciliary entry of KIF17 is dependent on its binding to the IFT-B complex via IFT46-IFT56 as well as on its nuclear localization signal. Molecular Biology of the Cell, 28(5). https://doi.org/10.1091/mbc.E16-09-0648

Gadadhar, S., Bodakuntla, S., Natarajan, K., & Janke, C. (2017). The tubulin code at a glance. Journal of Cell Science, 130(8). https://doi.org/10.1242/jcs.199471

Gadelha, A. P. R., Cunha-e-Silva, N. L., & Souza, W. de. (2013). Assembly of the Leishmania amazonensis flagellum during cell differentiation. Journal of Structural Biology, 184(2), 280–292. https://doi.org/10.1016/j.jsb.2013.09.006

Gagnon, C., White, D., Cosson, J., Huitorel, P., Eddé, B., Desbruyères, E., Paturle-Lafanechère, L., Multigner, L., Job, D., & Cibert, C. (1996). The polyglutamylated lateral chain of alpha-tubulin plays a key role in flagellar motility. Journal of Cell Science, 109(6). https://doi.org/10.1242/jcs.109.6.1545

Garcia-Gonzalo, F. R., & Reiter, J. F. (2017). Open Sesame: How transition fibers and the transition zone control ciliary composition. Cold Spring Harbor Perspectives in Biology, 9(2). https://doi.org/10.1101/cshperspect.a028134

Gluenz, E., Ginger, M. L., & McKean, P. G. (2010). Flagellum assembly and function during the Leishmania life cycle. In Current Opinion in Microbiology (Vol. 13, Issue 4). https://doi.org/10.1016/j.mib.2010.05.008

Gossage, S. M., Rogers, M. E., & Bates, P. A. (2003). Two separate growth phases during the development of Leishmania in sand flies: Implications for understanding the life cycle. International Journal for Parasitology, 33(10). https://doi.org/10.1016/S0020-7519(03)00142-5

Halliday, C., Billington, K., Wang, Z., Madden, R., Dean, S., Sunter, J. D., & Wheeler, R. J. (2019). Cellular landmarks of Trypanosoma brucei and Leishmania mexicana. Molecular and Biochemical Parasitology, 230. https://doi.org/10.1016/j.molbiopara.2018.12.003

Han, L., Rao, Q., Yang, R., Wang, Y., Chai, P., Xiong, Y., & Zhang, K. (2022). Cryo-EM structure of an active central apparatus. Nature Structural and Molecular Biology, 29(5). https://doi.org/10.1038/s41594-022-00769-9

Hao, L., Thein, M., Brust-Mascher, I., Civelekoglu-Scholey, G., Lu, Y., Acar, S., Prevo, B., Shaham, S., & Scholey, J. M. (2011). Intraflagellar transport delivers tubulin isotypes to sensory cilium middle and distal segments. Nature Cell Biology, 13(7). https://doi.org/10.1038/ncb2268

Harris, J. A., Liu, Y., Yang, P., Kner, P., & Lechtreck, K. F. (2016). Single-particle imaging reveals intraflagellar transport-independent transport and accumulation of EB1 in Chlamydomonas flagella. Molecular Biology of the Cell, 27(2). https://doi.org/10.1091/mbc.E15-08-0608

Hazime, K. S., Zhou, Z., Joachimiak, E., Bulgakova, N. A., Wloga, D., & Malicki, J. J. (2021). STORM imaging reveals the spatial arrangement of transition zone components and IFT particles at the ciliary base in Tetrahymena. Scientific Reports, 11(1). https://doi.org/10.1038/s41598-021-86909-5

He, K., Ling, K., & Hu, J. (2020). The emerging role of tubulin posttranslational modifications in cilia and ciliopathies. Biophysics Reports, 6(4). https://doi.org/10.1007/s41048-020-00111-0

Hirano, T., Katoh, Y., Nakayama, K., & Marshall, W. (2017). Intraflagellar transport - A complex mediates ciliary entry and retrograde trafficking of ciliary G protein-coupled receptors. Molecular Biology of the Cell, 28(3). https://doi.org/10.1091/mbc.E16-11-0813

Holwill, M. E. J. (1977). Some Biophysical Aspects of Ciliary and Flagellar Motility. Advances in Microbial Physiology, 16(C). https://doi.org/10.1016/S0065-2911(08)60046-6

Höög, J. L., Lacomble, S., O'Toole, E. T., Hoenger, A., McIntosh, J. R., & Gull, K. (2014). Modes of flagellar assembly in Chlamydomonas reinhardtii and Trypanosoma brucei. ELife, 3. https://doi.org/10.7554/elife.01479

Huang, K., Diener, D. R., & Rosenbaum, J. L. (2009). The ubiquitin conjugation system is involved in the disassembly of cilia and flagella. Journal of Cell Biology, 186(4). https://doi.org/10.1083/jcb.200903066

Huangfu, D., Liu, A., Rakeman, A. S., Murcia, N. S., Niswander, L., & Anderson, K. v. (2003). Hedgehog signalling in the mouse requires intraflagellar transport proteins. Nature, 426(6962). https://doi.org/10.1038/nature02061

Ikegami, K., Heier, R. L., Taruishi, M., Takagi, H., Mukai, M., Shimma, S., Taira, S., Hatanaka, K., Morone, N., Yao, I., Campbell, P. K., Yuasa, S., Janke, C., MacGregor, G. R., & Setou, M. (2007). Loss of α-tubulin polyglutamylation in ROSA22 mice is associated with abnormal

targeting of KIF1A and modulated synaptic function. Proceedings of the National Academy of Sciences of the United States of America, 104(9). https://doi.org/10.1073/pnas.0611547104

Ishida, Y., Tasaki, K., Katoh, Y., & Nakayama, K. (2022). Molecular basis underlying the ciliary defects caused by IFT52 variations found in skeletal ciliopathies. Molecular Biology of the Cell, 33(9), ar83. https://doi.org/10.1091/mbc.E22-05-0188

Janke, C., & Magiera, M. M. (2020). The tubulin code and its role in controlling microtubule properties and functions. In Nature Reviews Molecular Cell Biology (Vol. 21, Issue 6). https://doi.org/10.1038/s41580-020-0214-3

Jékely, G., & Arendt, D. (2006). Evolution of intraflagellar transport from coated vesicles and autogenous origin of the eukaryotic cilium. In BioEssays (Vol. 28, Issue 2). https://doi.org/10.1002/bies.20369

Jiang, Y. Y., Lechtreck, K., & Gaertig, J. (2015). Total internal reflection fluorescence microscopy of intraflagellar transport in Tetrahymena thermophila. Methods in Cell Biology, 127. https://doi.org/10.1016/bs.mcb.2015.01.001

Johnson, K. A. (1998). The axonemal microtubules of the Chlamydomonas flagellum differ in tubulin isoform content. Journal of Cell Science, 111(3). https://doi.org/10.1242/jcs.111.3.313

Jordan, M. A., Diener, D. R., Stepanek, L., & Pigino, G. (2018). The cryo-EM structure of intraflagellar transport trains reveals how dynein is inactivated to ensure unidirectional anterograde movement in cilia. In Nature Cell Biology (Vol. 20, Issue 11). https://doi.org/10.1038/s41556-018-0213-1

Kamhawi, S. (2006). Phlebotomine sand flies and Leishmania parasites: friends or foes? In Trends in Parasitology (Vol. 22, Issue 9). https://doi.org/10.1016/j.pt.2006.06.012

Kato, C., Miyazaki, K., Nakagawa, A., Ohira, M., Nakamura, Y., Ozaki, T., Imai, T., & Nakagawara, A. (2004). Low expression of human tubulin tyrosine ligase and suppressed tubulin tyrosination/detyrosination cycle are associated with impaired neuronal differentiation in neuroblastomas with poor prognosis. International Journal of Cancer, 112(3). https://doi.org/10.1002/ijc.20431

Katoh, Y., Terada, M., Nishijima, Y., Takei, R., Nozaki, S., Hamada, H., & Nakayama, K. (2016). Overall architecture of the intraflagellar transport (IFT)-B complex containing cluap1/IFT38 as an essential component of the IFT-B peripheral subcomplex. Journal of Biological Chemistry, 291(21). https://doi.org/10.1074/jbc.M116.713883

Kee, H. L., Dishinger, J. F., Lynne Blasius, T., Liu, C. J., Margolis, B., & Verhey, K. J. (2012). A size-exclusion permeability barrier and nucleoporins characterize a ciliary pore complex that regulates transport into cilia. Nature Cell Biology, 14(4). https://doi.org/10.1038/ncb2450

Khan, Y. A., Andrews, N. W., & Mittra, B. (2018). ROS regulate differentiation of visceralizing Leishmania species into the virulent amastigote form . Parasitology Open, 4. https://doi.org/10.1017/pao.2018.15

Kobayashi, T., Ishida, Y., Hirano, T., Katoh, Y., & Nakayama, K. (2021). Cooperation of the IFT-A complex with the IFT-B complex is required for ciliary retrograde protein trafficking and GPCR import. Molecular Biology of the Cell, 32(1). https://doi.org/10.1091/MBC.E20-08-0556

Kozminski, K. G., Johnson, K. A., Forscher, P., & Rosenbaum, J. L. (1993). A motility in the eukaryotic flagellum unrelated to flagellar beating. Proceedings of the National Academy of

Sciences of the United States of America, 90(12), 5519–5523.
https://doi.org/10.1073/pnas.90.12.5519

Kubo, T., Brown, J. M., Bellve, K., Craige, B., Craft, J. M., Fogarty, K., Lechtreck, K. F., & Witman, G. B. (2016). Together, the IFT81 and IFT74 N-termini form the main module for intraflagellar transport of tubulin. Journal of Cell Science, 129(10).
https://doi.org/10.1242/jcs.187120

Kurup, S. P., & Tarleton, R. L. (2014). The trypanosoma cruzi flagellum is discarded via asymmetric cell division following invasion and provides early targets for protective CD8+ T cells. Cell Host and Microbe, 16(4), 439–449. https://doi.org/10.1016/j.chom.2014.09.003

Lacey, S., Foster, H., & Pigino, G. (2022). The Molecular Structure of Anterograde Intraflagellar transport trains. BioRxiv.

Langmead, B., & Salzberg, S. (2013). Bowtie2. Nature Methods, 9(4).

Latour, B. L., van de Weghe, J. C., Rusterholz, T. D. S., Letteboer, S. J. F., Gomez, A., Shaheen, R., Gesemann, M., Karamzade, A., Asadollahi, M., Barroso-Gil, M., Chitre, M., Grout, M. E., van Reeuwijk, J., van Beersum, S. E. C., Miller, C. v., Dempsey, J. C., Morsy, H., Bamshad, M. J., Nickerson, D. A., … Doherty, D. (2020). Dysfunction of the ciliary ARMC9/TOGARAM1 protein module causes Joubert syndrome. Journal of Clinical Investigation, 140(8).
https://doi.org/10.1172/JCI131656

Lechtreck, K. F. (2013). In vivo imaging of IFT in Chlamydomonas flagella. In Methods in Enzymology (Vol. 524). https://doi.org/10.1016/B978-0-12-397945-2.00015-9

Lechtreck, K. F. (2015). IFT-Cargo Interactions and Protein Transport in Cilia. In Trends in Biochemical Sciences (Vol. 40, Issue 12, pp. 765–778). Elsevier Ltd.
https://doi.org/10.1016/j.tibs.2015.09.003

Lechtreck, K. F., & Geimer, S. (2000). Distribution of polyglutamylated tubulin in the flagellar apparatus of green flagellates. Cell Motility and the Cytoskeleton, 47(3).
https://doi.org/10.1002/1097-0169(200011)47:3<219::AID-CM5>3.0.CO;2-Q

Lechtreck, K. F., Johnson, E. C., Sakai, T., Cochran, D., Ballif, B. A., Rush, J., Pazour, G. J., Ikebe, M., & Witman, G. B. (2009). The Chlamydomonas reinhardtii BBSome is an IFT cargo required for export of specific signaling proteins from flagella. Journal of Cell Biology, 187(7).
https://doi.org/10.1083/jcb.200909183

Lechtreck, K. F., Mengoni, I., Okivie, B., & Hilderhoff, K. B. (2018). In vivo analyses of radial spoke transport, assembly, repair and maintenance. Cytoskeleton, 75(8).
https://doi.org/10.1002/cm.21457

Lechtreck, K. F., Yiliu, Dai, J., Alkhofash, R. A., Butler, J., Alford, L., & Yang, P. (2022). Chlamydomonas ARMC2/PF27 is an obligate cargo adapter for intraflagellar transport of radial spokes. ELife, 11. https://doi.org/10.7554/eLife.74993

Lentini, G., dos Santos Pacheco, N., & Burleigh, B. A. (2018). Targeting host mitochondria: A role for the Trypanosoma cruzi amastigote flagellum. Cellular Microbiology, 20(2).
https://doi.org/10.1111/cmi.12807

Leon, L. L., Soares, M. J., & Temporal L, R. M. (1995). Effects of Temperature on Promastigotes of Several Species of Leishmania. Journal of Eukaryotic Microbiology, 42(3).
https://doi.org/10.1111/j.1550-7408.1995.tb01569.x

L'Hernault, S. W., & Rosenbaum, J. L. (1983). Chlamydomonas α-tubulin is posttranslationally modified in the flagella during flagellar assembly. Journal of Cell Biology, 97(1). https://doi.org/10.1083/jcb.97.1.258

L'Hernault, S. W., & Rosenbaum, J. L. (1985). Reversal of the posttranslational modification on Chlamydomonas flagellar α-tubulin occurs during flagellar resorption. Journal of Cell Biology, 100(2). https://doi.org/10.1083/jcb.100.2.457

Li, R., & Zhu, J. (2022). Effects of aneuploidy on cell behaviour and function. Nature Reviews Molecular Cell Biology. https://doi.org/10.1038/s41580-021-00436-9

Li, S., Wan, K. Y., Chen, W., Tao, H., Liang, X., & Pan, J. (2020). Functional exploration of heterotrimeric kinesin-II in IFT and ciliary length control in Chlamydomonas. ELife, 9. https://doi.org/10.7554/eLife.58868

Liang, Y., Meng, D., Zhu, B., & Pan, J. (2016). Mechanism of ciliary disassembly. In Cellular and Molecular Life Sciences (Vol. 73, Issue 9). https://doi.org/10.1007/s00018-016-2148-7

Luo, W., Ruba, A., Takao, D., Zweifel, L. P., Lim, R. Y. H., Verhey, K. J., & Yang, W. (2017). Axonemal Lumen Dominates Cytosolic Protein Diffusion inside the Primary Cilium. Scientific Reports, 7(1). https://doi.org/10.1038/s41598-017-16103-z

Ma, M., Stoyanova, M., Rademacher, G., Dutcher, S. K., Brown, A., & Zhang, R. (2019). Structure of the Decorated Ciliary Doublet Microtubule. Cell, 179(4). https://doi.org/10.1016/j.cell.2019.09.030

Mangeol, P., Prevo, B., & Peterman, E. J. G. (2016). KymographClear and KymographDirect: Two tools for the automated quantitative analysis of molecular and cellular dynamics using kymographs. Molecular Biology of the Cell, 27(12). https://doi.org/10.1091/mbc.E15-06-0404

Marchese-Ragona, S., & Holwill, M. E. J. (1980). Motile flagellar axonemes with a 9 + 1 microtubule configuration. Nature, 287(5785). https://doi.org/10.1038/287867a0

Marshall, W. F., & Rosenbaum, J. L. (2001). Intraflagellar transport balances continuous turnover of outer doublet microtubules: Implications for flagellar length control. Journal of Cell Biology, 155(3). https://doi.org/10.1083/jcb.200106141

Marshall, W. F., Wemmer, K., & Ludington, W. (2019). Testing the role of intraflagellar transport in flagellar length control using length-altering mutants of Chlamydomonas. https://doi.org/10.1098/rstb.2019.0159

Marszalek, J. R., & Goldstein, L. S. B. (2000). Understanding the functions of kinesin-II. In Biochimica et Biophysica Acta - Molecular Cell Research (Vol. 1496, Issue 1). https://doi.org/10.1016/S0167-4889(00)00015-X

Martinez-Rojano, H., Mancilla-Ramirez, J., Quiñonez-Diaz, L., & Galindo-Sevilla, N. (2008). Activity of hydroxyurea against Leishmania mexicana. Antimicrobial Agents and Chemotherapy, 52(10). https://doi.org/10.1128/AAC.00124-08

McInally, S. G., Kondev, J., & Dawson, S. C. (2019). Length-dependent disassembly maintains four different flagellar lengths in giardia. ELife, 8. https://doi.org/10.7554/eLife.48694

McKeithan, T. W., Lefebvre, P. A., Silflow, C. D., & Rosenbaum, J. L. (1983). Multiple forms of tubulin in Polytomella and Chlamydomonas: Evidence for a precursor of flagellar α-tubulin. Journal of Cell Biology, 96(4). https://doi.org/10.1083/jcb.96.4.1056

Milic, B., Andreasson, J. O. L., Hogan, D. W., & Block, S. M. (2017). Intraflagellar transport velocity is governed by the number of active KIF17 and KIF3AB motors and their motility properties under load. Proceedings of the National Academy of Sciences of the United States of America, 114(33). https://doi.org/10.1073/pnas.1708157114

Minocha, N., Kumar, D., Rajanala, K., & Saha, S. (2011). Kinetoplast morphology and segregation pattern as a marker for cell cycle progression in Leishmania donovani. Journal of Eukaryotic Microbiology, 58(3). https://doi.org/10.1111/j.1550-7408.2011.00539.x

Moran, J., Mckean, P. G., & Ginger, M. L. (2014). Eukaryotic Flagella: Variations in Form, Function, and Composition during Evolution. 64(12), 1103–1114. https://doi.org/10.2307/90006997

Morga, B., & Cilia. (2013). Getting to the heart of intraflagellar transport using Trypanosoma and Chlamydomonas models: the strength is in their differences (Vol. 2). http://www.ciliajournal.com/content/2/1/16

Mukhopadhyay, S., Wen, X., Chih, B., Nelson, C. D., Lane, W. S., Scales, S. J., & Jackson, P. K. (2010). TULP3 bridges the IFT-A complex and membrane phosphoinositides to promote trafficking of G protein-coupled receptors into primary cilia. Genes and Development, 24(19). https://doi.org/10.1101/gad.1966210

Nakayama, K., & Katoh, Y. (2020). Architecture of the IFT ciliary trafficking machinery and interplay between its components. In Critical Reviews in Biochemistry and Molecular Biology (Vol. 55, Issue 2). https://doi.org/10.1080/10409238.2020.1768206

Neofotis, P., Temple, J., Tessmer, O. L., Bibik, J., Norris, N., Pollner, E., Lucker, B., Weraduwage, S. M., Withrow, A., Sears, B., Mogos, G., Frame, M., Hall, D., Weissman, J., & Kramer, D. M. (2021). The induction of pyrenoid synthesis by hyperoxia and its implications for the natural diversity of photosynthetic responses in Chlamydomonas. ELife, 10. https://doi.org/10.7554/eLife.67565

Nievergelt, A. P., Zykov, I., Diener, D., Chhatre, A., Buchholz, T.-O., Delling, M., Diez, S., Jug, F., Štěpánek, L., & Pigino, G. (2022). Conversion of anterograde into retrograde trains is an intrinsic property of intraflagellar transport. Current Biology. https://doi.org/10.1016/j.cub.2022.07.033

O'Hagan, R., Piasecki, B. P., Silva, M., Phirke, P., Nguyen, K. C. Q., Hall, D. H., Swoboda, P., & Barr, M. M. (2011). The tubulin deglutamylase CCPP-1 regulates the function and stability of sensory cilia in C. elegans. Current Biology, 21(20). https://doi.org/10.1016/j.cub.2011.08.049

Orbach, R., & Howard, J. (2019). The dynamic and structural properties of axonemal tubulins support the high length stability of cilia. Nature Communications, 10(1). https://doi.org/10.1038/s41467-019-09779-6

Ostrowski, L. E., Blackburn, K., Radde, K. M., Moyer, M. B., Schlatzer, D. M., Moseley, A., & Boucher, R. C. (2002). A proteomic analysis of human cilia: identification of novel components. Molecular & Cellular Proteomics : MCP, 1(6). https://doi.org/10.1074/mcp.M200037-MCP200

Ounjai, P., Kim, K. D., Lishko, P. v., & Downing, K. H. (2012). Three-dimensional structure of the bovine sperm connecting piece revealed by electron cryotomography. Biology of Reproduction, 87(3). https://doi.org/10.1095/biolreprod.112.101980

Pan, J., & Snell, W. J. (2005). Chlamydomonas shortens its flagella by activating axonemal disassembly, stimulating IFT particle trafficking, and blocking anterograde cargo loading. Developmental Cell, 9(3), 431–438. https://doi.org/10.1016/j.devcel.2005.07.010

Pan, X., Ou, G., Civelekoglu-Scholey, G., Blacque, O. E., Endres, N. F., Tao, L., Mogilner, A., Leroux, M. R., Vale, R. D., & Scholey, J. M. (2006). Mechanism of transport of IFT particles in C. elegans cilia by the concerted action of kinesin-II and OSM-3 motors. Journal of Cell Biology, 174(7). https://doi.org/10.1083/jcb.200606003

Patra, S., Jülicher, F., & Chowdhury, D. (2020). Flagellar length control in biflagellate eukaryotes: Time-of-flight, shared pool, train traffic and cooperative phenomena. New Journal of Physics, 22(8). https://doi.org/10.1088/1367-2630/ab9ee4

Pazour, G. J., Agrin, N., Leszyk, J., & Witman, G. B. (2005). Proteomic analysis of a eukaryotic cilium. Journal of Cell Biology, 170(1). https://doi.org/10.1083/jcb.200504008

Pazour, G. J., Wilkerson, C. G., & Witman, G. B. (1998). A dynein light chain is essential for the retrograde particle movement of intraflagellar transport (IFT). Journal of Cell Biology, 141(4). https://doi.org/10.1083/jcb.141.4.979

Phillips, D. M. (1969). Exceptions to the prevailing pattern of tubules (9 + 9 + 2) in the sperm flagella of certain insect species. The Journal of Cell Biology, 40(1). https://doi.org/10.1083/jcb.40.1.28

Pigino, G., Geimer, S., Lanzavecchia, S., Paccagnini, E., Cantele, F., Diener, D. R., Rosenbaum, J. L., & Lupetti, P. (2009). Electron-tomographic analysis of intraflagellar transport particle trains in situ. Journal of Cell Biology, 187(1). https://doi.org/10.1083/jcb.200905103

Pimenta, P. F. P., Turco, S. J., McConville, M. J., Lawyer, P. G., Perkins, P. v., & Sacks, D. L. (1992). Stage-specific adhesion of Leishmania promastigotes to the sandfly midgut. Science, 256(5065). https://doi.org/10.1126/science.1615326

Piperno, G., Huang, B., & Luck, D. J. L. (1977). Two dimensional analysis of flagellar proteins from wild type and paralyzed mutants of Chlamydomonas reinhardtii. Proceedings of the National Academy of Sciences of the United States of America, 74(4). https://doi.org/10.1073/pnas.74.4.1600

Piperno, G., LeDizet, M., & Chang, X. J. (1987). Microtubules containing acetylated alpha-tubulin in mammalian cells in culture. The Journal of Cell Biology, 104(2). https://doi.org/10.1083/jcb.104.2.289

Piperno, G., Siuda, E., Henderson, S., Segil, M., Vaananen, H., & Sassaroli, M. (1998). Distinct mutants of retrograde intraflagellar transport (IFT) share similar morphological and molecular defects. Journal of Cell Biology, 143(6). https://doi.org/10.1083/jcb.143.6.1591

Plotnikova, O. v., Pugacheva, E. N., & Golemis, E. A. (2009). Primary cilia and the cell cycle. Methods in Cell Biology, 94, 137–160. https://doi.org/10.1016/S0091-679X(08)94007-3

Porter, M. E., Bower, R., Knott, J. A., Byrd, P., & Dentler, W. (1999). Cytoplasmic dynein heavy chain 1b is required for flagellar assembly in Chlamydomonas. Molecular Biology of the Cell, 10(3). https://doi.org/10.1091/mbc.10.3.693

Prensier, G., Vivier, E., Goldstein, S., & Schrével, J. (1980). Motile flagellum with a "3+0" ultrastructure. Science, 207(4438). https://doi.org/10.1126/science.7189065

Price, H. P., Peltan, A., Stark, M., & Smith, D. F. (2010). The small GTPase ARL2 is required for cytokinesis in Trypanosoma brucei. Molecular and Biochemical Parasitology, 173(2). https://doi.org/10.1016/j.molbiopara.2010.05.016

Prigent, Y., Kann, M. L., Lach-Gar, H., Péchart, I., & Fouquet, J. P. (1996). Glutamylated tubulin as a marker of microtubule heterogeneity in the human sperm flagellum. Molecular Human Reproduction, 2(8). https://doi.org/10.1093/molehr/2.8.573

Qin, H., Diener, D. R., Geimer, S., Cole, D. G., & Rosenbaum, J. L. (2004). Intraflagellar transport (IFT) cargo: IFT transports flagellar precursors to the tip and turnover products to the cell body. Journal of Cell Biology, 164(2). https://doi.org/10.1083/jcb.200308132

Rajagopalan, V., Subramanian, A., Wilkes, D. E., Pennock, D. G., & Asai, D. J. (2009). Dynein-2 affects the regulation of ciliary length but is not required for ciliogenesis in tetrahymena thermophila. Molecular Biology of the Cell, 20(2). https://doi.org/10.1091/mbc.E08-07-0746

Ramalho-Ortigao, M., Saraiva, E. M., & Traub-Csekö, Y. M. (2010). Sand fly-Leishmania interactions: Long relationships are not necessarily easy. In Open Parasitology Journal (Vol. 4, Issue SPEC. ISS.1). https://doi.org/10.2174/1874421401004010195

Regnard, C., Desbruyères, E., Denoulet, P., & Eddé, B. (1999). Tubulin polyglutamylase: Isozymic variants and regulation during the cell cycle in HeLa cells. Journal of Cell Science, 112(23). https://doi.org/10.1242/jcs.112.23.4281

Reignault, L. C., Alcantara, C. de L., Barrias, E. S., & de Souza, W. (2019). 3D reconstruction of Trypanosoma cruzi-macrophage interaction shows the recruitment of host cell organelles towards parasitophorous vacuoles during its biogenesis. Journal of Structural Biology, 205(2). https://doi.org/10.1016/j.jsb.2018.12.010

Reiter, J. F., & Leroux, M. R. (2017). Genes and molecular pathways underpinning ciliopathies. In Nature Reviews Molecular Cell Biology (Vol. 18, Issue 9). https://doi.org/10.1038/nrm.2017.60

Renzaglia, K. S., & Garbary, D. J. (2001). Motile gametes of land plants: Diversity, development, and evolution. In Critical Reviews in Plant Sciences (Vol. 20, Issue 2). https://doi.org/10.1080/20013591099209

Richter, F., Morton, S. U., Qi, H., Kitaygorodsky, A., Wang, J., Homsy, J. G., DePalma, S., Patel, N., Gelb, B. D., Seidman, J. G., Seidman, C. E., & Shen, Y. (2020). Whole Genome De Novo Variant Identification with FreeBayes and Neural Network Approaches. BioRxiv Genomics.

Ringo, D. L. (1967). Flagellar motion and fine structure of the flagellar apparatus in Chlamydomonas. The Journal of Cell Biology, 33(3). https://doi.org/10.1083/jcb.33.3.543

Rogers, M. B., Hilley, J. D., Dickens, N. J., Wilkes, J., Bates, P. A., Depledge, D. P., Harris, D., Her, Y., Herzyk, P., Imamura, H., Otto, T. D., Sanders, M., Seeger, K., Dujardin, J. C., Berriman, M., Smith, D. F., Hertz-Fowler, C., & Mottram, J. C. (2011). Chromosome and gene copy number variation allow major structural change between species and strains of Leishmania. Genome Research, 21(12). https://doi.org/10.1101/gr.122945.111

Rogowski, K., Juge, F., van Dijk, J., Wloga, D., Strub, J. M., Levilliers, N., Thomas, D., Bré, M. H., van Dorsselaer, A., Gaertig, J., & Janke, C. (2009). Evolutionary Divergence of Enzymatic Mechanisms for Posttranslational Polyglycylation. Cell, 137(6). https://doi.org/10.1016/j.cell.2009.05.020

Rogowski, K., van Dijk, J., Magiera, M. M., Bosc, C., Deloulme, J. C., Bosson, A., Peris, L., Gold, N. D., Lacroix, B., Grau, M. B., Bec, N., Larroque, C., Desagher, S., Holzer, M., Andrieux, A., Moutin, M. J., & Janke, C. (2010). A family of protein-deglutamylating enzymes associated with neurodegeneration. Cell, 143(4). https://doi.org/10.1016/j.cell.2010.10.014

Rosenbaum, J. L., & Witman, G. B. (2002). Intraflagellar transport. In Nature Reviews Molecular Cell Biology (Vol. 3, Issue 11, pp. 813–825). https://doi.org/10.1038/nrm952

Ross, S., & Schwartz, S. (2022). Total Internal Reflection Fluorescence (TIRF) Microscopy . Https://Www.Microscopyu.Com/Techniques/Fluorescence/Total-Internal-Reflection-Fluorescence-Tirf-Microscopy.

Ruba, A., Luo, W., & Yang, W. (2018). Application of high-speed super-resolution speed microscopy in live primary cilium. Journal of Visualized Experiments, 2018(131). https://doi.org/10.3791/56475

Salloum, T., Tokajian, S., & Hirt, R. P. (2021). Advances in Understanding Leishmania Pathobiology: What Does RNA-Seq Tell Us? In Frontiers in Cell and Developmental Biology (Vol. 9). https://doi.org/10.3389/fcell.2021.702240

Santi, A. M. M., & Murta, S. M. F. (2022). Impact of Genetic Diversity and Genome Plasticity of Leishmania spp. in Treatment and the Search for Novel Chemotherapeutic Targets. In Frontiers in Cellular and Infection Microbiology (Vol. 12). https://doi.org/10.3389/fcimb.2022.826287

Sanyal, C., Pietsch, N., Ramirez Rios, S., Peris, L., Carrier, L., & Moutin, M. J. (2021). The detyrosination/re-tyrosination cycle of tubulin and its role and dysfunction in neurons and cardiomyocytes. In Seminars in Cell and Developmental Biology. https://doi.org/10.1016/j.semcdb.2021.12.006

Sasse, R., & Gull, K. (1988). Tubulin post-translational modifications and the construction of microtubular organelles in Trypanosoma brucei. Journal of Cell Science, 90 (Pt 4). https://doi.org/10.1242/jcs.90.4.577

Sayers, E. W., Bolton, E. E., Brister, J. R., Canese, K., Chan, J., Comeau, D. C., Connor, R., Funk, K., Kelly, C., Kim, S., Madej, T., Marchler-Bauer, A., Lanczycki, C., Lathrop, S., Lu, Z., Thibaud-Nissen, F., Murphy, T., Phan, L., Skripchenko, Y., … Sherry, S. T. (2022). Database resources of the national center for biotechnology information. Nucleic Acids Research, 50(D1). https://doi.org/10.1093/nar/gkab1112

Schneider, A., Plessmann, U., & Weber, K. (1997). Subpellicular and flagellar microtubules of Trypanosoma brucei are extensively glutamylated. Journal of Cell Science, 110(4). https://doi.org/10.1242/jcs.110.4.431

Schneider, A., Sherwin, T., Sasse, R., Russell, D. G., Gull, K., & Seebeck, T. (1987). Subpellicular and flagellar microtubules of Trypanosoma brucei brucei contain the same α-tubulin isoforms. Journal of Cell Biology, 104(3). https://doi.org/10.1083/jcb.104.3.431

Scholey, J. M. (2008). Intraflagellar transport motors in cilia: Moving along the cell's antenna. In Journal of Cell Biology (Vol. 180, Issue 1). https://doi.org/10.1083/jcb.200709133

Schouteden, C., Serwas, D., Palfy, M., & Dammermann, A. (2015). The ciliary transition zone functions in cell adhesion but is dispensable for axoneme assembly in C. elegans. Journal of Cell Biology, 210(1). https://doi.org/10.1083/jcb.201501013

Schwabl, P., Boité, M. C., Bussotti, G., Jacobs, A., Andersson, B., Moreira, O., Freitas-Mesquita, A. L., Meyer-Fernandes, J. R., Telleria, E. L., Traub-Csekö, Y., Vaselek, S., Leštinová, T., Volf, P., Morgado, F. N., Porrozzi, R., Llewellyn, M., Späth, G. F., & Cupolillo, E. (2021). Colonization and genetic diversification processes of Leishmania infantum in the Americas. Communications Biology, 4(1). https://doi.org/10.1038/s42003-021-01658-5

Secundino, N. F. C., Eger-Mangrich, I., Braga, E. M., Santoro, M. M., & Pimenta, P. F. P. (2005). Lutzomyia longipalpis peritrophic matrix: Formation, structure, and chemical composition. Journal of Medical Entomology, 42(6). https://doi.org/10.1093/jmedent/42.6.928

Sedmak, T., & Wolfrum, U. (2010). Intraflagellar transport molecules in ciliary and nonciliary cells of the retina. Journal of Cell Biology, 189(1). https://doi.org/10.1083/jcb.200911095

Shillingford, J. M., Murcia, N. S., Larson, C. H., Low, S. H., Hedgepeth, R., Brown, N., Flask, C. A., Novick, A. C., Goldfarb, D. A., Kramer-Zucker, A., Walz, G., Piontek, K. B., Germino, G. G., & Weimbs, T. (2006). The mTOR pathway is regulated by polycystin-1, and its inhibition reverses renal cystogenesis in polycystic kidney disease. Proceedings of the National Academy of Sciences of the United States of America, 103(14). https://doi.org/10.1073/pnas.0509694103

Silflow, C. D., & Rosenbaum, J. L. (1981). Multiple α- and β-tubulin genes in chlamydomonas and regulation of tubulin mRNA levels after deflagellation. Cell, 24(1). https://doi.org/10.1016/0092-8674(81)90503-1

Silverman, M., & Simon, M. (1974). Flagellar rotation and the mechanism of bacterial motility. Nature, 249(5452). https://doi.org/10.1038/249073a0

Sinclair, A. N., Huynh, C. T., Sladewski, T. E., Zuromski, J. L., Ruiz, A. E., & de Graffenried, C. L. (2021). The Trypanosoma brucei subpellicular microtubule array is organized into functionally discrete subdomains defined by microtubule associated proteins. PLoS Pathogens, 17(5). https://doi.org/10.1371/journal.ppat.1009588

Sloboda, R. D. (2009). Posttranslational protein modifications in cilia and flagella. Methods in Cell Biology, 94. https://doi.org/10.1016/S0091-679X(08)94018-8

Smith, A. E. (2013). The centriole in evolution: from motility to mitosis.

Snow, J. J., Ou, G., Gunnarson, A. L., Walker, M. R. S., Zhou, H. M., Brust-Mascher, I., & Scholey, J. M. (2004). Two anterograde intraflagellar transport motors cooperate to build sensory cilia on C. elegans neurons. Nature Cell Biology, 6(11). https://doi.org/10.1038/ncb1186

Stepanek, L., & Pigino, G. (2016). Microtubule doublets are double-track railways for intraflagellar transport trains. Science, 352(6286). https://doi.org/10.1126/science.aaf4594

Sunter, J. D., Moreira-Leite, F., & Gull, K. (2018). Dependency relationships between IFT-dependent flagellum elongation and cell morphogenesis in Leishmania. Open Biology, 8(11). https://doi.org/10.1098/rsob.180124

Sunter, J., & Gull, K. (2017). Shape, form, function and Leishmania pathogenicity: from textbook descriptions to biological understanding. In Open biology (Vol. 7, Issue 9). https://doi.org/10.1098/rsob.170165

Szymanska, K., & Johnson, C. A. (2012). The transition zone: An essential functional compartment of cilia. In Cilia (Vol. 1). https://doi.org/10.1186/2046-2530-1-10

Takao, D., & Verhey, K. J. (2016). Gated entry into the ciliary compartment. In Cellular and Molecular Life Sciences (Vol. 73, Issue 1). https://doi.org/10.1007/s00018-015-2058-0

Taschner, M., Bhogaraju, S., & Lorentzen, E. (2012). Architecture and function of IFT complex proteins in ciliogenesis. Differentiation, 83(2). https://doi.org/10.1016/j.diff.2011.11.001

Taschner, M., & Lorentzen, E. (2016). The intraflagellar transport machinery. In Cold Spring Harbor Perspectives in Biology (Vol. 8, Issue 10). Cold Spring Harbor Laboratory Press. https://doi.org/10.1101/cshperspect.a028092

Taschner, M., Mourão, A., Awasthi, M., Basquin, J., & Lorentzen, E. (2017). Structural basis of outer dynein arm intraflagellar transport by the transport adaptor protein ODA16 and the intraflagellar transport protein IFT46. Journal of Biological Chemistry, 292(18). https://doi.org/10.1074/jbc.M117.780155

Tetley, L., & Vickerman, K. (1985). Differentiation in Trypanosoma brucei: host-parasite cell junctions and their persistence during acquisition of the variable antigen coat. In J. Cell Sci (Vol. 74).

Ti, S.-C. (2022). Reconstituting Microtubules: A Decades-Long Effort From Building Block Identification to the Generation of Recombinant α/β-Tubulin. Frontiers in Cell and Developmental Biology, 10. https://doi.org/10.3389/fcell.2022.861648

Ti, S.-C., Alushin, G. M., & Kapoor, T. M. (2018). Human b-Tubulin Isotypes Can Regulate Microtubule Protofilament Number and Stability Developmental Cell Human b-Tubulin Isotypes Can Regulate Microtubule Protofilament Number and Stability. Developmental Cell, 47.

Toropova, K., Zalyte, R., Mukhopadhyay, A. G., Mladenov, M., Carter, A. P., & Roberts, A. J. (2019). Structure of the dynein-2 complex and its assembly with intraflagellar transport trains. Nature Structural and Molecular Biology, 26(9). https://doi.org/10.1038/s41594-019-0286-y

van de Weghe, J. C., Aaron Harris, J., Kubo, T., Witman, G. B., & Lechtreck, K. F. (2021). Diffusion rather than intraflagellar transport likely provides most of the tubulin required for axonemal assembly in Chlamydomonas. Journal of Cell Science, 133(17). https://doi.org/10.1242/jcs.249805

van den Hoek, H., Klena, N., Jordan, M. A., Alvarez Viar, G., Schaffer, M., Erdmann, P. S., Wan, W., Plitzko, J. M., Baumeister, W., Pigino, G., Hamel, V., Guichard, P., Engel, B. D., Klena, N., Jordan, M. A., Alvarez Viar, G., Schaffer, M., Erdmann, P. S., Wan, W., … Engel, B. D. (2021). In situ architecture of the ciliary base reveals the stepwise assembly of IFT trains. BioRxiv, 548(July).

van der Heiden, K., Groenendijk, B. C. W., Hierck, B. P., Hogers, B., Koerten, H. K., Mommaas, A. M., Gittenberger-de Groot, A. C., & Poelmann, R. E. (2006). Monocilia on chicken embryonic endocardium in low shear stress areas. Developmental Dynamics, 235(1). https://doi.org/10.1002/dvdy.20557

Vannuccini, E., Paccagnini, E., Cantele, F., Gentile, M., Dini, D., Fino, F., Diener, D., Mencarelli, C., & Lupetti, P. (2016). Two classes of short intraflagellar transport train with different 3D structures are present in Chlamydomonas flagella. Journal of Cell Science, 129(10). https://doi.org/10.1242/jcs.183244

Vashishtha, M., Walther, Z., & Hall, J. L. (1996). The kinesin-homologous protein encoded by the Chlamydomonas FLA10 gene is associated with basal bodies and centrioles. Journal of Cell Science, 109(3). https://doi.org/10.1242/jcs.109.3.541

Vaughan, S., & Gull, K. (2016). Basal body structure and cell cycle-dependent biogenesis in Trypanosoma brucei. In Cilia (Vol. 5, Issue 1). https://doi.org/10.1186/s13630-016-0023-7

Vieillard, J., Paschaki, M., Duteyrat, J. L., Augière, C., Cortier, E., Lapart, J. A., Thomas, J., & Durand, B. (2016). Transition zone assembly and its contribution to axoneme formation in Drosophila male germ cells. Journal of Cell Biology, 214(7). https://doi.org/10.1083/jcb.201603086

Vincensini, L., Blisnick, T., Bertiaux, E., Hutchinson, S., Georgikou, C., Ooi, C. P., & Bastin, P. (2018). Flagellar incorporation of proteins follows at least two different routes in trypanosomes. Biology of the Cell, 110(2). https://doi.org/10.1111/boc.201700052

Vitre, B., Guesdon, A., & Delaval, B. (2020). Non-ciliary Roles of IFT Proteins in Cell Division and Polycystic Kidney Diseases. In Frontiers in Cell and Developmental Biology (Vol. 8). https://doi.org/10.3389/fcell.2020.578239

Wakid, M. H., & Bates, P. A. (2004). Flagellar attachment of Leishmania promastigotes to plastic film in vitro. Experimental Parasitology, 106(3–4), 173–178. https://doi.org/10.1016/j.exppara.2004.03.001

Ward, S., Thomson, N., White, J. G., & Brenner, S. (1975). Electron microscopical reconstruction of the anterior sensory anatomy of the nematode caenorhabditis elegans. Journal of Comparative Neurology, 160(3). https://doi.org/10.1002/cne.901600305

Wei, Q., Xu, Q., Zhang, Y., Li, Y., Zhang, Q., Hu, Z., Harris, P. C., Torres, V. E., Ling, K., & Hu, J. (2013). Transition fibre protein FBF1 is required for the ciliary entry of assembled intraflagellar transport complexes. Nature Communications, 4. https://doi.org/10.1038/ncomms3750

Wheeler, R. J., Gluenz, E., & Gull, K. (2011). The cell cycle of Leishmania: Morphogenetic events and their implications for parasite biology. Molecular Microbiology, 79(3), 647–662. https://doi.org/10.1111/j.1365-2958.2010.07479.x

Wheeler, R. J., Gluenz, E., & Gull, K. (2015). Basal body multipotency and axonemal remodelling are two pathways to a 9+0 flagellum. Nature Communications, 6. https://doi.org/10.1038/ncomms9964

WHO. (2022). Leishmaniasis. 2022. https://www.who.int/news-room/fact-sheets/detail/leishmaniasis

Williams, C. L., Mcintyre, J. C., Norris, S. R., Jenkins, P. M., Zhang, L., Pei, Q., Verhey, K., & Martens, J. R. (2014). Direct evidence for BBSome-associated intraflagellar transport reveals distinct properties of native mammalian cilia. Nature Communications, 5. https://doi.org/10.1038/ncomms6813

Wingfield, J. L., Mekonnen, B., Mengoni, I., Liu, P., Jordan, M., Diener, D., Pigino, G., & Lechtreck, K. (2021). In vivo imaging shows continued association of several IFT-A, IFT-B and dynein complexes while IFT trains U-turn at the tip. Journal of Cell Science, 134(18). https://doi.org/10.1242/jcs.259010

Wingfield, J. L., Mengoni, I., Bomberger, H., Jiang, Y. Y., Walsh, J. D., Brown, J. M., Picariello, T., Cochran, D. A., Zhu, B., Pan, J., Eggenschwiler, J., Gaertig, J., Witman, G. B., Kner, P., & Lechtreck, K. (2017). IFT trains in different stages of assembly queue at the ciliary base for consecutive release into the cilium. ELife, 6. https://doi.org/10.7554/eLife.26609

Wloga, D. et. al. (2017). Tubulin post-translational modifications and microtubule dynamics. In International Journal of Molecular Sciences (Vol. 18, Issue 10). https://doi.org/10.3390/ijms18102207

Wloga, D., Joachimiak, E., Louka, P., & Gaertig, J. (2017). Posttranslational modifications of Tubulin and cilia. Cold Spring Harbor Perspectives in Biology, 9(6). https://doi.org/10.1101/cshperspect.a028159

Wloga, D., Webster, D. M., Rogowski, K., Bré, M. H., Levilliers, N., Jerka-Dziadosz, M., Janke, C., Dougan, S. T., & Gaertig, J. (2009). TTLL3 Is a Tubulin Glycine Ligase that Regulates the Assembly of Cilia. Developmental Cell, 16(6). https://doi.org/10.1016/j.devcel.2009.04.008

Wolff, A., de Nechaud, B., Chillet, D., Mazarguil, H., Desbruyeres, E., Audebert, S., Edde, B., Gros, F., & Denoulet, P. (1992). Distribution of glutamylated α and β-tubulin in mouse tissues using a specific monoclonal antibody, GT335. European Journal of Cell Biology, 59(2).

Wong-Riley, M. T. T., & Besharse, J. C. (2012). The kinesin superfamily protein KIF17: One protein with many functions. In Biomolecular Concepts (Vol. 3, Issue 3). https://doi.org/10.1515/bmc-2011-0064

Wood, C. R., Wang, Z., Diener, D., Zones, J. M., Rosenbaum, J., & Umen, J. G. (2012). IFT proteins accumulate during cell division and localize to the cleavage furrow in chlamydomonas. PLoS ONE, 7(2). https://doi.org/10.1371/journal.pone.0030729

Woods, A., Sherwin, T., Sasse, R., MacRae, T. H., Baines, A. J., & Gull, K. (1989). Definition of individual components within the cytoskeleton of Trypanosoma brucei by a library of monoclonal antibodies. Journal of Cell Science, 93(3). https://doi.org/10.1242/jcs.93.3.491

Woolley, D., Gadelha, C., & Gull, K. (2006). Evidence for a sliding-resistance at the tip of the trypanosome flagellum. Cell Motility and the Cytoskeleton, 63(12). https://doi.org/10.1002/cm.20159

Wordeman, L., & Vicente, J. J. (2021). Microtubule targeting agents in disease: Classic drugs, novel roles. In Cancers (Vol. 13, Issue 22). https://doi.org/10.3390/cancers13225650

Wren, K. N., Craft, J. M., Tritschler, D., Schauer, A., Patel, D. K., Smith, E. F., Porter, M. E., Kner, P., & Lechtreck, K. F. (2013). A differential cargo-loading model of ciliary length regulation by IFT. Current Biology, 23(24). https://doi.org/10.1016/j.cub.2013.10.044

Xia, L., Hai, B., Gao, Y., Burnette, D., Thazhath, R., Duan, J., Bré, M. H., Levilliers, N., Gorovsky, M. A., & Gaertig, J. (2000). Polyglycylation of tubulin is essential and affects cell motility and division in Tetrahymena thermophila. Journal of Cell Biology, 149(5). https://doi.org/10.1083/jcb.149.5.1097

Xue, B., Liu, Y. X., Dong, B., Wingfield, J. L., Wu, M., Sun, J., Lechtreck, K. F., & Fan, Z. C. (2020). Intraflagellar transport protein RABL5/IFT22 recruits the BBSome to the basal body through the GTPase ARL6/BBS3. Proceedings of the National Academy of Sciences of the United States of America, 117(5). https://doi.org/10.1073/pnas.1901665117

Yanase, R., Moreira-Leite, F., & Sunter, J. (2022). Formation and three-dimensional architecture of Leishmania adhesion in the sand fly vector. BioRxiv.

Yi, P., Li, W. J., Dong, M. Q., & Ou, G. (2017). Dynein-Driven Retrograde Intraflagellar Transport Is Triphasic in C. elegans Sensory Cilia. Current Biology, 27(10). https://doi.org/10.1016/j.cub.2017.04.015

Zauli, R. C., Yokoyama-Yasunaka, J. K. U., Miguel, D. C., Moura, A. S., Pereira, L. I. A., da Silva, I. A., Lemes, L. G. N., Dorta, M. L., de Oliveira, M. A. P., Pitaluga, A. N., Ishikawa, E. A. Y., Rodrigues, J. C. F., Traub-Cseko, Y. M., Bijovsky, A., Ribeiro-Dias, F., & Uliana, S. R. B. (2012). A dysflagellar mutant of Leishmania (Viannia) braziliensis isolated from a cutaneous leishmaniasis patient. Parasites and Vectors, 5(1), 11. https://doi.org/10.1186/1756-3305-5-11

Zilberstein, D., & Shapira, M. (1994). The role of pH and temperature in the development of Leishmania parasites. In Annual Review of Microbiology (Vol. 48). https://doi.org/10.1146/annurev.mi.48.100194.002313